University of Glasgow

Deciphering the Vascular Disease Mechanisms Underlying Hypertensive Disorders of Pregnancy

Kayley Scott

BSc (Hons), MRes

This document is submitted in fulfilment of the requirements for the degree of Doctor of Philosophy (PhD) within the School of Cardiovascular and Metabolic Health for the College of Medical, Veterinary and Life Sciences.

Date of Deposition: 27/09/2023

Author's Declaration

I declare that the contents of this document are entirely my own work and not of any other person, with the exception of urine biochemistry assays performed by Ms. Elaine Bulter, qRT-PCR of neonatal tissues performed by Miss. Lara Peden, Miss. Sol Olivera and Miss. Cara Trivett. The RNA sequencing data was previously generated by Dr. Hannah Morgan and the bioinformatics associated with differential expressional analysis was conducted by Glasgow Polyomics. Pathway Analysis was performed with guidance from Dr. Martin McBride. Myography of isolated uterine arteries was performed by Dr. Hannah Morgan. This work was supervised by Dr. Christian Delles and Dr. Delyth Graham. This document as a whole has not previously been submitted in any form to the University of Glasgow or to any other institution for assessment or any other purpose.

PRINTED NAME: ___**KAYLEY SCOTT**_____

SIGNATURE: _____

09/2023

Acknowledgements

First and foremost, I would like to thank my supervisors Dr. Christian Delles and Dr. Delyth Graham, without whom none of this research would have been possible. Special thanks are extended to Del and Dr. Martin McBride. Del and Martin have provided endless confidence in me and unwavering support in the face of what would have otherwise been insurmountable obstacles and conflicts (both professional and personal). Without you both to guide me, I would not be half the scientist and human being that I am today. Special mentions must go to those that graciously allowed me to mentor them and helped me during my research journey: Sol Olivera, Lara Peden and Cara Trivett. To you all, thank you for giving me that opportunity to learn and I am so incredibly proud to say that I believe each of you are already tour de forces in your areas of research interest. I wish you guys nothing but happiness and joy in your future endeavours. And, of course, I must thank the British Heart Foundation for their funding of my PhD Studentship and for making this possible.

Special thanks to the Biological Services staff of the CVRU, namely Joanne Battersby and Seonagh Henderson. Seonagh, your love of animals and science as well as your unending work ethic inspired me every single day I worked alongside you. I am so privileged to call you not only a colleague, but a now very dear friend. As long as I work with animals in science, I will strive to be like you.

I would also like to extend thanks to every single individual in the BHF GCRC who has helped me in some way. Everyone has been so warm and welcoming and has made me feel part of an amazing community. To all my fellow PhD students who were with me in the trenches so to speak, I will never tire of seeing you all succeed. I miss you all.

Finally, I am so grateful to my friends and partner. Toni and Karina, thank you for listening to me endlessly drone on about placentas and blood vessels, for the late night venting sessions when everything felt too much and for helping me back on my feet every single time. And Martin, without you cheering me on I would have given up long ago. Thank you for every hug, for every smile and every time you told me “you can do this”. I love you, thank you so much for all that you’ve done to help me get here and become my best self, in and out of the lab.

COVID-19 Impact Statement

The work contained within this thesis was carried out in the period 2019 – 2022. During 2020-2021 the coronavirus (COVID-19) pandemic occurred with effects that altered research globally. Given the *in vivo* nature of the work in this thesis, the pandemic presented major challenges and disruptions to data collection, resource availability and laboratory access.

At the time of UK lockdown, significant progress had been made in optimising a model of super-imposed pre-eclampsia in rats (Chapter 3) and work was underway on optimising a protocol for the isolation of primary uterine artery vascular smooth muscle cells (Chapter 6) as well as plans to begin investigating the use of magnesium sulphate in our rodent model (Chapter 4). All of this work was suspended during the pandemic due to travel restrictions preventing any and all work on-campus. This substantially hindered the final outputs presented in this thesis.

Due to the impact of COVID-19, *n* numbers involving uterine artery vascular smooth muscle cells are low and cannot be statistically tested for significance. Additionally, the pause in *in vivo* research created significant batch variability in the magnesium sulphate study that is discussed further in its relevant chapter. Had these disruptions not taken place, I believe the results of Chapters 4 and 6 would be clearer to interpret and both studies would have been able to obtain higher *n* numbers. Therefore, the results presented would have been able to better inform the hypotheses of each study.

To mitigate the impact of COVID-19, the focus of the thesis was broadened to include *in silico* analysis of an in-house transcriptomic data set to investigate alterations in gene expression during early rodent pregnancy. This later informed a publication which is presented in Chapter 5.

Summary

As the prevalence of hypertensive orders increases, particularly pre-eclampsia superimposed on a background of chronic hypertension (SPE), so too does the global disease burden they represent. Not only are these disorders detrimental to both mother and child during the course of pregnancy, they also have lasting long-term effects to future cardiovascular health for both. Despite this, relatively little is known about the generation and development of these multifactorial disorders. In combination with the effects of potential treatments to offspring health, the resultant scope for therapeutic interventions is severely limited. The stroke-prone spontaneously hypertensive (SHRSP) rat is an established model of chronic hypertension during pregnancy that can be further stressed by infusion of angiotensin II (ANGII) in mid-gestation to create a pre-eclamptic phenotype that closely mimics the clinical manifestation of SPE in humans.

This thesis aimed to optimise and characterise a novel rodent model of SPE to provide a useful tool in understanding the underlying pathophysiology of the condition and in testing potential therapeutic strategies. The objectives were to assess the maternal, fetoplacental and neonatal response to SPE development in the SHRSP; evaluate the use of magnesium sulphate ($MgSO_4$) as a preventative therapeutic in the context of SPE; investigate the underlying genetic mechanisms that may influence abnormal uterine artery remodelling due to maternal hypertension; and, finally, to validate these genetic mechanisms *in vitro*. A variety of *in vivo* and *ex vivo* techniques were employed in the generation and assessment of the optimised SPE rodent model. Pregnant SHRSP dams infused with 750ng/kg/min ANGII were found to exhibit signs of impaired maternal cardiovascular, renal and placental function alongside the abnormal uterine artery remodelling already characteristic of the SHRSP. Further, the offspring of these dams were more likely to be growth restricted and preliminary evidence suggested neonatal gene expression may be altered. When $MgSO_4$ was administered in a preventative capacity in daily drinking water, it was shown to improve maternal blood pressure, proteinuria and weight. However, $MgSO_4$ was ineffective at improving maternal cardiac function or uteroplacental flow and was observed to worsen fetal growth restriction. To better understand the maternally-derived factors in this impaired uterine artery remodelling associated with hypertensive pregnancy, RNA-sequencing was used to assess the genetic profiles of early

pregnancy uterine arteries in SHRSP and normotensive WKY. Though the two strains shared a conserved response to pregnancy, there were striking differences in pathways related to vascular function, notably reactive oxygen species (ROS) production and calcium (Ca^{2+}) signalling. Finally, using a combination of whole uterine arteries and vascular smooth muscle cells (UAVSMCs) derived from them, the gene expression patterns relating to ROS and Ca^{2+} were investigated to validate them. Though studies were preliminary and sample sizes small, there was evidence of altered ROS production, NOX subunit expression and UAVSMC Ca^{2+} release between WKY and SHRSP.

This work has provided information on an optimised, novel rodent model of super-imposed pre-eclampsia that may be used as a potential tool in investigating the pathophysiology of the condition or in assessing the long-term consequences of an adverse *in utero* environment. It has also deepened our understanding of the effects of prolonged $MgSO_4$ exposure during pregnancy and highlighted the need for an optimised, standardised dosing regime in humans. Furthermore, this work has generated novel insights into the genetic factors that influence uterine artery remodelling and their functional consequences in early hypertensive pregnancy.

Table of Contents

List of Tables

List of Figures

List of Abbreviations

°C	Degrees Celsius
ng	nanogram
nm	nanometre
µg	Micrograms
µL	Microlitre
µmol	Micromole
µM	Micromolar
µm	Micrometre
mg	Milligram
mL	Millilitre
mM	Millimolar
mm	Millimetre
cm	Centimetre
g	gram
kg	kilogram
mol	Mole
L	Litre
ms	Millisecond
min	Minutes
hr	Hour
wk	Weeks
Δ	Delta
ACE	Angiotensin converting enzyme
ACE2	Angiotensin converting enzyme 2
ACR	Albumin to creatinine ratio
Ang(1-7)	Angiotensin (1-7)
Ang(1-9)	Angiotensin (1-9)
ANGI	Angiotensin I
ANGII	Angiotensin II
ASB4	Ubiquitin ligase ankyrin repeat and SOCS box containing 4
AT_1R	Angiotensin type 1 receptor
AT_2R	Angiotensin type 2 receptor
AT_1-AA	Angiotensin type 1 receptor autoantibodies
ATP	Adenosine triphosphate
AVP	Arginine vasopressin
AWT(s/d)	Anterior wall thickness (systole/diastole)
BP	Blood pressure
BPH/5	Borderline hypertensive 5
Ca^{2+}	Calcium ion
$CaCl_2$	Calcium chloride
Calm1	Calmodulin 1
cDNA	Complimentary DNA
CO	Cardiac output
CO_2	Carbon dioxide
COVID-19	Coronavirus
CP	Chorionic plate
CSF	Cerebrospinal fluid
CT	Cycle threshold
CTB	Cytotrophoblast
Cyba	Cytochrome b-245 α chain; p22-phox
Cybb	Cytochrome b-245 β chain; gp91

DBP	Diastolic blood pressure
DEG	Differentially expressed gene
dH_2O	Deionised water
D_i	Internal diameter
D_e	External diameter
DMEM	Dulbecco's Modified Eagle Medium
DMSO	Dimethyl sulfoxide
DNA	Deoxyribonucleic acid
dNTP	Deoxyribonucleotide triphosphate
DT'E	Deceleration time taken for the E wave to return from peak to baseline
E:A	Ratio between the peaks of the E and A waves
EDD	End diastolic diameter
EDTA	Ethylenediaminetetraacetic acid
EDV	End diastolic velocity
EF	Ejection fraction
eNOS	Endothelial nitric oxide synthase
EPR	Electron paramagnetic resonance
ESD	End systolic diameter
ESV	End systolic velocity
EVT	Extravillous trophoblast
FBS	Fetal bovine serum
FGR	Fetal growth restriction
FPKM	Fragments per kilobase of transcript per million mapped reads
FS	Fractional shortening
G	Gauge
GAPDH	Glyceraldehyde-3-phosphate dehydrogenase
GD	Gestational day
GFR	Glomerular filtration rate
GHz	Gigahertz
GOI	Gene of interest
Gpx1	Glutathione peroxidase 1
HDP	Hypertensive disorder of pregnancy
HELLP	Haemolysis, elevated liver enzymes and low platelets
HEPES	(4-(2-hydroxyethyl)-1-piperazineethanesulfonic acid)
HIF-1α	Hypoxia inducible factor 1α
HR	Heart rate
IPA®	Ingenuity Pathway Analysis®
Itpr2	Inositol 1,4,5-triphosphate receptor type 2
IU	International units
Jx	Junctional zone
K^+	Potassium ion
KCl	Potassium chloride
KH_2PO_4	Potassium dihydrogen phosphate; $K(PH_2O_4)$
kPa	Kilopascals
Lab	Labyrinth zone
L-NAME	Ω-nitro-$_L$-arginine methyl ester
lncRNA	Long non-coding RNA
LVM	Left ventricular mass
MAP	Mean arterial pressure
Mes	Mesometrial triangle
Mg^{2+}	Magnesium ion
$MgCl_2$	Magnesium chloride

$MgSO_4$	Magnesium sulphate
MHC	Major histocompatibility complex
mmHg	Millimetres of mercury
MMP	Matrix metalloprotease
mRNA	Messenger RNA
mV	Millivolts
Myh6	Myosin heavy chain 6
Mylk	Myosin light chain kinase
Na^+	Sodium ion
Na_2HPO_4	Disodium hydrogen phosphate
NaCl	Sodium chloride
NADPH	Nicotinamide adenine dinucleotide phosphate-oxidase
NaH_2CO_3	Sodium dihydrogen bicarbonate
NFW	Nuclease free water
NK	Natural killer cell
NOX	NADPH oxidase
NOX2	NADPH oxidase 2
NOX4	NADPH oxidase 4
NP	Non-pregnant
ns	Non-significant
O_2	Oxygen
$O_2^{\bullet-}$	Superoxide anion
P	Pregnant
p0	Passage 0
p40-phox	Neutrophil cytosolic factor 4; Ncf4
p67-phox	Neutrophil cytosolic factor 2; Ncf2
padj	Adjusted *p*-value for false discovery rate
PAS	Periodic acid Schiff
PBS	Phosphate buffered saline
PCA	Principal component analysis
PCR	Polymerase chain reaction
PE	Pre-eclampsia
PKC	Protein kinase C
PLC	Phospholipase C
Plc1	Phospholipase C like 1
Plcg2	Phospholipase C γ 2
PlGF	Placental growth factor
PP	Pre-pregnancy
Pparα	Peroxisome proliferator activated receptor α
Prkcb	Protein kinase C β
PSV	Peak systolic velocity
PVR	Peripheral vascular resistance
PWT(s/d)	Posterior wall thickness (systole/diastole)
qPCR	Quantitative polymerase chain reaction
qRT-PCR	Quantitative reverse transcriptase polymerase chain reaction
RAAS	Renin-angiotensin-aldosterone system
RBC	Red blood cell
REML	Restricted maximum likelihood
RI	Resistance index
RNA	Ribonucleic acid
RNA-Seq	RNA sequencing
ROS	Reactive oxygen species
rpm	Revolutions per minute

RQ	Relative quantity
RUPP	Reduced uteroplacental perfusion
RWT	Relative wall thickness
S/D	Systolic to diastolic ratio
SBP	Systolic blood pressure
SE	Standard error
SEM	Standard error of the mean
sEng	Soluble transforming growth factor β co-receptor endoglin
sFlt-1	Soluble FMS-like tyrosine kinase 1
SHR	Spontaneously hypertensive rat
SHRSP	Stroke-prone spontaneously hypertensive rat
siRNA	Short interfering RNA
SpA	Spiral arteries
SPE	Super-imposed pre-eclampsia
Spp1	Osteopontin
SSIV	Superscript IV
STB	Syncytiotrophoblast
STOX1	Storkhead box 1
SV	Stroke volume
TGF-β1	Transforming growth factor β-1
TNF-α	Tumour necrosis factor α
U	Units
UAVSMC	Uterine artery vascular smooth muscle cell
uNK	Uterine natural killer cell
v/v	Volume to volume
VEGF	Vascular endothelial growth factor
vs	Versus
VSMC	Vascular smooth muscle cell
WHO	World Health Organisation
w/v	Weight to volume
WKY	Wistar Kyoto
xg	G-force

List of Published Works and Awards

Journal Articles

Scott, K., Morgan, H.L., Delles, C., Fisher, S., Graham, D. and McBride, M.W. (2021). Distinct uterine artery gene expression profiles during early gestation in the stroke-prone spontaneously hypertensive rat. *Physiological Genomics.* **53** (4), p. 160-171.

Mary, S., Boder, P., Rossitto, G., Graham, L., Scott, K., Flynn, A., Kipgen, D., Graham, D. and Delles, C. (2021). Salt loading decreases urinary excretion and increases intracellular accumulation of uromodulin in stroke-prone spontaneously hypertensive rats. *Clinical Science (London)*. **135** (24), p.2749-2761.

Casey, H., Dennehy, N., Fraser, A., Lees, C., McEinery, C., Scott, K., Wilkinson, I.B. and Delles, C. (2023). Placental Syndromes and Maternal Cardiovascular Health. *Clinical Science (London)*. **137** (16), p.1211-1224.

Abstracts

Scott, K., Olivera, S., Peden, L., McBride, M.W., Delles, C. and Graham, D. 'Magnesium Sulphate Treatment During Hypertensive Pregnancy Improves Maternal but not Fetal Outcomes in Rats.' Scottish Lipid Forum and Scottish Heart and Arterial Disease Risk Prevention Hybrid Meeting, November 2021. (Oral and Poster communication).

Scott, K. Morgan, H.L., Delles, C., McBride, M.W., Fisher, S., Frazier, S., Trueba, L.G., Olivera, S. and Graham, D. 'Modelling Hypertensive Pregnancy in the stroke-prone spontaneously hypertensive rat.' Sex and Gender Aspects of Cardiovascular Disease, Universities of Glasgow and Sydney, August 2021. (Online communication).

Scott, K., Morgan, H.L., McBride, M.W., Graham, D. and Delles, C. 'Hypertension During Early Pregnancy Impairs Genetic Priming of Uterine Arteries Prior to Remodelling in Rodents.' European Society of Hypertension-International Society of Hypertension Joint Meeting, April 2021. (Online communication).

Scott, K., Morgan, H.L., Graham, D. and Delles, C. 'Characterising a Novel Model of Super-imposed Pre-eclampsia.' European Society of Hypertension-International Society of Hypertension Joint Meeting, April 2021. (Online communication).

Scott, K., Morgan, H.L., McBride, M.W., Graham, D. and Delles, C. 'Hypertension During Early Pregnancy Impairs Genetic Priming of Uterine Arteries Prior to Remodelling in Rodents.' 24th Annual Scottish Cardiovascular Forum Meeting, February 2021. (Online communication).

Scott, K., Morgan, H.L., Delles, C., Fisher, S., McBride, M.W. and Graham, D. 'Hypertension During Early Pregnancy Impairs Genetic Priming of Uterine Arteries Prior to Remodelling in Rodents.' Placenta-Interface Virtual Seminar Series, Universities of Florida and Pittsburgh, February 2021. (Online communication)

Scott, K., Morgan, H.L., Graham, D. and Delles, C. 'Characterising a Novel Model of Super-imposed Pre-eclampsia.' Maternal obesity and pre-eclampsia: common pathways, Biochemical Society and World Obesity Federation Joint Meeting, November 2019. (Poster communication).

Scott, K., Morgan, H.L, Mary, S. and Graham, D. 'Dissecting the Underlying Disease Mechanisms of Hypertensive Pregnancy.' British Heart Foundation Student Conference, April 2019. (Oral communication).

Scott, K., Morgan, H.L. and Graham, D. 'Optimising a Novel Model of Super-imposed Pre-eclampsia.' 10th Glasgow Paediatric Research Day, November 2019. (Poster communication).

Scott, K., Morgan, H.L. and Graham, D. 'The Contribution of Fetoplacental Genes in the Development of Abnormal Uterine Artery Remodelling During Pregnancy in the SHRSP Rat.' 9th Glasgow Paediatric Research Day, November 2018. (Poster communication).

Awards

Onsite Poster Presentation Award: Best Poster (2019) - £100 awarded for poster presented at the Maternal obesity and pre-eclampsia: common pathways, Biochemical Society and World Obesity Federation Joint Meeting, Amsterdam, Netherlands.

Introduction to Omics Training Fund (2019) - £200 awarded to attend the 'Introduction to Omics' course held by Glasgow Polyomics.

ISH 2022 Kyoto Presenter Travel Grant (2022) – Waiver of the meeting registration fee (¥20000 JPY), hotel accommodation and $600 USD travel expenses. Due to online participation, registration fee waiver only was awarded.

Non-Peer Reviewed Articles

Scott, K. (2018). Taking a Look *in Utero*: Tackling Cardiovascular Disease During Pregnancy. *Pharmacology Matters*. **11** (3), p.15-17.

Manuscripts in Submission (Unpublished)

Loughrey, C., Smith, G., Matsuda, R., Toda, M., Shinozaki, M., Scott, K., Costa, A.D.S., Martin, T., Dobi, S., Saxena, P., Shimamoto, K., Ishikawa, T., Kambayashi, R., Riddell, A., Elliot, E., McCarroll, C., Sakai, T., Yamano, M., Hirano, S., Kusano, K., Ionue, Y., Nakamura, M., Kikuchi, M., Toyoda, S., Taguchi, I., Fujiwara, T., Sugiyama, A., Kumagai, Y. and Iawata, K. (2022). A novel ryanodine receptor 2 stabilizer, M201-A, demonstrating an atrial selective anti-arrhythmic effect without detrimental hemodynamics. *Communications Medicine*. [Manuscript submitted for publication].

Chapter 1: Introduction

1.1 Adapting to the Normal Pregnancy

The average human pregnancy typically lasts between 266 to 294 days, or 38 to 42 weeks, from the time of conception (normally determined by the date of the last menstrual period of the mother) (Bhat and Kushtagi, 2006). During this relatively short gestational time frame, almost all of the maternal biological systems are placed under significant stress. To adapt to this stress, these maternal systems undergo major physiological adaptations in order to support the growing fetus whilst protecting the mother. Developing an understanding of these changes is key in identifying areas at risk of derangement and subsequent pathological states (Soma-Pillay *et al*, 2016). Amongst these systems, those that control blood pressure and vascular remodelling are particularly sensitive to changes induced by pregnancy.

1.1.1 Placental Development

Perhaps one of the biggest maternal adaptations to pregnancy in all mammals is the development of the placenta. The placenta is a unique organ that is only found during pregnancy and is immediately lost upon delivery. Its primary function is to facilitate the exchange of gases, nutrients and waste products between the mother and developing fetus whilst keeping the two circulatory systems separate (Ji *et al*, 2013). It also functions as the fetal renal, respiratory, hepatic, gastrointestinal and immune systems whilst producing several pregnancy-associated hormones and growth factors designed to protect the fetus from the maternal immunological response (Guttmacher *et al*, 2014; Ji *et al*, 2013). Placental development varies greatly between species and is usually categorised based on gross shape and the histological structure of the maternal-fetal interface. There are four placentation types based on structure: diffuse, multicotyledonary, zonary and discoid (or bidiscoid) (Furukawa *et al*, 2014, Fig. 1.1). Though there is great variation in terms of placental structure, the main cell types, molecular mechanisms and functions are conserved across mammalian species. Placentae can also be categorised by the histologic relationship between the chorion and uterine wall into three types: epitheliochorial, endotheliochorial and haemochorial (Furukawa *et al*, 2014, Fig. 1.1). Both humans and rats share a haemochorial placental structure that is distinguished by its depth of trophoblast invasion into the maternal tissues.

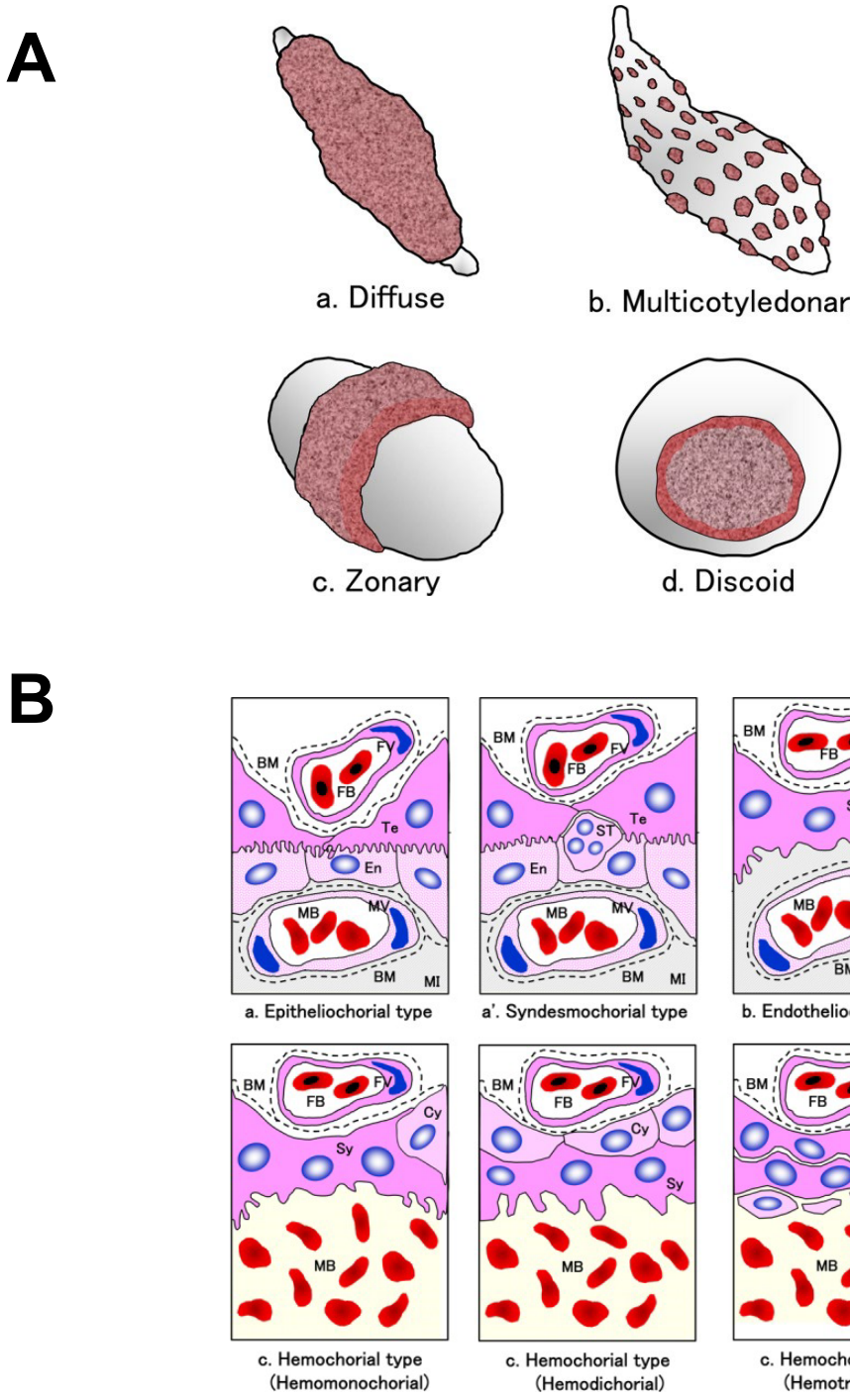

Figure 1.1: Summary of Placental Structure Classifications (Sourced: Furukawa et al, 2014).

(A) Illustrations of the classification of mammalian placentae based on gross structure of materno-fetal exchange area in relation to the chorionic sac. (B) Illustrations of the classification of mammalian placentae based on histologic relationship between chorion and uterine wall. (BM; basement membrane, Cy; cytotrophoblast, En; endometrium, FB; fetal blood, FV; fetal vessel, MB; maternal blood, MI; maternal interstitium, MV; maternal vessel, ST; specific trophoblast, Sy; syncytiotrophoblast, Te; trophectoderm).

1.1.1.1 Human

In humans, the placenta is the first organ to form in the pregnancy and originates from the blastocyst- formed by sequential divisions of the fertilized ovum (Fig. 1.2, Clift and Schuh, 2013). A successful pregnancy may only occur when the endometrium has been altered by ovarian hormones that are secreted in a cyclic fashion, otherwise known as the luteal phase of the menstrual cycle. This limits the period of receptivity for implantation. Once the blastocyst is formed following fertilisation, implantation is initiated by rising levels of oestrogen and progesterone (Gude *et al* 2004). This occurs 6-7 days post-conception following blastocyst formation (Frank, 2017). The blastocyst is formed of two distinct cell populations: the inner cell mass (or embryoblast), and the trophectoderm (or trophoblast) (Maltepe and Fisher, 2015). Upon adhering to the uterine epithelium, the blastocyst immediately begins dividing to create new cell populations that will become the distinct placental layers and invades deep into the uterine wall (Ji *et al*, 2013). The trophoectoderm is composed of a single layer of cytotrophoblasts (CTBs). Following implantation to the uterine wall, these trophoblasts located at the pole of the blastocyst proliferate to form a double layer. These layers fuse in a process known as syncytial fusion to create the first syncytiotrophoblasts (STBs) of the developing placenta, occurring approximately two weeks post-conception (Frank, 2017; Gerbaud and Pidoux, 2015). During this time, a constant cycle of CTB proliferation and fusion maintains these two populations and creates the fetal portion of the placenta- the chorionic plate (Maltepe and Fisher, 2015). From the initial population of CTBs, some penetrate the newly formed layer of STBs to become extravillous cytotrophoblasts (EVTs, also known as endovascular trophoblast) (Gude *et al*, 2004). These EVTs invade the maternal decidua, myometrium and uterine spiral arteries in a retrograde fashion (Lyall *et al*, 2001). The spiral arteries undergo substantial dilatation and the vascular smooth muscle cells become dedifferentiated and the maternal endothelium is replaced by EVTs for the duration of the pregnancy (Fig. 1.3, Frank, 2017).

1.1.1.2 Rodent

The placentae of rodents (mice and rats) can be separated into distinct layers: the decidua and mesometrial triangle (or metrial glands), the junctional zone (also referred to as the basal zone), the labyrinth zone and the chorionic plate (Fig. 1.4, Small *et al*, 2016a). Human placentae share all of these layers with the exception

that the labyrinth zone in rodents, containing three trophoblast layers, equates to the placental villi, containing only one layer, in humans with both having different gross structures (De Rijk *et al,* 2002). Placental development in rats begins with stem cells that originate from the trophoectoderm of the blastocyst following implantation, similar to humans (Soares *et al*, 2012). A key differentiation between human and rodent placentation is the means by which the endometrium is altered to receive the blastocyst at implantation. In humans, decidualisation of the endometrium is triggered by hormone fluctuations during the menstrual cycle. In rodents, however, decidualisation is triggered in response to the implantation itself, usually occurring at days 4 or 5 of pregnancy (Fonseca *et al*, 2012). Additionally, whilst the blastocyst first attaches on the anti-mesometrial side of the uterus in both species (Fig 1.3), the mature placenta in rats is formed on the mesometrial side (Fig 1.4, De Rijk, 2002). Following successful implantation, the trophoectoderm consisting of two layers, mular and polar respectively, begins to differentiate into various populations of trophoblast. The mular trophoectoderm becomes primary trophoblastic giant cells whilst the polar trophoectoderm differentiates into the ectoplacental cone, subsequently invading the decidua (Furukawa *et al*, 2019). Secondary giant trophoblast cells begin to arise at the margins of the ectoplacental cone (Fonesca *et al*, 2012). Beneath the trophoectoderm are two layers of STBs that undergo fusion, much like in human placental development to create further populations of CTBs that become either secondary giant trophoblast cells, spongiotrophoblasts (endocrine functions), glycogen cells or interstitial invasive trophoblasts (situated between the vasculature) (Furukawa *et al*, 2014; Fonesca *et al*, 2012; Soares *et al*, 2012). These secondary giant trophoblast cells are analogous to human EVTs and exhibit the same invasive activity, particularly in the uterine spiral arteries (Soares *et al*, 2012). The ectoplacental cone further differentiates to become the junctional and labyrinth zones (Furukawa, 2019). The mesometrial triangle is formed from decidualised endometrial stromal cells, uterine natural killer cells, spiral arteries and glycogen-cell origin trophoblasts as well as fibroblasts from early to mid-gestation (Furukawa *et al*, 2014).

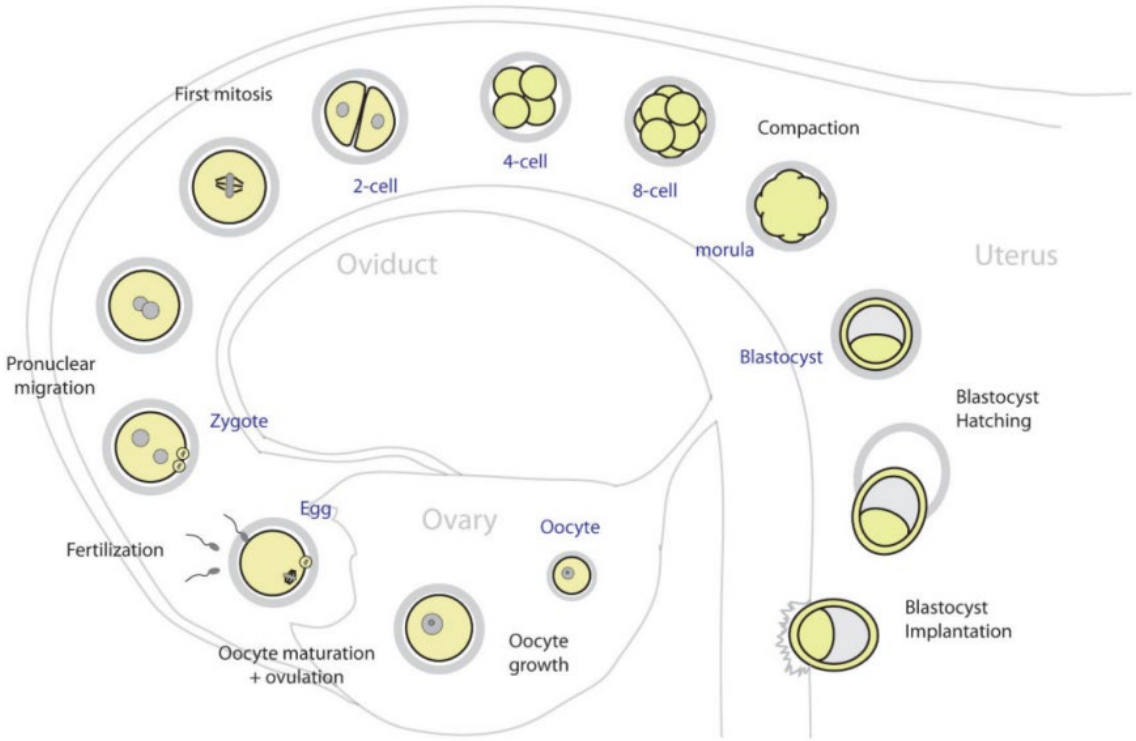

Figure 1.2: Formation of the Blastocyst Following Fertilisation (Sourced: Clift and Schuh, 2013).

Following fertilisation of the egg, the zygote travels along the fallopian tube towards the uterus. During this time, it undergoes successive rounds of cell division, eventually becoming the blastocyst, composed of two distinct cell populations. The blastocyst implants into the uterine wall and the fetus and placenta begin to develop via various cell lineages.

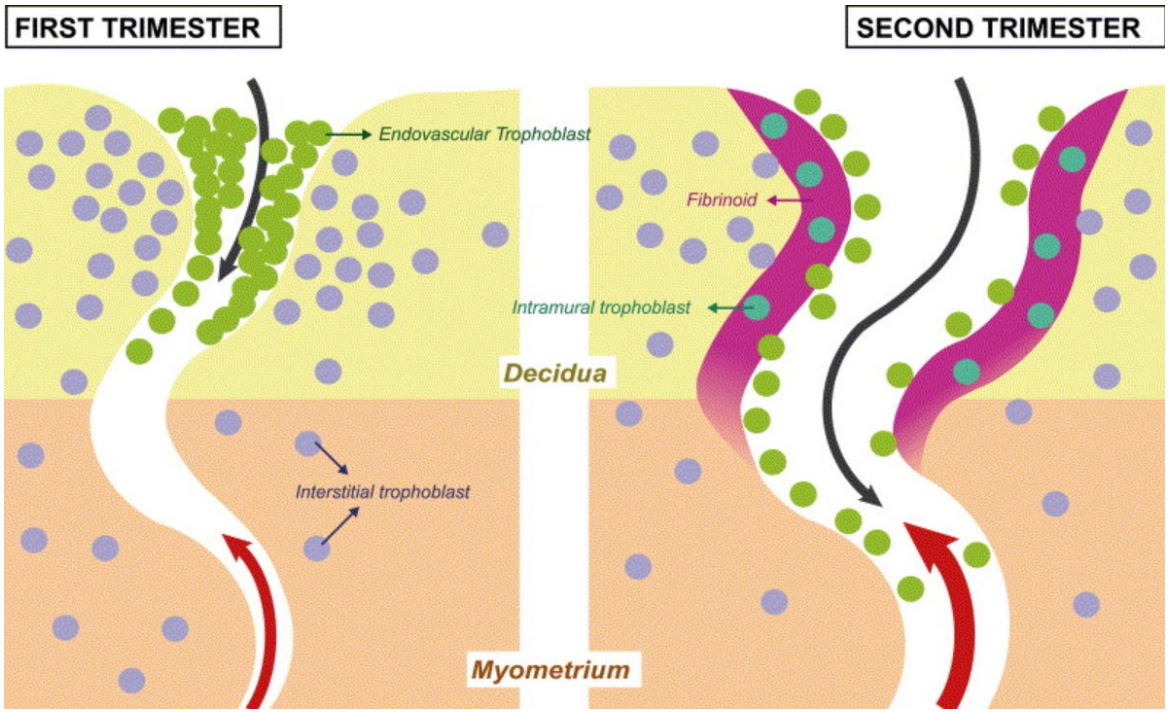

Figure 1.3: Invasion of the Maternal Vasculature by Extravillous Trophoblasts
(Sourced: Pijnenborg *et al*, 2006).

Once the population of EVTs has been established, they begin to invade the maternal uterine spiral arteries retrogradely, extending through the decidua and myometrium in the first trimester. The arteries dilate and become low-resistance vessels to increase uteroplacental perfusion to meet the demands of the fetus. They replace the maternal endothelium to give resistance to vasoconstrictors until term. Black arrows = direction of trophoblast invasion. Red arrows = direction and extent of blood flow. (EVT; extravillous cytotrophoblast).

A

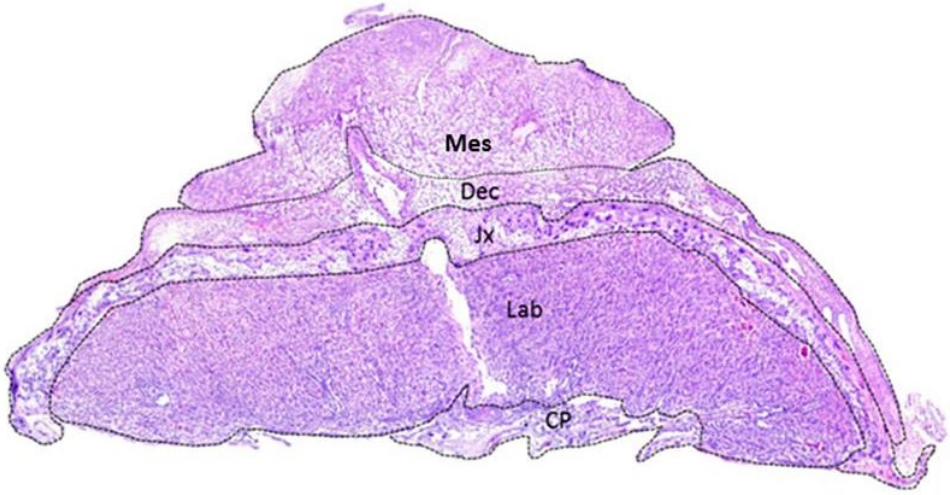

B

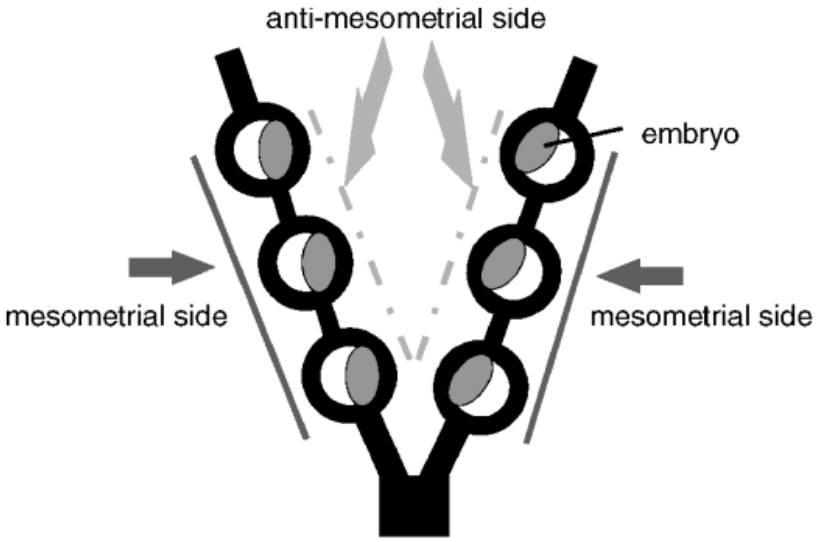

Figure 1.4: Representative Illustrations of Rat Placental Layers and Embryo Implantation Site (Sourced: Small *et al*, 2016a; De Rijk *et al*, 2002).

(A) Representative mid-sagittal section of a rat placenta in late gestation, stained with H&E, showing the mesometrial triangle (Mes), decidua (Dec), junctional zone (Jx), labyrinth zone (Lab) and chorionic plate (CP). (B) Illustration depicting embryo implantation in the uterus of the rat.

1.1.2 Cardiovascular & Haemodynamic Adaptations

Alterations to the maternal cardiovascular system are crucial in providing the developing fetus with an adequate environment that balances uteroplacental flow, oxygenation and nutrient delivery to the placenta. These changes also serve to protect the mother from the physiological stress of pregnancy (Melchiorre *et al*, 2012). Some of these adaptations have been well characterised for several years, with changes to maternal heart rate, cardiac output, blood pressure and vascular resistance among the first documented (Chapman *et al*, 1998; Davison and Dunlop, 1980; O'Day, 1997). Many of the physiological adaptations to pregnancy begin in early gestation reaching a plateau in mid-gestation that peaks once more at the time of delivery (Carlin and Alfirevic, 2008). Clapp and Capeless (1997) studied groups of nulliparous and multiparous participants prior to and throughout pregnancy. They documented a substantial increase in cardiac output (CO) by 8 weeks of gestation in both first and second pregnancy groups. Such findings have been found in multiple studies using both invasive and non-invasive techniques. It is now generally accepted that CO begins to rise in the first trimester, peaking in the third trimester to approximately 30-50% of non-pregnant measurements in singleton pregnancies (Abbas *et al*, 2005). In twin pregnancies, CO may rise a further 15% (Sanghavi and Rutherford, 2014). This increase in CO in early gestation is attributed to the concurrent rise in stroke volume occurring in the same time frame of 30% (Carlin and Alfirevic, 2008; Tan and Tan, 2013). In late gestation, the increase in CO is maintained by the increase in maternal heart rate of ~10-20bpm (Soma-Pillay *et al*, 2016). The increase in stroke volume is likely due to early increases in left ventricular mass and end-diastolic volume as the heart becomes dilated and increases myocardial contractility whilst afterload decreases in the first trimester (Soma-Pillay *et al*, 2016).

Both CO and stroke volume are linked to the rising maternal heart rate during pregnancy that functions to compensate for a decrease in peripheral vascular resistance (PVR). Decreases in PVR contribute to increased preload and reduced afterload in the maternal heart and can been seen as early as the seventh week of gestation, with PVR further decreasing by up to 40% (vs. non-pregnant values) by the time of the third trimester (Sanghavi and Rutherford, 2014). During pregnancy, there is a steady increase in blood and plasma volume that is apparent as early as week seven which plateaus at 32 weeks leading to a total increase between 45-

50% (O'Day, 1997). There is also an increase in red cell mass of ~25%, which also contributes to increased preload (Chapman *et al*, 1998; Carlin and Alfirevic, 2008). Whilst the increase in red cell mass facilitates a higher exchange of oxygen between mother and fetus, it is believed that the far more substantial rise in plasma volume prevents increased blood viscosity to promote placental perfusion and prevent thrombosis (Carlin and Alfirevic, 2008). Unlike stroke volume, diastolic and mean arterial pressures decrease by approximately 10% in healthy normotensive pregnancies by gestational week 7 to 8 continuing to fall until around week twenty-four and rising thereafter until term (Tan and Tan, 2013). Mean arterial pressure is directly proportional to CO and PVR. The rise in CO and fall in PVR appear to be parallel, explaining the comparatively small falls in mean arterial pressure and diastolic blood pressure (Melchoirre *et al*, 2012; Tan and Tan, 2013). Systolic pressure remains relatively stable throughout pregnancy but may decrease slightly in early to mid-gestation, though to a lesser extent than diastolic blood pressure (Abbas *e al*, 2005). It is likely that changes in blood pressure occur secondary to the fall in PVR and compensatory rise in CO, though they are not sufficient to prevent a small decrease in pressures (Carlin and Alfirevic, 2008). As a result of the various haemodynamic changes in the maternal cardiovascular system (summarised in Fig. 1.5) combined with increased maternal heart mass there is an increased consumption of oxygen (Thornburg *et al*, 2000). In tandem with these is a dramatic shift in cardiac metabolism from glucose utilisation in early pregnancy to fat burning in late pregnancy, a change that temporally parallels the fetal metabolic demand rather than the maternal haemodynamic demand and allows the heart to develop insulin resistance (Liu and Arany, 2014). Together, these alterations in cardiovascular function create an efficient transport system for oxygen and nutrients that meets the demands for both mother and fetus.

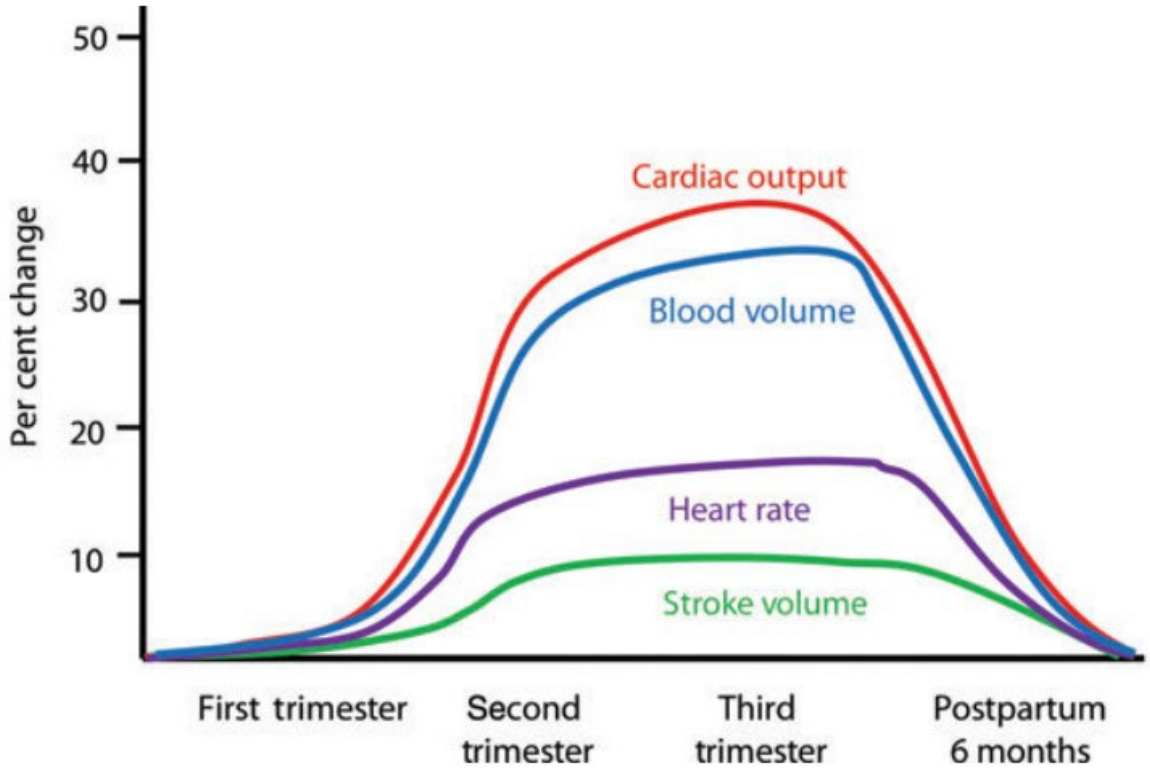

Figure 1.5: Summary of Cardiovascular Adaptations to a Normal Pregnancy (Sourced: Liu and Arany, 2014).

Over the course of a normal pregnancy heart rate, cardiac output, blood volume and stroke volume begin to rise in the first trimester, steadily increasing until birth before returning to normal levels post-partum. Additionally, systemic vascular resistance and mean arterial pressure decrease throughout pregnancy by approximately 10% whilst red cell mass increases on average by 20-30%.

1.1.2.1 Uterine Vascular Remodelling

The uterus is supplied by the main uterine artery, originating from the hypogastric artery, providing ~80% of total uteroplacental blood flow with the rest supplied by the ovarian arteries (Cicinelli *et al*, 2006; Osol and Moore, 2013). Upon contact with the myometrium the uterine artery branches into the arcuate arteries before further branching into the radial arteries. These run toward the endometrium where they branch once more into the spiral arteries (SpA), so called due to their normally tightly coiled shape, which run parallel to the endometrial surface before finally connecting to the endometrial veins via capillaries (James *et al*, 2017, Fig.

1.6). During the menstrual cycle, the SpA undergo a rapid period of arterial growth leading to the increased endometrial thickness that persists during pregnancy (Pijenborg *et al*, 2006). This rapid growth is characterised as outward hypertrophic remodelling, whereby the lumen of the SpA is doubled in humans (with similar findings in other mammals such as rats) with minimal thickening of the vascular wall itself, resulting in an increased cross-sectional area (Osol and Mandala, 2009). Additionally, in multiparous animals like the rat, the uterine arteries also increase their axial length to accommodate changes in the size of the uterus during pregnancy, though this has not yet been documented in humans (Osol and Moore, 2013).

As previously described, implantation of the blastocyst into the prepared endometrium results in the production of EVTs which invade the maternal decidua and SpA. Consequently, the SpA undergo significant structural and functional changes that transform the high-resistance, low-flow tightly coiled SpA into large diameter, high flow vessels that lack responsiveness to maternal vasoactive factors. This also occurs in the larger radial and arcuate vessels which dilate to increase blood flow towards the uterus and placenta (James *et al*, 2017). These remodelling processes begin at conception and are normally completed by the end of the second trimester and are proposed to occur in three stages (Chen *et al*, 2012). Successful remodelling of the vasculature is crucial for a normal, healthy pregnancy. The first stage is thought to be mediated by the decidua occurring pre-implantation, where cells originating from the decidualised endometrium secrete a variety of factors (including matrix metalloproteinases (MMPs), cytokines and growth factors) that stimulate or inhibit trophoblast invasion into the SpA and interstitium (Sharma *et al*, 2016). In the second stage, the vascular smooth muscle and endothelium of the vessel begin to deteriorate due to interstitial invasion post-implantation. This disorganisation results in the invasion of the arterial lumen by EVTs which replace the lost vascular smooth muscle and endothelium thereby transforming the SpA (Chen *et al*, 2012). EVTs within the vascular lumen begin to clump together during early pregnancy forming a vascular plug which functions to create a low-oxygen environment to stimulate further EVT invasion and placental development as well as protect the fetus from oxidative stress. (Pijenborg *et al*, 2006). The remodelling process is summarised in Fig. 1.7. As the pregnancy progresses, low-oxygen due to vascular plugging is slowly overcome by progressive arterial remodelling, breakdown of the plug and angiogenesis within

the placenta to prevent hypoxia (Chen *et al*, 2012; James *et al*, 2017). Following delivery, the vasculature reverts to its non-pregnant state following re-endothelisation of the SpA (Scott *et al*, 2009; Pijenborg *et al*, 2006).

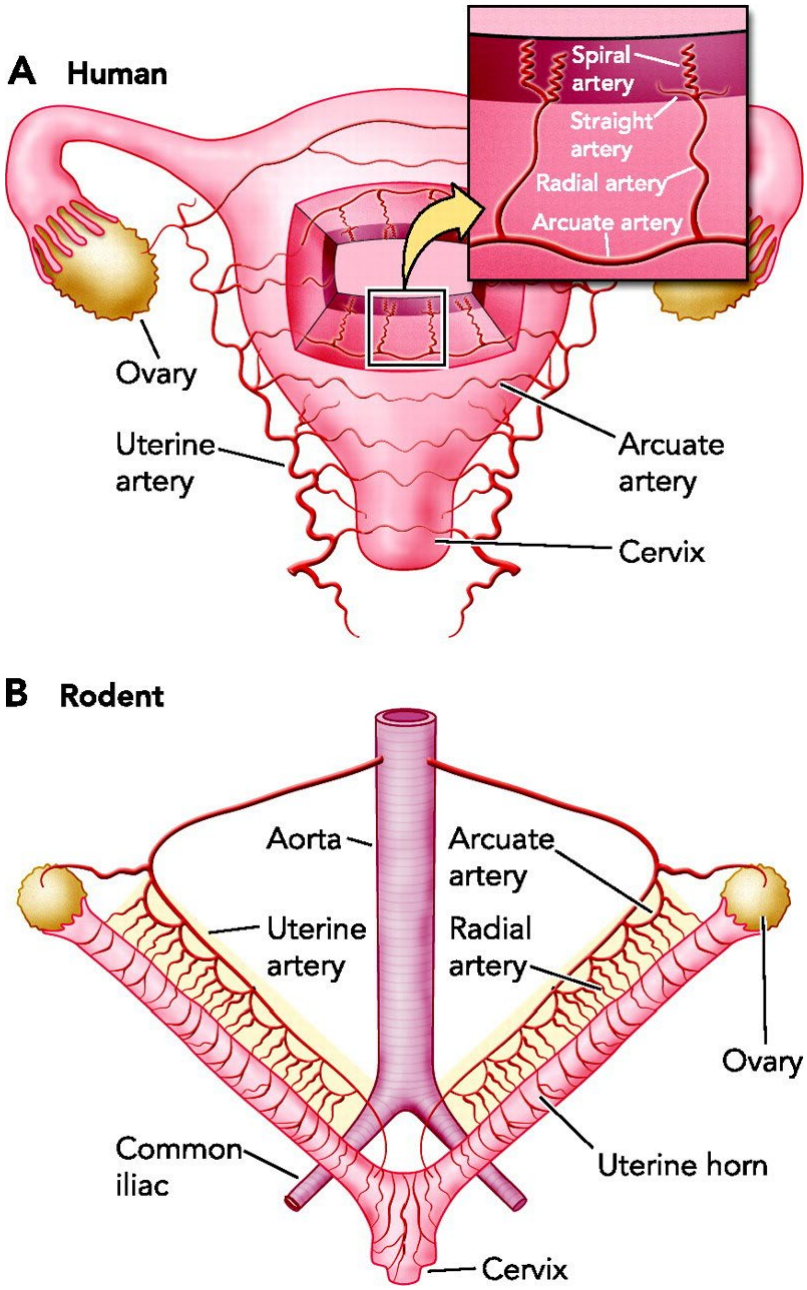

Figure 1.6: Comparative Anatomy of Uterine Vasculature in Humans and Rodents (Sourced: Osol and Mandala, 2009).

Illustrations showing the anatomy of the uterine circulation in humans (A) and rodents (B). The uterine arteries arise from the hypogastric artery in humans and from the aorta in rodents. The main artery branches into the arcuate arteries which branch into the radial arteries and finally the spiral arteries that run beneath the endometrial surface.

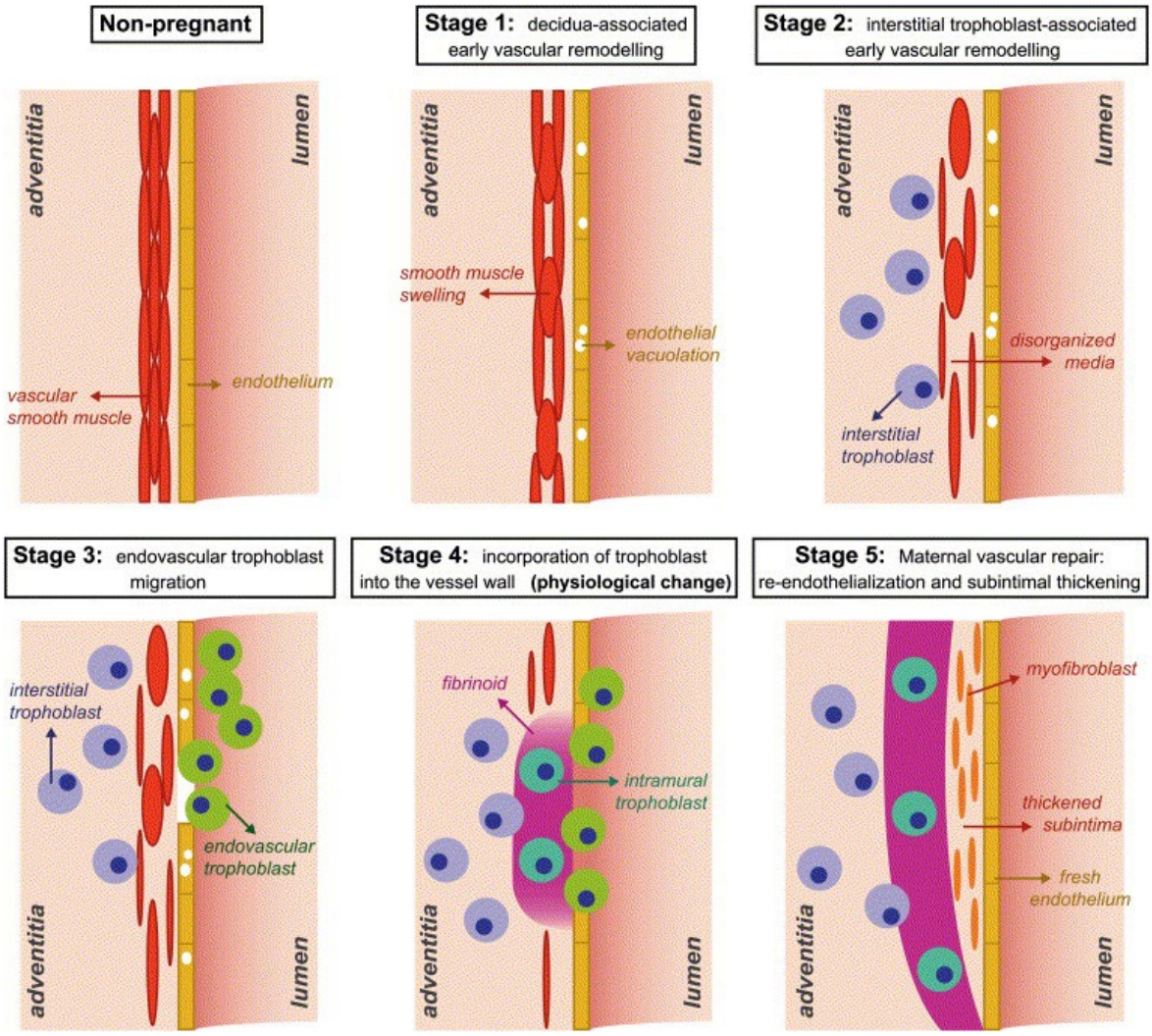

Figure 1.7: Illustration of the Events During Spiral Artery Remodelling
(Sourced: Pijenborg *et al*, 2006).

A depiction of the stages of trophoblast invasion and subsequent remodelling of the spiral arteries during pregnancy. The first stage is decidua-associated with the release of numerous factors that begin to alter the environment to promote trophoblast invasion. Interstitial trophoblasts begin to invade and disrupt vascular and endothelial cells. This allows for the further invasion of the arterial lumen by EVTs. The trophoblasts become embedded into the vessel walls, degrading the vascular and endothelial components which are replaced by trophoblasts, widening the lumen and increasing flow. At term, the maternal vasculature begins to reverse these processes through re-endothelisation. (EVTs; extravillous/endovascular trophoblasts).

1.1.3 Local Alterations in Immune Cells

Pregnancy is a strange phenomenon when viewed through the lens of the immune system. In a normal healthy pregnancy, the fetus arises from both maternal and paternal cells which in turn allows it to express paternal antigens, creating a semi-allogenic invasive entity that should be rejected by the maternal immune system (Jabrane-Ferrat and Siewiera, 2014). Though the maternal and fetal blood supplies never come into direct contact, fetal antigen shedding does occur in the intervillous space, and it is not yet understood whether maternal T cells sense these antigens at all or whether they make specific adjustments to ensure tolerance (Wallace *et al,* 2012). It has been proposed that the control of immune related functions during pregnancy is regulated by other immune cell types within the uterus. Of these cells, uterine natural killer cells (uNKs, also known as decidual natural killer cells) represent a substantial proportion (> 40%) and begin to accumulate in the decidua during the normal menstrual cycle and throughout early pregnancy (Wallace *et al*, 2012). During the first trimester uNKs amass in and around the SpA but by 20 weeks of gestation they begin to decline such that only small numbers are present at term (Pijenborg *et al*, 2006). Of note, uNKs differ from NKs normally found in the peripheral blood. uNKs express different surface markers such as CD69, CD9 and NKp44, show differential gene expression in comparison to peripheral blood NKs and have a higher expression of a number of receptors including chemokine receptors suggesting uNKs have specific pregnancy-related functions (Parham, 2004). The unique expression profile of uNKs favours a cytokine-secreting role as opposed to the cytotoxic defensive role of NKs in peripheral blood (Jabrane-Ferrat and Siewiera, 2014). Interestingly, as uNKs decline in late gestation they are replaced by a growing population of T cells that can represent up to 80% of the immune cell population at term (Wallace *et al*, 2012).

As discussed in 1.1.2.1, SpA remodelling is first initiated by cells residing within the decidua that secrete a variety of factors. The spatiotemporal distribution of uNKs suggests they participate in SpA remodelling. Indeed, many have speculated that uNKs play a direct role in remodelling by interacting with EVTs. This is supported by the finding that EVTs express MHC class I molecules, specifically those that function as excellent ligands for uNK receptors (Parham, 2004). Additionally, Smith and colleagues (2009) showed that uNKs and

macrophages were found within the SpA prior to EVT invasion and reported evidence of vascular smooth muscle cell loss and disruption alongside endothelial damage and layer separation. uNKs may also influence vascular remodelling independently of EVTs through the production of a variety of angiogenic factors including angiopoietins -1 and -2, and vascular endothelial growth factor (Robson *et al*, 2012). It is proposed in the literature that invading uNKs and decidual macrophages begin to disrupt vascular smooth muscle cells through the production of matrix metalloproteases (MMPs), particularly MMP-2 and MMP-9 (Chen *et al*, 2014; Robson *et al*, 2012). Concurrently, uNKs secrete chemokines and cytokines such as interleukin-8 which is known to attract fetal trophoblast cells and promote EVT invasion (Jabrane-Ferrat and Siewiera, 2014; Sharma *et al*, 2016). EVTs may also aid in the recruitment of uNKs and other immune cell types to the decidua by secretion of chemokines leading to a positive feedback loop (Jabrane-Ferrat and Siewiera, 2014). During the latter half of pregnancy once SpA remodelling is complete, the population of uNKs dwindles and is replaced by a period of mild systemic inflammation that persists until term as directed by the maternal-fetal interface (Parham, 2004). The complex and precise interactions between local maternal immune cells and fetal trophoblasts is necessary for the completion of a successful pregnancy. A disruption of any one of these interactions may subsequently lead to a pathological state.

1.1.4 Renal Adaptations

Due to the various changes to the maternal haemodynamic profile, during a normal pregnancy the kidneys undergo significant structural and functional changes to cope (Fig. 1.8). The decreases in PVR and mean arterial pressure lead to an increase in renal plasma flow and glomerular filtration rate (Hussein and Lafayette, 2014). Increased renal plasma flow during pregnancy leads to an increase in kidney size of 1-1.5 cm by mid-pregnancy (Soma-Pillay *et al*, 2016). Glomerular filtration rate has been found to increase by 20% as early as gestational week four, peaking at 180mL/min in the first trimester (Hussein and Lafayette, 2014; Carlin and Alfirevic, 2008). Complementary to the increase in glomerular filtration rate there is a decrease in serum creatinine levels and an increase in its urinary clearance, along with other urinary proteins (Odutayo and Hladunewich, 2012). These changes are reflected in changes to tubular function where glucose reabsorption in the proximal and collecting tubules is less effective

with varied levels of excretion (Soma-Pillay *et al*, 2016). The changes to glomerular filtration rate during gestation also result in an increase of filtered sodium and its subsequent reabsorption, leading to a net retention of sodium to sustain the increased plasma volume despite significant vasodilation (Tan and Tan, 2013). Several signalling systems are affected in a pregnancy-specific manner, particularly the renin-angiotensin aldosterone system.

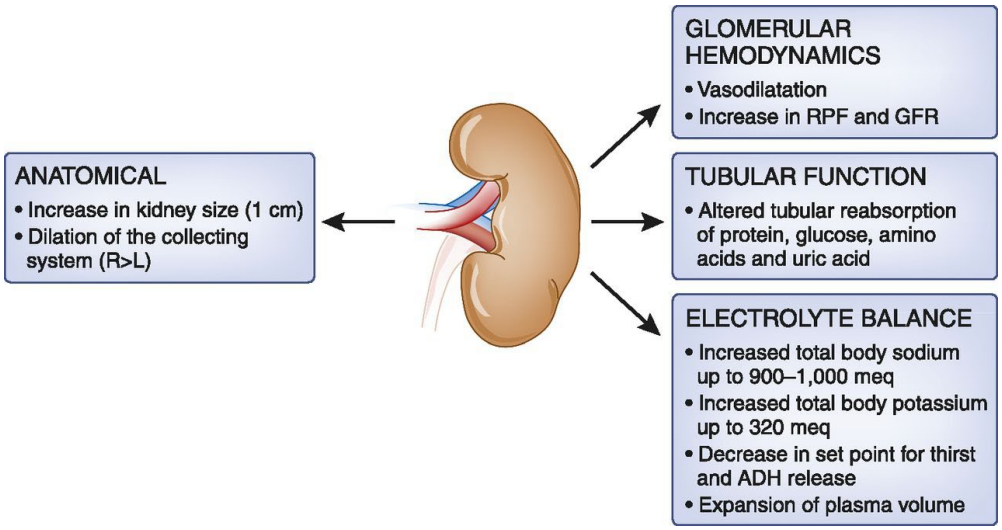

Figure 1.8: Summary of Renal Adaptations to a Normal Pregnancy (Sourced: Odutayo and Hladunewich, 2012).

During the normal pregnancy increases in RPF and GFR lead to an increase in kidney size. There is vasodilation of the renal vasculature and the collecting system. These lead to changes in tubular function and consequentially, electrolyte balance. These changes are, in part, controlled by changes in the response to the RAAS. (RPF; renal plasma flow, GFR; glomerular filtration rate, RAAS; renin-angiotensin-aldosterone system).

1.1.4.1 The Renin-Angiotensin Aldosterone System

The renin-angiotensin aldosterone system (RAAS) is one of the crucial players in determining maternal blood volume, and by extension blood pressure, vascular tone in the arteries and sodium homeostasis (Patel *et al*, 2017). Renin is the rate-limiting step of the RAAS and is formed by the proteolytic cleavage of prorenin, produced in the granular cells of the kidney (Patel *et al*, 2017). The release of

renin is tightly controlled by local baroreceptors located at the juxtaglomerular apparatus and by the uptake of NaCl at the macula densa (Sparks *et al*, 2014). In the classical RAAS, renin acts on angiotensinogen released from the liver, converting it to angiotensin I (ANGI). Renin has interactions with many other cells and is itself secreted by many cell types. In humans, a renin receptor has been identified and is expressed in the heart, brain and placenta with localisation in the uterine vessels where it has been shown to enhance the production of ANGI (Paul *et al*, 2006). ANGI is then converted to angiotensin II (ANGII) by angiotensin-converting enzyme (ACE). ANGII is the primary vasoactive peptide produced by the RAAS and has several functions throughout the body including direct vascular effects such as vasoconstriction, remodelling and angiogenesis and indirect effects such as alterations in fluid homeostasis and inflammation (Si *et al*, 2018; Mirabito Colafella *et al*, 2019). The vascular effects of ANGII are primarily initiated by the angiotensin type 1 receptor (AT_1R). The AT_1R is expressed in all of the organ systems that control blood pressure and signals through the inositol triphosphate pathway to stimulate the release of Ca^{2+} and via reactive oxygen species to activate downstream targets (Sparks *et al*, 2014; Forrester *et al*, 2018). Binding of ANGII to the AT_1R also causes aldosterone secretion leading to fluid retention and increased arterial pressure (Arendse *et al*, 2019). Activation of the AT_1R has also been found to induce transcription via Janus kinase (Sparks *et al*, 2014).

The classical RAAS has been well characterised by researchers for many years. This characterisation has led to the identification of an alternative axis to the RAAS, the so-called counter-regulatory axis (Ocaranza *et al*, 2020). In this axis ANGI is produced as normal but is converted to the angiotensin (1-7) and (1-9) (Ang-(1-7), Ang-(1-9)) peptides by ACE2, the only known homolog of ACE (Cohen *et al*, 2020). ACE2 may also utilise ANGII as its substrate in the production of Ang-(1-7) (Ocaranza *et al*, 2020). ACE2 expression is largely confined to the heart and kidneys, suggesting a role in blood pressure control (Paul *et al*, 2006). Ang-(1-7) signals via the Mas receptor and AT_2R whilst Ang-(1-9) signals via the AT_2R only (Patel *et al*, 2016). In contrast to the actions of ANGII, Ang-(1-7) activation of the Mas receptor results in nitric oxide release and vasodilation alongside a reduction in oxidative stress and inflammation (Cohen *et al*, 2020). Thus, it appears that Ang-(1-7) directly antagonises the actions of ANGII. Similarly, activation of the AT_2R is considered to be protective by eliciting vasodilatory, anti-proliferative and

anti-inflammatory actions (Mirabito Colafella *et al*, 2019). There is also evidence that the AT_2R may bind the AT_1R forming a heterodimer, directly influencing its function independently of AT_2R activation (Paul *et al*, 2006). The classical and counter-regulatory axes of the RAAS are summarised in Fig. 1.9.

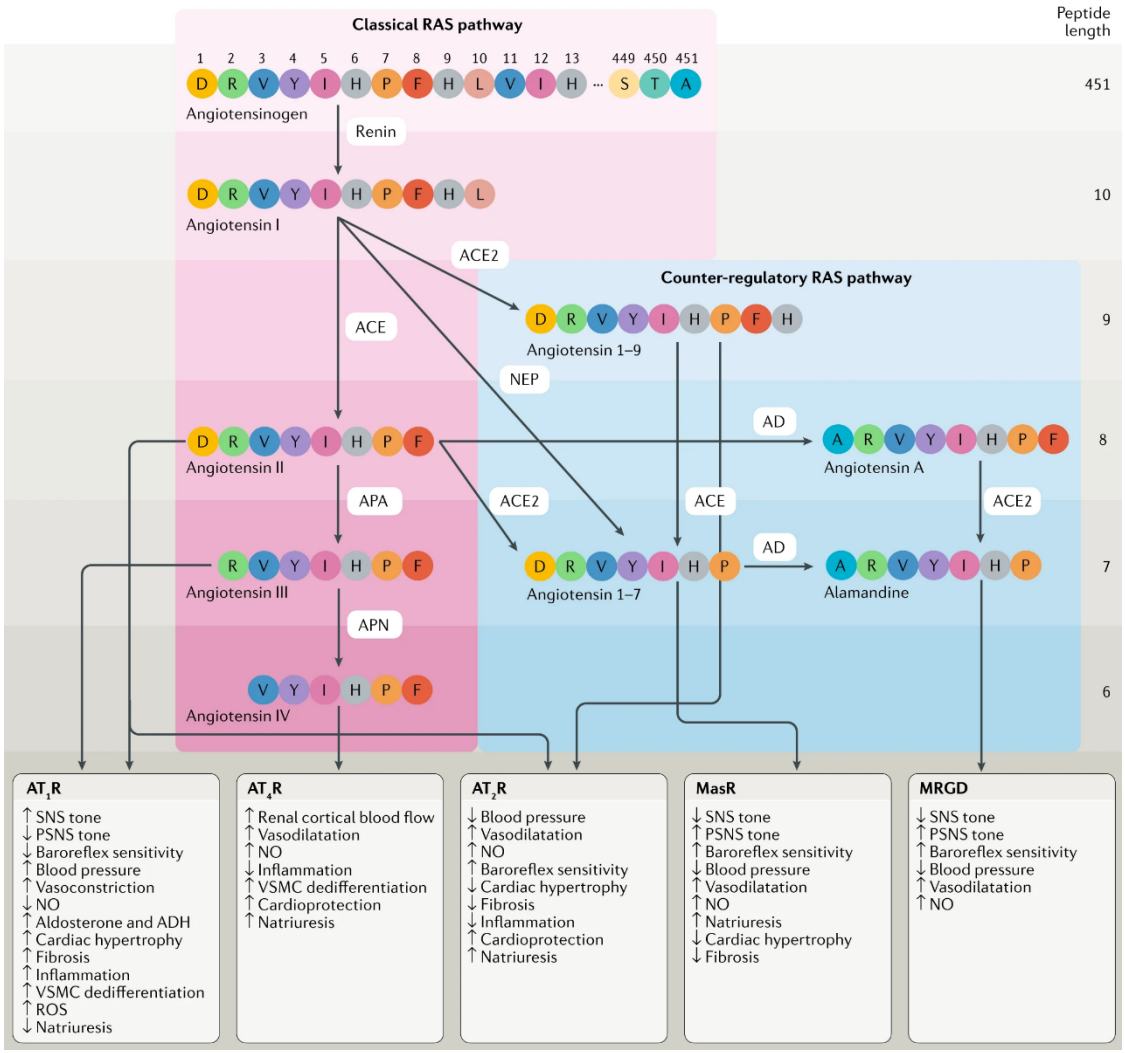

Figure 1.9: Summary of The Classical and Counter Regulatory Axes of the Renin-Angiotensin-Aldosterone System (Sourced: Ocaranza *et al*, 2020).

In the classical axis of the RAAS, angiotensinogen produced in the liver is converted to ANGI in the kidney by renin. This is then converted to ANGII by ACE which activates the AT_1R to increase vascular tone and consequently, blood pressure within the arteries. ANGII also promotes inflammation, fibrosis, oxidative stress and fluid retention. The counter regulatory axis branches at the point of ANGI production. From here ANGI is converted by ACE2 to Ang-(1-9) and Ang-(1-7) which activate the MasR and AT_2R. This produces a net anti-inflammatory, anti-proliferation, vasodilatory effect that lowers blood pressure. (ACE/ACE2; angiotensin-converting enzyme/two, ANGI; angiotensin I, ANGII; angiotensin II, $AT_{1/2}R$; angiotensin 1/2 receptor, Ang-(1-7)/ (1-9); angiotensin-(1-7)/ (1-9), RAS/RAAS; renin-angiotensin-aldosterone system, MasR; Mas receptor).

1.1.4.2 The Renin-Angiotensin Aldosterone System During Pregnancy

Normal pregnancy is associated with an upregulation of the renin-angiotensin-aldosterone system. This is required to fulfil the increased salt demand to support the expansion of the cardiovascular system (Lumbers *et al*, 2019). This is achieved by activation of the circulating and local tissue RAAS alongside the normal RAAS, which contain all of the components required to synthesise ANGII independently from the liver (Lumbers and Pringle, 2014). ACE expression, however, is unaltered by pregnancy (Fu *et al*, 2019). Tissue RAAS are present within the ovaries, uteroplacental unit and decidua during pregnancy and are activated to varied degrees dependant on the stage of gestation (Lumbers and Pringle, 2014). The placental RAAS is expressed from six weeks of gestation onwards and in addition to its roles in blood volume regulation, it stimulates angiogenesis and trophoblast invasion (Lumbers *et al*, 2019). Renin levels begin to rise as a result of production by the ovaries and decidua after week 20 (Patel *et al*, 2017; Cheung and Lafayette, 2013). This is preluded by rising prorenin levels. Prorenin, once thought to be biologically inactive, may signal via the prorenin receptor to produce ANGI and ANGII by exposing the renin catalytic site of prorenin prior to increases in renin itself (Lumbers and Pringle, 2014).

Circulating levels of angiotensinogen are also increased via an increase in its production by the liver (Lumbers and Pringle, 2014). The rising levels of angiotensinogen coincide with the rising levels of oestrogen produced by the placenta in early pregnancy (Sanghavi *et al*, 2014; Soma-Pillay *et al*, 2016). Together, these effects culminate in an increase in circulating ANGII (Cheung and Lafayette, 2013). It is therefore surprising that despite increases in ANGII, normal pregnancy is characterised by a fall in mean arterial pressure. This is due to a developed resistance to ANGII during gestation which is lost post-partum. This resistance may be explained by the presence of other vasoactive substances such as progesterone, vascular endothelial growth factor and relaxin (Cheung and Lafayette, 2013). Ang-(1-7) during pregnancy is increased and contributes to vasodilation alongside the downregulation and monomeric composition of the AT_1R and upregulation of AT_2R (Lumbers *et al*, 2019). The increased release of Ang-(1-7) may be due to the increased circulating levels of ANGII and high expression of ACE2 within the placenta that is observed in early pregnancy (Lumbers and Pringle, 2014). This heightened ACE2 expression is limited to non-

invasive syncytiotrophoblasts. Maternal activation of the mineralocorticoid receptor by rising levels of aldosterone, additionally, appears to be essential for trophoblast growth and normal placental function (Sanghavi *et al*, 2014).

1.2 Hypertensive Disorders of Pregnancy

Hypertensive disorders of pregnancy remain one of the most common complications of pregnancy, affecting 5-10% of all pregnancies (Moussa *et al*, 2014). They are regarded as syndromes, caused by the influence of both genetic and acquired factors (Umesawa and Kobashi, 2017). There are a variety of associated risk-factors that may lead to or exacerbate the negative outcomes associated with a pregnancy affected by these disorders including obesity, maternal age and multiparity, among others (Hutcheon *et al*, 2011). As the incidence of both hypertension and obesity continues to rise worldwide, understanding the underlying pathology of these disorders and identifying targeted therapies is becoming an area of great importance in order to translate research findings to clinical practice (Moussa *et al*, 2014).

1.2.1 Classification of Disorders

The classifications and diagnostic criteria of these disorders varies internationally but can generally be divided into four distinct categories based on their clinical presentation: (1) pre-existing or chronic hypertension, (2) gestational hypertension, (3) pre-eclampsia (PE) and (4) chronic hypertension with superimposed pre-eclampsia (SPE) (Naderi *et al*, 2017). All hypertensive disorders of pregnancy are categorised by an elevated blood pressure, or hypertension, defined as a systolic pressure ≥ 140mmHg and/or a diastolic pressure ≥ 90mmHg. Some patients may present with severe hypertension, that is a systolic pressure ≥ 160mmHg and diastolic pressure ≥ 110mmHg (Magee *et al*, 2015). Pre-eclampsia is additionally defined by the presence (or worsening) of proteinuria at 20 weeks or more of gestation. Proteinuria itself can be defined by a variety of measurements: either as a 24-hour urinary protein excretion ≥ 300mg or by an albumin/creatinine ratio ≥ 30mg/mol in singleton pregnancies (≥ 40mg/mol in multiple pregnancies) (Hutcheon *et al*, 2011; Magee *et al*, 2015).

1.2.1.1 Chronic and Gestational Hypertension

Chronic hypertension is characterised by the presence of an elevated blood pressure diagnosed prior to or in the first 20 weeks of gestation. Where hypertension is diagnosed after the first 20 weeks, it may only be classified as chronic hypertension if the blood pressure remains elevated for 12 weeks post-partum (Hutcheon *et al*, 2011). Chronic hypertension is associated with an

increased risk of PE, intrauterine growth restriction, pre-term delivery and premature separation of the placenta before term (Leeman *et al*, 2016; Magee *et al*, 2015). Chronic hypertension may be complicated by the development of SPE which can increase the likelihood of adverse maternal-fetal outcomes (Moussa *et al*, 2014). Essential, also known as primary, hypertension accounts for approximately 90% of chronic hypertension cases (Moussa *et al*, 2014).

Similar to chronic hypertension, gestational hypertension can be identified by an elevated blood pressure, however this must occur at greater than 20 weeks of gestation with the absence of proteinuria, and blood pressure must return to pre-pregnancy levels by 12 weeks post-partum (Naderi *et al*, 2017). For this reason, gestational hypertension is unique in that it can only be diagnosed in the post-partum period as opposed to during the pregnancy (Hutcheon *et al*, 2011). Gestational hypertension has an increased risk of PE that varies based upon fetal age at the time of presentation. Approximately 35% of those who present with gestational hypertension at <34 weeks develop PE in the following 5 weeks (Magee *et al*, 2015). However, patients who in previous pregnancies have experienced gestational hypertension are more likely to remain in this category than they are to develop PE (Magee *et al*, 2015). Where gestational hypertension presents at ≥ 37 weeks of gestation, it is unlikely to have a substantial effect on either maternal or perinatal morbidity. These patients do not usually require any interventions (Moussa *et al*, 2014).

1.2.1.2 Pre-eclampsia and Super-imposed Pre-eclampsia

In addition to meeting the criteria for hypertension, pregnancies affected by pre-eclampsia must do so at 20 weeks or more of gestation and additionally must also meet the criteria for proteinuria or one other severe feature of PE, described in Table 1.1 (Brown *et al*, 2018a). Though patients can be prescribed antihypertensives and modify their lifestyles, PE can be only resolved by delivery of the placenta. However, it may take 24-hours for improvements to be noticeable and blood pressure may not fall to normal levels for a further 6 weeks post-partum (Anthony *et al*, 2016). Interestingly, it has been found that PE can occur in the absence of fetus so long as there is a placenta, for example in the development of hydatidiform moles (Chaiworaponsa *et al*, 2014). Pre-eclampsia is generally regarded as the most severe hypertensive disorder of pregnancy and is known to

increase the future risk of cardiovascular disease in both mothers and their offspring (Tooher *et al*, 2017). It is unclear whether PE is causative of later life manifestations of cardiovascular disease or if it is an early indicator of cardiovascular disease (Bokslag *et al*, 2017). This difficulty in determining the association between the two is that many of the risk factors for developing hypertensive disorders of pregnancy are also risk factors for cardiovascular disease (Herrara-Garcia and Contag, 2014).

PE is complex in that it is a multi-organ disease with wide ranging effects to both mother and fetus. As a result, it is possible to reach a diagnosis of PE in the absence of proteinuria where there is at least one other severe feature of the disease that may pose a life-threatening risk to either mother or fetus (Table 1.1). As PE can affect multiple systems, it can vary in severity and duration from one pregnancy to another and in some cases may present as asymptomatic (Anthony *et al*, 2016). There are two distinct subtypes of PE distinguished by time of onset: early and late. Early-onset PE is considered the more severe, life-threatening of the two occurring prior to 34 weeks of gestation with late-onset occurring at 34 weeks or later (Lisonkova and Joseph, 2013). Early-onset PE is associated with placental vascular lesions; however, it only represents ~12% of all PE cases (Chaiworapongsa *et al*, 2014). It is unknown whether there are differing pathological mechanisms between early- and late-onset PE, or whether they represent gradients of severity. PE is considered dangerous not only due to end-organ damage, but for the potential progression to eclampsia- the sudden onset of grand mal seizures in the absence of other neurological conditions (Chen *et al*, 2014). HELLP syndrome (haemolysis, elevated liver enzymes and low platelets) is a particularly severe form of PE which is thought to occur as a result of substantial hepatocellular injury in the form of unruptured hepatic and subcapsular haematomas (Hutcheon *et al*, 2011). HELLP syndrome is difficult to diagnose as blood pressure may only be slightly elevated, contrary to the general criteria for PE (Moussa *et al*, 2014). It is now accepted that PE has a placental origin and is associated with abnormal remodelling of the maternal uterine vasculature (Fig. 1.10).

Similar to PE, SPE can be diagnosed on its own or with severe features. It is defined as the exacerbation of previously well-controlled hypertension and/or the onset of new proteinuria or worsening of existing proteinuria (Moussa *et al*, 2014).

SPE complicates 25% of cases of chronic hypertension during pregnancy (Brown *et al*, 2018a). The severe features of SPE include thrombocytopenia, elevated liver transaminases, new-onset or worsening renal insufficiency, pulmonary oedema and persistent cerebral or visual disturbances (Guedes-Martins, 2016).

Table 1.1 Summary of Low and High Severity Features of Pre-eclampsia

Affected System	Severity	
	Low	**High**
Central Nervous System	Headache	Cerebrovascular Haemorrhage leading to stroke, TIA or RIND
	Visual Disturbances (cortical blindness and retinal detachment	Progression to eclampsia
		Posterior reversible encephalopathy syndrome
Cardiovascular & Respiratory Systems	Chest pain	Uncontrollable or severe hypertension (SBP ≥ 160mmHg, DBP ≥ 110mmHg)
	Dyspnoea	Pulmonary oedema
	Falling O_2 saturation (<90%)	Myocardial ischaemia or infarction
Haematological	Increased WBC count	Thrombocytopenia (< 100 x 10^9/L)
	Increased aPPT	Required transfusion of blood products
	Decreased platelet count	
Renal	Increased serum creatinine (1.1mg/dL)	Acute kidney injury or marked decrease in renal function
	Increased serum uric acid	Required dialysis
Hepatic	Nausea and vomiting	Increased transaminase levels in the liver (> 2x the normal range)
	Epigastric pain	Possible haematoma and rupture
Feto-placental	IUGR	Stillbirth
	Absent or reversed EDF (assessed by Doppler ultrasound)	Placental abruption

The varied effects and presentations of pre-eclampsia in multiple systems in the body, categorised as low or high severity. High severity symptoms increase the risk of progression from pre-eclampsia to superimposed pre-eclampsia (on chronic hypertension), eclampsia and HELLP syndrome. (aPPT; activated partial thromboplastin time, DBP; diastolic blood pressure; EDF; end diastolic flow, IUGR; intrauterine growth restriction, RIND; reversible ischaemic neurological deficit, SBP; systolic blood pressure, TIA; transient ischaemic attack, WBC; white blood cell). (Anthony *et al*, 2016; Hutcheon *et al*, 2011; Leeman *et al*, 2016; Magee *et al*, 2015; Moussa *et al*, 2014; Naderi *et al*, 2017, Brown *et al*, 2018a).

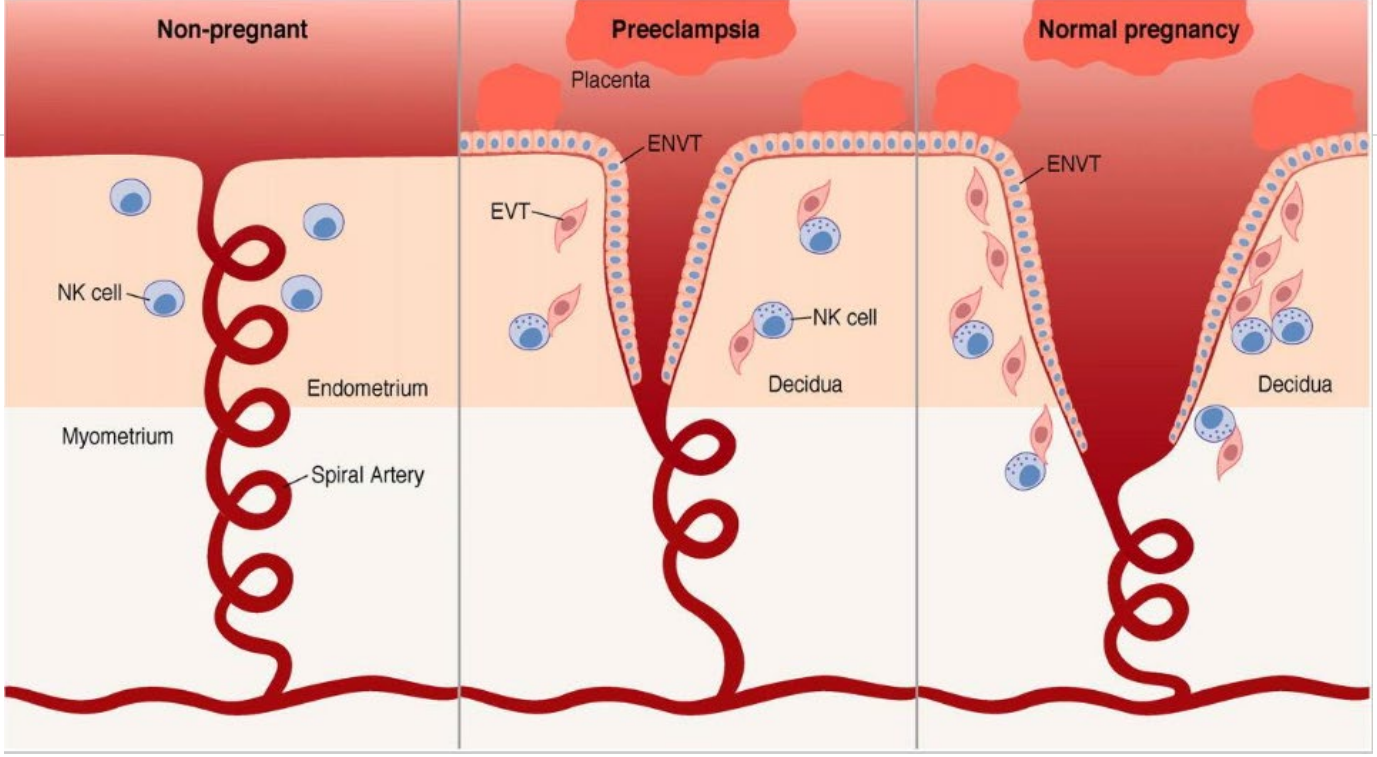

Figure 1.10: Abnormal Remodelling of the Maternal Vasculature in Pre-eclampsia (Sourced: Parham, 2004).

In a non-pregnant individual (left), the maternal uterine spiral arteries are high-resistance vessels with a small diameter, extending from the surface of the uterine wall to connect to the systemic blood supply. During a normal pregnancy (right) EVTs invade the spiral arteries to trigger remodelling, increasing the luminal size and blood flow towards the placenta. In pre-eclampsia (middle), this process is dysfunctional resulting in an inadequate remodelling of the maternal vessels, preventing sufficient blood flow to the fetus thereby limiting the delivery of nutrients and oxygen. (EVT; extravillous cytotrophoblast, NK cell; natural killer cell).

1.2.2 Prevalence and Impact

Despite continued efforts to reduce maternal mortality, it remains a large healthcare concern in developed and developing countries alike. Approximately five million people give birth each year in the European Union alone (Bouvier-Colle *et al*, 2012). According to the World Health Organisation (WHO), in 2017 approximately 295,000 individuals died during or following childbirth, with most being preventable deaths (World Health Organisation, 2019). WHO defines maternal mortality as the "death of a woman during pregnancy or within 42 days after its end regardless of duration or place of pregnancy" (Reinke *et al*, 2017). Indeed, maternal mortality has such an impact that it became a target of the United Nations Millennium Development Goals (MDG); aiming to reduce the maternal mortality ratio by 75% (for the period 1990 – 2015) (United Nations, 2015). Maternal mortality has declined globally by 45%, likely due to improved prenatal and antenatal care particularly in rural and developing countries, reflected by an increase in the number of skilled healthcare professionals attending births and in the number of antenatal care visits (Gaffey *et al*, 2015). Despite this decrease, it has still fallen short of the MDG's estimates and remains an area of concern in many countries.

Hypertensive disorders of pregnancy account for approximately 16% of maternal deaths (Deak and Moskovitz, 2012) and are the second largest cause of death in the maternal population, following haemorrhage (Say *et al*, 2014). Hypertensive disorders of pregnancy, on average, affect 5-10% of all pregnancies worldwide (Lai *et al*, 2017). Interestingly, unlike haemorrhage, deaths due to hypertensive disorders of pregnancy are similar between developed and developing countries (Say *et al*, 2014; Kassebaum *et al*, 2014). The prevalence of hypertensive disorders of pregnancy varies between countries and is dependent on the disorder (5.2-8.2% chronic hypertension; 1.8-4.4% gestational hypertension; 0.2-9.2% pre-eclampsia) (Umesawa and Kobashi, 2017). The disparity in maternal mortality rates between countries and between studies cannot be ignored and is commonly attributed to an under- or misreporting of maternal cause of death of up to 50% (Say *et al*, 2014; Bouvier-Colle *et al*, 2012). Additionally, it is unclear in many reports whether maternal death caused by hypertension during pregnancy is included as a co-morbidity (or indirect cause) or if it is a direct cause of death (Kassebaum *et al*, 2014). These issues in reporting maternal mortality make it

difficult to fully ascertain the impact of hypertensive disorders of pregnancy on a global scale and how this may change between countries. Consequentially, this creates difficulties in creating and managing preventative treatment strategies for various health care services.

Despite these difficulties in reporting maternal mortalities, clinical data collection has allowed us to identify important risk factors (Table 1.2) that may promote the development of a hypertensive disorder of pregnancy and to understand how those affected by these disorders may be affected in their futures. Of concern is that many of the risk factors identified for hypertensive disorders of pregnancy are also common risk factors for essential hypertension, such as, obesity, age and modifiable risk factors (Singh *et al*, 2016). These similarities make both hypertension during pregnancy and essential hypertension difficult to easily classify as both conditions are multifactorial and can be influenced by various different factors from genetic to environmental. These identified risk factors are also becoming more common in individuals of child-bearing age, thereby increasing the likelihood of a pregnancy to be affected by one of these disorders (Ebbing *et al*, 2017; Adam, 2017). As the incidence of hypertensive disorders of pregnancy rises, so too does the incidence of future cardiovascular disease in the very same population and in their offspring (Davis *et al*, 2012; Tooher *et al*, 2017). The ability to accurately predict high risk individuals and initiate one of the few preventative treatments available is key in reducing not only maternal and fetal mortality at the time of pregnancy, but in reducing the number of future cardiovascular disease cases that may arise from affected mothers and offspring.

Table 1.2. Common Risk Factors in the Development of Hypertensive Disorders of Pregnancy

Common Maternal Risk Factors
• Nulliparity • Multiparity • Familial history of hypertensive disorder of pregnancy, chronic hypertension, diabetes mellitus (types I or II) or renal disease • Pre-existing hypertension, proteinuria or other cardiovascular disease such as type I diabetes mellitus • Smoking (inversely related to PE risk) • Obesity – BMI ≥ 25kg/m^2 • Insulin resistance • Anaemia • Maternal age > 40 years • Pregnancy interval > 6 years

Common shared risk factors among hypertensive disorders of pregnancy. All of the indicated factors increase maternal risk for developing hypertensive disorders of pregnancy, with the exception of smoking which has an inverse risk associated with PE. These risk factors are also common to other types of cardiovascular disease out with pregnancy. (BMI, body mass index; PE, pre-eclampsia). Ebbing *et al*, 2017; Magee *et al*, 2015; Naderi *et al*, 2017; Tooher *et al*, 2017; Umesawa and Kobashi, 2016; Wenger, 2014).

1.2.3 Maladaptation's to Maternal Cardiovascular Function

As outlined in 1.1.2, the ability for the maternal cardiovascular system to adapt to the rapidly changing needs of the mother and fetus throughout gestation is key in the completion of a healthy pregnancy. Disruption of any one of these processes can lead to a number of pathophysiological states that are detrimental to mother and fetus. Understandably, hypertension during pregnancy is inexplicably linked to cardiovascular dysfunction. It has been posed by many that pregnancy acts as a stress test for the cardiovascular system and that development of a hypertensive disorder of pregnancy merely reflects underlying cardiovascular disease or is an indicator of those will go on to develop cardiovascular disease in later life (Naderi *et al*, 2017). This population of patients are also associated with a four-fold increase in the development of post-partum heart failure (deMartelly *et al*, 2021).

There are many similarities in pathophysiology between hypertensive disorders of pregnancy with few being specific to one disorder alone. In the following sections of this chapter, the focus will be on pre-eclampsia and super-imposed pre-eclampsia for brevity as most hypertensive disorders increase the risk for progression to one of these syndromes thus the underlying pathophysiology is largely similar.

During pregnancy there is a state of chronic volume expansion that is normally counteracted by the decrease in peripheral vascular resistance (Sanghavi and Rutherford, 2014). Studies utilising echocardiography have shown that a mismatch of these responses, even in healthy pregnancies, can lead to signs of cardiac maladaptation that typically resolve within 12 months post-partum (Buddeberg *et al*, 2018). These maladaptive changes occur in ~45% of PE pregnancies and show overt diastolic dysfunction that does not resolve with delivery (Buddeberg *et al*, 2018). Changes in cardiac function are evident long before placental development in both humans and rodents and literature suggests the volume-overload related dysfunction predisposes to uteroplacental hypoperfusion and placental stress which may alter the maternal endothelial response and subsequently give rise to PE (Gyselaers and Thilaganathan, 2019). Pregnancies affected by PE also show ECG abnormalities that precede the onset of clinical symptoms that are indicative of abnormal ventricular repolarisation (Raffaelli *et al*, 2014). Castleman and colleagues (2016.) also found evidence of left ventricular remodelling via increased left ventricular mass, in the form of concentric hypertrophy, and total vascular resistance in PE pregnancies. Despite speculation that late- and early-onset PE represent gradients of severity, studies have noted distinct differences in cardiac function between the two. Early-onset PE was found to be associated with diastolic dysfunction in the second trimester whilst this evolves in the latter half of pregnancy in late-onset cases suggesting the causative factors differ in each (Valensise *et al*, 2008; Fig. 1.11). Stroke volume has been found to be reduced in pregnancies with PE when compared to normal pregnancy in the first trimester alongside reductions in cardiac output, with both being more pronounced in early-onset cases (Castleman *et al*, 2016; Gyselaers and Thilaganathan, 2019).

Whilst the precise mechanisms that underlie the pathophysiological changes in the maternal heart during PE are not fully understood, it is hypothesised that a failure of the endothelium to elicit vasodilation to maintain falling total peripheral

resistance gives rise to hypertension, increasing systemic pressure and cardiac output, resulting in multi-organ effects (Anthony *et al*, 2016). Studies have found that biomarkers of endothelial activation are increased in PE alongside evidence of endothelial dysfunction in conduit vessels well before clinical presentation and this persists post-partum (Tannetta and Sargent, 2013). There is also an elevation of endothelial adhesion molecules vascular cell adhesion protein 1 (VCAM-1) and intracellular adhesion molecule 1 (ICAM-1) in severe PE when compared to normal pregnancy (Ahmed *et al*, 2016). Endothelial dysfunction in PE is thought to be induced by rising levels of the placentally-derived anti-angiogenic factors soluble FMS-like tyrosine kinase-1 (sFlt-1) and soluble transforming growth factor β (TGFβ) co-receptor endoglin (sEng). sFlt-1 levels are indeed raised in PE pregnancies and are thought to antagonise vascular endothelial growth factor (VEGF) and placental growth factor (PlGF), both of which are required for maintenance and integrity of the maternal endothelium (Ahmed *et al*, 2016; Tannetta and Sargent, 2013). sEng is known to antagonise the biological effects of TGFβ (required for vascular endothelial maintenance) in a severity dependant manner alongside sFlt-1 *in vivo* (Venkatesha *et al*, 2006). Walshe and colleagues (2009) found that overexpression of sEng in mice lead to endothelial activation and the expression of pro-inflammatory molecules involved in leukocyte function, suggesting the rises in sFlt-1 and sEng cause endothelial dysfunction that promotes a pro-inflammatory state in PE giving rise to its characteristic hypertension and proteinuria. Given that both sFlt-1 and sEng are produced within the placenta, it is unsurprising that abnormal maternal endothelial function has been linked by many studies to embryo implantation (Gyselaers and Thilaganathan, 2019). Literature suggests that an increased circulatory burden of trophoblastic tissue released by the abnormal placenta combines with components of oxidative stress, inflammation and anti-angiogenesis that alter systemic maternal endothelial function (Anthony *et al*, 2016).

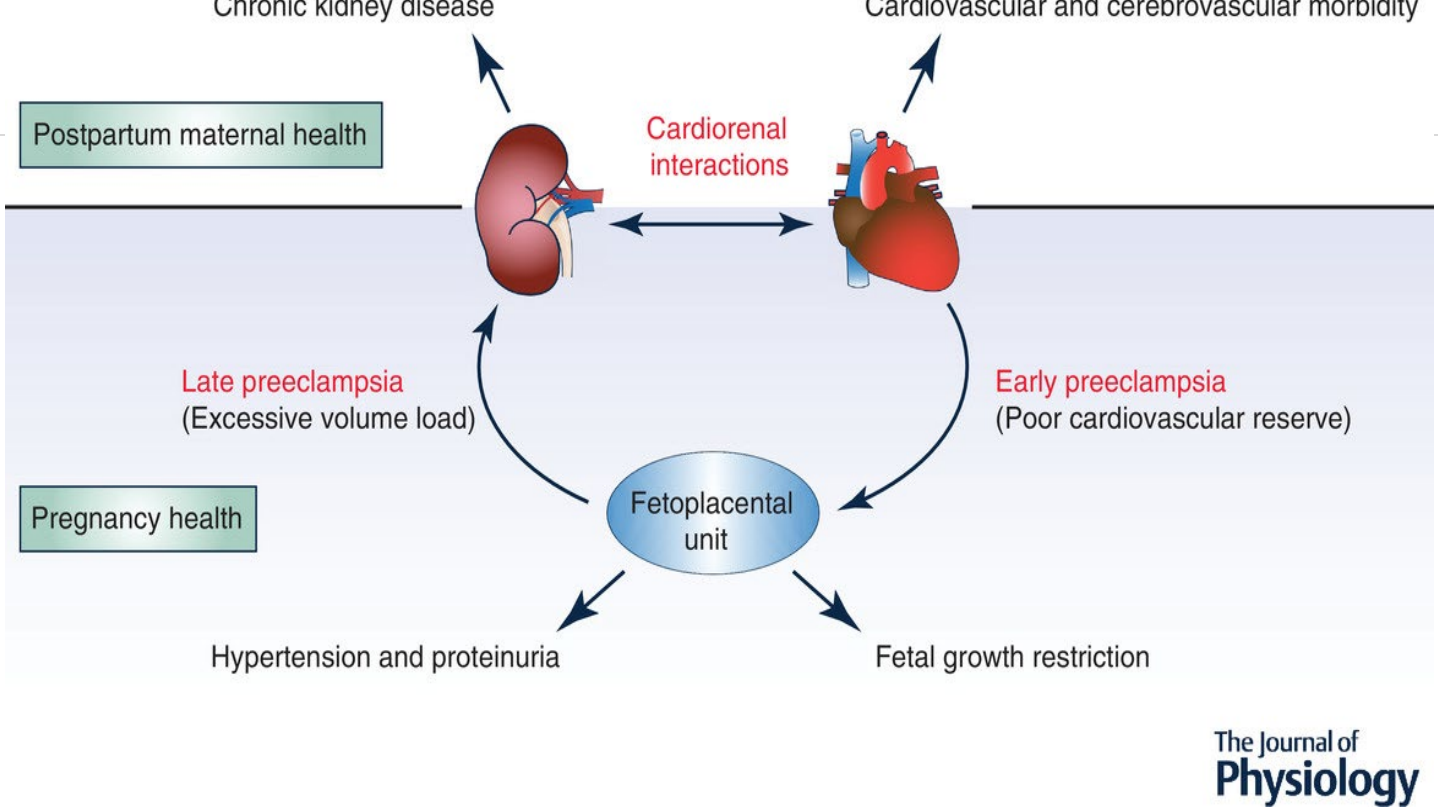

Figure 1.11: Cardiorenal Interactions Underlying Early- and Late-Onset Pre-eclampsia (Sourced: Gyselaers and Thilaganathan, 2019).

Illustrative representation of the pathophysiological mechanisms that contribute to the development of cardiac dysfunction in early- and late-onset PE. Early-onset PE is associated with a deficient cardiovascular reserve that gives rise to ventricular diastolic dysfunction by the second trimester. In contrast, ventricular diastolic dysfunction in late-onset PE is associated with a state of chronic volume overload that leads to the development of ventricular diastolic dysfunction in the latter half of pregnancy. (PE; pre-eclampsia).

1.2.4 Defective Vascular Remodelling

Vascular remodelling is crucial for the successful adaptation of the maternal systems to a normal pregnancy in order to account for the increase in blood volume and to adequately regulate maternal blood pressure. Placental pathologies typically begin to arise during the first trimester in humans but are often unable to be diagnosed until the last trimester where major functional and structural abnormalities are easily identifiable (Thompson *et al*, 2016). Similar changes can be seen in rodent models of hypertensive pregnancy, such as the spontaneously hypertensive stroke prone (SHRSP) rat where changes in gene expression have been identified at gestational day (GD) 6.5 (Scott *et al*, 2021), whilst structural changes become apparent in late pregnancy at GD18.5 (Small *et al*, 2016).

In order for a healthy pregnancy to succeed the maternal spiral uterine arteries must undergo significant remodelling during placentation, a process which is initiated by the invasion of EVTs, thereby allowing an adequate flow of blood towards the fetus. Failure of the EVTs to complete this process leads to ~50% reduction in uteroplacental flow (Davis *et al*, 2012). Incomplete invasion of EVTs causes a failure of the myometrial portion of the SpA to transform in the second trimester and increases the likelihood for atherosclerotic plaque-like lesions in these vessels (Chaiworapongsa *et al*, 2014; Fig. 1.10). It is not clear what prevents EVTs from invading the SpA in PE. The specificity of EVT invasion into the arteries suggests the involvement of oxygen or haemodynamics, in particular the influence of oxygen gradients in directing EVT migration. A persistent hypoxic state after 9 weeks of gestation may alter trophoblast differentiation resulting in shallow invasion and poor remodelling, though this theory is yet to be confirmed (Chaiworapongsa *et al*, 2014). This chronic hypoxic state is believed to trigger the release of reactive oxygen species, hypoxia-inducible factor 1-α and TGF-β1 (Verdonk *et al*, 2014). Indeed, elevated levels of HIF-1α have been noted in placentae of PE pregnancies (Chaiworapongsa *et al*, 2014). On the other hand, a study by Leno-Durán *et al* (2010) utilising immune-deficient mice showed that their lack of SpA remodelling did not lead to chronic hypoxia within the placenta. Additionally, levels of s-Flt-1 remain elevated in placental explants cultured in atmospheric conditions (Ahmad and Ahmed, 2004). Thus, the theory of persistent hypoxia as the initiating factor in EVT invasion failure is disputed.

One theory is the involvement of an irregular maternal immune response to the fetus involving uNKs. A study also utilising immune deficient mice lacking SpA remodelling found they remained normotensive and did not develop a PE-like phenotype (Burke *et al*, 2010). It has been suggested that uNK cells may 'prime' the uterus for vascular remodelling prior to EVT invasion through the secretion of various cytokines (interleukin-8, tumour necrosis factor-α and interferon-γ) and vasoactive factors (angiopoietin-1, ANGII, interferon-γ and VEGF), all of which possess corresponding receptors found in the spiral arteries (Wallace *et al*, 2012). There is conflicting evidence on uNK involvement with some studies showing increased uNK levels measured using immunohistochemistry and flow cytometry in PE patients, whilst others report a reduction in placental bed biopsies from those with PE at term (Ahmed *et al*, 2016). Finally, it has been proposed that pregnancy-associated hormones present at high concentrations at the fetal-maternal interface may also be responsible for the initiation of EVT invasion, namely human chorionic gonadotrophin, progesterone and oestradiol, with all having various actions such as promotion of angiogenesis, uNK recruitment and trophoblast differentiation (Chen *et al*, 2012).

The failure of the SpA to adequately transform inhibits uteroplacental perfusion and leads to a state of continuous ischaemia/reperfusion injury. This repeated injury promotes endoplasmic reticulum stress (Tanetta and Sargent, 2013). An inability of the endoplasmic reticulum to restore cellular haemostasis causes necrosis and apoptosis of the SBT layer and subsequent oxidative stress and inflammation. This is recognised by gross pathological changes that include placental infarctions and ischaemic lesions, particularly in severe PE (Tannetta and Sargent, 2013; Ma'ayeh *et al*, 2020). Ischaemia/reperfusion injury is also thought to increase the secretion of sFlt-1 and sEng into maternal serum and this underlies some of the maternal clinical presentation of PE (Ma'ayeh *et al*, 2020). The oxidative stress caused by recurring ischaemia/reperfusion injury not only increases trophoblast debris, but also generates pro-inflammatory cytokines and chemokines (Chaiworapongsa *et al*, 2014). Oxidative stress can also lead to DNA damage and inhibition of protein synthesis and nitration, all of which have been found in PE placentae (Ahmed *et al*, 2016). Furthermore, pregnancies affected by PE have been noted to show mitochondrial dysfunction in trophoblasts as well as decreased expression of superoxide dismutase and glutathione peroxidase, both crucial factors in maternal antioxidant mechanisms (Ma'ayeh *et al*, 2020; Ahmed *et*

al, 2016). Whether increased reactive oxygen species production and oxidative stress are initiators of PE or rather symptoms of it are still debated.

1.2.5 Dysregulation of the Maternal Renin-Angiotensin Aldosterone System

In order to compensate for the various haemodynamic changes that occur during pregnancy, the RAAS undergoes significant shifts in the expression and secretion of its various components. As the kidneys are heavily involved in the control of blood volume and therefore blood pressure, it is unsurprising that an inability of the RAAS to adapt to pregnancy-specific changes is associated with hypertension during pregnancy or that chronic renal disease is a prominent risk factor in their development (Vest and Cho, 2014). In contrast to the changes outlined in 1.1.4.2, during a PE pregnancy there is a marked decrease in plasma volume expansion which leads to an elevated blood pressure and insufficient uteroplacental perfusion (Verdonk *et al*, 2014).

Despite a decrease in circulating volume, almost all the components of the RAAS are downregulated in PE (Fig. 1.12) (Verdonk *et al*, 2014). Interestingly, though its expression is downregulated, there is an increase sensitivity to ANGII in PE that is apparent from 24 weeks of gestation, causing vasoconstriction (Hussein and Lafayette, 2014; Chaiworapongsa *et al*, 2014). The increased sensitivity to ANGII is due to an upregulation and heterodimerization of the AT_1R to bradykinin B_2 receptors and the production of AT_1R autoantibodies (Hussein and Lafayette, 2014). These autoantibodies are capable of activating AT_1Rs in the endothelium and vascular smooth muscle, stimulating NADPH oxidase (NOX) to produce ROS and stimulate placental sFlt-1 production (Chaiworapongsa *et al*, 2014; Chen *et al*, 2014). It is well known that the RAAS is heavily involved in angiogenesis in several tissues. ANGII is known to induce angiogenesis via an interaction with the AT_1R, a mechanism which may underlie placental angiogenesis and spiral artery transformation (Lumbers and Pringle, 2014). Thus, down-regulation of the RAAS in hypertensive disorders of pregnancy may contribute to defective vascular remodelling and abnormal placentation. Additionally, the presence of AT_1R autoantibodies may also have an effect in inhibiting angiogenesis. Whilst the circulating levels of angiotensinogen are unaltered in PE, there is an alteration in the type of angiotensinogen. That is, in PE there is an increase in a high molecular mass form of angiotensinogen complexed with proMBP (proform of eosinophil

major basic protein), altering the kinetics of its cleavage by renin and potentially contributing to the observed reduction in plasma renal activity (Verdonk *et al*, 2014). Renin production is known to be overall suppressed in PE; however, some theorise that increased local renin production within the placenta may occur in response to placental ischaemia (Hussein and Lafayette, 2014). Suppression of renin production in the kidneys is thought to be a result of AT_1R activation by autoantibodies thereby interfering with the ANGII-renin feedback loop (Verdonk *et al*, 2014). There is also evidence that both aldosterone and Ang-(1-7) are reduced in pregnancies affected by PE (Verdonk *et al*, 2014).

PE is often associated with glomerular lesions, where the glomeruli become enlarged and renal plasma flow is reduced due to swelling and hypertrophy of the endothelial cells within the glomerular capillaries (Karumanchi *et al*, 2005). This particularly affects the fenestrated endothelium of glomeruli where the swelling causes loss of fenestrations (Tannetta and Sargent, 2013). This endotheliosis results in a decreased glomerular filtration rate and recent studies have shown evidence that there is also a loss of size and charge selectivity of the glomerular barrier, contributing to the proteinuria that is characteristic of PE in particular (Karumanchi *et al*, 2005). It is hypothesised that these lesions are mediated by placental s-Flt-1/sEng associated inhibition of VEGF, PlGF and TGFβ triggered by autoantibodies (Gyselaers and Thilaganathan, 2019). Disruption of glomerular endothelial function can trigger further impairment of renal function via podocyte dysfunction whereby podocytes detach and are excreted in the urine. This is detectable well before onset of clinical PE symptoms (Gyselaers *et al*, 2019; Tannetta and Sargent, 2013).

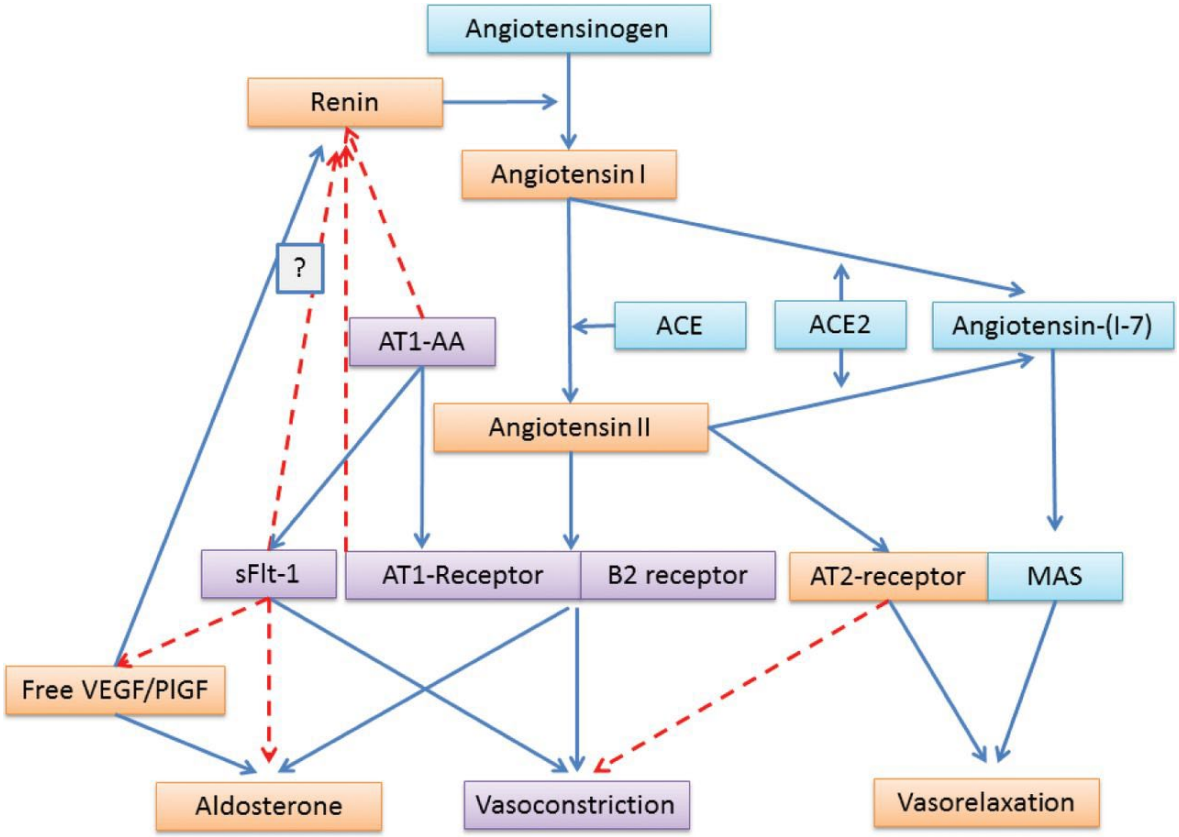

Figure 1.12: Changes in RAAS Expression in Pre-eclamptic vs. Normal Pregnancy
(Sourced: Verdonk *et al*, 2014).

During the normal pregnancy, components of the RAAS are upregulated. In contrast, the opposite is true of PE where almost all RAAS components are downregulated leading to renal dysfunction. This contributes to the elevated blood pressure, endothelial dysfunction, reduced blood volume and proteinuria characteristic of PE. Orange = suppressed levels vs normal pregnancy, purple squares = increased levels and blue squares no change. Solid lines = stimulation and dashed lines = inhibition. (PE; pre-eclampsia, RAAS; renin-aldosterone-angiotensin system).

1.2.6 Prediction, Prevention & Intervention Strategies

Perhaps the biggest therapeutic strategy for PE lies not in finding a cure, but rather screening pregnancies to predict the disorder. This includes screening for associated risk factors (Table 1.2), maternal history and routine blood pressure measurements during antenatal visits (Dadelszen and Magee, 2016). More recently, a first-trimester screening protocol has been developed that included monitoring of mean arterial pressure, uterine artery pulsatility index and serum

PlGF concentrations. This protocol has shown promising success, identifying 90% of cases of early-onset PE with a 5% false positive rate (Poon *et al*, 2009). However, the protocol was less successful in identifying late-onset cases. Despite this, the ratio of sFlt-1 to PlGF is still considered to be a useful biomarker in predicting PE, with serum levels of sFlt-1 increasing 4-5 weeks prior to clinical onset and decreasing PlGF levels observable at 9-11 weeks prior to clinical onset (Naderi *et al*, 2017). Second- and third-trimester screening targets for PE include placental perfusion measurements alongside assessment of maternal cardiac output and renal function (Dadelszen and Magee, 2016). Though there are many screening tools available, there is no one test that can accurately and reliably predict the development of PE.

Where an individual is considered to be at high risk for the development of PE one of many potential preventative strategies may be initiated. Many have reviewed the role of calcium supplementation (1-2g/day) and have found significant reductions in PE risk by 55% in normal dietary intake groups and 64% in low dietary calcium groups (Lassi *et al*, 2014). Calcium also appears to have a protective effect on maternal mortality as well as lowering the risk of low birth weight and still birth (Dadelszen *et al*, 2016). Magnesium homeostasis is also crucial during a healthy pregnancy and magnesium deficiency has been linked to PE development (de Araújo *et al*, 2020). Magnesium levels are reduced in erythrocyte membranes, brain, muscle and in the plasma of those with PE during pregnancy (Rylander, 2015). Similarly, magnesium deficiency has also been associated with cardiovascular death and stroke (Rylander, 2015). Indeed, studies have reported a reduced PE risk when pregnant individuals were given magnesium supplementation (de Araújo *et al*, 2020). On the other hand, a systematic review of ten clinical trials showed no significant effect of magnesium supplementation on PE risk, still birth or fetal growth restriction (Makrides *et al*, 2014) leaving the debate very much ongoing. Finally, aspirin, an anti-platelet agent thought to target the imbalance between vasoconstrictor thromboxane A_2 and vasodilator prostacyclin, may also be used to prevent pre-eclampsia in high-risk groups. Evidence has emerged that shows a consistent reduction in PE risk, preterm birth and other adverse pregnancy outcomes in those given low-dose daily aspirin (Lassi *et al*, 2014; Naderi *et al*, 2017; Ma'ayeh *et al*, 2020)

Despite a lack of understanding on the underlying pathology of PE, there are a wide variety of treatments designed to monitor and manage its symptoms that are becoming more common practice worldwide. When treating any hypertensive disorder of pregnancy, there must be a consideration for the health and well-being of both the fetus and the mother. For this reason, many antihypertensive agents are contraindicated that would normally be used such as ACE inhibitors and angiotensin-receptor blockers due to an increased risk of fetal hypotension, intrauterine growth restriction, renal failure and other congenital malformations (Folk, 2018). It should be noted that unless there are severe features of the disease present, antihypertensive treatment is reserved for mothers with chronic hypertension in lieu of non-pharmacological treatments such as lowering dietary sodium, regular blood pressure monitoring and blood tests and the potential for premature delivery depending on clinical circumstances (National Institute for Health and Care Excellence, 2011). Where the use of an antihypertensive is deemed appropriate, the target blood pressure is 140/90mmHg and a diastolic pressure no lower than 80mmHg to prevent compromised uteroplacental perfusion and fetal hypotension (National Institute for Health and Care Excellence, 2011). However, this is considered a borderline blood pressure and does not remove the risk of further complications.

Antihypertensive treatments that are approved for the control of maternal blood pressure are determined on the desired effect: long-term management postpartum or acute lowering of blood pressure. In the case of the former, oral agents are commonly used and include the α-/β-blocker labetalol, Ca^{2+}-channel blockers such as nifedipine, diltiazem or verapamil or centrally acting adrenergic agonists including methyldopa and clonidine (Moussa *et al*, 2014). Other options include second-line agents such as the diuretic hydrochlorothiazide, though these are avoided in PE patients suffering from volume depletion (Moussa *et al*, 2014). Labelatol and nifedipine may also be used in an acute setting as well as hydralazine or sodium nitroprusside (Lassi *et al*, 2014; Moussa *et al*, 2014). Whilst these agents may be effective in lowering maternal blood pressure, they merely treat the signs and symptoms of PE, thus new treatments are severely lacking.

Novel treatments for PE are currently being researched with a focus on immunological approaches. One such example is the use of an antidigoxin antibody fragment digibind to target the elevated levels of endogenous digitalis-like

factors, such as marinobufagenin, in PE which has been found to lower maternal blood pressure and preserve renal function in women with PE (Oparil and Schmieder, 2013). Other approaches include the use of short interfering RNAs to target the elevated levels of sFlt-1. Turanov and colleagues (2018) found that a single dose of hydrophobically modified asymmetric siRNAs targeted against sFlt-1 produced therapeutic benefit in a baboon model of PE in the absence of adverse outcomes for the fetus. However, many of these novel therapeutics require validation and are a long way from the clinic.

Other interventions during pregnancy are aimed at reducing the risk of further complication and progress to a more severe form of disease. Magnesium sulphate therapy ($MgSO_4$) is indicated in women with PE to prevent the progression to eclampsia and has been found in several trials to reduce stillbirths, maternal death and seizure reoccurrence (Lassi *et al*, 2014). However, $MgSO_4$ has shown other beneficial effects. In a rodent model of PE using Ω-nitro-L-arginine methyl ester (L-NAME), $MgSO_4$ significantly decreased proteinuria and maternal blood pressure, increased production of nitric oxide, decreased levels of serum sFlt-1 and sEng and reduced fetal mortality (Korish, 2012). Further, $MgSO_4$ improved cardiac function in *ex vivo* hearts of pregnant rats given L-NAME by preventing cardiac depression, maintaining stroke volume and prolonging diastolic relaxation (Coates *et al*, 2006). This lends further weight to the hypothesis that magnesium deficiency plays a role in the generation of PE.

1.3 Maternal and Fetal Genetics

Evidence in the literature suggests that maternal and fetal genetics play an influential role in the development of hypertensive disorders of pregnancy. Indeed, a familial maternal history of PE is a risk factor not only for the development of PE in subsequent pregnancies but also for future cardiovascular disease, particularly in early-onset cases (Herrera-Garcia and Contag, 2014). There is also evidence to suggest that paternal genes may play a role as seen by the effects of changing partners and an increased risk associated with fathers born from a PE pregnancy or those who had previously fathered a PE pregnancy (Burton *et al*, 2019). This is perhaps unsurprising given that by its nature the placenta obtains 50% of its genetic information from the father.

Though it is hypothesised that maternal, paternal and fetal genes influence the development of hypertensive disorders of pregnancy, most studies concerning the genetics of hypertensive disorders of pregnancy are focused on the placenta. The placental genome is normally identical to that of the fetus as both are derived from the same conceptus material. However, the human placenta has a high capacity for mosaicism- spontaneously arising chromosome aberrations- which may trigger abnormal placental development (Gobbo *et al*, 2020; Coorens *et al*, 2021). Additionally, epigenetic alterations occur frequently throughout gestation. DNA methylation is low at the time of implantation; however, it has been found to increase between 28-40 weeks in humans which is thought to alter placental gene expression in response to environmental factors such as smoking or diet (Novakovic *et al*, 2011). Though hypertensive disorders of pregnancy stem from a placental origin, maternal gene expression patterns should not be overlooked as a contributing player to placental dysfunction as it is the maternal genetic response that controls placentation, immunological tolerance of the fetus and appropriate adaptation of the cardiovascular system.

1.3.1 The Maternal-Fetal Gene Conflict Theory

Whilst it is clear that genetics plays a role in the pathology of pre-eclampsia, the contribution of maternal, paternal and fetal genes is unclear. One theory is that in a normal pregnancy, the fetal gene expression pattern increases the transfer of nutrients to the fetus whilst the maternal expression pattern functions to restrict this nutrient transfer within specific boundaries to ensure optimal maternal health

(Ali and Khalil, 2015). The placenta is known to alter its genetic and phenotypic response to a wide range of factors; studies have shown this can include changes in the surface area available for nutrient transfer as well as the abundance of nutrient transporters and metabolic rate (Burton and Fowden, 2012). This indicates that maternal nutrient allocation to the fetus can be manipulated directly by alterations to the placenta or indirectly by systemic changes in nutrient availability. Therefore, asymmetry in the genes expressed by the mother and fetus may create a situation where these genes are in conflict with one another. This conflict may lead to the inappropriate spatiotemporal initiation of signalling events that could precede or influence impaired placentation and vascular remodelling during pregnancy (Kobayashi, 2015).

This gene-conflict scenario is thought to be partially influenced by imprinted genes. Imprinted genes are preferentially expressed in a parent-of-origin manner within the placenta, such that imprinted paternal genes increase placental and fetal growth whilst imprinted maternal genes function in the opposite manner (Fowden and Moore, 2012). These imprinted genes are able to alter resource allocation by affecting trophoblast differentiation and organisation as well as vascularisation (Fowden and Moore, 2012). Indeed, a maternal familial history of hypertensive disorders of pregnancy is a known risk factor for their development. Epidemiological studies have found an increased prevalence of PE in daughters (23%) and daughters in-law (10%) related to those with a history of PE pregnancies. However, there was no association between paternal familial risk factors (Herrera-Garcia and Contag, 2014). Some studies contest this and claim to show an association between paternal familial history and PE (Burton *et al*, 2019). Despite the lack of information on the directional flow of information between fetus and mother, several studies have identified genes that may increase the susceptibility to develop disorders such as PE.

Genome-wide linkage studies have identified multiple gene loci on multiple chromosomes, suggesting PE is a multi-genic disorder (Ali and Khalil, 2015). Global gene expression patterns were analysed in the placentae of control and PE patients. Thirty-six differentially expressed genes were identified in PE placentae, of these thirty-one were downregulated including VEGF, hypoxia-inducible factor, leptin, angiotensinogen, various cytokines and tumour necrosis factor-α (Founds *et al*, 2009). In a more recent review, 250 differentially expressed genes were

identified across three data sets comparing control and PE placentae. Of these, 228 were upregulated and 22 were downregulated in PE (Mohamad *et al*, 2020). Other studies have shown altered maternal gene expression in pathways related to pregnancy maintenance, metabolism, oxidative stress and metabolism, embryogenesis and development, implantation, placentation and decidualisation, immune modulation and vascular function (Kobayashi, 2015). It has been shown by Doridot and colleagues (2013) that fetal/paternal genes can also greatly impact pregnancy outcome. When transgenic male mice overexpressing STOX1 (a transcription factor associated with impaired trophoblast invasion) were crossed with wild-type females to create heterozygous fetuses, mothers showed severe gestational hypertension, proteinuria and an increased plasma level of anti-angiogenic factors alongside alterations to kidney and placental histology similar to the changes seen in PE (Doridot *et al,* 2013). This lends weight to the gene-conflict theory. However, it is unclear in these studies to what degree, if any, these expression changes were causative of a poorer pregnancy outcome like PE, or whether they represent a response to placental and vascular dysfunction.

Though these studies can provide information on potential genetic drivers of hypertensive disorders of pregnancy, they are not without their limitations. As aforementioned, the placenta has a high capacity for spontaneous mutations that are unrelated to either maternal or paternal gene expression patterns. These somatic mutations have been shown to alter pregnancy outcome (Coorens *et al*, 2021; Eggenhuizen *et al*, 2021). Whilst this chromosomal mosaicism is most prevalent in the pre-implantation stages and embryos appear to select against cells carrying spontaneous mutations, it is estimated that one third of embryos reaching the blastocyst stage still present with spontaneous chromosome abnormalities (Eggenhuizen *et al*, 2021). These mutations can give rise to a number of phenotypes in the fetus such as aneuploidy, with most resulting in miscarriage in the early embryo (Gobbo *et al*, 2020). However, in cases where this mosaicism is confined to the placenta alone it is possible for the fetus to survive until term despite placental dysfunction. Though the fetus may survive, pregnancies affected by this confined mosaicism are associated with fetal growth restriction (Eggenhuizen *et al*, 2021). A study by Coorens *et al* (2020) found that the placenta is more akin to a patchwork of individually distinct genetic units that each vary from the last despite being sampled from the same placental region. Therefore, whilst genome-wide linkage studies can provide an indicator of

potential genes and pathways involved in hypertensive disorders of pregnancy, many of these studies used single samples from one region of the placenta. Additionally, there was little uniformity in the regions of the placenta sampled between studies. Given the high capacity for somatic mutations or mosaicism within the placenta, it is almost impossible to draw certain conclusions from genome-wide linkage studies.

1.3.2 Omics Technologies and Hypertensive Disorders of Pregnancy

Historically, understanding the pathophysiology of complex disorders, particularly multi-genic disorders, has focussed on protein-coding genes. In recent years, however, research has broadened our understanding of how disease states can arise not only from coding portions of the genome, but from non-coding portions. RNA, or ribonucleic acid, has been found to exist in a variety of structures and in a variety of locations playing multiple roles in protein coding, transcriptional regulation, nuclear architecture and messenger RNA (mRNA) stability as well as translation and post-translational modifications (Gong *et al*, 2021).

'Omics' technologies refer to a collection of disciplines aimed at characterising and quantifying pools of biological molecules that may translate to molecular structure, function and/or interactions. Genomics concerns the genome, transcriptomics examines transcribed genes (mRNA), proteomics is the large-scale study of proteins and metabolomics is the study of metabolite production. Omics technologies have been instrumental in the field of pregnancy research, particularly in the search for biomarkers of complex hypertensive disorders of pregnancy such as PE (Benny *et al*, 2020; Odenkirk *et al*, 2020; Liu *et al*, 2019). Both proteomics and metabolomics have been used to examine the placentae of patients with and without PE alongside investigating potential changes in proteins or metabolites in animal models of PE (Kedia *et al*, 2019; Mary *et al*, 2021).

1.3.2.1 Transcriptomics

Whole transcriptome analyses are also increasingly being employed as an unbiased approach to investigate the genetic and epigenetic contribution to disease manifestation. Due to the dynamic nature of pregnancy, transcriptome analysis can be used to understand the accompanying patterns of transient gene expression of the placenta in healthy and diseased conditions such as PE, recurrent pregnancy loss or fetal growth restriction, among others (Gong *et al*, 2021; Li *et al*, 2022). Generally speaking, across the literature two approaches are used to profile the transcriptome: microarrays and next-generation RNA sequencing (Yong and Chan, 2020). Microarrays use modified complementary DNA templates of an RNA sample set. These templates become hybridised to a set of DNA probes fixed to a solid surface (Cox *et al*, 2015). Binding to the DNA probes then elicits either direct or indirect detection of fluorescence which can be used to quantify gene expression (Cox *et al*, 2015). However, it is limited in that it cannot detect gene expression if the species-specific gene-probe is not present in the array. As microarrays provide information on specific genes rather than the whole genome, it is difficult across studies to reach a consensus due to differing study designs and probe choices. If studies were to use similar arrays there is the danger of artificially inflating the significance of certain expression changes. Moreover, much of the microarray data generated from placentae was produced when RNA biology was less well understood and not all transcripts were detectable by available probes (Yong and Chan, 2020). RNA sequencing is more sensitive when compared to microarrays and is able to detect rare or novel RNA transcripts in the coding and non-coding portions of the whole genome, is not bound by species and is able to detect single-nucleotide variations (Yong and Chan, 2020).

Several studies using microarray-based genome wide profiling have been conducted in placental tissues from human PE pregnancies to attempt to identify susceptibility genes. Literature reports the involvement of genes related to metabolism, oxidative and vascular stress and the immune system, among others (Louwen *et al*, 2012; Kobayashi, 2015). A review of single nucleotide polymorphism (SNP) arrays based on phenotype data generated from genome wide association studies by Benny and colleagues (2020) found associations with genes involved in calcium signalling and the control of follicle-stimulating hormone

levels. Profiling with RNA sequencing has shown the upregulation of genes with a known association with PE such as Flt-1, PlGF and VEGF as well as hypoxia signalling and transcription factor networks (Benny *et al*, 2020). Gong *et al* (2021) also reported an increased expression of follistatin-like 3 at the gene level which was reflected by an increased level of protein in the serum of patients with PE or fetal growth restriction and was identified by RNA sequencing.

The majority of these studies have focussed on protein-coding genes, and whilst this has been effective, the advent of sequencing technologies has allowed us to investigate non-coding RNAs. More than 93% of the genome is known to be transcribed, however, a mere 2% of this is mRNA with the remaining made up of non-coding RNAs (Casamassimi *et al*, 2017). These RNAs are small (<200 nucleotides in length) and include micro-RNA, piwi-interacting RNA, small interfering RNA, transfer RNA, circular RNA and small nucleolar RNA (Cox *et al*, 2015). A distinct subtype of non-coding RNAs are long non-coding RNAs (lncRNA) which are over 200 nucleotides in length. All of these RNA subtypes have been shown to have varied effects on gene expression including translational repression, mRNA degradation and silencing of transposons and repetitive sequences to maintain genomic stability (Casamassimi *et al*, 2017). LncRNAs appear to have additional functions as key regulators of gene expression including acting as micro-RNA host genes or sponges, antisense transcription factor decoys or guides for chromatin remodelling (Fig. 1.13). Unlike many other RNA subtypes, lncRNA research is still in its early days and characterisation of these lncRNAs and their potential involvement in pathophysiological states is complicated as a result.

Another obstacle in the application of transcriptomics to investigating hypertensive disorders of pregnancy is the use of placental tissue. Whilst these disorders stem from a placental origin, the placenta itself is composed of many distinct cell types each with specific roles and thus expression patterns. It has also been shown that the placental transcriptome provides dynamic, state-specific information and this transcriptome is distinct between each of the placental layers in rats (Shankar *et al*, 2012). Some studies have sought to counteract this by using single cell RNA sequencing. One such study focussed on the profiles of individual cell populations arising from the placenta and maternal decidua, thus informing our understanding of the maternofetal interface. Researchers found distinct transcriptional signatures

for decidual stromal and uterine natural killer cells (Nelson *et al*, 2016). However, this analysis was only able to detail the maternal response in relation to shallow trophoblast invasion without examining the maternal vasculature. Thus, whilst our understanding of specific pathways may be enhanced there is still no understanding of the ways in which these populations interact and thus influence one another. Additionally, most of these studies have focussed on placental or decidual tissue at term. The ethical limitations and inaccessibility issues surrounding uterine tissue samples from early gestational time points presents a significant barrier in determining whether these expression changes at term are causative of dysfunctional placentation or merely reflect a maternal adaptation to it. To add to this, very few studies as a result have used samples from the maternal spiral arteries, which are key in the development of a healthy pregnancy and hypertensive disorders of pregnancy, severely limiting our understanding of the early genetic events that underlie maternal vascular remodelling in response to functional and dysfunctional placentation.

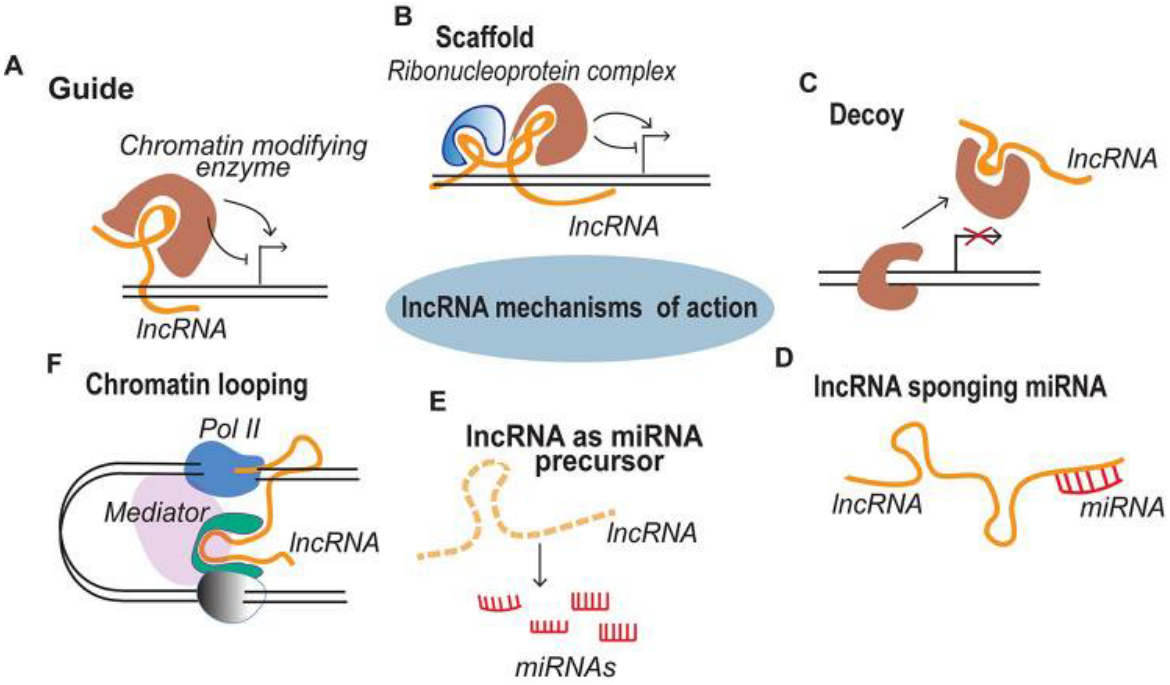

Figure 1.13: Diverse Functions of Long non-coding RNAs (Sourced: Sweta *et al*, 2019).

LncRNAs are now being recognised as key regulators of genome regulation via variety of actions. A) Guide lncRNAs may activate or inhibit gene expression through re-localisation of regulatory factors by chromatin modifying enzyme. B) Scaffold lncRNAs help transient ribonucleoprotein complex assembly. C) LncRNAs may also act as decoys, binding transcription factors to inhibit its regulation. D) LncRNA sponges are able to bind microRNA and inhibit their influence on gene expression. E) They may also function as primary microRNA precursors to direct specific microRNA expression. F) Finally, transcription of lncRNAs may also initiate long range gene regulation in regulatory portions of the genome.

1.4 Animal Models of Hypertensive Pregnancy

Modern biomedical research has benefitted substantially by the advent of accessible model organisms – particularly rodents – to study pathophysiological processes. This is particularly true in the context of hypertension and pregnancy. Whilst it is possible to study human placental samples at term, or in rare cases from elective abortions, this provides us with only a snapshot of the dynamic processes involved in healthy and hypertensive pregnancy (Guttmacher *et al*, 2014). Additionally, it is incredibly difficult to assess changes that occur in the cardiovascular, renal and uteroplacental systems in humans during pregnancy as the most reliable of these procedures are often invasive and confer additional risk to the fetus.

As outlined in 1.1.1, both humans and rats share a haemochorial placenta with only a few differences in gross structure and organisation. For this reason, they are an excellent model of pregnancy. However, the benefits of utilising rats to understand haemochorial placentation and the genetic and physiological changes of early gestation are not universally agreed upon with some expressing concerns of evolutionary divergence (Soares *et al*, 2012). Despite this, rodent models of pregnancy and its related disorders have proven useful in understanding both the underlying mechanisms and maternal responses to healthy and hypertensive pregnancy. It is important to note that no animal model is perfect in recapitulating human hypertensive pregnancy and researchers must exercise care when extrapolating from such models.

Hypertensive rat strains have proven to be very useful when investigating hypertensive pregnancy and range from the stroke-prone spontaneously hypertensive rat that is bred with a predisposition to hypertension to strains in which a high dietary salt intake is necessary to elicit hypertension, such as the Dahl salt-sensitive strain, mimicking the environmental factors that influence the development of hypertension in humans (Graham *et al*, 2005).

1.4.1 The Stroke-Prone Spontaneously Hypertensive Rat

The stroke-prone spontaneously hypertensive (SHRSP) rat is a genetic model of severe hypertension and cerebral stroke first derived by Okamoto and colleagues in 1974. This was achieved by selective breeding of Wistar Kyoto (WKY) rats that had spontaneously developed hypertension when fed a Japanese diet (high sodium, low potassium and protein) rather than the normal Western chow. After many generations of selective breeding, the strain known as the spontaneously hypertensive (SHR) rat was created. A subset of these severely hypertensive rats were observed to develop symptoms of stroke at high frequency when fed a high-salt diet. Further selective breeding of these animals led to the generation of the SHRSP strain (Carswell *et al*, 2005, Fig. 1.14A). As the use of this strain in research has increased worldwide, several smaller closed colonies have been created by successive inbreeding within institutions including the University of Glasgow which now maintains the SHRSP.Gcrc strain (Fig. 1.14B).

Male SHRSP rats have been found to develop severe hypertension with a systolic pressure between 170-200mmHg at 10-12 weeks of age in the SHRSP.Gcrc strain, with further rises in blood pressure as they age. The SHRSP have the highest systolic pressure of all spontaneously hypertensive strains with pressures as high as 240mmHg, compared to maximal systolic pressures in the SHR strain (Nabika *et al*, 2012). The SHRSP are also far more likely to suffer from stroke (80% vs 10% in SHR: Nabika *et al*, 2012). In contrast to the SHRSP and SHR, WKY rats show a stable normotensive systolic pressure of approximately 140-150mmHg from 6 weeks onwards (Kato *et al*, 2015). Further study of the SHRSP strain over the years has revealed that this hypertension is associated with endothelial dysfunction, left ventricular hypertrophy and renal damage (Harvey *et al*, 2017; He *et al*, 2014; Kato *et al*, 2015). These phenotypes closely mimic those seen in human essential hypertension. Additionally, as in humans, female SHRSP rats though hypertensive have a lower blood pressure than their male counterparts (Davidson *et al*, 1995).

It is known that genetic influences can contribute up to 50% of variability related to blood pressure in human essential hypertension (Saavedra, 2009). In parallel to the genetic studies taking place in humans, researchers have sought to understand the genetic development of hypertension in rodent models in hopes it

may aid in the identification of candidate genes. The use of these inbred models such as the SHRSP is advantageous as they provide genetic homogeneity and control of environmental factors alongside the usefulness of specific normotensive and hypertensive inter-crosses in studying genetic linkage that is otherwise impossible in human studies (Graham *et al*, 2005). The study of these models has largely utilised quantitative trait loci mapping, a phenotype-driven approach that has the potential to identify novel genes involved in disease (Carswell *et al*, 2005). However, no model is perfect. Though rodent models of hypertension do share common features, evidence suggests that the pathogenic mechanisms differ between strains, particularly inbred sub-strains maintained at different institutions despite sharing a similar genetic background (Saavedra, 2009). For example, the SHRSP/Izm sub-strain exhibits increased blood pressure from 6 weeks of age whilst the SHRSP/Kyo sub-strain did not exhibit increased blood pressure until 10 weeks of age (Kato *et al*, 2015). Despite these shortcomings, rodent models of hypertension continue to provide insights into the control of blood pressure in both humans and rats.

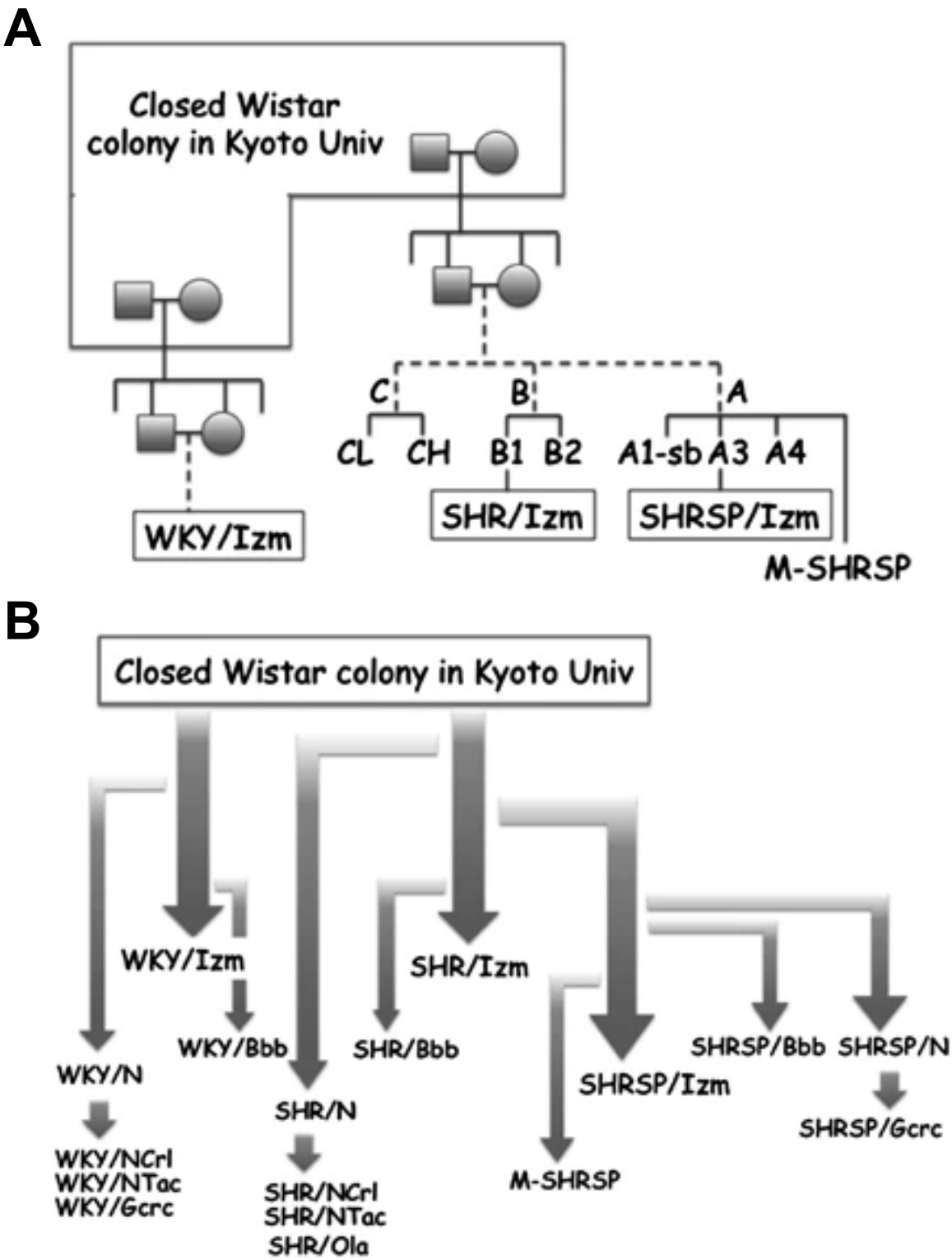

Figure 1.14: Generation of the WKY, SHR and SHRSP Strains and Their Inbred Sub-strains
(Sourced: Nabika *et al*, 2012).

(A) Selective breeding of WKY rats lead to the generation of the first SHR rats in the University of Kyoto, Japan by Okamoto in 1963. This was followed by the generation of the SHRSP strain in 1974. (B) Subsequent generations were bred worldwide in a variety of institutions and locations, leading to the array of inbred sub-strains now available including the Glasgow based strains, denoted as Gcrc.

1.4.1.1 Modelling Hypertensive Pregnancy in the SHRSP

The majority of studies investigating cardiovascular disease and hypertension in the SHRSP have focussed solely on males. This is, generally, due to the fact that male SHRSP rats tend towards a higher blood pressure and development of end-organ damage in comparison to females of the strain as well as the outdated assumption that the female oestrous cycle introduces population heterogeneity (Masineni *et al*, 2005; Plevkova *et al*, 2020). Whilst it is true that hormone fluctuations in female subjects, particularly during pregnancy, can affect drug metabolism- this has been proven to be of little consequence in most investigations of disease given that most diseases already show sex differences unrelated to hormone levels (Plevkova *et al*, 2020). This bias within preclinical research over the years has led to a lack of knowledge of vascular disease in females.

The SHRSP response to pregnancy was first described in the late 1970s and early 1980s (McCarthy and Kopin, 1978; Yamada *et al*, 1981). These studies described the maintenance of a hypertensive blood pressure profile throughout pregnancy in the SHRSP in contrast to a reduced blood pressure in pregnant WKY dams. These early studies also reported a reduced reproductive success (reflected by reduced litter size and rate of delivery) in pregnant SHRSP rats (Yamada *et al*, 1981). Subsequent research investigated changes within the placenta during pregnancy in the SHRSP showing a decreased blood flow and placental Na^+-K^+-ATPase activity and increased hypertrophy within blood vessels (Fuchi *et al*, 1995a; Fuchi *et al*, 1995b). Despite these early advances, far fewer studies have been conducted in the SHRSP than the SHR strain (23 results versus 314 results for the search terms “SHRSP pregnancy” and “SHR pregnancy” respectively, minus duplications; search conducted in PubMed, May 2022). Of these 23 studies examining SHRSP pregnancy, only eight have investigated the maternal vascular response. Of these eight, only five studies focussed on the remodelling of the uterine arteries themselves and the potential effects on placentation (Fuchi *et al*, 1995a; Small *et al*, 2016a; Small *et al*, 2016b; Barrientos *et al*, 2017; Scott *et al*, 2021).

The reduced cross-sectional area of SHRSP uterine arteries versus WKY first reported by Fuchi *et al* (1995a) was later seen by Small *et al* (2016a) in the

SHRSP.Gcrc versus WKY.Gcrc, alongside evidence of increased vessel stiffness and resorption rate, reduced uteroplacental flow and decreased litter size that was not reversible when blood pressure was controlled with the calcium channel blocker nifedipine. They also showed an increased mRNA expression of hypoxia-inducible factor 1α and superoxide dismutase 1 and glycogen cell loss in the SHRSP placenta, suggesting the deficient remodelling of the uterine arteries in the SHRSP may cause altered placental function though a direct link was not confirmed in the study (Small *et al*, 2016a). Further study by Small and colleagues (2016b), provided evidence that the dysfunctional vascular remodelling of SHRSP dams was influenced by the inflammatory response. They showed that treatment of pregnant SHRSP rats with the anti-inflammatory etanercept improved blood pressure, litter size, placental glycogen content and uteroplacental blood flow (Small *et al*, 2016b). Barrientos *et al* (2017) sought to characterise the remodelling of the spiral arteries of the SHRSP further via histological analysis of trophoblast invasion in the mesometrial triangle. They found that SHRSP placentae presented with defective endovascular trophoblast invasion in comparison to WKY (Barrientos *et al*, 2017). Recent work has sought to disseminate the underlying genetic factors that influence uterine vascular remodelling in the SHRSP prior to structural and functional changes within the vessels with several pathways identified as potentially having a causative role (Scott *et al*, 2021). Despite advancements in our understanding of the SHRSPs maternal response to pregnancy, particularly relating to vascular remodelling and placentation, it is still unclear why the SHRSP experience these impairments. Though our understanding of the SHRSP as model of chronic hypertension during pregnancy is far from complete, the similarities between the SHRSP and human hypertensive pregnancy make it an excellent tool in the study of hypertensive disorders of pregnancy.

1.4.2 The Reduced Uteroplacental Perfusion Model

Though the underlying mechanisms of PE are not fully understood, it is accepted that a key component of disease development is reduced uteroplacental perfusion leading to hypoxia and ischaemia/reperfusion injury as a result of impaired vascular remodelling and shallow trophoblast invasion (Li *et al*, 2012). The reduced uteroplacental perfusion (RUPP) procedure originated in the 1970s where clipping and complete ligation of the uterine and ovarian arteries was conducted in

female baboons, which was found to induce hypertension and proteinuria during pregnancy (Cavanagh *et al*, 1977). It was not until the 1990s that the RUPP procedure was carried out in rats to serve as a model of *de novo* PE development similar to humans (Casper and Seufert, 1995). The model has since been further optimised to the procedure now routinely used in rats by the Granger lab by clipping the lower abdominal aorta and ovarian arteries, as opposed to the previous method of clipping the aorta below the renal arteries, reducing uteroplacental flow by ≈40% in gravid rats (Alexander *et al*, 2001).

In detail, the RUPP procedure involves using silver clips to compress an occlude the lower abdominal aorta just above the iliac bifurcation. Due to compensatory blood flow to the placenta in rats occurring via an adaptive increase in ovarian blood flow, both the left and right ovarian arteries are also clipped before the first segmental artery to inhibit the uterine blood supply (Fig 1.15A; Fushima *et al*, 2016). This procedure is carried out in mid-gestation, normally on GD14, and has been shown to mimic the physiological features of PE in humans. These include hypertension, proteinuria, fetal growth restriction (decreased litter size and pup weight), impaired renal function (reduced glomerular filtration rate and renal plasma flow), increased vascular reactivity, endothelial dysfunction and increased peripheral resistance as well as impairment of cardiac function (Fushima *et al*, 2016; Li *et al*, 2012; Bakrania *et al*, 2022). RUPP rats have also been shown to have a pro-inflammatory response to pregnancy and increased serum and placental levels of sFlt-1 and decreased plasma VEGF and PlGF as seen in human PE cases (Li *et al*, 2012). Though the development of hypertension in this model is not spontaneous, the associated symptoms of RUPP surgery have been found to be pregnancy specific as surgical reduction in uteroplacental perfusion did not elicit a blood pressure response in virgin control rats (Alexander *et al*, 2001).

The RUPP model of PE is advantageous as it is able to capture a number of features of the disease seen in humans. Of note, the development of fetal growth restriction in this model is useful in understanding how impairment of the maternal response to hypertensive pregnancy influences fetal programming and future cardiovascular disease development- a feature that is not shared by all animal models of PE. Additionally, the surgery itself is not specific to rodents only allowing for the study of nonhuman primates (Li *et al*, 2012). The RUPP model can be a

useful tool in the study of potential therapeutic approaches that may not be appropriate for study in human pregnancy. However, the RUPP model does come with some substantial limitations. Firstly, an increase in blood pressure following RUPP surgery is not guaranteed across or even within species. This is due to the fact that the surgery itself is rather precise in nature with respect to the locations of arterial clips and gestational timing. Additionally, the average rat gestation is roughly 22 days. Thus, clipping of the arteries on GD14 leaves only a very narrow window for study. The use of nonhuman primates gives a much longer window of study with placentation that is much more akin to humans, however it is incredibly costly. Second, as the induction of hypertension in this model is surgical it is unable to recapitulate immune mechanisms, trophoblast invasion or vascular remodelling deficiencies that have been noted in early hypertensive pregnancy (Li *et al*, 2012). Third, as a result of the restriction of the abdominal aorta a common complication of the procedure is hindlimb ischaemia that can progress to complete paraplegia in approximately 8% of surgeries (Morton *et al*, 2019). Furthermore, it is difficult to ascertain whether the cardiovascular effects of RUPP surgery are solely pregnancy-specific or rather a response to the procedure itself. Evidence has been shown to suggest RUPP surgery has a distinct impact on sympathetic nerve activity and cardiac output that is not otherwise seen in rodent pregnancy and in cases of hindlimb ischaemia, the PE phenotype may be a result of systemic hypoxia rather than of the uteroplacental unit specifically (Morton *et al*, 2019; Sholook *et al*, 2007). This can be overcome by clipping the ovarian and uterine arteries only, so called the selective RUPP model, which has been shown to capture the physiology of PE without affecting hindlimb blood flow (Fig. 1.15B; Morton *et al*, 2019). Finally, the RUPP model is unable to mimic the glomerular endotheliosis of PE and the progression of severe PE to HELLP syndrome seen in humans (Li *et al*, 2012).

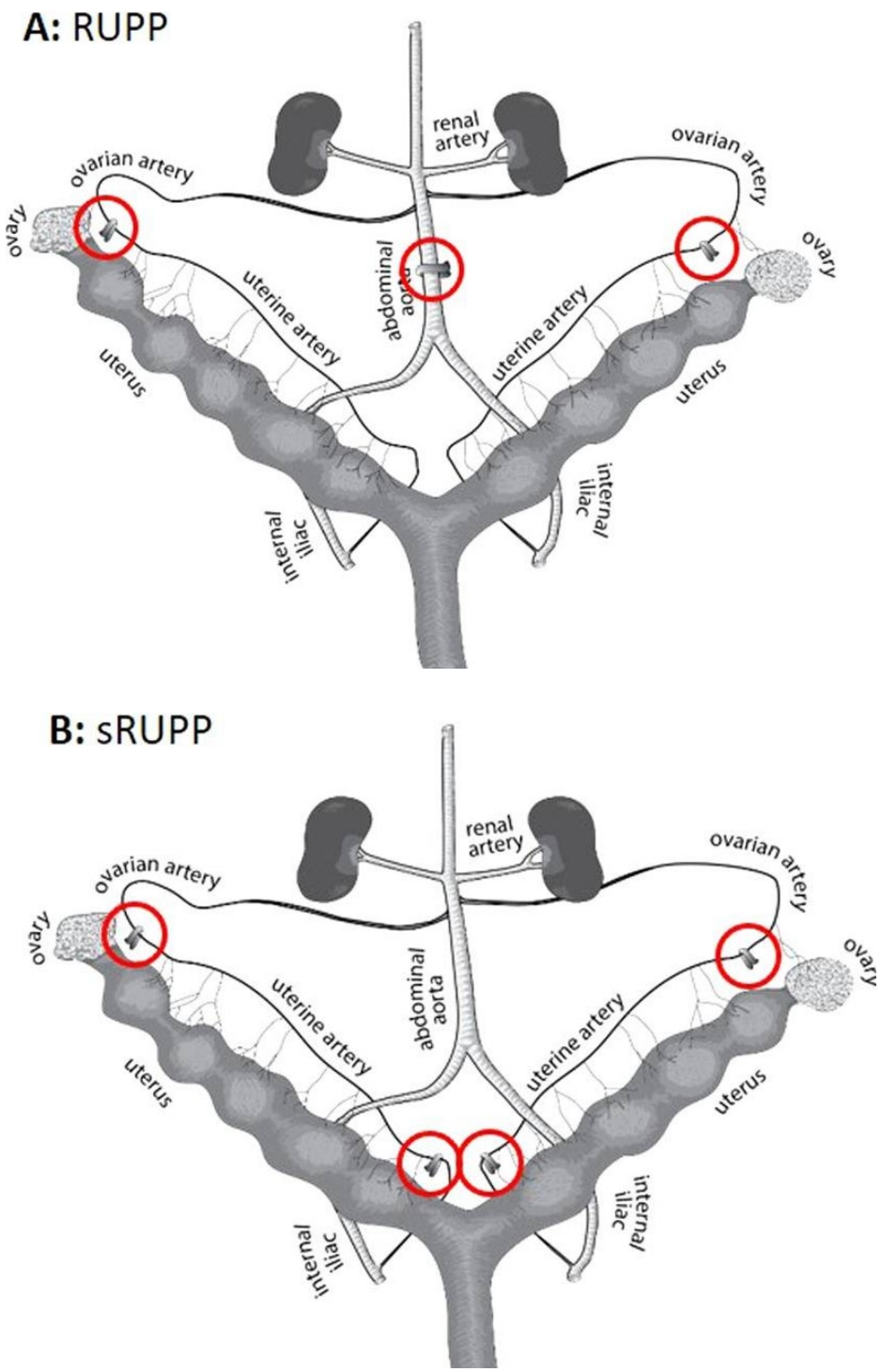

Figure 1.15: Illustrative Examples of Arterial Clipping in the RUPP and selective RUPP Models
(Sourced: Morton *et al*, 2019).

(A) In the RUPP model, silver clips are placed above the iliac bifurcation of the lower abdominal aorta and on the left and right ovarian arteries. (B) In the selective RUPP model, silver clips are placed in the left and right ovarian arteries between the ovary and uterine horn as well as the left and right uterine arteries just below the supply to the first fetus. (RUPP; reduced uteroplacental perfusion).

1.4.3 Genetic Models

As outlined in 1.3, maternal and fetal genetics are known to play a role in the development of hypertensive disorders of pregnancy such as PE. Though PE is a multifactorial, polygenic disease that is impossible to reproduce perfectly in animal models, a successful approach adopted by researchers involves focussing in on a specific phenotype and engineering genetic manipulations that mimic it. One such model is the endothelial nitric oxide synthase knockout ($eNOS^{-/-}$), which seeks to model endothelial dysfunction, common to PE. This approach was largely inspired by the finding that disruptions in nitric oxide related pathways alongside polymorphisms in the nitric oxide synthase gene have been identified in patients with PE (Alpoim *et al*, 2014; Alpoim *et al*, 2013). However, this has yielded mixed results. Pregnant $eNOS^{-/-}$ mice showed a decreased blood pressure whilst non-pregnant knockout mice showed a marked increase in blood pressure that returned following pregnancy (Cushen and Goulopoulou, 2017). $eNOS^{-/-}$ mice do show features of fetal growth restriction as in PE but the results with regards to maternal hypertension have been inconsistent, likely due to compensation by one of the other nitric oxide synthase isoforms (Huang *et al*, 1995; Shesely *et al*, 2001).

There have been several knockout models generated in attempts to understand placental vascularisation and artery remodelling as a result of trophoblast invasion. These include the ubiquitin ligase ankyrin repeat and SOCS box containing 4 (ASB4) knock-out, as variants of ASB4 - an imprinted gene - have been linked to human obesity, a known risk factor for PE (Mizuno *et al*, 2002; Vagena *et al*, 2022). In the placentae of ASB4 deficient mice, there was impaired trophoblast-to-endothelial cell differentiation resulting in poor vascularisation (Townley-Tilson *et al*, 2014; Li *et al*, 2016). The role of the immune system in vascular remodelling and placentation during healthy and hypertensive pregnancy has been well evidenced in the literature. It comes as no surprise then that several genetic manipulation models of components of the immune response have been generated. These include deficiencies in complement component 1q, interlukin-4 and interleukin-10 each of which show one or more symptoms that are similar to human PE including mild hypertension, proteinuria, renal pathology and elevated sFlt-1 though none showed features of fetal growth restriction (Bakrania *et al*, 2022; Cushen and Goulopoulou, 2017).

Other genetic models are concerned with the overexpression of select genes. One example is the storkhead box 1 (STOX1) transcription factor transgenic overexpression mouse model. STOX1 is expressed in EVTs and influences their invasion during normal placental development (Cushen and Goulopoulou, 2017). Studies have shown that the paternally inherited allele Y153H which results in STOX1 overexpression is a high-risk allele for decreased EVT invasion and PE development, though this association is highly debated (Yong *et al*, 2018). In response to this issue, Doridot and colleagues (2013) presented a mouse model of PE symptoms induced by paternally inherited STOX1 overexpression. Wild-type female mice with fetus' heterogenous for STOX1 overexpression exhibited severe gestational hypertension, proteinuria and increased circulating levels of sFlt-1 and sEng, common biomarkers of PE in humans (Doridot *et al*, 2013). Interestingly, female mice overexpressing STOX1 show a return to baseline measures following delivery but experience long-term alterations to cardiac function and the local cytokine profile mimicking the increased cardiovascular disease risk in post-PE patients (Miralles *et al*, 2019).

One of the best characterised genetically linked models of PE is the borderline hypertensive 5 (BPH/5) mouse strain. This strain has an elevated blood pressure throughout its adult life span and has a similar spontaneously increasing blood pressure profile during pregnancy to SPE (Davisson *et al*, 2002). Alongside hypertension these mice also experienced endothelial dysfunction, increased uterine vascular resistance, proteinuria, diminished litter size and placental dysfunction (Cushen and Goulopoulou, 2017). A more recent study has shown that BPH/5 mice also have abnormal trophoblast invasion (Bakrania *et al*, 2022). However, one thing all of these genetic models share is that they utilise mice rather than rats. Though mice do share some similarities with humans with regards to placental development the commonalities are not enough to extrapolate findings to humans, particularly those related to trophoblast invasion which is comparatively shallow in mice versus humans.

1.4.4 Pharmacological Intervention Models

Hypertensive disorders of pregnancy can be mimicked pharmacologically by the administration of substances known to cause vascular dysfunction through inflammation and endothelial damage. As with genetic models however, there is

no one pharmacological model that accounts for all the characteristics of human PE. A common clinical biomarker for the detection of PE is an elevated serum sFlt-1 (Naderi *et al*, 2017). Many animal models have been developed to mimic this phenotype to assess the effects on angiogenesis during pregnancy. One such model administered sFlt-1, which binds VEGF and PlGF, in both pregnant Sprague-Dawley rats via adenovirus injection into the tail vein (Maynard *et al*, 2003). Pregnant rats receiving sFlt-1 exhibited significant hypertension and proteinuria alongside glomerular endotheliosis but there was no analysis of fetal growth. Notably, those receiving a lower dose of sFlt-1 showed a milder phenotype, much like the varied severities of PE noted in humans (Maynard *et al*, 2003). The long-term effects of elevated sFlt-1 have also been studied in mice using the same model. Pruthi *et al* (2015) found that at two months post-partum following PE (adenoviral sFlt-1 injection), mice that experienced injury to the left common carotid artery showed histological features of abnormal vascular remodelling. However, a study by Bytautiene *et al* (2010) found that mice exposed to sFlt-1 during pregnancy did not show evidence of abnormal vascular function in the carotid artery at eight months post-partum. Thus, the usefulness of this model is debated.

Studies have shown that patients with PE show a two-fold increase in placental and plasma tumour necrosis factor-α (TNF-α) (Cornelius *et al*, 2019). TNF-α has also been shown to cause vascular dysfunction in both humans and rodents (Small *et al*, 2016b). For these reasons coupled with its involvement in the immune response, TNF-α has been utilised to model pregnancy-induced hypertension in rodents. Infusion of the proinflammatory cytokine has been found to elevate blood pressure and increase the expression of the precursor of endothelin-1, a known vasoconstrictor peptide (Bakrania *et al*, 2022; Schiffrin, 2001). The role of TNF-α as a potential therapeutic target in PE has also been investigated by utilising the SHRSP model of chronic hypertension during pregnancy. Pregnant SHRSP rats had elevated levels of placental TNF-α and were administered the TNF-α inhibitor etanercept. Following treatment, researchers showed improvements in blood pressure, placental glycogen levels, uterine artery function and uteroplacental flow but not in fetal growth measurements (Small *et al*, 2016b).

There are many models that seek to induce hypertension by inducing vasoconstriction. Of these, the most popular and most reviewed model is the L-

NAME model of PE. This model replicated the endothelial dysfunction of PE by inhibiting nitric oxide synthase- though it is not yet confirmed whether nitric oxide plays a definitive role in the pathogenesis of PE (Sunderland *et al*, 2010). Pregnant Sprague-Dawley rats that were administered L-NAME by means of osmotic mini pump on GD17 onwards showed evidence of hypertension, fetal growth restriction, proteinuria and elevated levels of sFlt-1 and sEng (Yallampali and Garfield, 1993; Ramesar *et al*, 2011). However, the role of nitric oxide in PE has not reached a consensus as genetic knockout of its production, as discussed prior, does not produce a PE phenotype during pregnancy. Despite this, the L-NAME model has been used extensively in hypertensive pregnancy research to study therapeutic agents (Sunderland *et al*, 2010).

As our understanding of the various pathways implicated in the generation of PE grows, more novel pharmacological intervention models are being generated. One such model involves infusion of the peptide hormone arginine vasopressin (AVP). AVP plays a crucial role in osmotic homeostasis and thus blood pressure regulation (Cushen and Goulopoulou, 2017). AVP secretion is not measured directly, but by its surrogate marker plasma copeptin. Copeptin was first shown to be elevated as early as the sixth week of gestation in pregnancies that subsequently developed PE by Santillan *et al* (2003). This led to the development of the AVP infusion model whereby mice received a mini pump 3 days prior to mating that administered AVP throughout gestation. These mice showed evidence of hypertension, proteinuria, renal glomerular endotheliosis, fetal growth restriction and an increased rate of embryo resorption (Santillan *et al*, 2003). Though this novel model seems promising, the underlying mechanisms of its PE-like symptoms are not well understood. Whilst the links between AVP and PE are not fully characterised, a recent study showed that a polymorphism of the AVP promoter region was associated with pre-eclampsia in humans thus it still shows promise as a model of PE (Erfanian *et al*, 2019).

1.4.5 Renin-Angiotensin Aldosterone System Manipulation Models

The RAAS is incredibly important in the development of a healthy pregnancy in both humans and rodents and dysregulation of this system has long been associated with hypertensive disorders of pregnancy, particularly PE (Verdonk *et al*, 2014). Alterations to the RAAS in rodents have been utilised in many ways in

attempts to model PE. Some groups have investigated the effects of genetic manipulation of certain RAAS components to mimic the changes observed in PE, such as the angiotensinogen-renin transgenic overexpression model. In this model, female Sprague-Dawley rats overexpressing angiotensinogen are crossed with males overexpressing renin. Crossing these strains caused dams to develop severe gestational hypertension, proteinuria, elevated levels of circulating and uteroplacental ANGII and decreased fetal weight in late gestation similar to late-onset PE and SPE (Bohlender *et al*, 2000; Hering *et al*, 2010). Interestingly, this cross does not work in the reverse order i.e., males overexpressing angiotensinogen and females overexpressing renin. A similar model has been created in mice which also develop a SPE-like phenotype (Bakrania *et al*, 2022; Takimoto *et al*, 1996). Though this model does exhibit the symptoms of PE the overexpression of RAAS elements does not replicate the decreased levels of renin noted in these patients (Hussein and Lafayette, 2014).

Though there is an overall decrease in ANGII expression during PE pregnancies there is an increased ANGII sensitivity that results in vasoconstriction (Hussein and Lafayette, 2014; Chaiworapongsa *et al*, 2014). This is, in part, due to the production of autoantibodies against the AT_1 receptor (AT_1-AA) which upon binding to and activation of the AT_1R lead to downstream activation of NADPH oxidase. This results in the production of ROS and subsequent activation of the transcription factor NF-κB, increasing the production of inflammatory mediators (Herse *et al*, 2008; Campbell *et al*, 2019). Studies have shown that individuals who suffered from pre-eclampsia during pregnancy still produced these autoantibodies up to eight years post-partum (Rieber-Mohn *et al*, 2018). This has resulted in the creation of the AT_1-AA chronic excess model in which purified rodent AT_1-AA are administered from GD12 to GD19 in pregnant Sprague-Dawley rats. These animals experience significantly increased mean arterial pressure and placental endothelin-1, however no effects were observed on fetal or placental weights (LaMarca *et al*, 2009). Further investigation has revealed this model also has mitochondrial dysfunction and elevated levels of sFlt-1 and sEng (Cunningham *et al*, 2019; LaMarca *et al*, 2012). Of note, hypertension in this model can be attenuated by an endothelin-1 receptor type A antagonist or TNF-α blockade, seemingly replicating the angiogenic imbalance and proinflammatory states associated with PE (Sunderland *et al*, 2010).

Both of these models have highlighted the important role of ANGII in association with the increased sensitivity to it seen in human PE. ANGII has previously been used to induce hypertension in normotensive animals to study alterations in cardiac function and reactive oxygen species production (Nishiyama *et al*, 2001; Laursen *et al*, 1997). When ANGII is delivered to normotensive rodents during pregnancy, they develop a PE-like phenotype with impaired vascular remodelling, increased blood pressure, placental inflammation and fetal growth restriction as a result of increased cardiovascular stress (Xue *et al*, 2017; Shirasuna *et al*, 2015). This model has been further developed by the Graham lab who utilise the chronically hypertensive SHRSP. By delivering ANGII via osmotic mini pump from GD10 onwards in the pregnant SHRSP they have developed a novel model of SPE that exhibits worsening hypertension, cardiac dysfunction, proteinuria and renal pathology, impaired uteroplacental flow, fetal and placental growth restriction and changes in placental gene expression, all mimicking the human phenotype (Morgan *et al*, 2018). These symptoms increase in severity as the dose of ANGII increases. Though this model shows promise further work is required to fully understand the underlying mechanisms of these pathological changes in response to ANGII and how these can potentially inform our understanding of PE and SPE in humans.

1.5 Hypothesis and Aims

The SHRSP rat serves as an excellent model of genetically linked chronic hypertension during pregnancy that can be stressed further to produce a phenotype similar to superimposed pre-eclampsia.

The Graham lab has previously modelled SPE in the SHRSP with ANGII at doses of 500 and 1000ng/kg/min but experienced a failure of the model to significantly mimic the severity of the human phenotype at the low dose and welfare concerns at the high dose. These welfare concerns included a total body weight loss of >20% of pre-pregnancy weight and a general deterioration of animal health resulting in early sacrifice alongside total pregnancy loss in the days following infusion of 1000ng/kg/min in some SHRSP dams. We hypothesised this model could be optimised and fully characterised at a dose of 750ng/kg/min ANGII. In Chapter 3, we aimed to achieve this by implantation of an osmotic mini pump and assessment of maternal and fetal outcomes.

$MgSO_4$ is routinely used in clinical practice to prevent the progression from pre-eclampsia to eclampsia. It is also known to induce production of NO and improve endothelial function. We hypothesised $MgSO_4$, administered as a 1% w/v solution in drinking water, could serve as a preventative therapeutic in our optimised rodent model of SPE. We aimed to test this in Chapter 4 by utilising the optimised model generated in Chapter 3 and assessing maternal and fetal outcomes.

The Graham lab has previously generated transcriptomic data derived from the uterine arteries of pregnant (GD6.5) and non-pregnant SHRSP and WKY dams. We utilised this data set to further examine the changes in gene expression profiles in response to pregnancy in both strains in Chapter 5, hypothesising that SHRSP dams would show distinct changes in gene expression that preceded structural and functional changes. Further to investigating gene expression changes, we hypothesised that the changes noted for calcium signalling and ROS production could be validated *in vitro*. In Chapter 5, we aimed to achieve this by isolating primary vascular smooth muscle cells from the uterine arteries of both SHRSP and WKY (pregnant and non-pregnant) and examining calcium release, measuring ROS generation and validating gene expression levels via Taqman® PCR.

Chapter 2: General Materials and Methods

2.1 General Laboratory Practice

All procedures noted in this thesis were conducted in a laboratory setting following local regulations pertaining to laboratory health and safety. A laboratory coat, non-powdered nitrile gloves and, where appropriate, safety glasses were worn at all times during *in vitro* procedures. For *in vivo* procedures, local practices related to animal handling and safety were followed at all times. During animal experimentation, colour-coded scrubs provided by the university were worn. Reagents considered to be hazardous to human health were handled and disposed of according to the manufacturer's safety data sheets and the Control of Substances Hazardous to Health regulations. Risk assessments, where appropriate, were completed prior to experimental work.

Laboratory equipment and reagents were of the highest grade commercially available. All equipment was ensured to be in working order and cleaned thoroughly prior to and after use. Glassware and re-usable plasticware were cleaned by soaking in Decon 75 detergent (Decon Laboratories Ltd., Sussex) and rinsed with distilled water before being dried at 37ºC. All other plastics were single use and sterile. This included eppendorfs ranging in volume from 0.5 to 2mL (Greiner Bio-One, Gloucestershire, UK), 15 and 50mL Corning® centrifuge tubes (VWR, Leicestershire, UK), 5 and 20mL Sterilin™ containers (VWR, Leicestershire, UK) and Corning® cell culture flasks and plates (VWR, Leicestershire, UK).

To measure volumes of liquid ranging from 0.1µL to 1000µL a calibrated Gilson pipette was used with appropriately sized, sterile tips (Greiner Bio-One, Gloucestershire, UK). In experiments involving ribonucleic acid, RNAse free eppendorfs and pipette tips were used as well as nuclease-free water (Qiagen, Manchester, UK). For volumes of 1mL to 25mL Stripette® serological pipettes were used with an electronic pipette filler (ThermoFisher Scientific, Paisley, UK). For volumes larger than 25mL, a clean measuring cylinder was used. Solid reagents were weighed on either a Mettler Toledo PB1501 balance (sensitive to 0.1g) or a Sartorius Extend balance (sensitive to 0.0001g).

Solutions were dissolved using a Jenway 1000 combination hotplate/stirrer (Fisher Scientific, Loughborough, UK). To mix solutions, a mini vortex 2800 rpm Lab

Dancer was used (Fisher Scientific, Loughborough, UK). Samples with volume <2mL were centrifuged using a desktop Eppendorf 5145 R microcentrifuge (Sigma Aldrich, Dorset, UK) in a temperature range of 4-20ºC. Volumes larger than 2mL or 96/384 well plates were centrifuged using a Mega star 3.0R centrifuge (VWR, Leicestershire, UK). pH adjustments to solutions were made using an Orion STAR A111 pH meter calibrated using 4.0, 7.0 and 10.0 pH standards prior to each use as per the manufacturer's instructions (ThermoFisher Scientific, Paisley, UK).

2.2 General Laboratory Techniques

2.2.1 Nucleic Acid Extraction

All RNA extractions were performed on animal tissues that were snap-frozen in liquid nitrogen at time of sacrifice using a Qiagen RNeasy Mini Kit (Qiagen, Manchester, UK). RPE, RW1 and RLT buffers were prepared prior to use by addition of 100% ethanol as per the manufacturer's instructions.

Tissue homogenisation was achieved by disruption in 350µL of RLT buffer via bead-milling in a TissueLyser II with 3mm steel beads (Qiagen, Manchester, UK) at 25Hz for 30s twice. Samples were placed on ice between lysis periods. Bead-milling was performed as the tissues that were used- uterine arteries and neonatal tissues- were harvested in small amounts. Lysates were then centrifuged at maximum speed for 3 minutes and the supernatant removed for further use.

RNA was extracted from lysates immediately following homogenisation. 350µL of 70% ethanol was added to the lysate. The sample was transferred to a RNeasy spin column with 2mL collection tube and centrifuged for 15 seconds at 8000x*g*. 700µL of RW1 buffer was added to the column and centrifuged for 15 seconds at 8000x*g*. This was followed by 500µL of RPE buffer, centrifuging for 15 seconds, another 500µL of RPE buffer and centrifugation for two minutes at 8000x*g*. Finally, 40µL of nuclease free water was added to the column and centrifuged at 8000 *g* for one minute to elute RNA. In some cases, this was repeated to ensure all RNA had eluted from the column due to the small size of the starting material.

RNA concentration and purity were determined using a Nanodrop spectrophotometer (ThermoFisher Scientific, Paisley, UK). Nucleic acids were detected at absorbance readings of 260nm (A_{260}). Protein contamination was detected at 280nm (A_{280}) and organic or solvent contamination from the extraction process at 230nm. A ratio of A_{260}/A_{280} between 1.9 and 2.1 was considered to indicate suitable purity. RNA samples were then stored at -80ºC until further use.

2.2.2 Reverse Transcriptase Polymerase Chain Reaction (RT-PCR)

Complementary DNA (cDNA) was prepared with between 50-2000ng of input RNA in a 20µL reaction volume using the SuperScript™ IV (SSIV) First-Strand Synthesis kit (ThermoFisher Scientific, Paisley, UK).

The RT-PCR was conducted in a 96-well plate with the final concentrations in each well detailed in Table 2.1. The total reaction volume within each well was achieved by addition of NFW up to 20µL. No-template (lacking RNA samples replaced by NFW) and blank controls (NFW only) were also conducted on the same plate at the same time. Plates were sealed using adhesive PCR film (ThermoFisher Scientific, Paisley, UK) and centrifuged at 8000x*g* for 30 seconds to ensure all reagents were well mixed.

The RT-PCR was carried out on a MJ Research Tetrad PTC-225 Thermal Cycler (MJ Research, Massachusetts USA). The temperature cycles are detailed in Table 2.2. Following generation of cDNA, plates were cooled to 4ºC and stored at -20ºC until further use.

Table 2.1 Additions and Final Well Concentrations of RT-PCR Reagents for cDNA Synthesis

Reagents	Volume Added (µL)	Final well concentration
5x SSIV reverse transcriptase buffer	4.0	1x
10mM dNTP mix (10mM each)	1.0	0.5mM each
100mM DTT (dithioreitol)	1.0	5mM
50µM random hexamers	1.0	2.5µM
40 U/µL RNase OUT™, RNase inhibitor	1.0	2.0 U/µL
200 U/µL SSIV reverse transcriptase	1.0	10.0 U/µL

A summary of the various reagents used in RT-PCR to generate cDNA from an initial RNA input of 50-2000ng in a 20µL reaction. Details of volumes per reagent added to each well and the resultant final well concentration per well are given.

Table 2.2 Temperature Cycles for RT-PCR cDNA Synthesis

Thermal Cycler Stage	Temperature (ºC)	Duration (min)
Anneal primers	25.0	10
Transcription and	48.0	30
Enzyme heat denaturation	95.0	5
Cooling	4.0	Until target temperature is reached

A summary of the thermal cycler stages in RT-PCR for cDNA synthesis from RNA.

2.2.3 Real Time Quantitative Polymerase Chain Reaction (qPCR)

2.2.3.1 Taqman® Gene Expression Assay

The Taqman® assay utilises fluorescently labelled probes, with either VIC™ or FAM™ dyes, specified to the target gene of interest (GOI). This allows for the incorporation of the probe into the double stranded structure of DNA during the reaction, followed by its cleavage in the subsequent cycle where the dye is separated from a non-fluorescent quencher. The intensity of fluorescence generated is proportional to the resultant amount of PCR product. The specific probes used in this assay were from ThermoFisher Scientific (Paisley, UK) and are detailed in Table 2.3.

Taqman® assays were prepared in 384-well MicroAmp™ Reaction Plates (ThermoFisher Scientific, Paisley, UK) with 1.0µL (for uterine and mesenteric arteries) or 2.0µL (for neonatal tissue) of cDNA, generated in section 2.2.2. Assays were carried out in duplex (uterine arteries) or triplicate (neonatal tissue) depending on the starting material. The GOI was labelled with a FAM™ probe, and the housekeeper GAPDH was labelled with a VIC™ probe. The final volume of 5µL/well was achieved by addition of Taqman® Universal Master Mix II (ThermoFisher Scientific, Paisley, UK). Plates were sealed with adhesive PCR film (ThermoFisher Scientific, Paisley, UK) and centrifuged at 8000x*g* for 30 seconds to ensure reagents were incorporated and at the base of the well. Taqman® assays were conducted using a QuantStudio 12K Flex Real-Time PCR system (ThermoFisher Scientific, Paisley, UK) under standard cycling conditions. Ct values were analysed using the $2^{(-\Delta\Delta Ct)}$ method (Livak and Schmittgen, 2001).

Table 2.3 Details of Rat Specific Taqman® Probes for qPCR

Gene Name	Gene Symbol	Assay ID	Fluorescent Label
Angiotensin I converting enzyme 2	Ace2	Rn01416293_m1	FAM-MGB
p22phox	Cyba	Rn00577357_m1	FAM-MGB
Gp91-phox	Cybb	Rn00576710_m1	FAM-MGB
Glutathione peroxidase 1	Gpx1	Rn00577994_m1	FAM-MGB
Peroxisome proliferator activated receptor alpha	Pparα	Rn005566193_m1	FAM-MGB
Osteopontin	Spp1	Rn00681031_m1	FAM-MGB

A summary of the rat specific Taqman® probes used to quantify gene expression during real time qPCR. The suffix _m1, under Assay ID, denotes that the probe spans exon junctions and thus quantifies only specific forms of mRNA, preventing the detection of genomic DNA.

2.2.4 Biochemical Urine Analysis

Urine samples were collected at a variety of gestational time points, as outlined in section 2.3.5. Samples were thawed and briefly centrifuged at low speed (<1000x*g*) at 4ºC to remove any debris from collection. 200µL of urine was used for biochemical analysis. The concentrations of albumin and creatinine were determined for each sample using the Roche Cobas C311 Analyser (Roche Diagnostics Ltd., West Sussex, UK). Albumin was detected using the Albumin Gen.2 Tina-Quant assay and creatinine was detected using the Creatinine Jaffe Gen.2 assay. These assays are designed for the photometric detection of their respective proteins in urine. These were used in conjunction with the Total Protein Urine/CSF assay control kit (all from Roche Diagnostics Ltd., West Sussex, UK). The concentrations of each protein were then expressed as a ratio of albumin to

creatinine, as creatinine should remain constant despite strain, treatment or gestational time point differences.

2.2.5 Tissue Processing and Sectioning

Upon harvesting at time of sacrifice, detailed in section 2.4, tissues were fixed in 10% neutral buffered formalin for 12-24 hours at room temperature (Sigma Aldrich, Dorset, UK). Tissues were washed two times in phosphate buffered saline [137mM NaCl, 2.7mM KCl, 4.3mM Na_2HPO_4, 1.47mM KH_2PO_4; pH 7.4] (PBS) to remove traces of fixative and stored in 70% ethanol at room temperature until further processing. Tissues were placed in labelled histology cassettes (ThermoFisher Scientific, Paisley, UK) which were then placed in 60ºC paraffin wax inside a Citadel 1000 processor (Fisher Scientific, Loughborough, UK). Tissues were processed by exposure to a timed sequence of alcohol and xylene at different concentrations over a period of 8 hours and 30 minutes, as outlined in Table 2.4. Following this, tissues were embedded in paraffin wax (≤60ºC) using the Shandon Histocentre 3 embedding centre (ThermoFisher Scientific, Paisely, UK). Blocks were cooled at -20ºC overnight prior to sectioning with a Leica RM2235 Microtome (Leica Biosystems, Milton Keyes, UK). Placentae and kidneys were cut transversely through the centre and placed cut side down. Sections were 5µm in thickness and were placed in 40ºC water before being transferred to a silane treated microscope slide and then baked overnight at 60ºC. Prior to staining, slides were deparaffinised by soaking in Histo-Clear (FisherScientific, Loughborough, UK) and rehydrated by soaking in decreasing concentrations of ethanol (100-70%) following by deionised water (dH_2O). All staining procedures were carried out at room temperature. Once staining was complete, slides were dehydrated by reversing the previous ethanol gradient (70-100%) followed by Histo-Clear (Table 2.5). Coverslips were mounted over stained sections using DPX mounting medium that was allowed to set overnight (Sigma Aldrich, Dorset, UK).

Table 2.4 Processing Conditions for Formalin Fixed Rodent Tissues

Solution	Incubation Time
70% Ethanol	15 minutes
85% Ethanol	15 minutes
90% Ethanol	25 minutes
95% Ethanol	25 minutes
100% Ethanol	15 minutes
100% Ethanol	15 minutes
100% Ethanol	15 minutes
Xylene	30 minutes
Xylene	30 minutes
Paraffin Wax	30 minutes
Paraffin Wax	30 minutes

A summary of the individual steps of formalin fixed tissue processing, detailing the solutions and incubation times of each step. The resultant tissues were embedded in paraffin wax blocks for use in histology.

Table 2.5 Summary of Slide Preparation Prior to and Following Staining

Stage	Solution	Incubation Time
Deparaffinisation	Histo-Clear	2 x 5 minutes
Rehydration	100% Ethanol	5 minutes
	90% Ethanol	5 minutes
	70% Ethanol	5 minutes
	dH_2O	5 minutes
Staining		
Dehydration	70% Ethanol	5 minutes
	90% Ethanol	5 minutes
	100% Ethanol	5 minutes
Deparaffinisation	Histo-Clear	2 x 5 minutes

A summary of the individual steps to prepare sections mounted onto silane treated slides for staining. Slides deparaffinised, rehydrated and stained. Following staining, slides are dehydrated and deparaffinised once more.

2.2.6 Histology

2.2.6.1 Periodic Acid Schiff Staining

Periodic Acid Schiff staining was used to detect polysaccharides and therefore identify glycogen containing cells in placental sections. Reagents were left on the benchtop to acclimatise to room temperature prior to use. Sections were incubated in 0.5% w/v periodic acid (in dH_2O) for 5 minutes. This was followed by rinsing three times with dH_2O for approximately 3 minutes each, for a total of 10 minutes, to remove excess stain. Sections were then incubated in Schiff's reagent (Sigma Aldrich, Dorset, UK) under dark condition for 15 minutes. The sections were washed under a running tap for 5 minutes before counter-staining with Harris haematoxylin (CellPath, Powys, UK) for 2 minutes. Sections were washed for a final time under a running tap for 5 minutes to remove excess stain and then dehydrated according to Table 2.5.

2.2.6.2 Picrosirius Red Staining

Picrosirius red staining was used to identify fibrosis by staining for total collagen in kidney sections. Following deparaffinisation and rehydration (Table 2.5), sections were transferred to Weigert's Haemotoxylin (freshly made according to manufacturer's instructions; Sigma Aldrich, Dorset, UK) and incubated for 10 minutes. Sections were then washed under a running tap for a further 10 minutes. A 0.1% picrosirius red solution was prepared using 0.1% w/v Sirius red F3B (Sigma Aldrich, Dorset, UK) in dH_2O. Sections were incubated in the picrosirius red solution for 60 minutes under dark conditions. This was followed by removal of excess stain by washing twice for 5 minute each time in acidified water (0.01N v/v hydrochloric acid in dH_2O). Excess moisture was removed before mounting coverslips as detailed in section 2.2.5.

2.2.6.3 Threshold Quantification of Staining in ImageJ

All slides were blinded prior to imaging. Approximately 5-6 images were taken with a 4x objective on an EVOS XL Core Imaging System (ThermoFisher Scientific, Paisley, UK). These images were images laced together using Microsoft Image Composite Editor 2.0 (Microsoft, Washington, USA). Positive staining was identified and quantified using the threshold quantification method in ImageJ software (National Institutes of Health, Bethesda, USA). The image type was

converted to a red:blue:green stack and viewed using the green channel for both Periodic Acid Schiff and Picrosirius red stains. The threshold was set to maximum to capture all pixels in the image before being adjusted to identify areas of positive staining only. This process gave values for the total area and positively stained area. This was then expressed as a percentage of whole tissue as positively stained area / total area x 100.

2.3 *In Vivo* Procedures

2.3.1 Animals

The stroke-prone spontaneously hypertensive (SHRSP) and Wistar Kyoto (WKY) rat strains used in this thesis were generated from inbred strains that have been maintained in-house by brother x sister mating in the University of Glasgow since 1991. Animals were housed under a controlled 12hour light/dark cycle with a constant temperature of 21±3ºC. They were maintained on a normal diet with *ad libtum* access to food and water (Rat and Mouse No.1 Maintenance Diet Expanded, Special Dietary Services, UK). All animal procedures were approved by the Home Office according to the Animals (Scientific Procedures) Act (1986) and ARRIVE guidelines (Kilkenny *et al*, 2010). Animal procedures were carried out under project licenses 60/9021 and PP0895181.

2.3.1.1 Time Mating

Age-matched, virgin female SHRSP and WKY rats were bred between 12-14 weeks of age. They were time mated for up to four days with males of the same strain in a mesh bottomed breeding cage. Successful mating was confirmed by the presence of a coital plug and denoted as gestational day 0.5.

2.3.2 Anaesthetic Procedures

When necessary, rats were anaesthetised using an induction box filled with 5% isoflurane in 1.5L/min of medical oxygen connected to an activated charcoal fluosorber filter canister (Harvard Apparatus, Massachusetts, USA). Once anaesthetised, rats were transferred to a mask in either a supine or prone position or on their side with nose and mouth fully secured inside the mask. Once transferred, anaesthesia was maintained at 1.5-2% isoflurane for recovery procedures. Where anaesthesia was terminal, rats were maintained at 5% isoflurane.

2.3.3 Radiotelemetry

Radiotelemetry involves the use of an implanted transmitter in the abdominal aorta of rats to enable continuous live monitoring of haemodynamic measurements. Systolic, diastolic and mean arterial pressures alongside heart rate and activity were directly monitored using the Ponemah telemetry system (Data Sciences International, Minneapolis St Paul, USA). Prior to implantation, the probe was sterilised by 24-hour incubation in Actril ® cold sterilant (VWR, Leicestershire, UK) at room temperature and calibrated within ±5mmHg.

Surgery was conducted at 10 weeks of age under aseptic conditions. The operating table was covered with a sterile surgical cover and a sterile surgical gown and gloves were worn at all times. Instruments were sterilised by autoclaving prior to use. Where multiple animals were receiving surgery in a single day a new set of gloves was worn for each animal and instruments were resterilised. Virgin female rats were anaesthetised as outlined for recovery procedures in section 2.3.2. Prior to the procedure animals received 5mg/kg carprofen analgesic subcutaneously. Hair was removed from the abdomen and swabbed with a 4% w/v chlorhexidine gluconate solution (HiBiScrub®). A no.11 scalpel was used to perform a midline laparotomy through the abdominal wall. The peritoneal cavity was cleared to expose the abdominal artery and iliac bifurcation. Once the surrounding connective tissue and fat had been cleared away, three MERSILK® Ethicon suture ties (NuCare, Bedfordshire, UK) were placed around the arteries as depicted in Figure 2.1 to temporarily occlude blood flow. A 22-guage needle bent to an approximate 45º angle was used to make an incision just above the iliac bifurcation. The catheter of the sterile probe was inserted up towards the renal arteries and secured with a small cellulose patch and tissue adhesive. The probe was secured into place by suturing to the abdominal wall using ETHILION® Ethicon nylon sutures (NuCare, Bedfordshire, UK) and the animal closed using VICRYL® Ethicon re-absorbable sutures (NuCare, Bedfordshire, UK) Animals were recovered on surgical Vetbed bedding in a 37ºC incubator and returned to their home cage atop the matching receiving pad. Following a two-week recovery period, animals were time mated as described in section 2.3.1.1 and returned to their home cage following successful mating. After confirmation, probes were switched on and data collected at a sampling rate of 10 seconds every five

minutes until parturition where they were sacrificed under terminal anaesthesia (2.3.2).

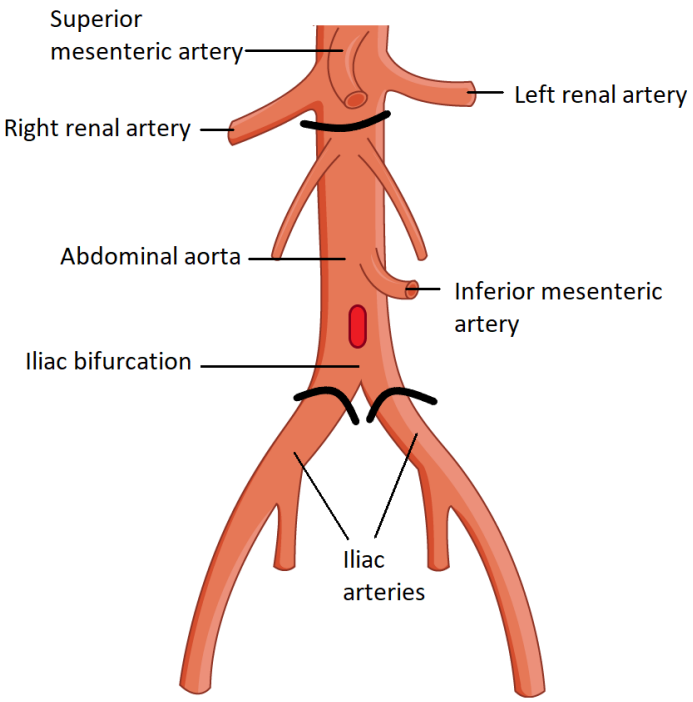

Figure 2.1: Illustration of Ligation Points During Radiotelemetry Probe Implantation
(Adapted from: Servier Medical Art)

A depiction of the structure of the arteries proximal and distal to the abdominal aorta. Prior to implantation, blood flow was occluded by ligating the abdominal and iliac arteries as indicated by the thick **black** curves. An incision was made just above the iliac bifurcation (shown by **red** oval) and the catheter of the probe inserted upwards along the abdominal aorta. The probe was secured to the abdominal wall. This illustration was created using artwork from Servier Medical Art, licensed under the Creative Commons Attribution 3.0 Unported License.

2.3.4 Tail Cuff Plethysmography

Systolic blood pressure was measured prior to pregnancy and on gestational days 6.5, 14.5 and 18.5 using tail-cuff plethysmography. Measurements were generally made in the early afternoon between 12:00 and 14:00 hours to minimise diurnal variation. The animals were acclimatised to the procedure prior to pregnancy. Animals were warmed in a pre-warmed induction box with heat lamps at approximately 30-32ºC for 10-20 minutes to induce vasodilation of the tail arteries.

Animals were gently restrained using a warm, dry towel and placed on an electric blanket to maintain body temperature with the tail exposed. A blood pressure occlusion cuff followed by a pressure transducer cuff, which measures blood pressure based on volume changes, were placed at the base of the tail. These were connected to a programmed electro sphygmomanometer to ensure consistent inflation-deflation in 1mmHg steps up to 250mmHg and register pressure changes detected by the transducer cuff. Upon inflation, systolic pressure was measured when blood flow to the tail artery was occluded by pressure in the cuff. An average of six readings per animal were taken and used to calculate mean systolic blood pressure.

2.3.5 Metabolic Cage Urine Sampling

Rats were placed into individual metabolic cages prior to pregnancy and at gestational days 6.5 and 18.5. All animals were acclimatised to the cages for two hours on two occasions before 24-hour measurements were made at pre-pregnancy and beyond. Rats had access to 200mL of drinking water and the standard diet *ad libtum*. The final remaining volume and any lost to spillage was recorded following a 24-hour time period. Urine and faecal matter were separated, and total urine volume was recorded before aliquoting into 2mL eppendorfs and storage at -80ºC.

2.3.6 Blood Sampling by Tail Venesection

Blood samples were collected from the tail vein prior to pregnancy and on gestational days 6.5, 14.5 and 18.5. Animals were heated in pre-warmed incubation boxes for 10 minutes prior to the procedure to induce vasodilation. Rats were anaesthetised for recovery procedures as in 2.3.2. Following confirmation of anaesthesia, rats were placed on their side. One of three tail veins (two lateral and one dorsal) were punctured with the tip of a sterile no.11 scalpel at an approximate 45º angle. Where multiple animals were being sampled, a new scalpel was used for each animal. Roughly 0.5mL of blood was collected into a heparinised collection tube on ice and gentle pressure was applied upon withdrawal of the scalpel at the puncture wound to stop any bleeding prior to recovery from anaesthesia. Heparin inhibits thrombin formation and thus clotting, allowing for plasma separation. Haematocrit was performed by transfer of a small volume of blood into specialised haematocrit capillary tubes sealed at one end and

centrifugation at 5000rpm for 15 minutes to separate the plasma. Percentage red blood cell (RBC) mass was calculated as RBC length (mm)/Total length (mm) x 100. The remainder of the samples were centrifuged for 15 minutes at 5000rpm and 4ºC to isolate plasma. This was aliquoted and stored at -80ºC.

2.3.7 Transthoracic Echocardiography

Echocardiography was performed at pre-pregnancy and at gestational days 6.5, 14.5 and 18.5. Rats were lightly anaesthetised throughout the procedure according to section 2.3.2. The thoracic and abdominal fur was removed by shaving and the area cleaned of stray hair. Rats were placed in a supine position. Aquasonic ultrasound gel (BioMedical Instruments, Zöllnitz, Germany) was applied to exposed skin as an ultrasound coupling medium. Rats were imaged trans-abdominally and trans-thoracically using an Acuson Sequoia C256 imager fitted with a 15 MHz linear array transducer (Siemans, Surrey, UK). The heart was imaged along a para-sternal short-axis view to obtain M-mode images for 6-7 cardiac cycles, repeated two times. Hearts were then imaged along an apical 4-chamber view to assess mitral valve flow using pulse wave Doppler for 6-7 cardiac cycles in duplicate. During the procedure tibial length was also measured to standardise measurements.

Analysis of the echocardiographic images was carried out using ImageJ software (National Institutes of Health, Bethesda, USA). Distance (in mm) between M-mode waveform peaks and troughs was measured (shown in Fig. 2.2A) and used to calculate estimations of stroke volume (SV), cardiac output (CO), left ventricular mass (LVM), ejection fraction (EF), fractional shortening (FS) and relative wall thickness (RWT). Calculations can be found in the appendix. Mitral flow images were analysed by measuring the ratio between the peak of the E wave and the A wave (E:A) and deceleration time taken for the E wave to return from peak to baseline (DT'E) (Fig. 2.2B).

2.3.8 Doppler Ultrasound of Uterine Arteries

Uterine artery Doppler ultrasound was conducted at the same time as echocardiography and prepared as described in 2.3.7. The uterine artery was located lateral to the uterus in the lower abdomen using the colour Doppler P-mode. Once location was confirmed, the transducer was placed parallel to the

artery and the pulse wave Doppler recorded for 6 cycles in duplicate (Fig. 2.3). In cases where an animal was only pregnant in one horn, measures were only taken from the pregnant horn. Peak systolic velocity (PSV) and end diastolic velocity (EDV) were measured from six consecutive cardiac cycles in duplicate. Resistance index (RI) was calculated as (*RI = [PSV-EDV]/PSV*) and systolic/diastolic ratio (*S/D*; calculated as *PSV/EDV*; Fig. 2.3). As pregnancy progresses, it is possible to detect the fetal heartbeat by sweeping the transducer over the lower abdomen until a fetus is identified. The fetal heartbeat was then recorded for approximately 6 cycles to confirm viability of the pregnancy. Doppler ultrasound images were analysed using ImageJ software (National Institutes of Health, Bethesda, USA).

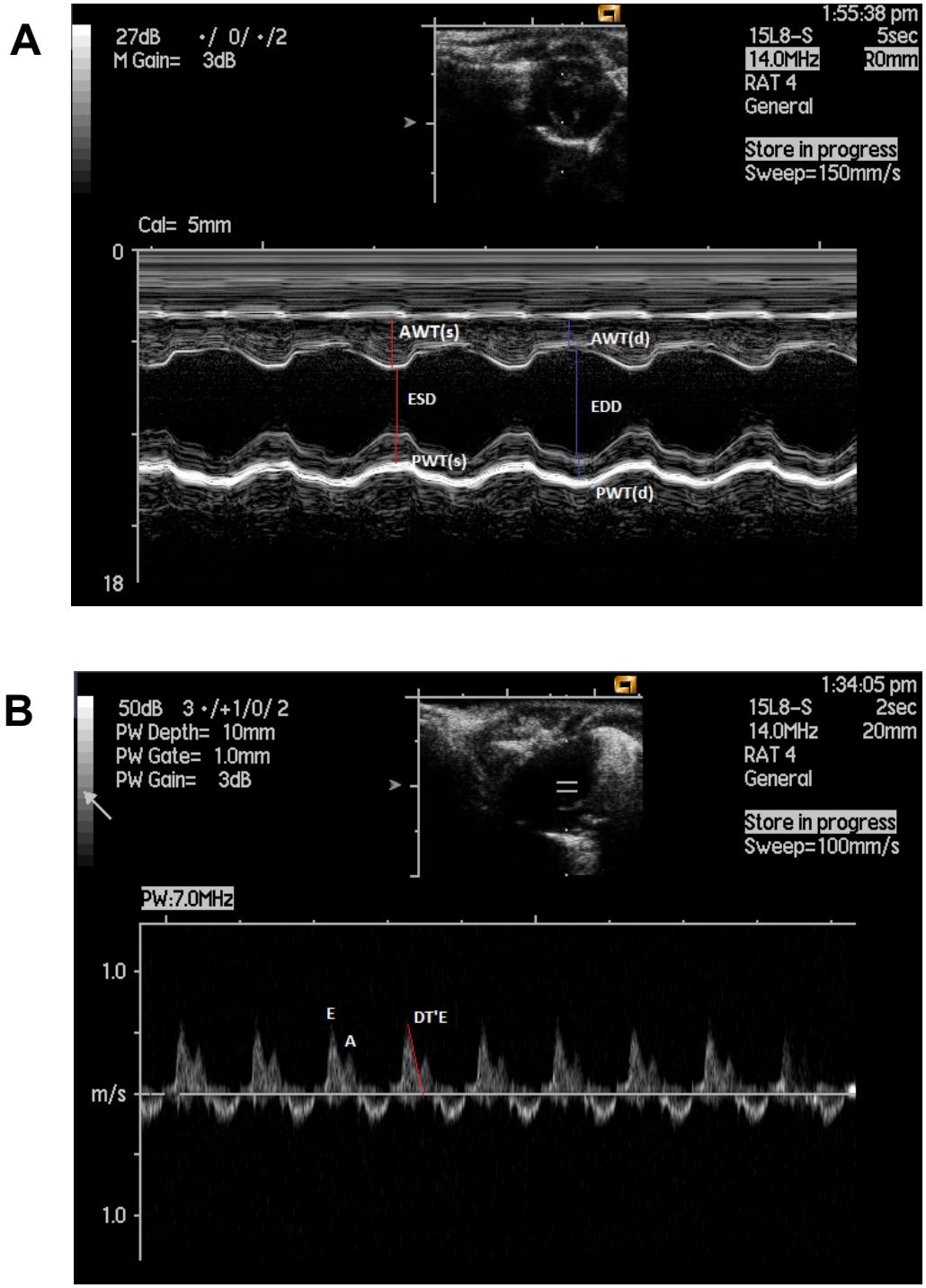

Figure 2.2: Representative Echocardiography Images

Cardiac functional parameters were calculated using a short-axis parasternal view to visualise the left ventricle for M-mode images (A) and mitral flow assessed using an apical four-chamber view (B). M-mode images were analysed by measuring the AWT and PWT for both systole and diastole as well as ESD and EDD. Images of the mitral valve were analysed by calculating the ratio of the E wave (passive filling) to the A wave (active filling) and the DT'E. (AWT(s/d); anterior wall thickness in systole/diastole, ESD; end systolic diameter, EDD; end diastolic diameter, PWT(s/d); posterior wall thickness in systole/diastole, DT'E; deceleration time of the E wave).

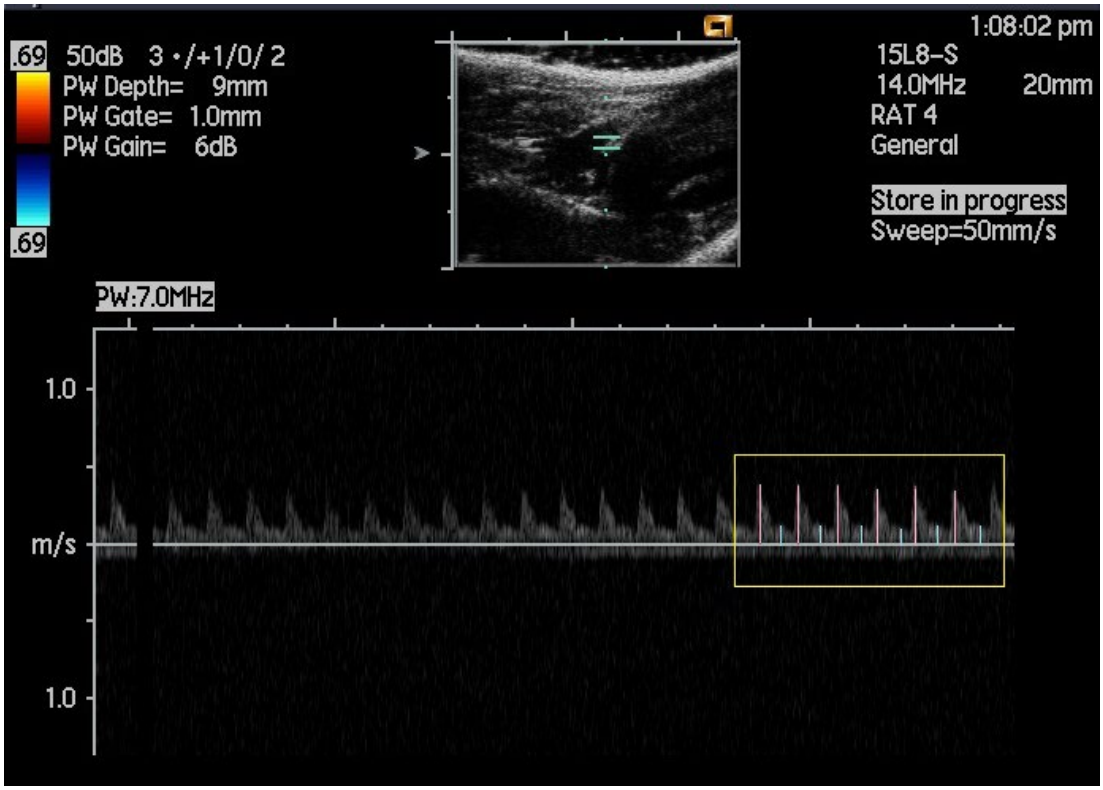

Figure 2.3: Representative Doppler Ultrasound Image of the Uterine Artery

Uteroplacental flow was calculated using colour Doppler ultrasound in the uterine arteries. Images were analysed by measuring PSV (long **pink** lines) and EDV (short **blue** lines) over six consecutive cardiac cycles (shown by **yellow** box). Where animals were only pregnant in one horn, measurements were taken from the pregnant horn only. (PSV; peak systolic velocity, EDV; end diastolic velocity).

2.4 Sacrifice Procedure

Animals were euthanised on gestational day 6.5, 18.5 or following parturition by exsanguination under terminal anaesthesia as in section 2.3.2. Some animals were sacrificed as virgin controls in the same manner as pregnant animals. Exsanguination was performed by creating a midline incision and opening of the thoracic cavity by blunt dissection and breaking of the rib cage on either side. Once the heart was exposed, the aorta was severed, and the heart removed for further processing. The method of culling was also the method for confirmation of death, as removal of the heart ensures permanent cessation of the circulation.

2.4.1 Cardiac Puncture Blood Sampling

Blood sampling via cardiac puncture was conducted just prior to exsanguination under terminal anaesthesia (2.3.2). Once the heart was exposed as detailed in 2.4, a 21-guage needle attached to a 5mL syringe was inserted into the apex of the heart and the left ventricle. Approximately 4-5mL of blood was slowly drawn into the syringe. The total volume of blood harvested was then split equally between either a heparin coated or EDTA coated BD Vacutainer ® tube (NuCare, Bedfordshire, UK) and kept on ice for haematocrit measurement and plasma isolation (detailed in section 2.3.6).

2.4.2 Maternal Tissue Collection

Following blood collection, maternal tissues were harvested and cleaned. Whole organ weights (unless otherwise indicated) were recorded using a Sartorius Extend balance (Appendix 7.1.1). Following whole organ weighing, the atria and right ventricle were removed from the maternal heart and the left ventricle weighed before dissection. The lower apex was removed, and the upper portion halved. The middle section of the heart was placed in 10% neutral buffered formalin for histological assessment (section 2.2.5) and the apex halves and upper left ventricle were snap frozen in liquid nitrogen. Whole organ weights were also recorded for the lungs, liver, left and right kidneys with renal fascia removed, brain and spleen. The right kidney, brain and lungs were halved with one half in formalin and the other snap frozen in liquid nitrogen. The liver and spleen were cut into three portions with one snap frozen and another placed in formalin. The left kidney was quartered and snap frozen. The adrenals were also removed and snap frozen or placed in formalin. All snap frozen tissues were stored at -80ºC until use.

A hysterectomy was performed, and the entire gravid/non-gravid uterus was removed and weighed. It was then placed in chilled calcium free phosphate buffered saline (PBS) to humanely euthanise the fetuses (if appropriate) by cooling followed by decapitation to confirm death by cessation of the circulation. The uterine arteries and veins were dissected from each uterine horn and placed on ice in calcium free PBS to preserve them for later dissection (2.4.3). Dams with <4 fetuses were excluded from further study (Table 2.6). One animal in the SHAM+$MgSO_4$ group of Chapter 4 was excluded due to a sudden death with no obvious cause (Table 2.6). The number of successfully implanted fetuses and resorptions were recorded alongside their locations, if applicable. The intestines were also collected in their entirety and placed into chilled calcium free PBS and kept on ice until further dissection (2.4.3).

Table 2.6 Summary of Dams Excluded From Further Study in Chapters 3 & 4

Chapter 3 – Experimental Group	**No. Recruited**	**<4 fetuses**	**Final *N* No.**
WKY	9	0	9
SHAM	13	2	11†
ANGII	20	1	19*
Chapter 4 – Experimental Group	**No. Recruited**	**<4 fetuses**	**Final *N* No.**
SHAM	2	0	2
ANGII	3	0	3
SHAM+$MgSO_4$	5	0**	4
ANGII+$MgSO_4$	6	1	5

A summary of the number of dams excluded from further study per group in each chapter based on the exclusion criteria of <4 fetuses present at time of sacrifice. *5 animals progressed to partition for neonatal and/or telemetry measurements. †3 animals progressed to partition for neonatal and/or telemetry measurements. **1 animal was excluded out with the given criteria due to a sudden death that following post-mortem did not have any obvious cause.

2.4.3 Artery Dissection

Uterine arteries were dissected and snap frozen for later RNA extraction (section 2.2.1) or reactive oxygen species measurement (section 6.3.2) or stored in chilled calcium free PBS for vascular smooth muscle cell isolation (section 2.5.1). The main uterine artery (Fig. 2.4) was dissected using a microscope in a sterile sylgard-coated plate in calcium free PBS. After careful removal of the surrounding adipose tissue to expose the artery, it was gently separated from the uterine vein and the vein discarded. The arteries were halved and either snap frozen in liquid nitrogen or transferred to chilled, sterile F-12 Hams Nutrient Mix media [1mM L-glutamine, 14mM sodium bicarbonate, 1mM sodium pyruvate] (Thermofisher Scientific, Paisley, UK) supplemented with 100IU/mL penicillin, 100µg/mL streptomycin, 2mM L-glutamine (all ThermoFisher Scientific, Paisley, UK) and stored at 4ºC for up to one hour before use in vascular smooth muscle isolation.

In the case of mesenteric artery dissection, the intestines were transferred and spread out on a sterile sylgard-coated plate in calcium free PBS. The 1st order mesenteric artery was identified, and the arterial tree followed down to the 3rd order mesenteric arteries. These 3rd order arteries were microscopically dissected in the same manner as the uterine arteries. Third order mesenteric arteries were then either snap frozen for RNA extraction (section 2.2.5) or reactive oxygen species measurement (section 6.3.2).

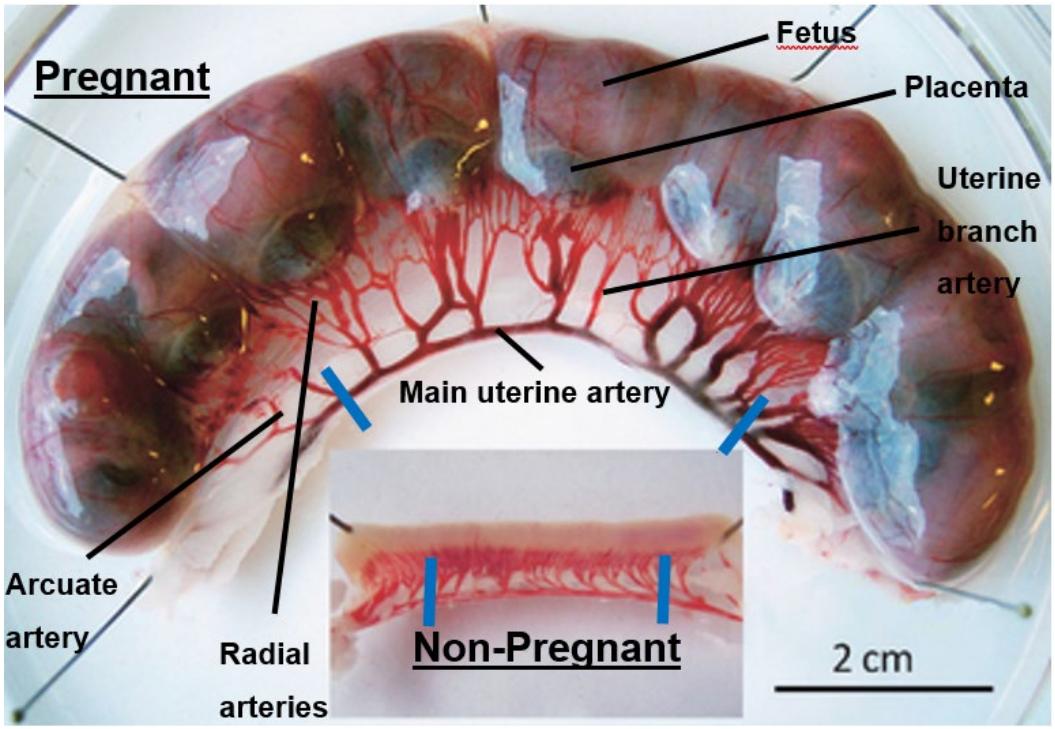

Figure 2.4: The Anatomy of the Pregnant versus Non-Pregnant Rat Uterine Vasculature
(Adapted from: Mandala and Osol, 2011).

Comparative images of a pregnant and non-pregnant uterine horn from a rat, showing the arrangement of the major fetoplacental units and vascular structure. The portion of the main uterine artery, minus the uterine vein, used in experiments is shown between the thick **blue** lines in the pregnant and non-pregnant uterine horns. This dissection was repeated on the opposite uterine horn in each animal.

2.4.4 Fetoplacental Tissue Collection

At gestational day 18.5, each fetoplacental unit was carefully dissected in chilled calcium free PBS. The amniotic fluid was drained by puncturing the amniotic sac and the fetal membranes removed. Both fetal and placental tissues were gently blotted on absorbent paper towel to remove excess fluids. The umbilical cord was severed, and the fetus and its matching placenta weighed whole and recorded (Appendix 7.1.2). Two placentae from each dam were chosen at random. These placentae were not weighed, rather, one was placed whole (including the mesometrial triangle) into 10% neutral buffered formalin for 24 hours at room temperature and one was snap frozen whole in liquid nitrogen. Of the placentae that were weighed whole, three were randomly chosen. These three placentae were carefully dissected into their individual placental layers: mesometrial triangle/decidua, junctional zone, chorionic plate and labyrinth (Fig. 1.4).

2.4.4.1 Assessment of Fetal Growth and Weight Distribution

Anthropomorphic measurements of fetal growth were performed for each fetus of each litter. Fetuses were weighed whole and measurements of fetal crown-rump length, head circumference and abdominal circumference were recorded using a length of MERSILK® Ethicon suture tie (NuCare, Bedfordshire, UK) soaked in PBS (Kusinski *et al*, 2012; Fig. 2.5). Following this, the head was removed. Each individual body was weighed followed by its matching head and recorded (Appendix 7.1.2). Fetal growth trajectories were determined by plotting the average fetal weight. The individual fetal weights were pooled for all fetuses of that strain and/or treatment group. These weights were used to construct a histogram of fetal weight distribution using frequency distribution bin centres of 0.05g. A non-linear regression was performed with Gaussian distribution for each strain and/or treatment group which presented the data as a percentage of the total population. Clinically, fetal growth restriction is determined by calculating the lowest 5th percentile of predicted fetal weight (Nardozza *et al*, 2017). The lowest 5th percentile was determined in the WKY and vehicle control groups and the percentage of fetuses that fell below this threshold for other strain/treatment groups was calculated. If a recorded fetal weight fell into this category the fetus was diagnosed with growth restriction.

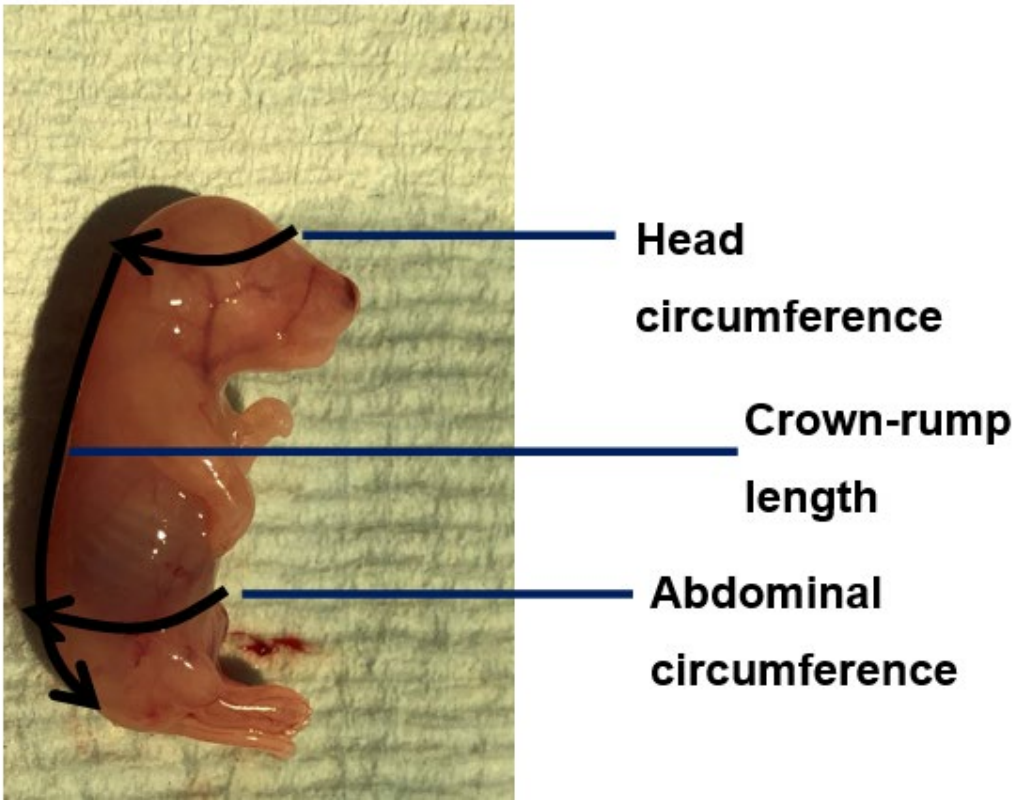

Figure 2.5: A Representation of Anthropomorphic Measurements of Fetal Growth

The morphometry of each fetus was measured using a length of MERSILK® Ethicon suture tie soaked in PBS and a ruler. Head circumference was measured just above the eyes and nose. Abdominal circumference was measured where the umbilical cord inserts into the abdomen. Crown-rump length was measured from the top of the head (intersecting with the head circumference) down to the base of the tail, following the curvature of the spine. This image depicts a GD18.5 SHRSP fetus.

2.4.5 Neonatal Sacrifice and Tissue Collection

Neonates were sacrificed on either day 1 or day 5 following birth by overdose of anaesthetic. Neonates were injected intra-peritoneally with 200µL of Dolethal 200mg/mL solution (pentobarbital sodium) followed by decapitation to confirm death by cessation of the circulation. The thoracic cavity was opened, and the neonatal heart, thoracic aorta and kidneys were dissected and snap frozen in liquid nitrogen before storage at -80ºC until they were used for RNA extraction (section 2.2.1).

2.5 Uterine Vascular Smooth Muscle Cell Culture

2.5.1 Primary Cell Isolation

Uterine arteries were dissected from non-pregnant and GD6.5 rats as described in section 2.4.3. Once dissected and stored in chilled F-12 Hams Nutrient Mix media [1mM L-glutamine, 14mM sodium bicarbonate, 1mM sodium pyruvate, supplemented with 100IU/mL penicillin, 100µg/mL streptomycin, 2mM L-glutamine] (all ThermoFisher Scientific, Paisley, UK) arteries were stored at 4ºC for up to one hour until use. The 4 artery segments from each animal (each artery from the left and right uterine horns halved) were divided into two eppendorfs and digested in F-12 media supplemented with 2mg/mL bovine serum albumin (Sigma, Dorset, UK), 250U/mL collagenase type-I (ThermoFisher Scientific, Paisley, UK or Worthington Biochemical, Berkshire, UK), 0.5U/mL elastase (Sigma, Dorset, UK) and 0.4mg/mL soybean trypsin inhibitor (Sigma, Dorset, UK) pre-incubated at 37ºC for five minutes to aid enzyme activation. During digestion, two artery segments from the same horn of the same animal were placed in 1mL of warmed enzyme supplemented F-12 media and incubated at 37ºC for 30-40 minutes with gentle agitation in a Biometra OV2 mini hybridisation oven (Thistle Scientific, Glasgow, UK). The incubation was halted when artery segments had softened and appeared 'fluffy'. The vessels were homogenised using a 1mL syringe and needles of increasing gauge size; 21G, 23G and 25G respectively. The vessels and digestion media were passed through each needle size five times in the same syringe. Homogenised arteries were centrifuged at 1200x*g* for three minutes at room temperature. The digestion media was removed, and the pellet resuspended in 500µL of pre-warmed, 37ºC complete F-12 media [100IU/mL penicillin, 100µg/mL streptomycin, 2mM L-glutamine, 10% v/v bovine serum albumin] (Gibco™ ThermoFisher Scientific, Paisley, UK). The primary cell suspension of 1mL per animal was split between 3 wells (300µL/well) in a 12-well culture plate and topped up with 1.7mL of complete F-12 media which was incubated at 37ºC with 5% CO_2 in a Heracell™ 240i CO_2 incubator (FisherScientific, Loughborough, UK). Each plate contained UAVSMCs isolated from 2 animals in triplicate. Of the remaining 6 wells, 3 were filled with 2mL of sterile PBS and 3 with 2mL of complete media to act as controls. Cell culture plates were incubated between 48-72 hours to allow for adhesion. Following adhesion, the media was changed to complete Dulbecco's Modified Eagles Medium (DMEM) with Glutamax™ supplement [4mM L-glutamine, 5.5mM D-glucose, 1mM sodium pyruvate, 44mM

sodium bicarbonate] (Gibco™ ThermoFisher Scientific, Paisley, UK) and 100IU/mL penicillin, 100µg/mL streptomycin, 2mM L-glutamine and 10% v/v fetal bovine serum.

2.5.2 Maintenance of the Primary Cell Line

Cells were monitored daily by visual inspection, and the culture medium was refreshed every 48-72 hours. Cells were used for live-cell fluorescent Ca^{2+} imaging when they reached 80% confluency at p0. To freeze cells, they were trypsinized and resuspended as above in 1mL complete DMEM media with 10% sterile dimethyl sulfoxide, a cryoprotective agent that maintains the cellular osmotic balance. This suspension was placed into a cryovial (Alpha-Laboratories, Hampshire, UK) which was placed into a room temperature Mr. Frosty™ Freezing Container (ThermoFisher Scientific, Paisley, UK) filled with isopropanol. The container was then placed in -80ºC conditions to ensure slow, uniform cooling of the cells to reduce intracellular crystal formation. Cells were removed from the Mr. Frosty containers after 24 hours and stored at -80ºC.

2.6 Statistical Analysis

Animals were assigned to different treatment or gestational groups randomly and following the ARRIVE (Animal Research: Reporting of *In Vivo* Experiments) guidelines (Kilkenny *et al*, 2010) for all *in vivo* studies. Results are presented as the mean ± the standard error of the mean (SEM) unless stated otherwise. Telemetry data obtained from the Ponemah system included hourly averages which were converted into 12-hour averages for each parameter to mimic the day/night cycle of lighting (section 2.3.1). Maternal and fetal data were compared between treatment and/or strain groups by restricted maximum likelihood (REML) mixed model effects analysis with Tukey's *post hoc* testing unless otherwise stated. For all analyses, *N* is used to represent the number of adult females and *n* is used to represent the number of individual offspring. The cycle threshold values of gene expression data obtained from Taqman® qPCR were normalised to the housekeeper gene, GAPDH (glyceraldehyde-3-phosphate dehydrogenase) to obtain delta cycle threshold (ΔCT) values. ΔCT values were used for statistical analysis using students t-tests. ΔCT values were used to express the relative quantity of gene expression by normalisation to the relevant control group (WKY non-pregnant or SHRSP vehicle control) and expressed as $2^{-\Delta\Delta CT}$. Statistical

analyses were conducted, and graphical data representations constructed using Prism 9.4.0 GraphPad Software© (California, USA). Statistical significance was determined by *p* value less than 0.05 with confidence intervals of 95%. Further information on specific statistical tests are detailed in the following results chapters.

Chapter 3: Optimisation and Characterisation of a Novel Rodent Model of Superimposed Pre-eclampsia

3.1 Introduction

Of all hypertensive disorders of pregnancy, pre-eclampsia superimposed on a background of pre-existing hypertension complicates 25% of cases of chronic hypertension during pregnancy (Brown *et al*, 2018a). SPE is defined clinically as the occurrence or worsening of proteinuria at 20 weeks or more of gestation in addition to pre-existing hypertension, or any other feature used to diagnose pre-eclampsia as outlined in Table 1.1 (Hutcheon *et al*, 2011; Magee *et al*, 2015; Vest and Cho, 2014). The prevalence of SPE is increasing, likely due to an increase in the presence of maternal risk factors in those of childbearing age such as increasing maternal age, multiparity, pre-existing cardiovascular disease and its comorbidities or an increased body mass index, among others (Agrawal and Wenger, 2020). Given the increased incidence of SPE, particularly in the Western world, detection of the disease is crucial as it can impact high risk individuals with pre-existing hypertension whose condition may deteriorate rapidly. This can be further complicated by the fact that those that are premenopausal are not routinely screened for hypertension throughout their entire reproductive period despite evidence that alterations in ovarian hormones play an important role in blood pressure regulation (Maric-Bilkan *et al*, 2014). Additionally, SPE can be difficult to distinguish from worsening of chronic hypertension. Indeed, pre-existing hypertension that could potentially develop to SPE can be masked in the first and second trimesters by the physiological pregnancy-associated decrease in blood pressure that naturally occurs (Khedagi and Bello, 2021).

Despite its significant impact, the pathology of SPE is poorly understood. As discussed in section 1.1.4.2, activation of the renin-angiotensin-aldosterone system (RAAS) is required for a successful pregnancy. This functions to support the expansion of the cardiovascular system and contributes heavily to the increased blood volume and cardiac output observed in healthy pregnancy (Lumbers *et al*, 2019). In order to maintain the RAAS during gestation extra-renal sources of renin are utilised. The largest extra-renal sources of renin are the ovaries and placenta, which regulate the local RAAS and increased production of ANGII (angiotensin II) during gestation (Patel *et al*, 2017; Cheung and Lafayette, 2013). Paradoxical to the rise in ANGII production, there is diminished sensitivity to its pressor response (Cheung and Lafayette, 2013). Hypertensive disorders of pregnancy have been associated with dysregulation of the RAAS and subsequent

hypersensitivity to ANGII which contributes to the elevated maternal blood pressure, proteinuria, endotheliosis and volume retention characteristic of these disorders (Hussein and Lafayette, 2014). Additionally, ANGII has been shown to induce angiogenesis via interaction with one of its receptors, AT_1R- a mechanism that may underlie spiral artery transformation and healthy development of the placenta, thus dysregulation of the RAAS may also affect uterine vascular remodelling (Lumbers and Pringle, 2014).

Unsurprisingly, ANGII infusion has been utilised by several groups as an experimental model of hypertension in normotensive rodents to induce cardiac, renal and vascular pathologies (Nyugen *et al*, 2015; Ruddy *et al*, 2017; Blanc *et al*, 2004). Far fewer studies have investigated the impact of ANGII infusion during pregnancy, particularly the effects on maternal outcomes. One such study by Shirasuna and colleagues (2015), found that high dose ANGII infusion in normotensive wild-type and immune deficient mice resulted in maternal hypertension and proteinuria and reduced fetal weight that was associated with placental inflammation. Similar maternal effects were observed by Xue *et al* (2017), who found that male offspring of pregnant Sprague-Dawley rats infused with ANGII had an increased pressor response to ANGII in adulthood that was associated with an increased renal nerve activity and abundance of proinflammatory cytokines in the brain. Other studies have utilised transgenic models (section 1.4.5) that stimulate ANGII overproduction in the placenta (Bohlender *et al*, 2000; Hering *et al*, 2010). These have shown that an upregulation of placental-specific ANGII results in similar maternal and fetal outcomes to ANGII infusion. Together, these studies share the consensus that an increase in both local and circulating ANGII during gestation results in the clinical features commonly associated with pre-eclampsia and SPE in humans.

As previously discussed in section 1.4.1.1, the stroke-prone spontaneously hypertensive rat (SHRSP) demonstrates an elevated blood pressure throughout gestation with evidence of reduced uteroplacental blood flow and fetal and placental abnormalities conjunctive with common hypertensive complications in human pregnancy (Small *et al*, 2016a). Furthermore, SHRSP demonstrate a failure to respond to the cardiovascular demands of pregnancy even in the absence of chronic hypertension (Small *et al*, 2016b). Interestingly, these complications do not prevent the SHRSP from successfully carrying their fetuses

to term, producing viable offspring. Morgan *et al* (2018) have shown that the SHRSP can be stressed via the infusion of ANGII to develop a superimposed pre-eclamptic phenotype alongside chronic hypertension. This novel rodent model of superimposed pre-eclampsia was initially characterised at a low dose of 500ng/kg/min and a high dose of 1000ng/kg/min ANGII which was delivered subcutaneously from GD10.5 to GD18.5 via osmotic mini pump. Whilst the model was successful in inducing changes associated with SPE such as reduced uteroplacental flow (Morgan *et al*, 2018), the low dose failed to accurately recapitulate the disease in full whilst the high dose was associated with a reduced survival rate, early removal from the study and subsequent welfare concerns.

3.2 Hypothesis & Aims

We hypothesised that the rodent model of superimposed pre-eclampsia developed by Morgan and colleagues (2018) could be optimised and fully characterised at a dose of 750ng/kg/min of ANGII following the same timeline and protocols previously published.

We aimed to achieve this by delivering an insult to the cardiovascular system at mid-gestation by surgically implanting an osmotic mini pump in pregnant SHRSP dams to mimic the 20-week time point in human gestation. Once implanted the mini pump subcutaneously infused ANGII until the end of the study. We investigated both maternal and fetal outcomes in response to SPE development in treated SHRSP rats. A small number of animals were allowed to progress to parturition. This allowed us to additionally investigate the neonatal response to ANGII *in utero*. We hypothesised that a dose of 750ng/kg/min ANGII would have a detrimental impact on maternal, fetal and neonatal outcomes and would mimic the human phenotype of the disease without causing any significant welfare concerns.

3.3 Materials and Methods

Animals were housed and mated as previously described in section 2.3.1. Phenotypic measurements including blood pressure (section 2.3.4), blood sampling (2.3.6) echocardiography (2.3.7) and uterine artery doppler assessment (2.3.8), were taken one week prior to mating (pre-pregnancy, PP) and at gestational days (GD) 6.5, 14.5 and 18.5. Metabolic cage urine sampling was conducted at PP and on GD 6.5 and 18.5 to analyse proteinuria (sections 2.2.4, 2.3.5). A subset of SHAM and ANGII animals underwent telemetry probe implantation surgery (section 2.3.3) two weeks prior to time mating to provide a continuous measurement of blood pressure, heart rate and activity throughout gestation. These animals were allowed to progress to parturition and their offspring used to assess the neonatal response to hypertensive pregnancy. Maternal, fetal and placental tissues and measurements were collected at GD18.5, just prior to the fall in maternal blood pressure seen at the end of SHRSP pregnancy (Small *et al*, 2016a). Full details of tissue collection and dissection can be found in sections 2.4.2, 2.4.3, 2.4.4 and 2.4.5. Placentae were harvested and either fixed for histological analysis or snap frozen to investigate gene expression and reactive oxygen species generation. Further details of these methods can be found in the general materials and methods (sections 2.2.3, 2.2.6). Neonatal tissues were collected as detailed in section 2.4.5 to investigate potential changes in gene expression (2.2.3) in response to hypertensive pregnancy.

3.3.1 Angiotensin II Infusion via Osmotic Mini Pump

ANGII at a dose of 750ng/kg/min or 0.9% w/v NaCl saline solution were delivered via osmotic mini pumps implanted subcutaneously. The dose was determined using results and guidance from Morgan *et al* (2018) who developed the model. Prior to pump implantation, SHRSP dams were weighed on GD9.5 and randomly assigned to one of two groups: SHAM (saline) or ANGII. A group of age-matched control WKY dams were weighed for saline pump implantation.

ANGII or saline solutions were infused at an approximate constant rate of 0.5µL/hr from GD10.5 for 8 days until termination at GD18.5 using AZLET® 2002 osmotic mini pumps (Charles River, Kent, UK). The flow rate was constant for 14 days, thus ANGII delivery was stable throughout gestation. Preparation of the ANGII solution was carried out in a sterile environment and the pump was handled whilst

wearing sterile, latex- and powder-free gloves at all times. A stock ANGII solution of 50µg/µL was created by dissolving 50mg of human ANGII (Sigma Aldrich, Dorset, UK) in NFW. The volume reservoir of the AZLET® 2002 mini pump is 200µL, therefore doses were prepared at 300µL to allow for overfilling of the pump to ensure complete filling and that no air was present in the pump. Individual doses for each animal were calculated using the weight obtained on GD9.5 and assigned group as well as pump flow rate. Once prepared, mini pumps were stored overnight at room temperature in sterile 5mL Sterilin™ containers filled with sterile saline solution. This was to prime the pumps to ensure that upon implantation the pump would begin to deliver either ANGII or saline immediately.

3.3.2 Mini Pump Implantation Surgery

Surgery was carried out on GD10.5 under standard aseptic conditions. SHRSP and WKY dams were anaesthetised as in section 2.3.2 and maintained at 2% isoflurane in 1.5L/min of oxygen in a prone position. Prior to the procedure animals received 5mg/kg carprofen analgesic subcutaneously. The right flank of the animal was shaved, cleaned and swabbed with a 4% w/v chlorhexidine gluconate solution (HiBiScrub®). A superficial incision approximately 3cm in length was made in the skin parallel to the shoulder with surgical scissors. This incision was lifted carefully with toothed forceps and the muscle and skin layers gently separated by opening and closing blunt tipped surgical scissors to create a subcutaneous pocket for the pump. The mini pump was removed from saline solution and carefully placed within this subcutaneous pocket, with the flow moderator pointing towards the rear of the animal. The incision was closed by suturing with VICRYL® Ethicon re-absorbable sutures (NuCare, Bedforshire, UK). Animals were then recovered in their home cages. Welfare checks were carried out daily from this point until study end.

3.4 Results

3.4.1 The Maternal Response to Hypertensive Pregnancy

3.4.1.1 ANGII Influence on Changes in Maternal Weight

A normal healthy pregnancy is associated with a reversible increase in weight due to development of the fetus and increases in maternal adipose, specific organs and blood volume. There was a significant treatment effect of ANGII on body weight across gestation (p<0.0001), non-gravid weight (p<0.0001) and the percentage change in body weight (p=0.0314). WKY control dams exhibited a gradual increase in weight throughout gestation (196.3±7.2g PP vs 252.3±4.4g GD18.5). SHRSP vehicle treated dams also experienced a gradual increase in maternal weight with a similar trajectory (142.6±3.4g PP vs 219.1±4.8g GD18.5) though they weighed significantly less than WKY dams (p<0.0001). Though dams receiving ANGII exhibited a pregnancy-associated increase in weight from PP (148.9±4.5g) to GD6.5 (183.0±3.9g), this plateaued once the pump was inserted on GD10.5 with only a slight increase noticeable at GD18.5 (192.5±7.1g). By GD18.5, ANGII dams weighed significantly less than SHAM (p<0.05). ANGII dams weighed significantly less than WKY dams across pregnancy (p<0.0001, Fig. 3.1A). Both SHAM and ANGII groups had significantly lower non-gravid weights (maternal weight independent of the uteroplacental unit) when compared to the WKY control group (p<0.001, Fig. 3.1B). The percentage change in body weight across gestation revealed that there was a statistically significant strain-dependant difference between WKY (15.6±1.6%) and SHAM (21.7±0.7%) dams at GD6.5 (p<0.05). Though there was no significant difference between WKY and ANGII dams at GD6.5, the percentage of weight gain was similar in SHAM and ANGII dams (22.0±2.5%). Following pump implantation, ANGII-infused dams saw a reduction in the percentage of weight gain such that by GD18.5 both ANGII (34.3±3.4%) and WKY (30.7±3.3%) dams had a significantly reduced weight gain that was not seen in SHAM (49.0±3.2%) treated animals (p<0.05, Fig. 3.1C). Thus, infusion of ANGII in mid-gestation led to a reduction in weight gain when compared to SHAM.

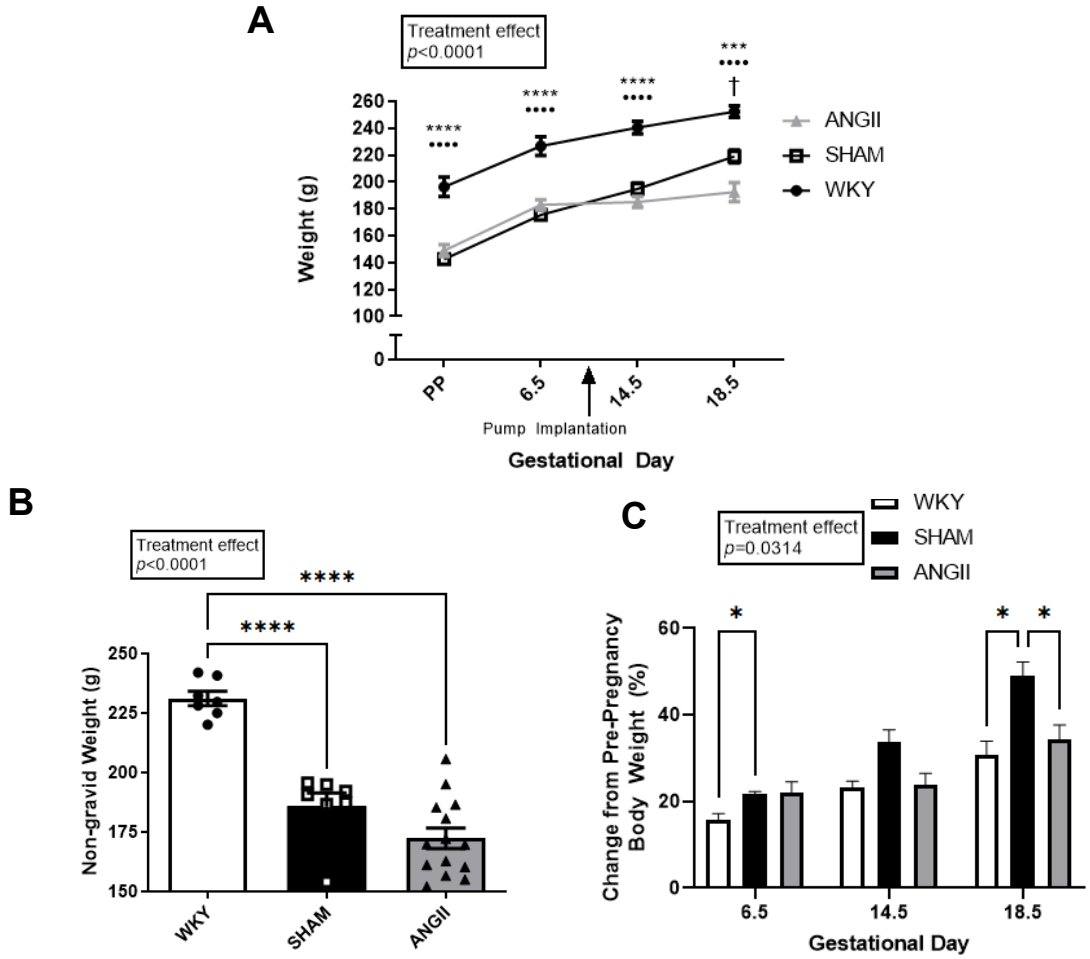

Figure 3.1: Changes in Maternal Weight from Pre-Pregnancy to Term

Maternal weight was recorded prior to and throughout pregnancy. There was a significant treatment effect of ANGII on body weight across gestation (p<0.0001), non-gravid weight (p<0.0001) and the percentage change in body weight (p=0.0314). (A) The weight change across pregnancy, including the uteroplacental unit, showed all groups experienced an increase in maternal weight prior to mini pump implantation (GD10.5) though there was a significant strain-dependant effect between WKY and SHAM/ANGII dams (****p<0.0001/••••p<.0001). Following pump implantation, both WKY (N=7) and SHAM (N=6) dams showed a continued increase in weight, though SHAM dams weighed significantly less than WKY dams at GD18.5 (****p<0.0001). In dams receiving ANGII (N=12), maternal weight plateaued between pump implantation and GD14.5. ANGII dams showed a further slight increase in weight by GD18.5 but weighed significantly less than WKY and SHAM animals (•••p<0.001, †p<0.05). Data analysed using restricted maximum likelihood mixed-effects analysis with Tukey's *post hoc* testing. (B) The pregnancy-independent maternal weight at GD18.5 was significantly lower in both SHAM and ANGII groups when compared to WKY controls (****p<0.0001). Data analysed by one-way ANOVA with Tukey's *post hoc* testing. (C) The percentage change in body weight (relative to PP measures) showed that at GD6.5 there was a significant strain-dependant difference between WKY and SHRSP (*p<0.05). Following ANGII infusion, the rate of weight gain slowed in infused SHRSP dams such that both WKY and ANGII had a significantly lower percentage weight gain than SHAM at GD18.5 (*p<0.05). Significant main effects of ANGII treatment were found for all measures. Data analysed by restricted maximum likelihood mixed effects analysis with Tukey's *post hoc* testing.

3.4.1.2 Blood Pressure Profile of ANGII-Infused SHRSP Dams

Systolic blood pressure was monitored throughout gestation in all groups by tail-cuff plethysmography; detailed in the general materials and methods in section 2.3.4. A small subset of SHAM and ANGII animals were monitored using surgically implanted radio-telemetry probes (section 2.3.3). All SHRSP dams were borderline hypertensive prior to pregnancy when compared to WKY dams as a reference strain (SHAM: 145.1±5.6mmHg, ANGII: 142.1±4.1mmHg, WKY: 137.2±4.8mmHg, ns.). Figure 3.2A illustrates the blood pressure profile of each group at PP and GD6.5, 14.5 and 18.5 by tail-cuff. There was a significant main treatment effect of ANGII on blood pressure (p=0.002). WKY mothers showed an initial decrease in systolic blood pressure (SBP) between PP and GD6.5 (128.9±4.3mmHg GD6.5), followed by a rise (143.1±10.5mmHg) before a final small decrease at GD18.5 (139.8±7.1mmHg). By contrast, SHAM mothers exhibited an early pregnancy increase in SBP (153.1±4.3mmHg GD6.5) before a gradual decline in SBP by GD18.5 (124.1±3.3mmHg). Animals that received ANGII treatment shared a similar SBP profile to SHAM animals from PP to GD6.5 (145.1±8.3mmHg). Upon pump implantation on GD10.5 this group experienced a worsening of their hypertension by GD14.5 (171.6±5.4mmHg, p<0.05 vs WKY) with SBP continuing to rise until GD18.5 (181.2±7.6mmHg, p<0.0001 vs SHAM, p<0.001 vs WKY). The systolic, diastolic (DBP) and mean arterial (MAP) blood pressure profiles of animals that underwent telemetry surgery mirrored the results from tail-cuff (Fig. 3.2B-D). Both SHAM and ANGII dams shared a similar profile from PP to the time of mini pump implantation, though both groups tended have higher blood pressure levels than those that were monitored via tail-cuff. Following mini pump surgery, SHAM dams showed a gradual decrease in blood pressure with a small increase at parturition. ANGII dams demonstrated an immediate increase in blood pressure followed by a decrease from GD13.5 to GD16.5, at which time blood pressure began to continuously rise until parturition. Heart rate was also monitored in these groups. There were no significant differences in heart rate throughout gestation between SHAM and ANGII dams. ANGII animals appeared to have a loss of diurnal regulation of heart rate following pump implantation until GD13.5 where diurnal differences were restored.

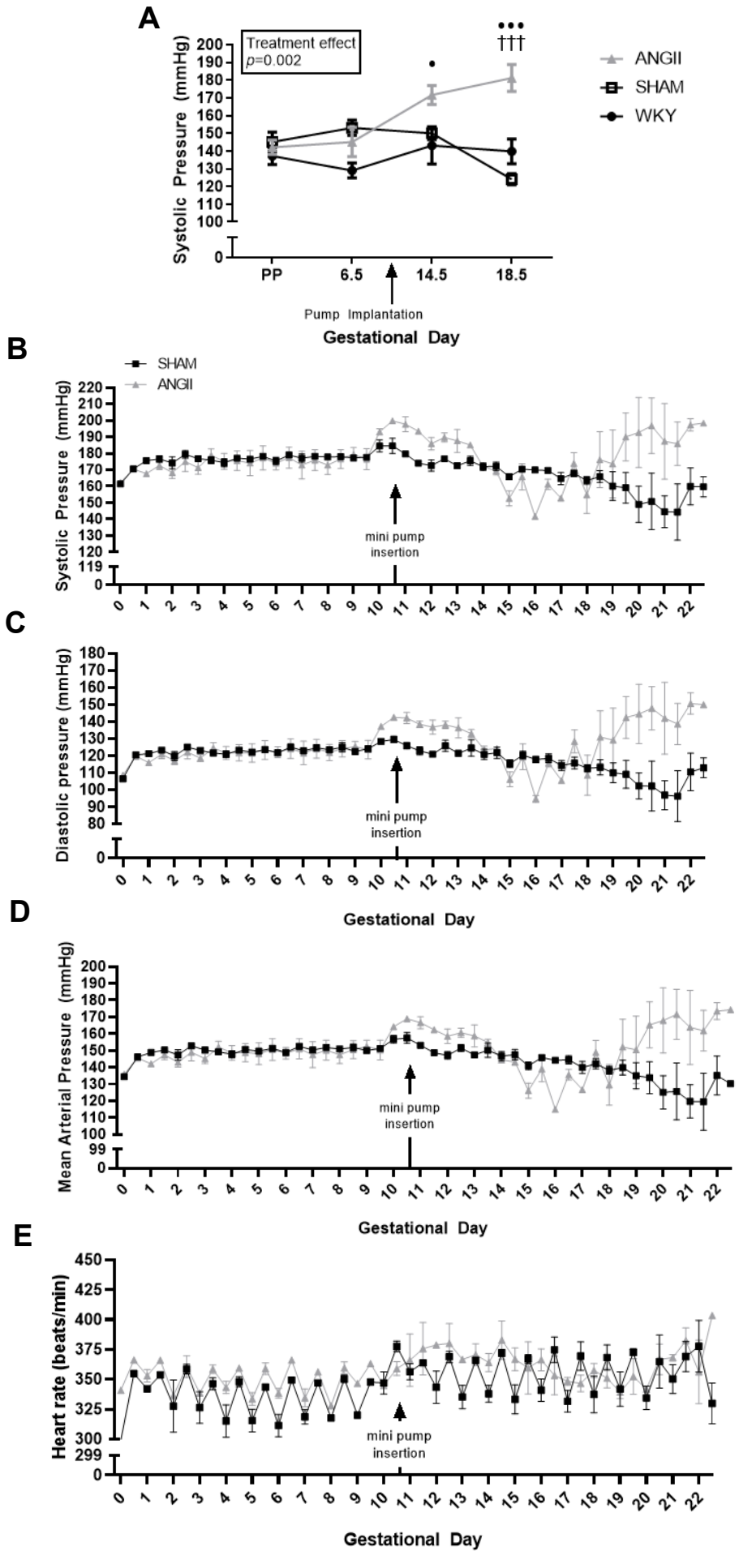
A
Treatment effect
p=0.002
Systolic Pressure (mmHg)
ANGII
SHAM
WKY
PP
6.5
14.5
18.5
Pump Implantation
Gestational Day
B
SHAM
ANGII
Systolic Pressure (mmHg)
mini pump insertion
C
Diastolic pressure (mmHg)
mini pump insertion
Gestational Day
D
Mean Arterial Pressure (mmHg)
mini pump insertion
Gestational Day
E
Heart rate (beats/min)
mini pump insertion
Gestational Day

Figure 3.2: The Maternal Blood Pressure Profile from Pre-Pregnancy to Term in Response to ANGII Treatment

Systolic blood pressure was recorded at pre-pregnancy (PP) and three specific gestational time points (pre ANGII: GD6.5, post-ANGII: 14.5 and 18.5) in WKY (nuclease free water), SHRSP SHAM (saline) and ANGII treated dams (750ng/kg/min). (A) Alterations in SBP across pregnancy measured by tail-cuff plethysmography. SHRSP dams in both groups were borderline hypertensive prior to pregnancy in comparison to normotensive WKY dams as a reference strain. There was a significant main treatment effect of ANGII on blood pressure (p=0.002). At GD6.5 WKY (N=8) dams showed a decrease in SBP whilst SHAM (N=7) and ANGII (N=14) dams showed a rise in SBP (*p<0.05). By GD14.5 SHAM SBP had fallen to a range comparable to WKY. ANGII animals suffered a further increase in SBP (•p<0.05) that continued to GD18.5 whilst SBP in both SHAM and WKY dams continued to fall gradually (•••/†††p<0.001). Data analysed using restricted maximum likelihood mixed-effects analysis with Tukey's*post hoc* testing. Blood pressure profiles for systolic (B), diastolic (C) and mean arterial (D) pressure were recorded prior to and continuously throughout pregnancy in a small number of SHAM (N=2) and ANGII (N=2) animals via implanted radiotelemetry probes. Heart rate (D) was also recorded. The profiles of SBP, DBP and MAP aligned with the measurements generated by tail-cuff. Heart rate did not differ significantly between SHAM and ANGII animals, however between GD10.5 and GD13 ANGII animals appeared to lose diurnal variation in heart rate. This was restored on GD13 and remained comparable to SHAM animals until parturition where SHAM animals exhibited a sharp decline in heart rate whilst ANGII animals a sharp increase. No statistical testing.

3.4.1.3 Cardiac Function in Response to ANGII Treatment in SHRSP Dams

Echocardiographic assessment of cardiac function was carried out prior to and throughout pregnancy in all groups (section 2.3.7). Significant main treatment effects of ANGII were found in stroke volume (p=0.0230), cardiac output (p=0.0011) and relative wall thickness (p=0.0180). Figure 3.3A shows that in a normotensive pregnancy, stroke volume remains stable as pregnancy progresses (0.26±0.03mL PP vs 0.28±0.05mL GD18.5) whilst cardiac output tended to gradually increase (81.02±9.07mL/min PP vs 97.50±20.55mL/min GD18.5, Fig. 3.3B). SHAM mothers also shared a relatively stable stroke volume across pregnancy (0.26±0.01mL PP vs 0.25±0.02mL GD18.5), however, cardiac output did not increase in this group. Rather, it also remained constant throughout gestation (95.67±8.7mL/min PP vs 84.64±11.1mL/min GD18.5). ANGII treatment in SHRSP dams resulted in a marked fall in stroke volume by GD14.5, though this was not significant, (0.25±0.03mL PP vs 0.17±0.02mL GD14.5, p=0.06) that persisted until time of sacrifice (0.19±0.02mL). A similar pattern was observed in cardiac output in this group, with a significant drop following mini pump implantation (74.93±8.15mL/min PP vs 52.28±7.59mL/min GD14.5, p<0.05 vs WKY). This effect was sustained though cardiac output increased somewhat by GD18.5 (61.86±5.89mL/min, p<0.05 vs WKY). Relative wall thickness (RWT) was used as a measure of left ventricular hypertrophy and therefore dysfunction in pregnant dams (Fig. 3.3C). There were no significant differences in RWT across gestation in WKY or SHAM groups, however RWT increased significantly on GD14.5 in the ANGII treated group (p<0.05, 0.48±0.02 PP vs 0.63±0.06mm GD14.5). On GD14.5 RWT was significantly increased in ANGII animals when compared to WKY (0.44±0.03mm) and SHAM (0.41±0.03mm, p<0.05 vs WKY, p<0.01 vs SHAM). By GD18.5 there were no significant differences between groups in RWT, though the ANGII had a higher RWT than WKY or SHAM groups (0.49±0.06mm WKY; 0.39±0.04mm SHAM; 0.56±0.07mm ANGII). Ejection fraction (Fig. 3.3D) was not significantly different across pregnancy in each of the groups.. This effect was also observed in fractional shortening (Fig. 3.3E). Echocardiographic estimations of left ventricular mass were normalised to tibial length, as upon reaching sexual maturity at ~12 weeks tibial growth slows significantly such that tibial length was stable for the duration of the study, and no changes were observed over the course of gestation or between groups (Fig.

3.3F). The left ventricles were dissected and weighed at time of sacrifice. These weights were normalised to tibial length and were in agreement with echocardiography data (Fig. 3.3G). Further investigation revealed no significant effect of ANGII infusion on blood flow through the mitral valve, a measure of diastolic dysfunction (Fig. 3.3H). However, there appeared to be a strain dependant effect at GD18.5 with SHAM dams (2.76±0.84) showing a higher E:A ratio than WKY (1.54±0.14) on GD18.5 that was not observed in the ANGII group (1.97±0.33). This strain dependent difference may also be present in the deceleration time of the E wave between WKY and SHRSP animals at pre-pregnancy, with a potentially increased deceleration time in WKY compared to ANGII dams (Fig. 3.3I, 68.797±5.852msec WKY; 49.984±3.241msec ANGII).

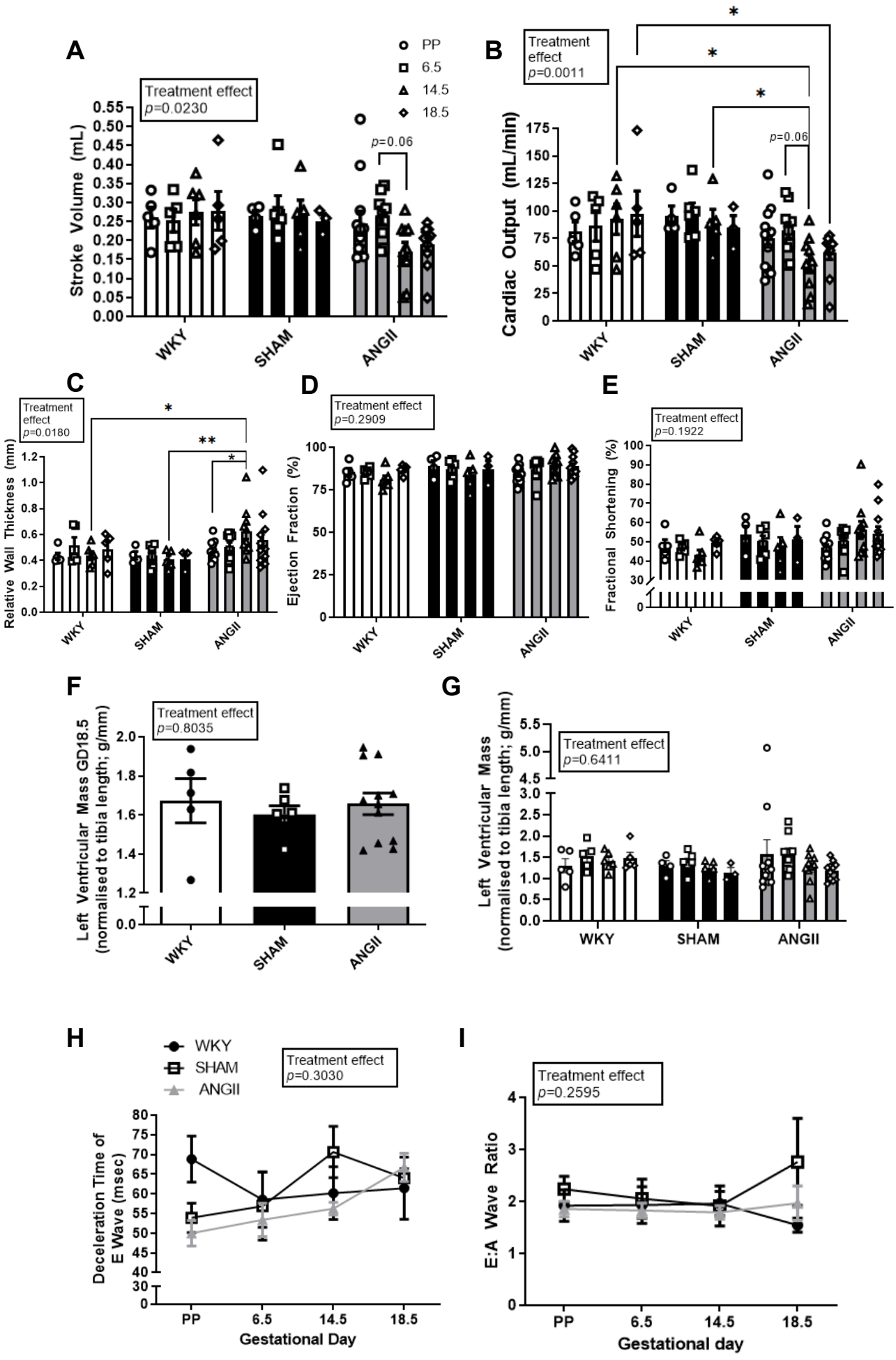
A
PP
6.5
14.5
18.5
Treatment effect
p=0.0230
Stroke Volume (mL)
p=0.06
WKY
SHAM
ANGII
B
Treatment effect
p=0.0011
Cardiac Output (mL/min)
p=0.06
C
Treatment effect
p=0.0180
Relative Wall Thickness (mm)
D
Treatment effect
p=0.2909
Ejection Fraction (%)
E
Treatment effect
p=0.1922
Fractional Shortening (%)
F
Treatment effect
p=0.8035
Left Ventricular Mass GD18.5 (normalised to tibia length; g/mm)
G
Treatment effect
p=0.6411
Left Ventricular Mass (normalised to tibia length; g/mm)
H
WKY
SHAM
ANGII
Treatment effect
p=0.3030
Deceleration Time of E Wave (msec)
Gestational Day
I
Treatment effect
p=0.2595
E:A Wave Ratio
Gestational day

Figure 3.3: Echocardiographic Estimations of Cardiac Function and Left Ventricular Mass Pre- and Post-ANGII Infusion

Echocardiography was carried out pre-pregnancy (PP) and on GD6.5, 14.5 and 18.5. Significant main treatment effects of ANGII were found in stroke volume (p=0.0230), cardiac output (p=0.0011) and relative wall thickness (p=0.0180). (A) Stroke volume remained stable throughout pregnancy in WKY (N=6) and SHAM (N=6) but decreased following ANGII (N=12) infusion in the treatment group (p=0.06). (B) Cardiac output gradually increased during the course of pregnancy in WKY dams. SHAM mothers experienced an initial increase followed by a decrease in cardiac output following mini pump surgery. ANGII infusion resulted in a significant decrease in cardiac output compared to WKY and SHAM that was not recovered by GD18.5 (*p<0.05). (C) RWT was significantly increased at GD14.5 in ANGII dams when compared to WKY dams (*p<0.05) as was ejection fraction. Ejection fraction as also increased relative to SHAM (*p<0.05) (D). This was also observed in fractional shortening (E). There were no differences in left ventricular mass (F,G) or mitral valve function (H,I) as a result of ANGII infusion. Data analysed using restricted maximum likelihood mixed-effects analysis with Tukey's *post hoc* testing or one-way ANOVA with Tukey's *post hoc* testing, as appropriate.

3.4.1.4 Uterine Artery Blood Flow Measured *In Vivo*

Uterine artery blood flow was analysed in the uterine artery using Doppler ultrasound imaging throughout gestation (section 2.3.8, Fig. 3.4A). Arterial blood flow was determined by calculating the systolic/diastolic (S/D, Fig. 3.4B) ratio and the resistance index (RI, Fig. 3.4C). A significant main treatment effect of ANGII was noted for RI (p<0.001) but not S/D. RI was significantly increased at GD18.5 in ANGII dams (0.57±0.02) in comparison to WKY dams (0.38±0.02, p<0.01). S/D was not significantly different between WKY, ANGII and SHAM animals following mini pump implantation. RI was significantly increased in ANGII (5.73±0.66) versus SHAM (3.01±0.32) at GD6.5 prior to surgery (p<0.05). This may have been due to operator technical error or poor image quality as at GD6.5 there was no difference in treatment between the groups. Similar to ANGII treated mothers, SHAM mothers also showed a significantly increased RI at GD18.5 when compared to WKY mothers (0.62±0.05, p<0.05).

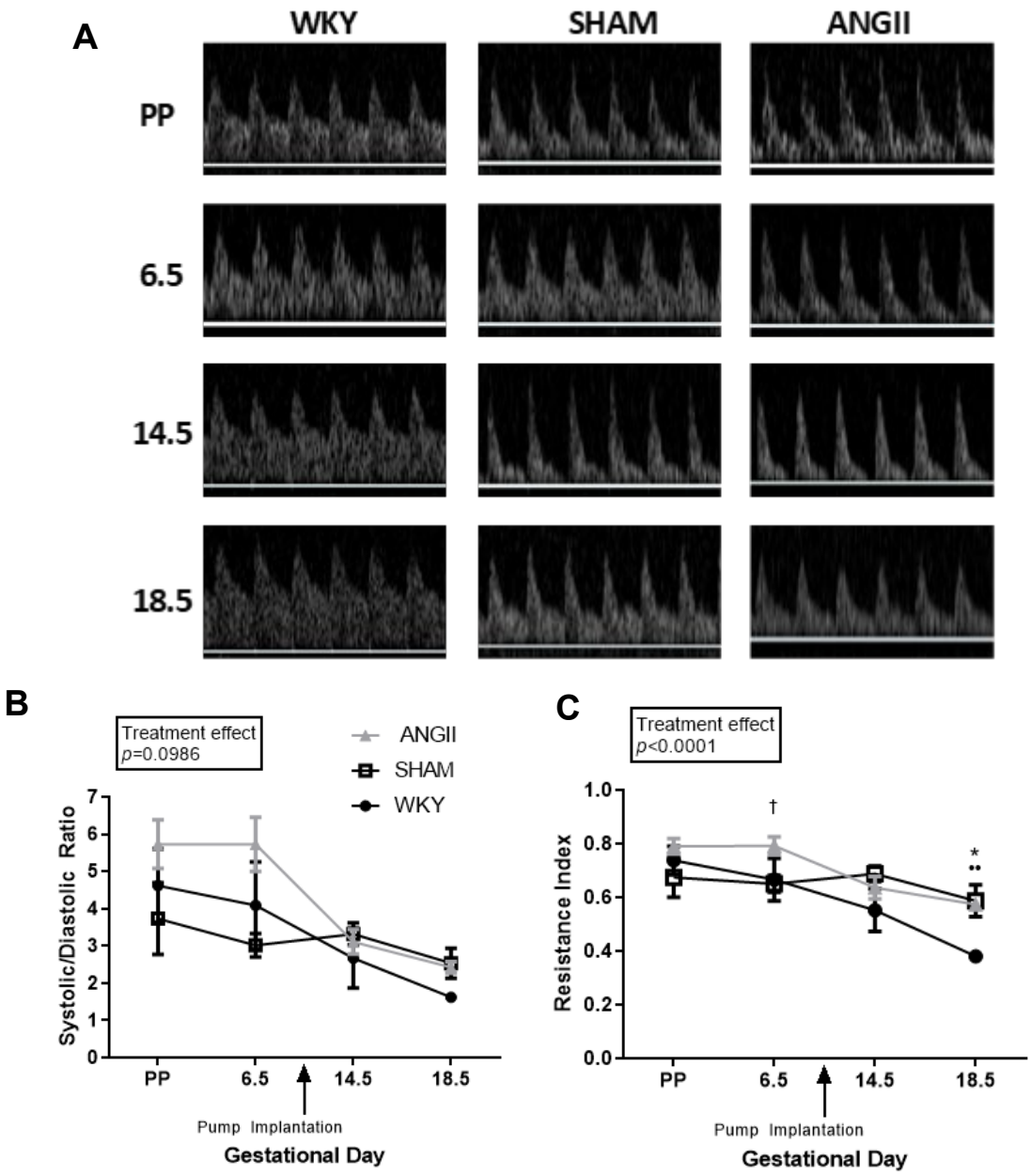

Figure 3.4: Pulse Wave Doppler Ultrasound Assessment of the Uterine Artery

Blood flow through the uterine artery was assessed by analysing waveform measurements captured prior to and throughout pregnancy. (A) Representative examples of these waveforms. A significant main treatment effect of ANGII was noted for RI (p<0.001) but not S/D. (B) Peak end systolic and diastolic volumes were calculated as detailed in the methods and expressed as a ratio. S/D was not different between ANGII (N=12) versus WKY (N=6) or SHAM (N=6) at GD18.5. (C) Resistance index was calculated using the peak end systolic and diastolic volumes. RI was significantly increased in both SHAM and ANGII mothers compared to WKY mothers at GD18.5 (*p<0.05, ••p<0.01). RI was significantly increased in ANGII versus SHAM groups on GD6.5 (†p<0.05). Data analysed using restricted maximum likelihood mixed-effects analysis with Tukey's *post hoc* testing, where appropriate.

3.4.1.5 Influence of ANGII Infusion on the Renal System

Twenty-four hour water intake and urine output were measured at pre-pregnancy (PP) and on GD6.5 and 18.5 using metabolic cages (2.3.5). There was a significant main treatment effect of ANGII on water intake (p=0.0089), urine output (p=0.0001) and water intake proportional to urine output (p=0.0003). There were no differences in water intake in early pregnancy (Fig. 3.5A). By GD18.5, water intake was significantly decreased in SHAM versus WKY and ANGII groups (33.3±0.8mL, 52.6±7.5mL and 53.4±3.1mL, respectively, p<0.001 SHAM vs WKY, p<0.0001 SHAM vs ANGII). A similar pattern was observed in urine output (Fig. 3.5B), which was significantly decreased at GD6.5 (p<0.05) and 18.5 (p<0.0001) in SHAM mothers compared to WKY mothers (. At GD18.5 urine output was significantly increased in ANGII versus SHAM mothers (33.8±2.9mL vs. 12.29±0.8mL, p<0.0001). The effect of ANGII treatment on urine output was preserved when corrected for fluid intake and expressed as a proportional urine excretion (Fig. 3.5C, GD6.5: p<0.05 SHAM vs WKY, GD18.5: p<0.0001 SHAM vs WKY, p<0.001 SHAM vs ANGII).

Urinary samples collected at the time points mentioned previously were analysed to determine the albumin:creatinine ratio (ACR, Fig. 3.5E) as an indication of proteinuria (2.2.4). ACR appeared to increase over the course of pregnancy in WKY animals (1.26±0.24µg/µmol/L PP vs 3.93±0.40µg/µmol/L GD18.5, ns.) whilst SHAM animals saw an apparent decrease across pregnancy (0.34±0.14µg/µmol/L PP vs 0.16±0.01µg/µmol/L GD18.5, ns.). ACR seemed to increase following ANGII infusion in SHRSP dams (0.39±0.06µg/µmol/L PP vs 163.06±98.6µg/µmol/L GD18.5, p<0.01). This increase appeared to far exceeded levels experienced by WKY and SHAM dams with ACR increased at GD18.5 relative to both.

Kidney morphology was assessed following sacrifice using picrosirius red staining (Fig. 3.5D). The assessment of positive staining was restricted to the cortex and medulla regions and expressed as a percentage of total kidney area (Fig. 3.5F). There was a significant main treatment effect of ANGII on picosirius red staining within the kidneys (p=0.0215). Positive staining was markedly increased in SHRSP dams that received ANGII in comparison to SHAM dams (27.80±7.23% vs 3.32±0.63%, *p<0.05). Though positive staining was higher in kidneys from ANGII

treated SHRSP than in WKY kidneys (12.73±3.88%) this was not statistically significant.

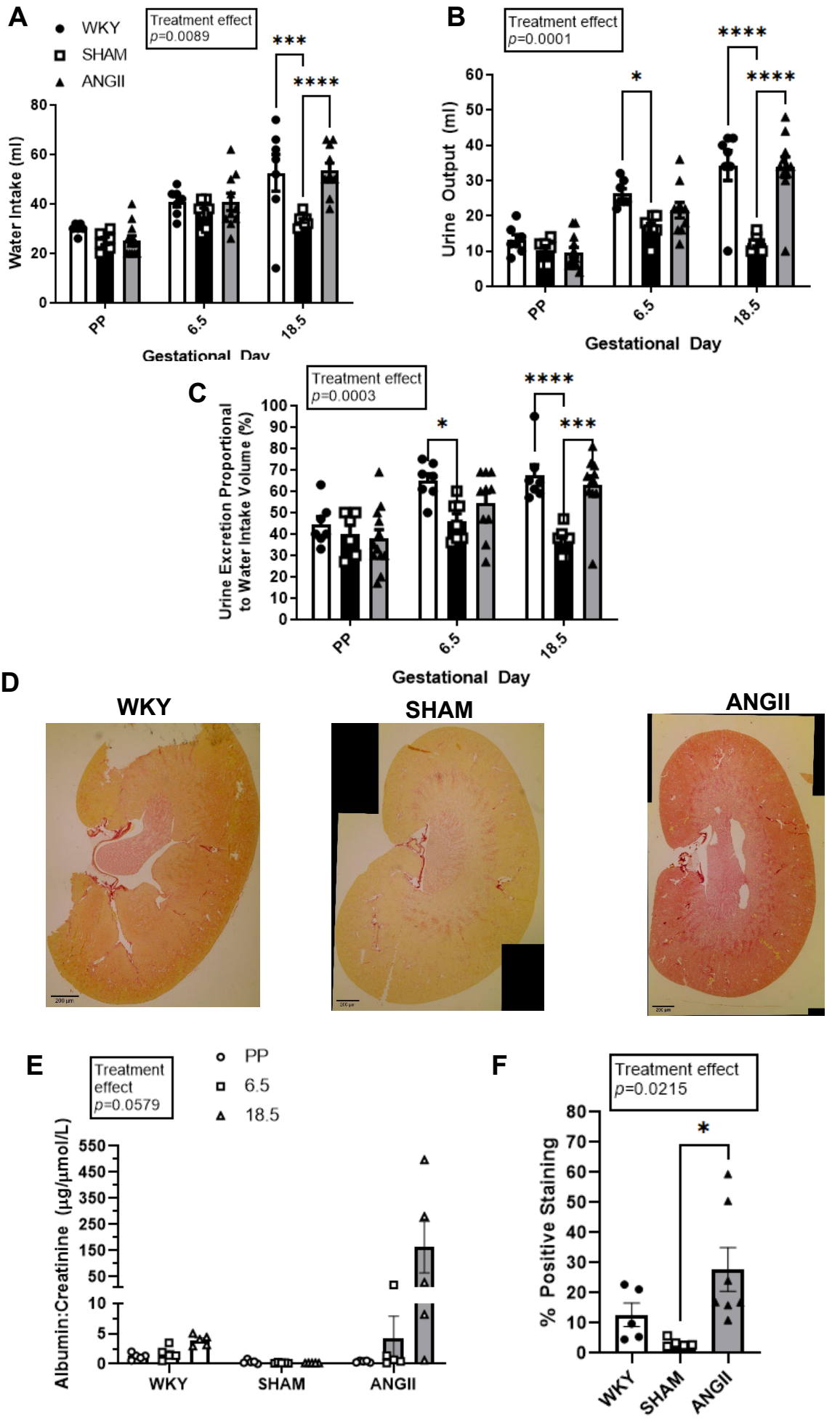
A
WKY
SHAM
ANGII
Treatment effect
p=0.0089
***
****
Water Intake (ml)
0
20
40
60
80
PP
6.5
18.5
Gestational Day
B
Treatment effect
p=0.0001
*
****
****
Urine Output (ml)
0
10
20
30
40
50
60
PP
6.5
18.5
Gestational Day
C
Treatment effect
p=0.0003
*
****
***
Urine Excretion Proportional to Water Intake Volume (%)
0
10
20
30
40
50
60
70
80
90
100
PP
6.5
18.5
Gestational Day
D
WKY
SHAM
ANGII
E
Treatment effect
p=0.0579
PP
6.5
18.5
Albumin:Creatinine (µg/µmol/L)
0
5
10
50
150
250
350
450
550
WKY
SHAM
ANGII
F
Treatment effect
p=0.0215
*
% Positive Staining
0
10
20
30
40
50
60
70
80
WKY
SHAM
ANGII

Figure 3.5: Influence of ANGII Infusion on Kidney Function and Morphology

Metabolic cages were used to collect twenty-four hour measurements of water intake and urine output prior to and throughout pregnancy. There was a significant main treatment effect of ANGII on water intake (p=0.0089), urine output (p=0.0001) and water intake proportional to urine output (p=0.0003). (A) Water intake was significantly increased in WKY (N=7) and ANGII (N=12) dams at GD18.5 compared to saline treated SHAM N=8) dams (***p<0.001, ****p<0.0001). (B) Urine output was significantly decreased during early pregnancy in SHAM mothers versus WKY (GD6.5, *p<0.05). Urine output was significantly lower in SHAM animals than in WKY or ANGII treated animals at GD18.5 (****p<0.0001). This effect was preserved when urine output was corrected for fluid intake (C). Data analysed by restricted maximum likelihood mixed-effects analysis with Tukey's *post hoc* testing. (D) Representative images of positive picrosirius red staining in kidneys from all groups. (E) ACR was significantly increased following ANGII (N=5) infusion and was significantly higher than WKY (N=5) or SHAM (N=5) (GD18.5, **p<0.01). Data analysed by two-way ANOVA with Tukey's *post hoc* testing, (F) There was a significant main treatment effect of ANGII on positive staining within the kidneys (p=0.0215). Positive picrosirius staining in kidneys from GD18.5 was significantly higher in ANGII (N=7) versus SHAM (N=6) but not WKY (N=5) animals (*p<0.05). Data analysed by one-way ANOVA with Tukey's *post hoc* testing.

3.4.2 Offspring Outcomes in Hypertensive Pregnancy

3.4.2.1 Fetal Weight and Size Distribution

ANGII treatment did not significantly affect the number of pups in each litter at either the fetal (Fig. 3.6A) or neonatal (Fig. 3.6B) stages. Fetal weights and anthropomorphic measurements were collected at GD18.5 following sacrifice. Fetuses that were exposed to ANGII *in utero* appeared to have a reduced fetal weight (1.00±0.09g; Fig. 3.7A) compared to those born to SHAM (1.32±0.11g) mothers but were similar to those born to WKY mothers (1.13±0.02g). Abdominal circumference appeared to be decreased in SHAM relative to ANGII (Fig. 3.7C, ns.). Offspring from ANGII dams appeared to have a slightly decreased head circumference than those from WKY or SHAM (24.5±1.3mm, 25.6±0.9mm, and 26.6±1.1mm respectively, ns.; Fig. 3.7B). Analysis via one-way ANOVA revealed a significant main treatment effect of ANGII on crown-rump length (p=0.0078). Crown-rump length was significantly increased in SHAM offspring only versus WKY (p<0.01, Fig. 3.7D). ANGII offspring crown-rump length was significantly lower than SHAM (p<0.05). There was no statistically significant difference in the head:body ratio (an indicator of head sparing fetal growth restriction) between

groups (Fig. 3.7E). Fetal weight data was also expressed as a weight distribution curve to represent the data in a more clinically relevant format (Fig. 3.7F). The 5th centile for WKY fetal weights was calculated as weights that fell below 1.02g. This centile threshold was used as a control reference to determine which fetuses would be classified as clinically growth restricted in this model. It was calculated that 33.33% of ANGII offspring fell below the threshold for fetal growth restriction whilst 0.00% of SHAM offspring were classified as growth restricted.

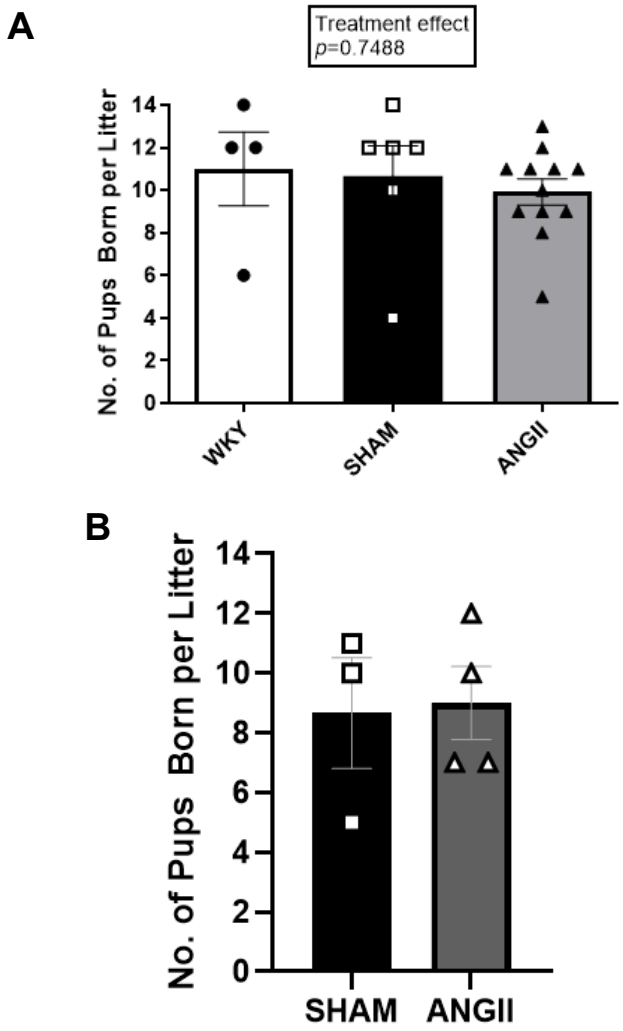

Figure 3.6: The Number of Offspring per litter at the Fetal and Neonatal Stages

The number of offspring in each litter was recorded at GD18.5 to capture the fetal stage and at the time of live birth for neonatal. (A) Infusion of ANGII (*N*=12) into SHRSP dams did not significantly influence the number of offspring per litter on GD18.5 when compared to SHAM (*N*=6) or WKY (*N*=4) dams. Data analysed by one-way ANOVA. (B) There was no significant effect of ANGII (*N*=4) treatment versus SHAM (*N*=3) animals on neonatal litter size. Data analysed by two-tailed unpaired *t test*.

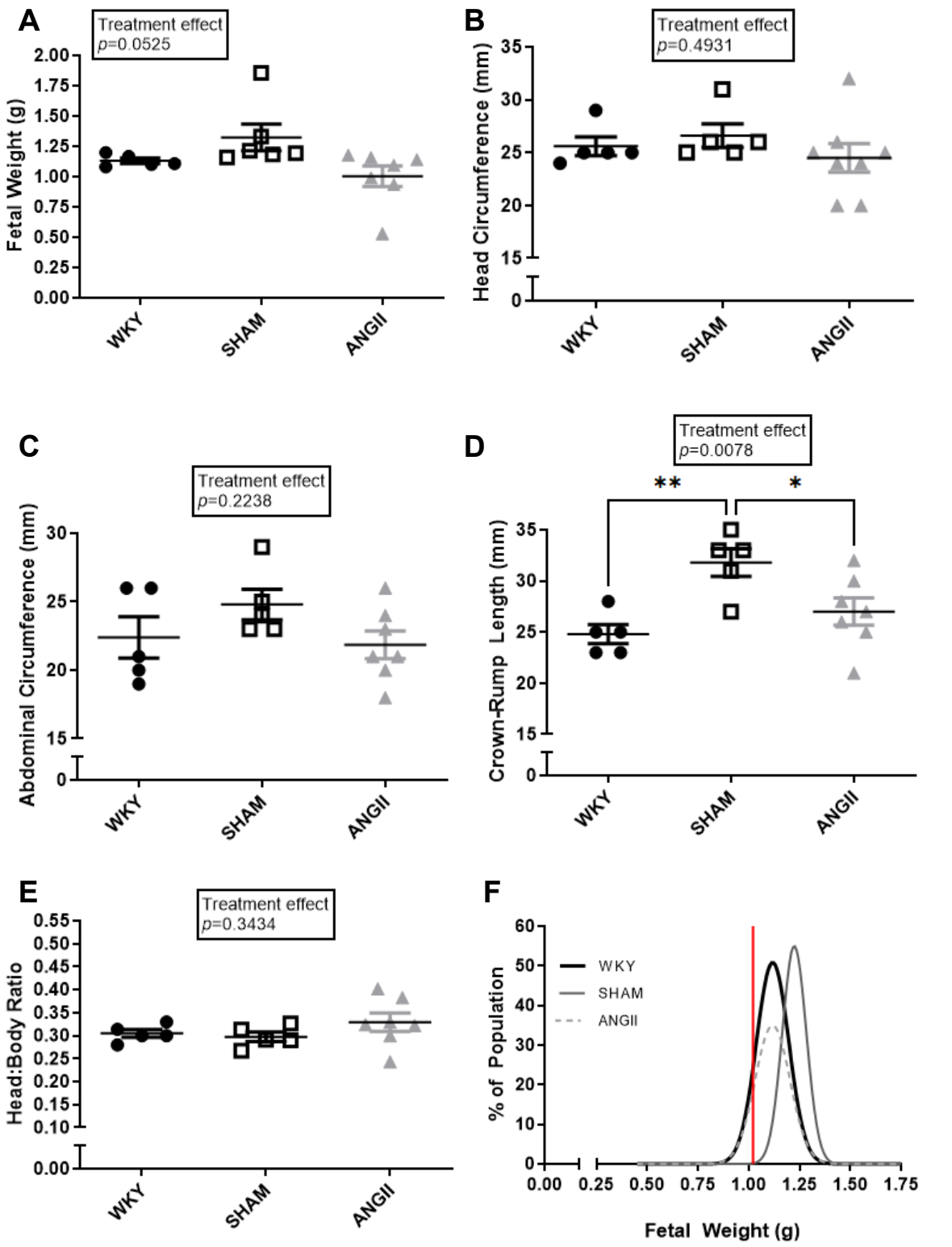
A
Treatment effect
p=0.0525
Fetal Weight (g)
2.00
1.75
1.50
1.25
1.00
0.75
0.50
0.25
0.00
WKY
SHAM
ANGII
B
Treatment effect
p=0.4931
Head Circumference (mm)
35
30
25
20
15
0
WKY
SHAM
ANGII
C
Treatment effect
p=0.2238
Abdominal Circumference (mm)
30
25
20
15
0
WKY
SHAM
ANGII
D
Treatment effect
p=0.0078
**
*
Crown-Rump Length (mm)
35
30
25
20
15
0
WKY
SHAM
ANGII
E
Treatment effect
p=0.3434
Head:Body Ratio
0.55
0.50
0.45
0.40
0.35
0.30
0.25
0.20
0.15
0.10
0.00
WKY
SHAM
ANGII
F
% of Population
60
50
40
30
20
10
0
WKY
SHAM
ANGII
0.00
0.25
0.50
0.75
1.00
1.25
1.50
1.75
Fetal Weight (g)

Figure 3.7: Fetal Growth Parameters in Response to Chronic Hypertension and ANGII Infusion

At GD18.5, fetuses were removed from the uterine horn and all amniotic fluid, placental tissue and associated membranes were removed. Analysis via one-way ANOVA revealed a significant main treatment effect of ANGII on crown-rump length (p=0.0078). (A) There was an observed decrease in fetal weight in ANGII (N=7,) offspring when compared to SHAM (N=6) that was similar to WKY (N=5) offspring. (B) No significant differences in head circumference were observed. (C) Abdominal circumference appeared to be lower in ANGII compared to SHAM offspring. (D) There was a significantly increased crown-rump length in SHAM versus WKY offspring (**p<0.01). ANGII offspring had a significantly lower crown-rump length than SHAM but not WKY offspring (*p<0.05). (E) No significant differences in head:body were found between groups though ANGII offspring may have had an increased ratio that may indicate head-sparing growth restriction. Data analysed by one-way ANOVA with Tukey's *post hoc* testing. (F) The proportion of total fetal weights at GD18.5 that fell below the 5th centile (**red** line) was determined by constructing a non-linear fit of frequency distributions for each group. The 5th centile was determined from WKY controls. ANGII (n=33 pups), SHAM (n=23 pups) and WKY (n=44 pups).

3.4.3 Placental Characteristics

Placental weight appeared to be reduced in offspring from ANGII dams (0.233±0.02g) when compared to those from SHAM dams (0.284±0.02g, p=0.09, Fig. 3.8A). Placental weight was not significantly different between WKY offspring (0.242±0.01g) and those from SHAM or ANGII groups. The fetal:placental ratio did not significantly differ between treatment groups, however ANGII offspring ratios (4.05±0.38) appeared to be lower than WKY or SHAM offspring (4.82±0.19 and 4.79±0.22, respectively, ns., Fig. 3.8B). Gross placental morphology was assessed using periodic acid Schiff staining to the various placental layers. A significant main treatment effect of ANGII was seen in positive staining within the junctional zone (p=0.0014). The intensity of positive staining within the junctional zone was significantly decreased in both SHAM (11.97±2.57%, p<0.01) and ANGII (16.94±2.84, p<0.01) placentae when compared to those from WKY pregnancies (30.92±2.86%, Fig. 3.8D).

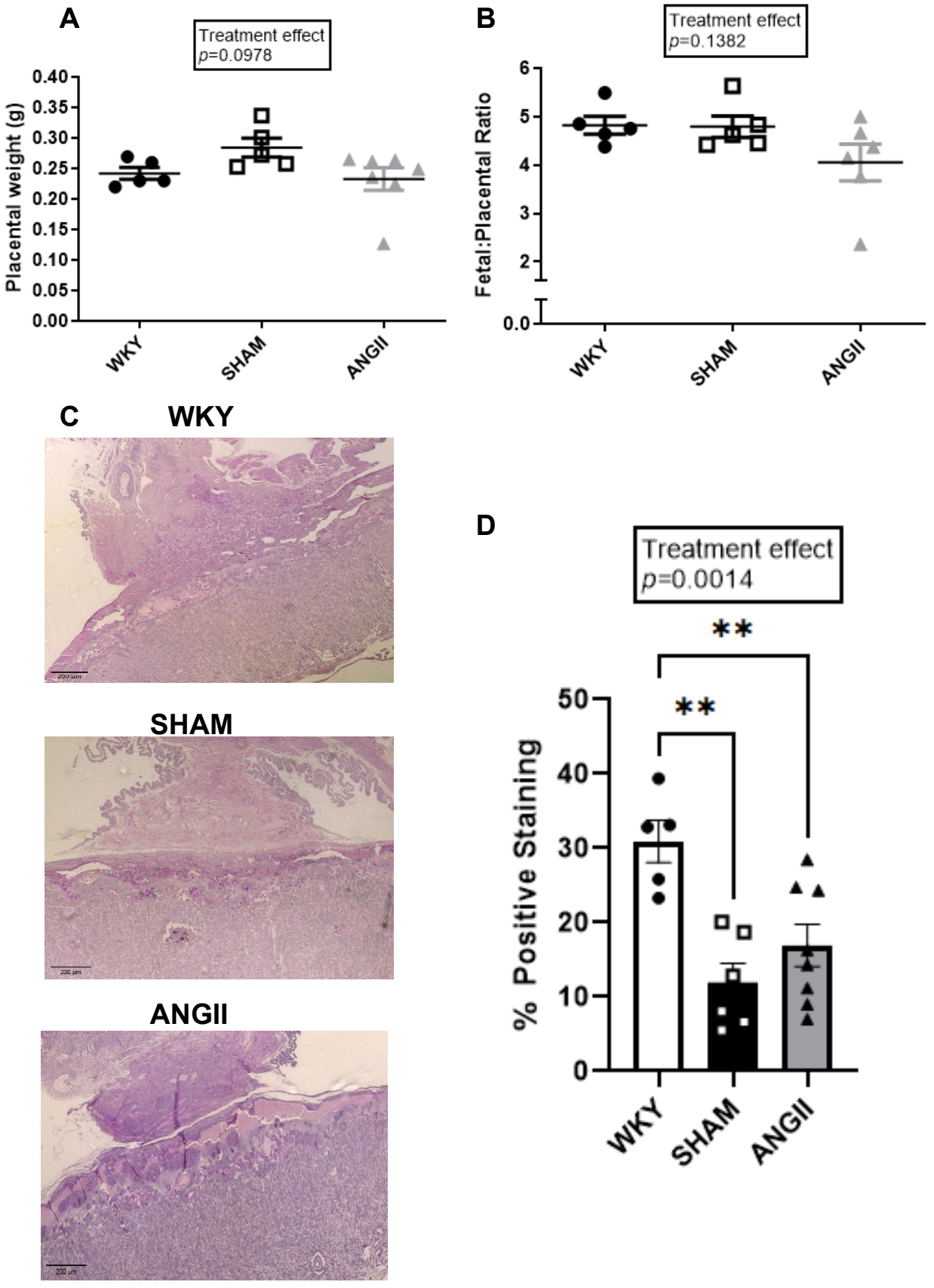
A
Treatment effect
p=0.0978
Placental weight (g)
0.40
0.35
0.30
0.25
0.20
0.15
0.10
0.05
0.00
WKY
SHAM
ANGII
B
Treatment effect
p=0.1382
Fetal:Placental Ratio
6
5
4
3
2
0.0
WKY
SHAM
ANGII
C
WKY
SHAM
ANGII
200 µm
D
Treatment effect
p=0.0014
**
**
% Positive Staining
50
40
30
20
10
0
WKY
SHAM
ANGII

Figure 3.8: Placental Characteristics Following ANGII Infusion

Once separated from the fetus, each placenta was gently blotted with absorbent paper to remove excess fluid. (A) Treatment with ANGII (*N*=7) may have resulted in a decrease in placental weight when compared to SHAM (*N*=5) placentae, though this was not significantly different to the weights of WKY (*N*=5) placentae. (B) The fetal:placental ratio did not significantly differ between groups though there may be a tendency towards a decreased ratio in ANGII (*N*=6) offspring when compared to both SHAM (*N*=5) and WKY (*N*=5) groups. (C) Representative images of positive periodic acid Schiff staining in placentae from all groups. (D) A significant main treatment effect of ANGII was seen in positive staining within the junctional zone (*p*=0.0014). Positive periodic acid Schiff staining of the junctional zone of the placenta was significantly decreased in both SHAM (*N*=6, ***p*<0.01) and ANGII (*N*=8, ***p*<0.01) treated placentae when compared to those from WKY (*N*=5) pregnancies. Data analysed by one-way ANOVA with Tukey's *post hoc* testing.

3.4.4 Neonatal Outcomes

3.4.4.1 Neonatal Weight

A subset of animals in the SHAM and ANGII groups were allowed to progress to parturition to examine the neonatal response to hypertensive pregnancy. The number of live births per litter was recorded on the day of birth (Fig. 3.6B). There were no differences in the number of neonates per litter between SHAM and ANGII treated dams. Neonatal weight was recorded on the day of birth and at 5 days after birth. A significant main treatment effect of ANGII was observed in neonatal weight ($p<0.0001$). At both day 1 and day 5 after birth, neonates from dams treated with 750ng/kg/min ANGII weighed significantly less than those from SHAM dams (5.40±0.06g vs. 3.83±0.12g, $p<0.0001$ day 1, 8.07±0.10g vs. 5.04±0.18g, $p<0.0001$ day 5, Fig. 3.9).

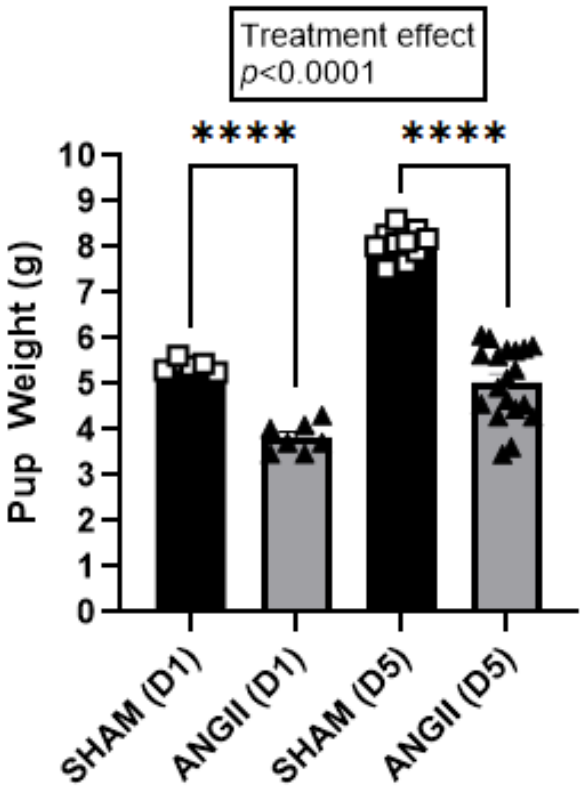

Figure 3.9: Live Neonatal Weight on Day 1 and Day 5 After Birth

Neonatal weights were recorded on the day of birth (D1) and at 5 days after birth (D5). A significant main treatment effect of ANGII was observed in neonatal weight (p<0.0001). At D1, neonatal weights in offspring exposed to ANGII *in utero* (n=5 pups) were significantly decreased versus weights from offspring born to SHAM mothers (n=7 pups, ****p<0.0001). This pattern between SHAM (n=10 pups) and ANGII (n=19 pups) was even more pronounced at D5 (****p<0.0001). Data analysed by two-way ANOVA with Tukey's *post hoc* testing.

3.4.4.2 Changes in Neonatal Gene Expression

qRT-PCR was performed to investigate the neonatal expression of genes including *Nox2*, *Ace2*, *Pparα*, *Gpx1* and *Spp1* in kidneys, hearts and thoracic aortae from ANGII and SHAM pregnancies (Fig. 3.10). These genes were chosen due to their known involvement in vascular remodelling and function as well as their known correlation with cardiovascular disease. Tissue from one neonate from a single litter per group were analysed, hence each group represents triplicate measures in n=1. Due to n=1/group/tissue no statistical analysis was conducted. Variation between the technical replicates was detected for all genes tested, suggesting the assay was not of high quality. This operator variability limited any conclusions that could be drawn about the data.

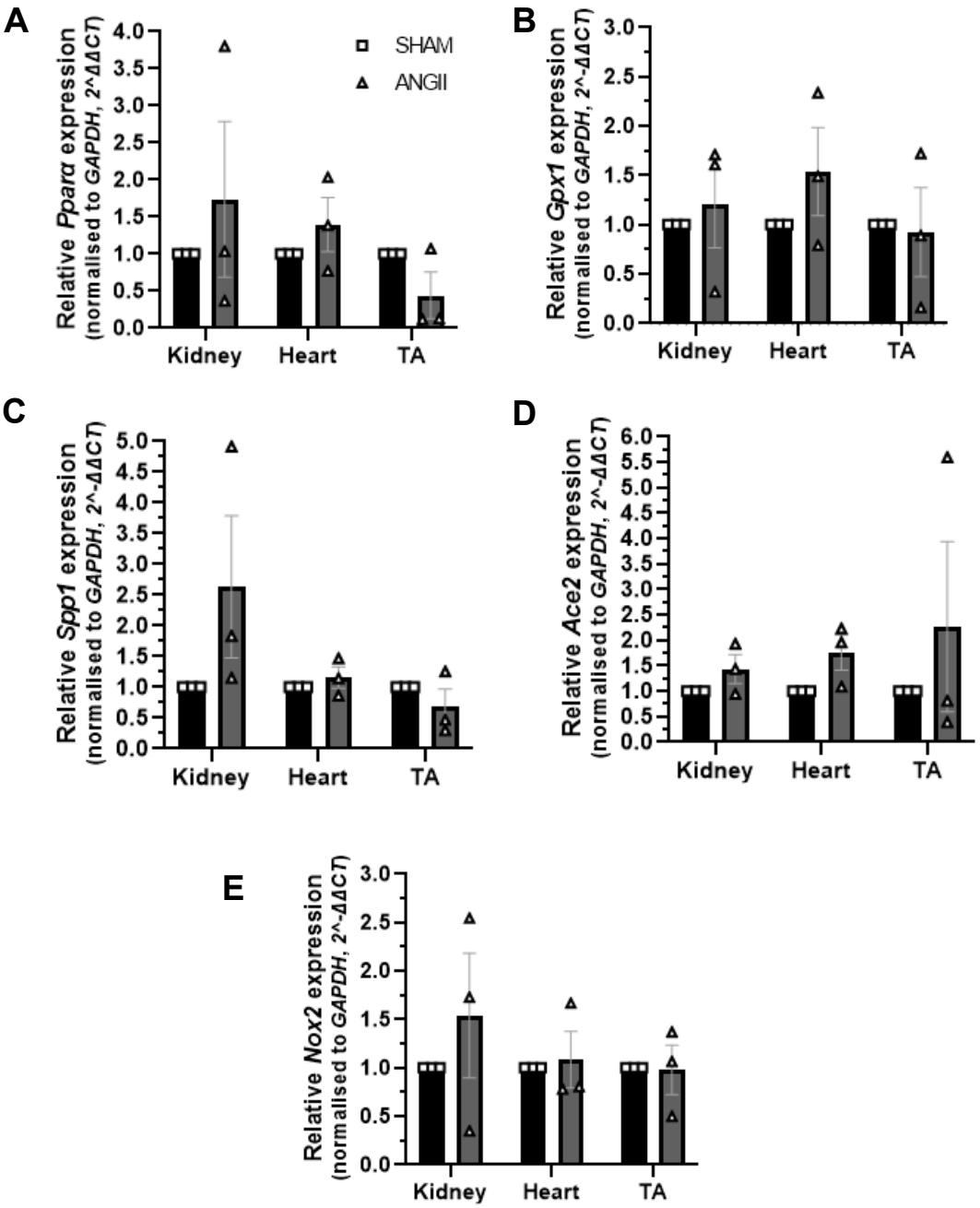

Figure 3.10: Gene Expression of Genes Related to Cardiovascular Disease in Neonatal Tissue

Gene expression of the genes (A) *Pparα*, (B) *Gpx1*, (C) *Spp1*, (D) *Ace2* and (E) *Nox2* were analysed using qRT-PCR and are presented as a relative expression normalised to the housekeeper gene *Gapdh* calculated from $2^{\Delta\Delta CT}$. Due to limited *n* numbers (*n*=1/group/tissue in triplicate) and high operator variability no statistical analysis was conducted.

3.5 Discussion

This chapter has provided evidence that super-imposed pre-eclampsia can be mimicked in SHRSP rats at a dose of 750ng/kg/min when delivered mid-gestation without causing extreme weight loss. The data presented indicates that SHRSP dams treated with ANGII had significant impairment of their haemodynamic and cardiovascular response to pregnancy when compared to SHAM treated SHRSP and normotensive WKY dams. Clinical indicators of severe pre-eclampsia such as a further elevated blood pressure, decreased cardiac output and proteinuria alongside evidence of fetal growth restriction and placental abnormalities were all documented in ANGII treated dams.

The SHRSP has a genetically determined predisposition towards chronic hypertension that makes it an ideal candidate for the study of hypertensive disorders of pregnancy such as pre-eclampsia. This study utilised normotensive WKY animals treated with saline to mimic a normal pregnancy as well as hypertensive SHRSP dams that also received saline to represent a treatment control group. Vehicle treated WKY dams demonstrated a consistent weight gain throughout pregnancy as did vehicle treated SHAM dams. Weight gain plateaued in ANGII-treated SHRSP dams at GD14.5 and by GD18.5 was significantly lower than SHAM. . A healthy pregnancy in humans is associated with an increase in total body weight, with the gravid uterus accounting for only 10% of this weight gain (Thornburg *et al*, 2015). This is due to the increase in the maternal heart alongside an increase in blood volume, and its increased consumption of oxygen and therefore energy requirements, leading to an increase in cardiac output to ensure adequate organ and placental perfusion to maintain the fetus (Thornburg *et al*, 2000). This also results in a shift in cardiac metabolism to meet the metabolic demands of the fetus in late gestation as fetal growth increases (Liu and Arany, 2014). Though ANGII administration slowed maternal weight gain it did not prevent it, however it did significantly decrease non-gravid weight relative to WKY mothers. The ANGII group also suffered from diminished cardiac output in late gestation following ANGII delivery when compared to SHAM and WKY. Reduced maternal weight gain and impaired cardiac output are associated with poorer fetal outcomes and increased severity of pre-eclampsia in humans (Wallace *et al*, 2017, Stott *et al*, 2018).

Both tail cuff plethysmography and radiotelemetry confirmed that ANGII administration was responsible for the observed increase in systolic and diastolic pressures. However, it is unclear why there were no differences in pre-pregnancy systolic pressures between WKY and SHRSP as has been previously reported (Small *et al*, 2016a, Small *et al*, 2016b). These differences were reported using radio-telemetry, whereas WKY dams were not investigated by telemetry in this study but rather by tail-cuff plethysmography. This deviation from the literature may be due to the different techniques used. In addition to this, radiotelemetry revealed that ANGII also resulted in a loss of diurnal regulation of heart rhythm. Short-term alterations to arterial blood pressure are mediated by the baroreceptor reflex. Normally, activation of the arterial baroreceptor reflex by a rise in systemic pressure (as was observed in this study) leads to a decreased activation of sympathetic neurons that innervate the heart and peripheral vessels. This results in bradycardia, reduced cardiac contractility and peripheral vasodilation to reduce heart rate and counteract the increase in systemic pressure (La Rovere *et al*, 2008). However, immediately following mini pump implantation surgery, SHRSP animals in this study exhibited an increase in heart rate. Heart rhythm returned to normal by GD11.5 in SHAM animals but continued to rise until GD12.5 in ANGII dams. This may be attributed to a blunting of the baroreceptor response by high levels of central ANGII prior to infusion on GD10.5. SHR rats have been shown to have increased central levels of renin, ACE and ANGII in comparison to WKY rats (Paull *et al*, 1997). This hyperactivation of the central RAAS may also be present in SHRSP dams and may explain the altered acute response to ANGII infusion in this study. This may also account for the loss of diurnal variation differences for a short-period following pump implantation in this group, as the constant firing of these receptors in addition to a sudden increase in circulating ANGII may have resulted in receptor desensitisation and thus temporary loss of diurnal control. ANGII dams also exhibited a significant increase in relative wall thickness on GD14.5 relative to WKY and SHAM dams, indicating hypertrophy as a result of hypertensive stress. This evidence, coupled with the finding that dams receiving ANGII also appeared to suffer from a decrease in stroke volume, is in agreement with the literature and echoes the hallmarks of cardiac dysfunction present in human cases of SPE (Buddeberg *et al*, 2018; Castleman *et al*, 2016).

Super-imposed pre-eclampsia is associated with endothelial dysfunction and defective vascular remodelling of the maternal uterine spiral artery, resulting in

intermittent placental ischaemia and subsequent reperfusion injury that gives rise to fetal growth restriction (Morgan *et al*, 2018; Small *et al*, 2016a). Small and colleagues (2016a) have previously shown that the SHRSP have defective pregnancy-dependant remodelling of the maternal uterine artery and reduced uteroplacental blood flow in comparison to their normotensive WKY counterparts. This effect was also seen in SHAM animals in this study. Treatment with ANGII did not significantly alter uterine artery blood flow *in vivo* when compared to SHAM. This may be due to the arteries of the SHRSP already being in a state of maximal impairment, thus treatment with ANGII is unable to further alter uterine artery function. It may be that the lack of response within the uterine artery in this study is a result of a low exposure time during pregnancy (8 days total) in comparison to studies in non-pregnant animals, or that delivering ANGII systemically does not affect the vessel in the same way that local uteroplacental ANGII would (Hering *et* al, 2010; Xue *et al*, 2017).

Treatment of pregnant SHRSP dams with ANGII resulted in altered renal function in reference to SHAM dams, as evidenced by an increased urine production and proteinuria. The ACR was significantly increased in ANGII mothers in comparison to both SHAM and WKY mothers despite an increase in water consumption and urine production. The increased urine production is in contrast to the normal physiological actions of ANGII in the kidney where it promotes water retention (Mirabito Colafella *et al*, 2019). This may be explained by the abnormalities in kidney morphology observed in this study. Kidneys exposed to ANGII during pregnancy had significantly higher positive staining for picrosirius red (an indicator of fibrosis) than their SHAM counterparts. Previous work has shown that ANGII infusion in the pregnant SHRSP also causes morphological abnormalities in the renal corpuscle (Morgan *et al*, 2018). This provides some evidence that ANGII infusion has a detrimental impact on renal function, however further assessment of glomeruli filtration rates would be beneficial in this model. Additionally, investigation of the expression levels of the various RAAS components would be beneficial in determining how closely this model recapitulates the human condition.

It is well known that this defective remodelling has an impact on offspring health and has been implicated in fetal growth restriction (FGR) (Davis *et al*, 2012). Alongside assessment of maternal health, this study also investigated the effect of elevated ANGII on fetal and placental development. Though there was no effect of

ANGII on litter size at either the fetal or neonatal stages, there was a significant decrease in fetal weight for offspring exposed to ANGII *in utero*. Neonatal weight was also significantly reduced in ANGII offspring at days 1 and 5 post-birth. Fetal growth restriction is defined as a failure of the fetus to reach its intrauterine potential for growth and development as a result of compromised placental function (Nardozza *et al*, 2017) and commonly occurs in pregnancies complicated by PE (Obata *et al*, 2020). Whilst FGR and PE may share some risk factors, FGR on its own confers additional risks to the fetus independently of its occurrence with PE such as increased risk of stillbirth, perinatal mortality and long-term health defects (Nardozza *et al*, 2017). In clinical practice, FGR is determined from the population average of fetal weights whereby fetuses weighing below the lowest 10^{th}, 5^{th} or 3^{rd} percentile of population weights are classified as growth restricted (Nardozza *et al*, 2017). In this study, 33.33% of ANGII fetuses fell below the 5^{th} percentile threshold for FGR confirming the fetal effects of this model at the study dose. Though this effect was confirmed to persistent in neonates, offspring development following parturition was studied in a limited capacity. A follow-up study of offspring exposed to ANGII *in utero* would be beneficial in determining whether this model also increases offspring risk of cardiovascular disease as is seen in those born from pre-eclamptic mothers in humans (Tooher *et al*, 2017).

Dysregulation of the maternal RAAS has been implicated in the dysfunctional spiral artery remodelling that leads to placental insufficiency in PE resulting in FGR and pathophysiological responses by the offspring in later life (Lumbers and Pringle, 2014; Xue *et al*, 2017). The cause of ANGII-infused FGR in this model is unclear as there was no effect of ANGII on uteroplacental blood flow, however placental weight was significantly reduced in ANGII dams. Although the fetal:placental ratio was not significantly different between groups, ANGII offspring appeared to have a decreased ratio compared to SHAM. This would suggest that there was no restriction to nutrient availability in the placenta and fetus from impaired flow, however neonatal weight was significantly lower in ANGII-treated offspring. It is possible that significant alterations to blood flow occurred after GD18.5 and were not measured in this study. This study did not investigate the spiral arteries of the placenta, but this would be of interest in future experiments perhaps by histological staining for markers of vascular remodelling within the mesometrial triangle, particularly given this models' links to the development of FGR and PE (Tanetta and Sargent, 2013). It may also be worth examining

placental function and transport in this model by investigating the expression of select transporter proteins as well as placental and fetal concentrations of their substrates. Though uteroplacental blood flow was unaffected, histological analysis of the placentae of both ANGII treated and SHAM SHRSP dams revealed abnormalities. Periodic acid-Schiff staining of the junctional zone showed a significantly decreased percentage of positive staining in the junctional zone in both SHAM and ANGII dams when compared to WKY dams. PAS staining identifies glycogen-containing cells within the placental layers which are known to disappear prior to parturition (Akison *et al*, 2017). Though the exact function of glycogen cells within the junctional zone is not fully understood, they are hypothesised to be a potential energy source in late gestation that is utilised by the placenta and/or the fetus (Coan *et al*, 2006). Therefore, depletion of glycogen cells following ANGII infusion may account for the changes in placental weight and FGR observed in this study despite there being no effect of ANGII on uteroplacental blood flow.

Current literature in the field fails to provide consistent results for the presence of metabolic and genetic markers of disease in offspring from mothers with pre-eclampsia in humans, therefore, further research is warranted. In addition to assessing the effects of ANGII-infusion on fetal growth, qRT-PCR was performed to investigate the expression of genes known for their involvement in vascular remodelling and various cardiovascular diseases. Due to the small sample size, statistical testing was not performed on this data. No conclusions could be made on the relative level of expression of the selected genes. All qPCR reactions were performed with the absence of standard curves; thus the validity of the assay could not be determined. Additionally, small sample sizes (n=1) and high variability between replicates of the same sample prevented the collection of any meaningful data.

Both *Pparα* and *Spp1* are involved in the functioning of the immune system and elevated levels of *Spp1* expression have been linked to chronic kidney disease and renal failure (Kaleta, 2019). Additionally, renal failure itself is a prominent risk factor for the development of cardiovascular disease, particularly hypertensive disorders of pregnancy (Vest and Cho, 2014). *Ace2* is a key component of the RAAS responsible for removing ANGII by converting it to Ang(1-7) in the heart and kidneys, which via its actions on the AT_2R antagonises the actions of ANGII

(Ocaranza *et al*, 2020; Cohen *et al*, 2020). *Ace2* can also be found in vascular endothelial cells and macrophages and its increased expression in these cell types has been observed in diseased states, suggesting *Ace2* may be implicated in hypertension and cardiovascular disease despite its vasodepressor actions or that its expression may be elevated as a secondary response to the disease process (Kuriakose *et al*, 2021). This suggests that an adverse *in utero* environment may alter offspring gene expression towards a pro-inflammatory, vasoconstrictive pathogenic state that increases the risk for later life cardiovascular and kidney disease (Davis *et al*, 2012; Tooher *et al*, 2017). *Gpx1* is known as the secondary defence against reactive oxygen species and free radicals in the mitochondria (Yeh *et al*, 2018). Conflicting results have been reported concerning the expression of *Gpx1* and its relationship to pre-eclampsia. Studies have reported both decreased and increased levels of *Gpx1* in whole blood, plasma and placentae of pre-eclamptic patients (Boutet *et al*, 2009). Due to the small sample size of neonatal tissue and variability in the technical replicates observed in this study, conclusions are limited. Increasing the number of samples by replicating this study with more *n* numbers would be beneficial to validate this finding. For any future qPCR studies, the inclusion of standard curves to enable assay validation and optimisation is crucial to ensure reliability in the data generated.

In summary, infusion of ANGII in the pregnant SHRSP rat significantly impacts maternal cardiovascular, renal and uteroplacental systems in addition to potentially restricting fetal growth. Fetal growth restriction in this model may be in part mediated by placental dysfunction. Though this study did investigate neonatal outcomes further study of offspring generated from this model would be a useful tool in understanding the impact of hypertensive disorders of pregnancy on adult SHRSP development. The changes observed in maternal systems closely mimicked those observed in human pre-eclampsia, thus this model could be utilised to investigate the long-term impacts of pre-eclampsia on maternal cardiovascular health post-pregnancy. This model was able to recapitulate human super-imposed pre-eclampsia in hypertensive rodents without negatively impacting animal welfare with regards to weight loss. We chose not to infuse WKY rats with ANGII in this study as previous work by a former student showed that WKY dams have an extremely low tolerance to ANGII infusion, even at a lowered dose of 500ng/kg/min, that resulted in excessive loss of body weight. These results demonstrate that this model has the potential to improve our understanding of pre-

eclamptic conditions, aid in determining the underlying causes and associated risks of pre-eclampsia in the chronically hypertensive population and provide a useful tool for the assessment of novel therapeutic strategies.

Chapter 4: Magnesium Sulphate as a Preventative Therapeutic in Rodent Super-imposed Pre-eclampsia

4.1 Introduction

The prevalence of hypertensive disorders of pre-eclampsia, including SPE, are on the rise and have become a leading cause of maternal and fetal mortality (Say *et al*, 2014). Whilst the underlying cause of SPE is not fully understood, many risk factors have been implicated in its development such as maternal weight or age, multiparity and maternal body mass index (Agrawal and Wenger, 2020). Though pharmacological interventions are severely lacking for SPE, one of the most commonly used approaches in clinical practice is the use of magnesium (Mg^{2+}) supplementation in the form of magnesium salts to prevent seizure occurrence in severe cases of SPE (Lassi *et al*, 2014).

Magnesium is the fourth most common cation in the human body, surpassed only by calcium (Ca^{2+}), potassium (K^{+}) and sodium (Na^{+}) (Chrysant and Chrysant, 2019). It is estimated that Mg^{2+} plays a role as a cofactor in as many as 325 enzymatic reactions related to the production of ATP (adenosine triphosphate), blood pressure control, muscle contraction, nerve conduction and bone strength, to name only a few (Severino *et al*, 2019). The recommended dietary intake of Mg^{2+} per day is approximately 280mg for an adult female and is mainly sourced from green leafy vegetables, cereals, meats and drinking water (James, 2010). During pregnancy, the recommended intake for Mg^{2+} increases to 360-400mg daily. Magnesium deficiency, or hypomagnesaemia (serum Mg^{2+} <0.74mmol/L), is becoming increasingly common in the Western world with foods in these regions containing 30-50% less Mg^{2+} than the recommended daily amount, exacerbated by the increasing consumption of processed foods (Fanni *et al*, 2021; Guerrera *et al*, 2009; Chrysant and Chrysant, 2019). Other factors such as gastrointestinal malabsorption or the use of medications such as diuretics or laxatives may also contribute to magnesium deficiency (Severino *et al*, 2019). Hypomagnesaemia has the potential to increase the onset of *de novo* hypertension or worsen pre-existing hypertension and increase the incidence of cardiovascular disease (Chrysant and Chrysant. 2019).

Studies have shown that hypomagnesemia is commonly observed in a wide range of cardiovascular diseases such as heart failure, diabetes mellitus, hypertension, stroke, arrhythmia and low serum levels of Mg^{2+} were a predictor for all-cause mortality (Liu and Dudley Jr., 2020; Guerrera *et al*, 2009). Magnesium is

additionally known to participate in metabolic and vascular homeostasis as well as modulate inflammation and oxidative stress. It is believed that hypomagnesaemia may also play a role in endothelial dysfunction and atherogenesis (Severino *et al*, 2019). Pregnant individuals are at particularly high risk of magnesium deficiency as Mg^{2+} levels decline during pregnancy, reaching their lowest at the end of the first trimester (James, 2010). Low Mg^{2+} levels have been linked to severe hypertension during pregnancy as early as 1998 (Khedun *et al*, 1998). Hypomagnesaemia during pregnancy may contribute to placental insufficiency and thus the development of SPE by inducing vasospasms in the uterine spiral arteries and increasing the risk for fetal growth restriction (James, 2010). Magnesium deficiency during pregnancy also increases the risk of premature labour as it can result in uterine excitability that may be exacerbated by maternal stress (Fanni *et al*, 2021). Literature suggests that low Mg^{2+} levels may impact fetal programming. A study by Schlegel and colleagues (2017) found that male rats that developed fetal hypomagnesaemia as a result of restriction of Mg^{2+} in the maternal diet presented in adulthood with signs of increased anxiety and a reduced expression of NMDA receptor subunits (*N*-methyl-D-aspartate) within the hippocampus. Other studies in animal models have found that restriction of maternal dietary Mg^{2+} intake results in abnormal fat metabolism, insulin resistance and diabetes (James, 2010).

The role of hypomagnesaemia in the generation of pre-eclampsia is debated, though magnesium deficiency is considered a predisposing factor to PE (Chiarello *et al*, 2018). It has been reported that pre-eclamptic individuals have lower red blood cell membrane and brain concentrations of Mg^{2+} than those with normal pregnancies (Nelander *et al*, 2017). During PE there is an accumulation of Mg^{2+} in the fetal circulation which is hypothesised to result from alterations in maternal Mg^{2+} metabolism (Borekci *et al*, 2009; Chiarello *et al*, 2018). Yang *et al* (2014) showed evidence of a reduced expression of the magnesium channel TRPM7 (M-type transient receptor potential channel 7) in hypoxic primary placental cells and in samples from pre-eclamptic placentae at term. The use of magnesium salts in pre-eclamptic pregnancy to prevent the increase of disease severity to eclampsia, seizures and maternal death has been a part of standard clinical care for many years (Chrysant and Chrysant, 2019; Guerrera *et al*, 2009). Administration of $MgSO_4$ has been found in various studies to reduce the risk of eclampsia by 50% as well as reduce hospital and intensive care unit admissions and was more

effective than other common treatments in eclampsia patients (Guerrera *et al*, 2009; Gröber *et al*, 2015; James, 2010). In the rat L-NAME model of PE (section 1.4.4) other beneficial actions of $MgSO_4$ were shown including decreased maternal blood pressure, proteinuria and reduced serum s-Flt1 and sEng alongside increased nitric oxide production (Korish, 2012). $MgSO_4$ also improved *ex vivo* heart function in this model (Coates *et al*, 2006). Despite this, the mechanism of action of this treatment has never been clearly defined nor has there been an agreement on the minimum effective dosing schedule in humans (Chiarello *et al*, 2018). A Cochrane review of magnesium supplementation concluded that based on cumulative evidence from ten trials involving 9090 pregnancies, there was no clear beneficial effect of Mg^{2+} during pregnancy, however it was noted that eight of the ten trials were of low to moderate quality (Makrides *et al*, 2014). This leaves the question of the relationship between hypomagnesaemia, $MgSO_4$ therapy and pre-eclampsia still unanswered.

4.2 Hypothesis & Aims

Utilising the rodent model of super-imposed pre-eclampsia optimised in chapter 3, we hypothesised that oral administration of $MgSO_4$ in place of normal drinking water may be beneficial to maternal and fetal outcomes in rodent SPE.

We aimed to investigate this by daily dosing of 1% w/v solution of $MgSO_4$ in place of normal drinking water. We examined both maternal and fetal outcomes in pregnant SHRSP rats infused with ANGII that received daily $MgSO_4$ from gestational day 0.5. We hypothesised that magnesium supplementation in the form of $MgSO_4$ would be beneficial in improving maternal blood pressure and uteroplacental flow as well as fetal growth in a rodent model of SPE.

4.3 Materials and Methods

Animals were housed and mated as outlined in section 2.3.1. Animals were randomly allocated to one of four treatment groups: saline only (SHAM), 750ng/kg/min ANGII (ANGII), saline with $MgSO_4$ (SHAM+$MgSO_4$) and ANGII with $MgSO_4$ (ANGII+$MgSO_4$). The ANGII dose was calculated and prepared as described in 3.3.1. ANGII was delivered by a subcutaneously implanted osmotic mini-pump that was present from GD10.5 (3.3.2). Phenotypical characterisation included blood pressure measurement (2.3.4), blood sampling (2.3.6), echocardiography (2.3.7) and uterine artery doppler assessment of uteroplacental blood flow (2.3.8). These measurements were conducted prior to pregnancy (PP) and at gestational days (GD) 6.5, 12.5 and 18.5. Proteinuria was assessed as described in section 2.2.4 using urine samples obtained at PP and on GD6.5 and 18.5 by metabolic cage sampling (2.3.5). Animals were sacrificed on GD18.5 and maternal, placental and fetal tissues and measurements were collected. Full details on tissue collection and dissection are discussed in sections 2.4.2 to 2.4.5. Placentae were harvested and either fixed for histological analysis or frozen for future studies. Further details of these methods can be found in the general materials and methods (sections 2.2.3, 2.2.6). Due to the impact of COVID-19 on research, data points from Chapter 3 from the SHAM and ANGII groups were included in the data analysis presented within this Chapter.

4.3.1 Magnesium Sulphate Dosing in Drinking Water

Animals in the SHAM+$MgSO_4$ and ANGII+$MgSO_4$ groups were treated from GD0.5 with a 1% w/v solution of $MgSO_4$ in place of their normal drinking water. $MgSO_4$ water was prepared by dissolving 10g of anhydrous magnesium sulphate (ThermoFisherScientific, Paisley, UK) in 1 litre of deionised water. Animals were provided with 200mL of $MgSO_4$ water that was refreshed daily. The concentration of $MgSO_4$ was determined from previous studies using rodents (Soltani *et al*, 2005; Hasanein *et al*, 2006).

4.4 Results

4.4.1 $MgSO_4$ and the Maternal Pregnancy Profile

4.4.1.1 $MgSO_4$ Improves Maternal Weight Gain in Hypertensive Pregnancy

A normal pregnancy is partially characterised by a reversible increase in weight that is independent of the uteroplacental unit, known as non-gravid weight gain. Non-gravid weight was determined on GD18.5 by weighing the whole carcass following removal of the uteroplacental unit (Fig. 4.1). Analysis by two-way ANOVA revealed no significant main effect of either ANGII or $MgSO_4$ on non-gravid weight. SHAM control dams showed a healthy weight gain with a non-gravid weight of 189.1±5.2g. $MgSO_4$ did not appear to have an effect on weight gain with the SHAM+$MgSO_4$ group non-gravid weight measuring 189.2±1.0g. Treatment with ANGII infusion in SHRSP dams resulted in an apparent decrease in non-gravid weight (174.0±3.7g). The addition of $MgSO_4$ drinking water in the ANGII group lead to an observed increase in non-gravid weight when compared to ANGII alone that was not statistically different from untreated SHAM animals (189.1±7.5g).

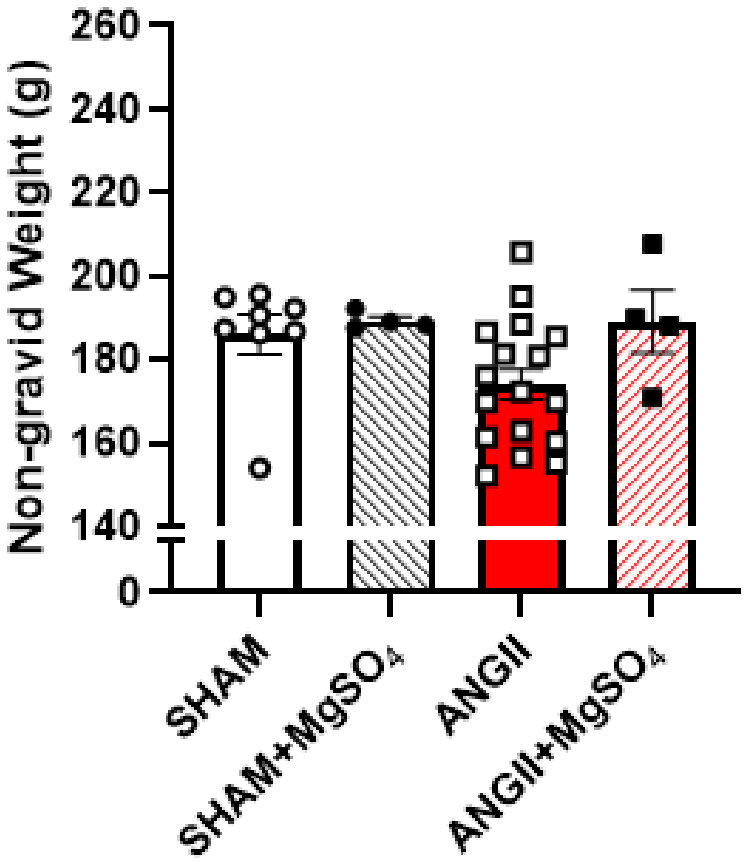

Figure 4.1: Non-gravid Weight at GD18.5 in Response to $MgSO_4$ Treatment

Maternal non-gravid weight was recorded on GD18.5 by removal of the entire uteroplacental unit following sacrifice and weighing the whole carcass. Analysis by two-way ANOVA revealed no significant main effect of either ANGII or $MgSO_4$ on non-gravid weight. SHAM animals receiving saline only (*N*=9) did not significantly differ from SHAM animals who also received $MgSO_4$ (*N*=4). Treatment of SHRSP dams with ANGII (*N*=17) resulted in an observed decrease in maternal non-gravid weight when compared to SHAM dams. The addition of $MgSO_4$ drinking water to ANGII treated animals (*N*=4) led to a non-significant increase in maternal non-gravid weight compared to ANGII alone. Data analysed by two-way ANOVA.

4.4.1.2 Blood Pressure Profiles in Response to $MgSO_4$

Systolic blood pressure was monitored throughout gestation in all groups by tail-cuff plethysmography; detailed in the general materials and methods in section 2.3.4. All animals in this study were borderline hypertensive prior to pregnancy. Using REML mixed-effects analysis, a significant main treatment effect on systolic blood pressure was found (p=0.0008). Figure 4.2 illustrates the systolic blood pressure profiles of each group at PP and on GD6.5, 12.5 and 18.5 by tail-cuff. Further analysis using *post hoc* multiple comparisons indicated both ANGII and $MgSO_4$ affected blood pressure. Both SHAM and ANGII dams exhibited an increase in blood pressure from PP to GD6.5 prior to mini pump surgery (SHAM: 143.6±4.0mmHg PP, 151.9±2.7mmHg GD6.5; ANGII: 139.9±3.7mmHg PP, 168.7±5.1mmHg GD6.5). In contrast, groups receiving $MgSO_4$ drinking water appeared to experience an initial decrease in blood pressure at GD6.5 that was lower when comparing the SHAM and ANGII to ANGII+$MgSO_4$ groups (SHAM+$MgSO_4$: 141.6±6.7mmHg PP, 137.5±11.2mmHg GD6.5; ANGII+$MgSO_4$: 139.2±3.6mmHg PP, 124.4±4.3mmHg GD6.5). SBP rose sharply following mini pump surgery in dams receiving ANGII by GD12.5. The use of $MgSO_4$ in SHAM animals led to a marked decrease in SBP (123.3±4.9mmHg GD12.5) in comparison to SHAM alone (149.7±2.8mmHg GD12.5; p=0.059) and ANGII alone (168.7±5.1mmHg GD12.5; p<0.001). There was no difference in blood pressure between ANGII and ANGII+$MgSO_4$ dams at GD12.5. By GD18.5, dams receiving ANGII only experienced a worsening of their hypertension with a blood pressure significantly higher than all other groups (178.4±7.1mmHg; p<0.01 vs. 142.9±2.6mmHg ANGII+$MgSO_4$; p<0.0001 vs. 128.0±3.4mmHg SHAM and 125.4±6.7mmHg SHAM+$MgSO_4$). There was no difference in blood pressure between SHAM and SHAM+$MgSO_4$ mothers at GD18.5.

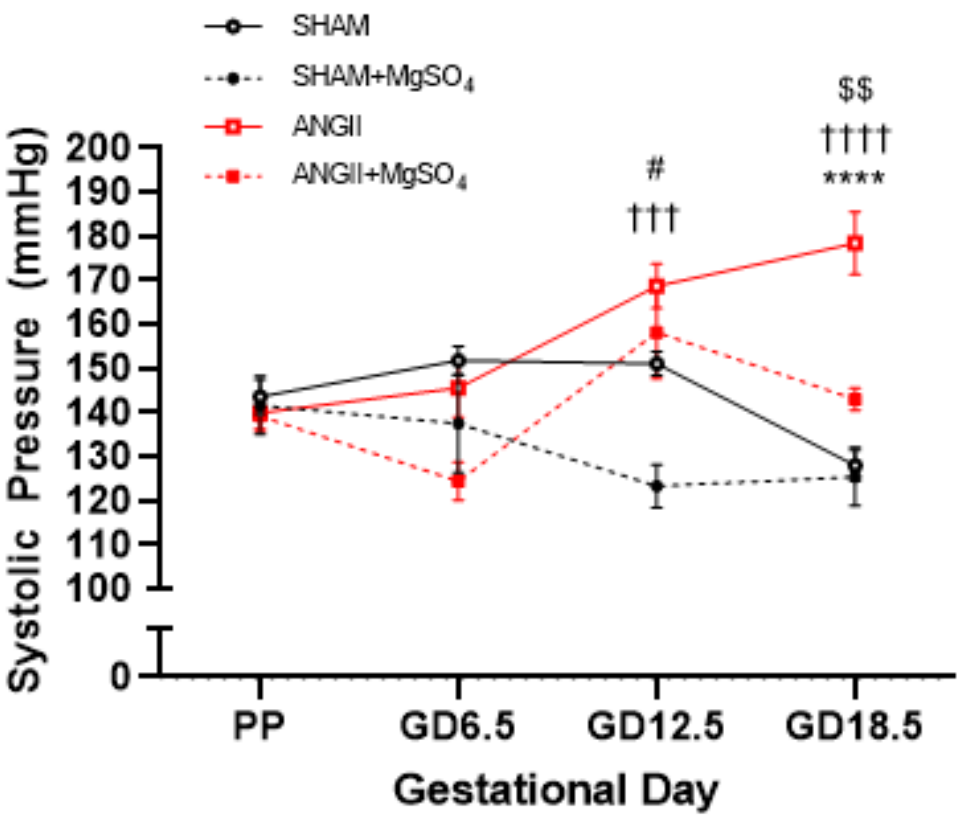

Figure 4.2: The Maternal Blood Pressure Profile Across Gestation in Response to ANGII and $MgSO_4$

Systolic blood pressure was recorded at pre-pregnancy (PP) and three specific gestational time points (pre ANGII: GD6.5, post-ANGII: GD12.5 and GD18.5) in SHRSP SHAM (saline) and ANGII treated dams (750ng/kg/min) with or without daily $MgSO_4$ drinking water. Alterations in SBP across pregnancy were measured by tail-cuff plethysmography. Statistical analysis showed a significant main treatment effect on blood pressure (p=0.0008) SHRSP dams in all groups were borderline hypertensive prior to pregnancy. Comparisons between groups during *post hoc* analysis revealed both ANGII and $MgSO_4$ affected blood pressure. At GD6.5 SHAM (N=10) and ANGII (N=17) dams exhibited an increase in SBP whilst SHAM+$MgSO_4$ (N=4) and ANGII+$MgSO_4$ (N=5) dams showed a decrease. Following pump implantation on GD10.5, animals receiving ANGII showed increased SBP by GD12.5 ($^{†††}p$<0.001 ANGII vs. SHAM+$MgSO_4$, $^{\#}p$<0.05 ANGII+$MgSO_4$ vs. SHAM+$MgSO_4$). On GD18.5, the ANGII group exhibited blood pressure that was significantly higher than all groups ($^{\$\$}p$<0.01 vs. ANGII+$MgSO_4$; ****/$^{††††}p$<0.0001 vs. SHAM/SHAM+$MgSO_4$). Though $MgSO_4$ water appeared to decrease SBP when compared to ANGII alone, ANGII+$MgSO_4$ mothers remained more hypertensive at GD18.5 than control SHAM mothers. Data analysed using restricted maximum likelihood mixed-effects analysis with Tukey's *post hoc* testing.

4.4.1.3 Echocardiographic Assessment Following ANGII and $MgSO_4$ Treatment in SHRSP Dams

Echocardiographic assessment of cardiac function was carried out prior to and throughout pregnancy in all groups (section 2.3.7). Following REML mixed-effects analysis, a significant main treatment effect was reported for stroke volume (p=0.0007), relative wall thickness (p=0.0053) and left ventricular mass measured weekly (p=0.0409). Figure 4.3A illustrates the changes in stroke volume throughout pregnancy in the groups. Stroke volume tended to remain relatively stable across gestation (0.26±0.02mL PP; 0.25±0.04mL GD12.5, 0.26±0.02mL GD18.5) in the control SHAM group. Addition of $MgSO_4$ to drinking water in SHAM dams lead to an observed increase in SV throughout pregnancy (0.18±0.02mL GD6.5; 0.27±0.01mL GD18.5, ns.). *Post hoc* comparisons between groups indicated that, following an initial increase in SV between PP (0.24±0.03mL) and GD6.5 (0.26±0.02mL), treatment with ANGII led to a significant decrease in SV by GD12.5 (0.17±0.02mL, p<0.05 vs. PP, p<0.01 vs. GD6.5) that did not recover to SHAM levels at GD18.5 (0.19±0.02mL, p<0.05). A similar observation, though non-significant, for SV was observed in those receiving both ANGII and $MgSO_4$ (0.17±0.03mL PP; 0.13±0.02mL GD12.5) that did not reach SHAM levels by GD18.5 (0.19±0.00mL). Relative wall thickness (RWT) was used as a measure of left ventricular hypertrophy and therefore dysfunction in pregnant dams (Fig. 4.3D). Tukey's *post hoc* analysis indicated that RWT was not significantly different between groups from PP to GD6.5. Treatment with ANGII resulted in a significant increase in RWT compared to SHAM (p<0.01, GD12.5). Addition of $MgSO_4$ in ANGII-infused dams led to a further significant increase in RWT relative to SHAM and SHAM+$MgSO_4$ groups (p<0.05, p<0.0001 respectively). RWT appeared to remain relatively consistent throughout pregnancy in the SHAM and SHAM+$MgSO_4$ groups. Ejection fraction (Fig. 4.3C) was not significantly different between groups or across gestation within groups. A similar result was observed for fractional shortening (Fig. 4.3B). Echocardiographic estimations of left ventricular mass were normalised to tibial length as upon reaching sexual maturity at ~12 weeks tibial growth slows significantly such that tibial length was stable for the duration of the study (Fig. 4.3E). When groups were compared during *post hoc* analysis, left ventricular mass (measured weekly) was significantly increased in the $MgSO_4$ groups when compared to ANGII alone on GD18.5 (1.21±0.1g/mm ANGII vs. 1.70±0.1g/mm ANGII+$MgSO_4$; 1.72±0.1g/mm SHAM+$MgSO_4$). The left

ventricles were dissected and weighed at time of sacrifice. These weights were normalised to tibial length but were not in agreement with echocardiography data, as there was no significant effect of either ANGII or $MgSO_4$ detected (Fig. 4.3F). This may represent operator variability in echocardiographic image capture or analysis rather than a true significant result.

Figure 4.4A shows the changes in maternal heart rate (HR) across gestation in all four groups. Batch variability was detected at PP. This variability was introduced due to a pause in research as a result of COVID-19 (see Impact Statement). All animals that received $MgSO_4$ treatment were studied one year later than SHAM or ANGII only animals and results for SHAM and ANGII groups included values from Chapter 3. Statistical analysis using REML mixed-effects analysis showed that there was significant main treatment effect in both HR (p=0.0003) and CO (p<0.0001). A significant main treatment effect was also noted for CO normalised to tibial length (p=0.0002). Tukey's multiple comparisons *post hoc* testing indicated that HR was significantly reduced in ANGII+$MgSO_4$ rats compared to ANGII at PP (*p<0.05) and a similar pattern was observed between SHAM+$MgSO_4$ and SHAM groups (ns.). This pattern persisted throughout gestation and by GD18.5, HR was significantly lower in ANGII+$MgSO_4$ dams compared to SHAM (*p<0.05) and ANGII dams (**p<0.01). HR was significantly reduced in SHAM+$MgSO_4$ animals versus ANGII animals at GD18.5 (*p<0.05) and appeared to be lower than SHAM only (ns.). Due to the variability between batches prior to treatment, it is unclear whether these changes in maternal heart rate are a result of $MgSO_4$ treatment. Of the estimates of cardiac function, cardiac output, is the only calculation that relies on HR. Therefore, the variability in maternal heart rate also affected cardiac output. To mitigate this effect, we calculated ∆cardiac output (∆CO) as the difference in cardiac output at each gestational time point relative to baseline (PP) measurements for each individual animal (Fig.4.4C), normalised cardiac output to tibial length (Fig. 4.4D) and presented these alongside the raw CO values (Fig. 4.4B). Following normalisation to tibial length, *post hoc* analysis indicated that cardiac output was significantly decreased in dams receiving ANGII only at GD12.5 (30.51±3.1mL/min/g, p<0.05) compared to PP values. This observation was also noted for raw cardiac output values, though to a higher degree of significance (p<0.01, PP vs GD12.5, ANGII). ∆CO in the SHAM group seemed to decline between GD6.5 (10.3±14.2%) and GD12.5 (-11.3±21.5%) before increasing on GD18.5 (26.9±34.1%) (Fig. 4.4C, ns.). The pattern in SV observed

in SHAM+MgSO4 animals was also observed in ΔCO (18.3±19.2% GD6.5; 92.6±23.0% GD18.5, ns.). ΔCO in the ANGII group followed a similar pattern to that of SHAM animals and was not significantly different. This was not the case with ANGII+MgSO4 dams, where there appeared to be a slight decrease between GD6.5 (21.2±37.6%) and GD12.5 (0.1±19.8%) that plateaued until GD18.5 (3.1±11.0%, ns.) indicating that by late gestation cardiac output was not significantly different to PP measurements. These corrections were unable to correct for the batch variation present between $MgSO_4$ groups and their normal drinking water counterparts.

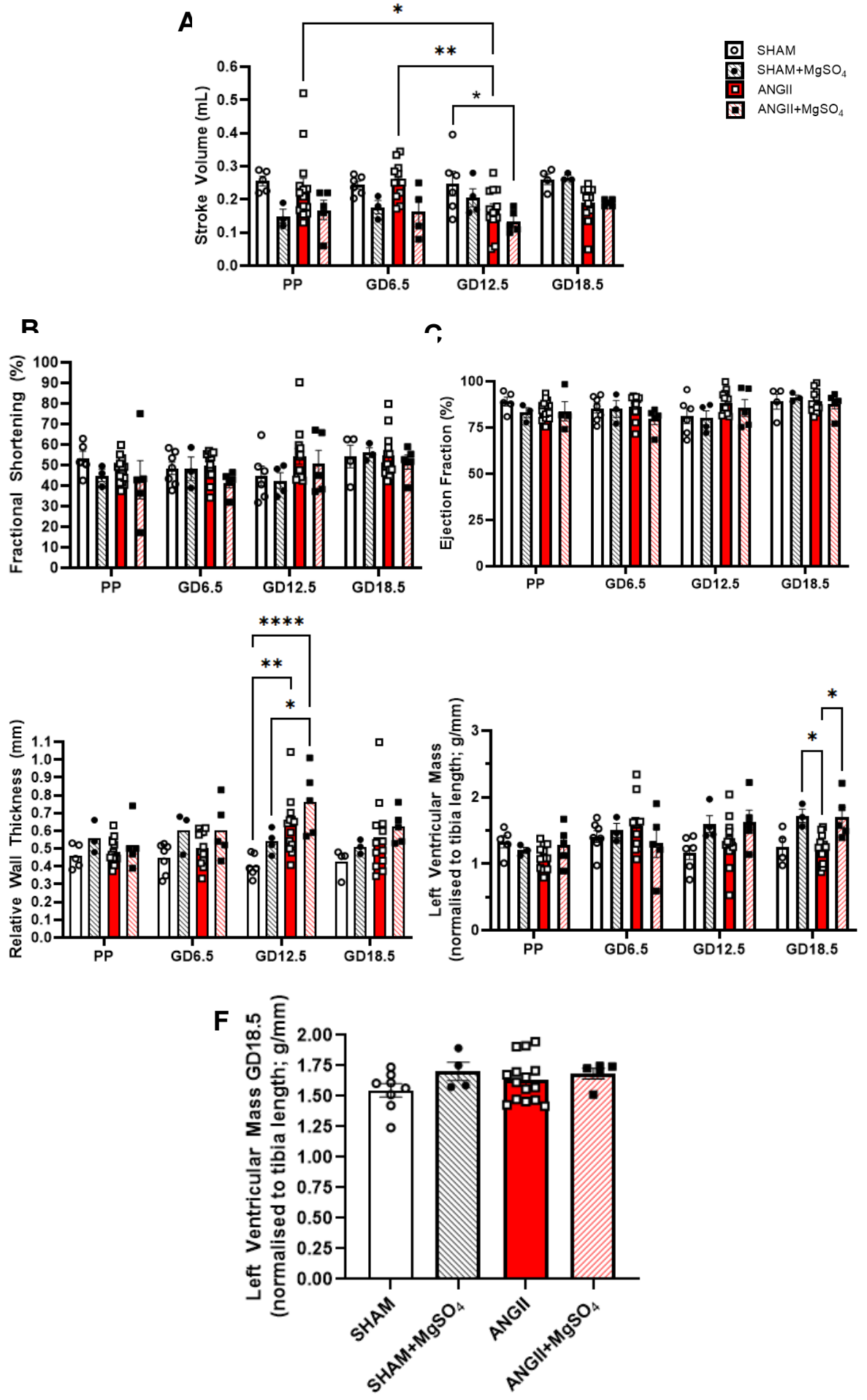
A
Stroke Volume (mL)
PP
GD6.5
GD12.5
GD18.5
SHAM
SHAM+MgSO4
ANGII
ANGII+MgSO4
B
Fractional Shortening (%)
C
Ejection Fraction (%)
Relative Wall Thickness (mm)
Left Ventricular Mass (normalised to tibia length; g/mm)
F
Left Ventricular Mass GD18.5 (normalised to tibia length; g/mm)

Figure 4.3: Echocardiographic Estimations of Cardiac Function Following $MgSO_4$ Intervention in Hypertensive Dams

Echocardiography was carried out pre-pregnancy (PP) and on GD6.5, 12.5 and 18.5. Following REML mixed-effects analysis, a significant main treatment effect was reported for stroke volume (p=0.0007), relative wall thickness (p=0.0053) and left ventricular mass (p=0.0409). (A) SV remained stable throughout pregnancy in SHAM (N=6) and steadily rose in SHAM+$MgSO_4$ dams (N=4) but decreased following ANGII infusion (N=14, */**p<0.05/0.01 PP/GD6.5 vs GD12.5). Addition of $MgSO_4$ to ANGII treated dams (N=5) drinking water did not prevent but rather appeared to exacerbate this decline in SV (*p<0.05 vs SHAM, GD12.5). (D) RWT was not significantly different between groups from PP to GD6.5. On GD12.5 ANGII+$MGSO_4$ animals showed a significantly increased RWT when compared to all other groups (*p<0.05 vs SHAM+$MgSO_4$, **p<0.0001 vs. SHAM). RWT was also significantly increased in SHAM vs ANGII (**p<0.01). These patterns were preserved at GD18.5 but were not significant. No differences between treatment groups were seen in calculated fractional shortening (B) or ejection fraction (C). Left ventricular mass (E) was significantly lower in ANGII vs $MgSO_4$ groups at GD18.5 (*p<0.05 vs SHAM+$MgSO_4$/ANGII+$MgSO_4$). Left ventricular mass at time of sacrifice (F) revealed this difference to be artificial as a result of image capture or analysis operator variability. Data analysed using restricted maximum likelihood mixed-effects analysis with Tukey's *post hoc* testing or two-way ANOVA with Tukey's *post hoc* testing where appropriate.

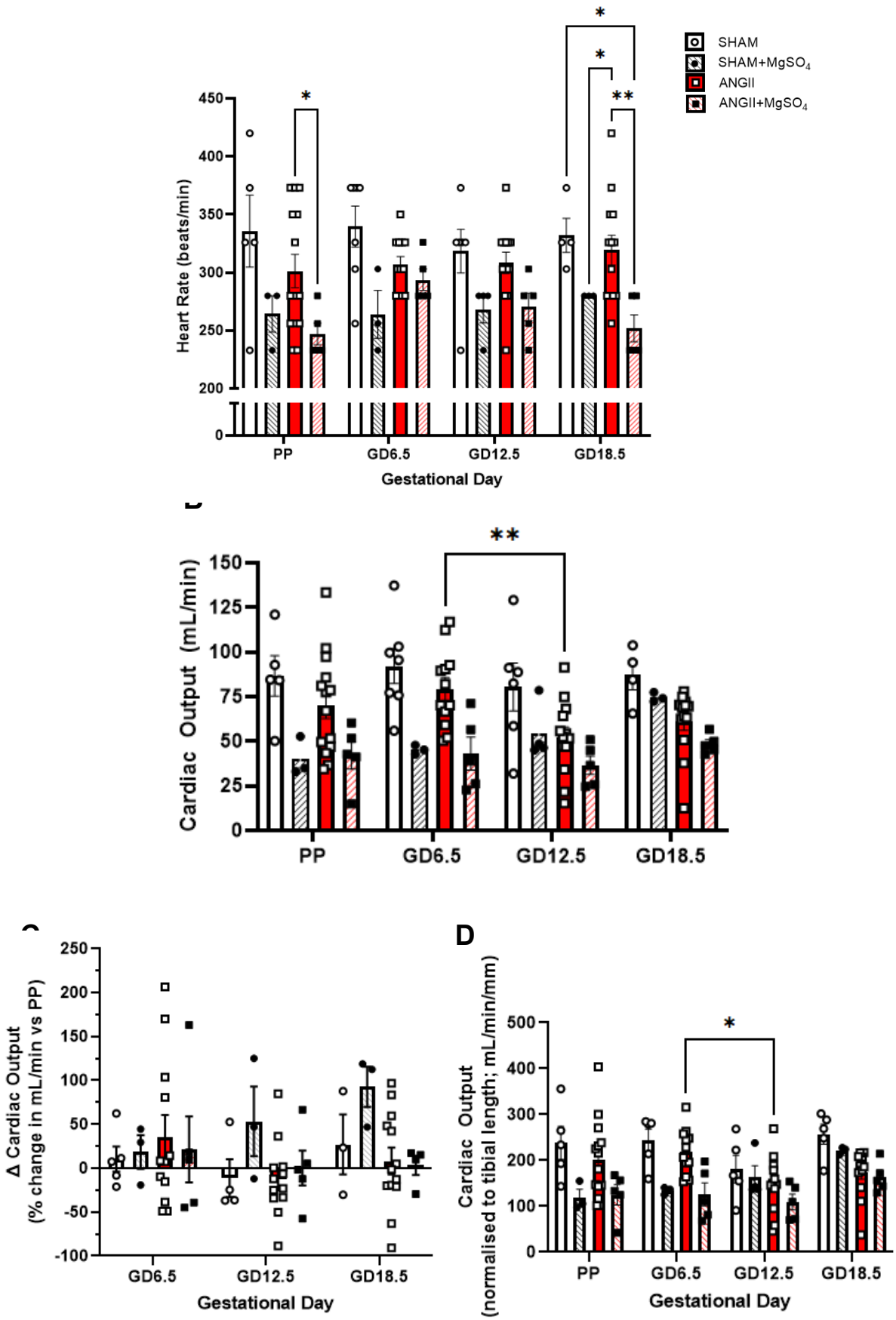
SHAM
SHAM+MgSO4
ANGII
ANGII+MgSO4
Heart Rate (beats/min)
Gestational Day
PP
GD6.5
GD12.5
GD18.5
Cardiac Output (mL/min)
Δ Cardiac Output (% change in mL/min vs PP)
Cardiac Output (normalised to tibial length; mL/min/mm)
D

Figure 4.4: Maternal Heart Rate and Cardiac Output Following $MgSO_4$ Intervention in Hypertensive Dams

Echocardiography was carried out pre-pregnancy (PP) and on GD6.5, 12.5 and 18.5. Statistical analysis using REML mixed-effects analysis showed that there was significant main treatment effect in both HR (p=0.0003) and CO (p<0.0001). A significant main treatment effect was also noted for CO normalised to tibial length (p=0.0002). (A) Maternal heart rate was significantly lower in ANGII+$MgSO_4$ (N=5) vs. ANGII (N=14) only rats at PP due to batch variability (*p<0.05). SHAM+$MgSO_4$ dams (N=4) also appeared to have a lower HR than SHAM (N=7) only at PP. This variability persisted throughout gestation. At GD18.5, HR was significantly reduced in the ANGII+$MgSO_4$ group compared to ANGII (**p<0.01) and SHAM (*p<0.05) groups. SHAM+$MgSO_4$ may have had a lower HR than SHAM at GD18.5 and a significantly lower HR than ANGII (*p<0.05). (B) Raw cardiac output values across gestation for all groups. CO significantly decreased following ANGII infusion in SHRSP dams (**p<0.01 GD6.5 vs. GD12.5). (C) ∆Cardiac output gradually increased during the course of pregnancy in SHAM+$MgSO_4$ dams (ns.). All other groups, however, experienced an initial increase followed by a decrease in ∆CO following mini pump surgery that appeared to be reversed by GD18.5 (ns.). (D) When CO was normalised to tibial length, ANGII led to a significant decrease in CO at GD12.5 (*p<0.05). Data analysed using restricted maximum likelihood mixed-effects analysis with Tukey's *post hoc* testing.

4.4.1.4 Uterine Artery Blood Flow Measured *In Vivo*

Uterine artery blood flow was analysed by Doppler ultrasound imaging throughout gestation (section 2.3.8, Fig. 4.5). Arterial blood flow was determined by calculating the systolic/diastolic (S/D, Fig. 4.5A) ratio and the resistance index (RI, Fig. 4.5B). There was no effect of either ANGII or $MgSO_4$ on either RI or S/D across gestation. There appeared to be an increase in S/D and RI in ANGII treated dams at GD6.5, though there was no significant main treatment effect. As this occurred prior to pump implantation, this rise at GD6.5 may be due to image quality or operator variability as no treatment was administered by this time.

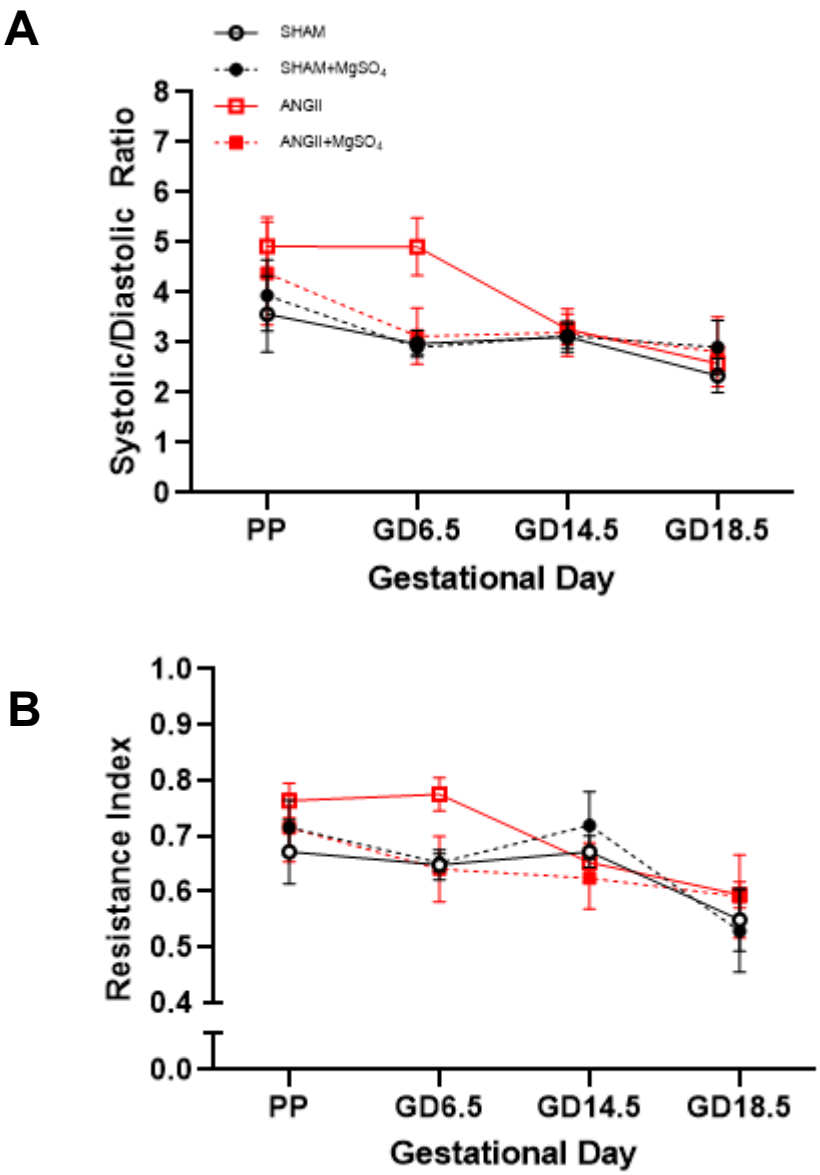

Figure 4.5: Pulse Wave Doppler Ultrasound Assessment of the Uterine Artery

Blood flow through the uterine artery was assessed by analysing waveform measurements captured prior to and throughout pregnancy. There was no significant main treatment effect on RI or S/D. (A) Peak end systolic and diastolic volumes were calculated as detailed in the methods and expressed as a ratio. S/D was not different between ANGII (*N*=13), SHAM (*N*=7), SHAM+$MgSO_4$ (*N*=3) or ANGII+$MgSO_4$ (*N*=5) dams . (B) Resistance index was calculated using the peak end systolic and diastolic volumes. RI was not significantly different across gestation or treatment groups. $MgSO_4$ had no effect on uterine blood flow in either SHAM or ANGII treated dams. Data analysed using restricted maximum likelihood mixed-effects analysis..

4.4.1.5 $MgSO_4$ Alters Water Homeostasis and Alleviates Proteinuria in ANGII-Infused SHRSP Dams

Twenty-four hour water intake and urine output were measured at pre-pregnancy (PP) and on GD6.5 and 18.5 using metabolic cages (2.3.5). Analysis via REML mixed-effects revealed there was a significant main treatment effect on water intake (p=0.0199) and urine output (p=0.0003). This significant main treatment effect persisted when these measures were expressed as a proportion (p=0.0003). At PP, there were no differences in water intake or urine output (Fig. 4.6A, 4.6B). No significant differences were noted between groups for either water intake or urine output at GD6.5. Using Tukey's *post hoc* multiple comparisons, it was observed that by GD18.5, animals receiving ANGII exhibited a significant increase in both water intake (51±3mL vs. 34±1mL) and urine output (31±3mL vs. 13±1mL) when compared to SHAM controls (p<0.0001, p<0.001, respectively). Addition of $MgSO_4$ to drinking water in ANGII-infused dams resulted in a significant decrease in both water intake and urine output compared to ANGII only (p<0.01, p<.0.0001, respectively). Following correction for fluid intake, urine output was expressed as a proportional urine excretion (Fig. 4.6C). No significant differences were noted at PP or GD6.5. The proportion of urine excretion to fluid intake was significantly increased on GD18.5 in the ANGII group relative to SHAM controls (60±4% vs. 39±2%, p<0.01). The effect of $MgSO_4$ in ANGII-infused dams was preserved when urine output was corrected (20±4%, p<0.001). Of note, proportional urine excretion in ANGII+$MgSO_4$ mothers was significantly decreased in comparison to SHAM controls (p<0.05).

Urinary samples collected from the aforementioned gestational time points were analysed to determine the albumin:creatinine ratio (ACR; Fig. 4.6D) as a measure of proteinuria (2.2.4). There was no significant main treatment effect detected in ACR. SHAM controls appeared to experience a decrease in proteinuria in early pregnancy that was sustained until GD18.5 (0.34±0.11µg/µmol/L PP; 0.16±0.04µg/µmol/L GD6.5; 0.13±0.03µg/µmol/L GD18.5, ns.). No additional effect of $MgSO_4$ drinking water on proteinuria in SHAM animals was detectable. ANGII-infused dams saw an apparent increase in proteinuria across pregnancy (0.39±0.06µg/µmol/L PP; 4.27±3.61µg/µmol/L GD6.5, ns.) that by GD18.5 was observed to be higher than SHAM controls (163.5±98.56µg/µmol/L; ns). $MgSO_4$ appeared to somewhat reverse the effect of ANGII infusion and decreased ACR at GD18.5 (11.96±5.81µg/µmol/L; ns).

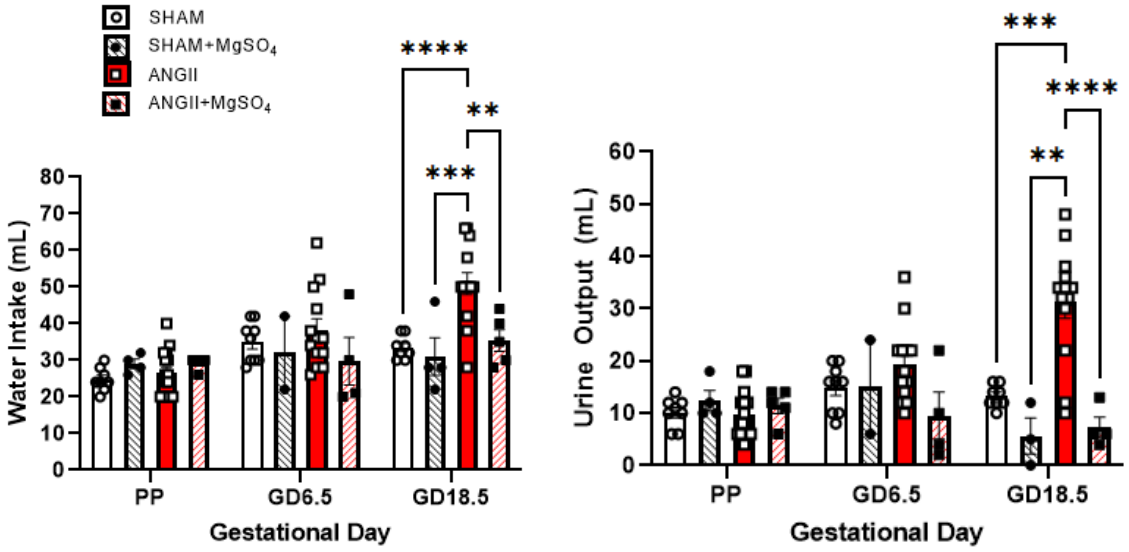
SHAM
SHAM+MgSO4
ANGII
ANGII+MgSO4
Water Intake (mL)
Urine Output (mL)
PP
GD6.5
GD18.5
Gestational Day
****
***
**
*

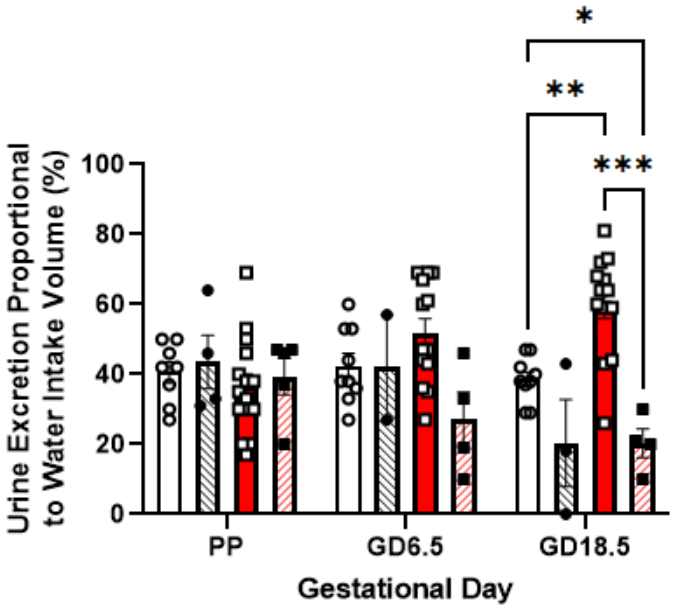
Urine Excretion Proportional to Water Intake Volume (%)
PP
GD6.5
GD18.5
Gestational Day
*
**
***

D

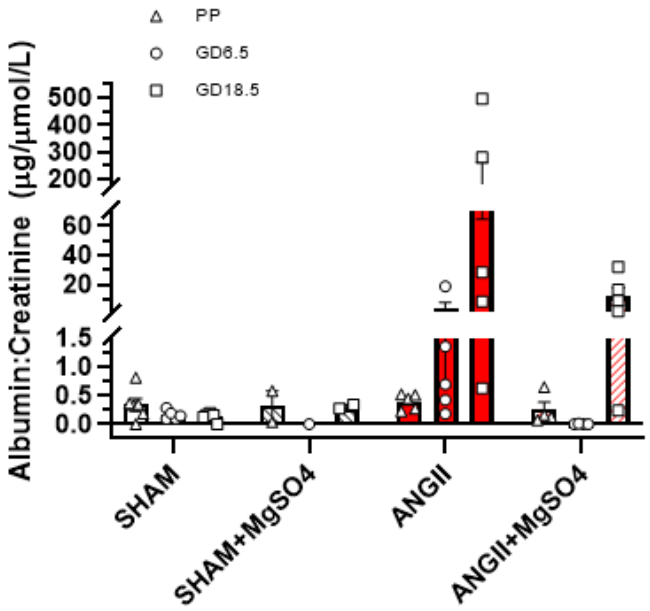
PP
GD6.5
GD18.5
Albumin:Creatinine (µg/µmol/L)
SHAM
SHAM+MgSO4
ANGII
ANGII+MgSO4

Figure 4.6: $MgSO_4$ Decreases Urine Output Proportionally to Water Intake and Proteinuria in ANGII-Infused Dams in Late Gestation

Metabolic cages were used to collect twenty-four hour measurements of water intake and urine output prior to and throughout pregnancy in SHAM (*N*=9), SHAM+$MgSO_4$ (*N*=4), ANGII (*N*=15) and ANGII+$MgSO_4$ (*N*=5 Analysis via REML mixed-effects revealed there was a significant main treatment effect on water intake (*p*=0.0199) and urine output (*p*=0.0003). This significant main treatment effect persisted when these measures were expressed as a proportion (*p*=0.0003). (A) Water intake, (B) Urine output. Urine output was expressed as a proportion to correct for fluid intake (C). When corrected, there were no significant differences in proportional urine excretion at PP or GD6.5 between groups. At GD18.5 ANGII-infusion significantly increased proportional urine excretion relative to SHAM controls (**p<0.01). $MgSO_4$ drinking water in ANGII-infused dams significantly decreased proportional urine excretion (***p<0.001 vs. ANGII) to levels that were also significantly lower than SHAM (*p<0.05). Data analysed by restricted maximum likelihood mixed-effects analysis with Tukey's *post hoc* testing. (D) ACR appeared to be increased following ANGII (*N*=5) infusion and seemed to be higher than SHAM (*N*=6) at GD18.5. ACR appeared reduced at GD18.5 when ANGII-infused dams were given $MgSO_4$ (*N*=5) drinking water throughout pregnancy. SHAM+$MgSO_4$ animals were not included in the analysis (*N*=2). Data analysed by restricted maximum likelihood mixed-effects analysis with Tukey's *post hoc* testing, as appropriate.

4.4.2 Fetal and Placental Outcomes in Response to ANGII and $MgSO_4$

4.4.2.1 Litter Size, Fetal Weight and Morphometry

Neither ANGII-infusion nor $MgSO_4$ drinking water significantly altered litter size (Fig. 4.7A). Fetal weights and anthropometric measurements were collected at GD18.5 following sacrifice. There was a significant main effect of both ANGII (*p*=0.0008) and $MgSO_4$ (*p*=0.0113) on fetal weight. Exposure to ANGII *in utero* resulted in a significant decrease in fetal weight when compared to SHAM (1.02±0.06g vs. 1.30±0.10g, p<0.05, Fig. 4.7B). This was not reversed with $MgSO_4$ (0.80±0.11g), which also resulted in a significantly decreased fetal weight compared to SHAM (p<0.01) and SHAM+$MgSO_4$ (p<0.05). This decrease was also observed compared to ANGII alone (0.80±0.11g, ns.). There may also have been a reduction in fetal weight in SHAM+$MgSO_4$ animals relative to SHAM controls (1.00±0.11g, ns.). A similar finding between the groups was observed in head circumference, where a significant main effect was detected for ANGII (*p*=0.0219) and $MgSO_4$ (*p*=0.0051). (Fig. 4.8A). There was a main effect of ANGII (*p*=0.0092) but not $MgSO_4$ in crown-rump length. Crown-rump length (Fig. 4.8B) appeared to be lower in SHAM+$MgSO_4$ (28±1mm) and was significantly lower in

ANGII (28±1mm, $p<0.05$) than in the SHAM group (32±1mm). Fetuses from the ANGII+$MgSO_4$ group had a crown-rump length that was significantly lower still than ANGII alone (27±2mm, $p<0.05$). Significant main effects for both ANGII ($p=0.0111$) and $MgSO_4$ ($p=0.0161$) were found in abdominal circumference (Fig. 4.8C). Abdominal circumference was significantly lower in ANGII+$MgSO_4$ (19±2mm) offspring when compared to those from SHAM (26±1mm) pregnancies ($p<0.01$). Though non-significant, it appeared that addition of $MgSO_4$ in either SHAM (22±1mm) or ANGII dams resulted in an observed decrease in abdominal circumference. ANGII alone (22±1mm) may also have decreased abdominal circumference when compared to SHAM (ns.) Analysis by two-way ANOVA revealed a significant main effect of $MgSO_4$ ($p<0.0001$) but not ANGII in the head:body ratio (Fig. 4.8D), which was used as indicator of head-sparing fetal growth restriction. *Post hoc* multiple comparisons showed that, *in utero* exposure of SHAM dams with $MgSO_4$ resulted in a significant increase in head:body ratio (0.50±0.03 SHAM+$MgSO_4$ vs. 0.34±0.03 SHAM, $p<0.0001$). A combination of ANGII infusion and $MgSO_4$ drinking water resulted in a significantly increased head:body ratio compared to both SHAM and ANGII only (0.56±0.03, $p<0.0001$ vs. ANGII, $p<0.001$ vs. SHAM).

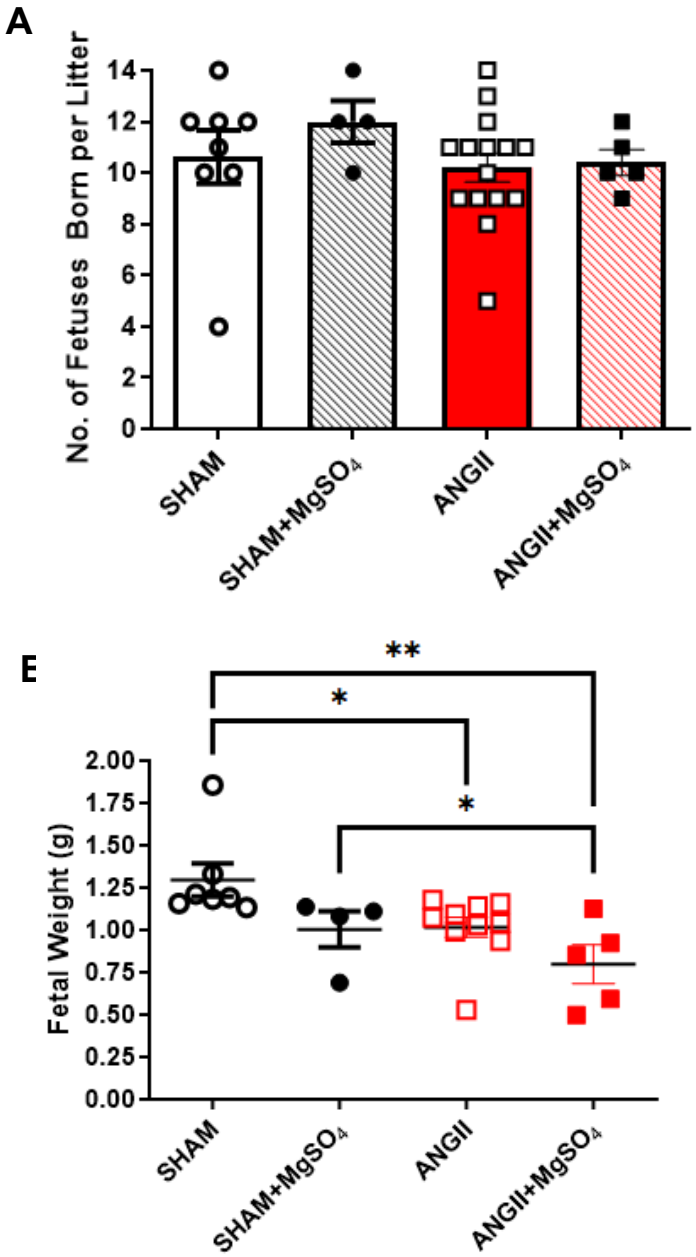

Figure 4.7: Litter Size and Fetal Weight Following ANGII and $MgSO_4$ Intervention

The number of offspring and fetal wight in each litter was recorded at GD18.5. (A) Infusion of ANGII (*N*=15) into SHRSP dams did not significantly influence the number of offspring per litter on GD18.5 when compared to SHAM (*N*=8). $MgSO_4$ did not have a significant influence on litter size in either the SHAM+$MgSO_4$ (*N*=4) or ANGII+$MgSO_4$ (*N*=5) groups. (B) There was a significant main effect of both ANGII (p=0.0008) and $MgSO_4$ (p=0.0113) on fetal weight. Fetal weight was significantly decreased as a result of ANGII infusion vs. SHAM (*p<0.05). There was also a significant decrease vs. SHAM in the ANGII+$MgSO_4$ group (**p<0.01) that may have been lower than ANGII. SHAM+$MgSO_4$ fetuses also appeared to have a reduced fetal weight compared to SHAM. Data analysed by two-way ANOVA with Tukey's *post hoc* testing, as appropriate.

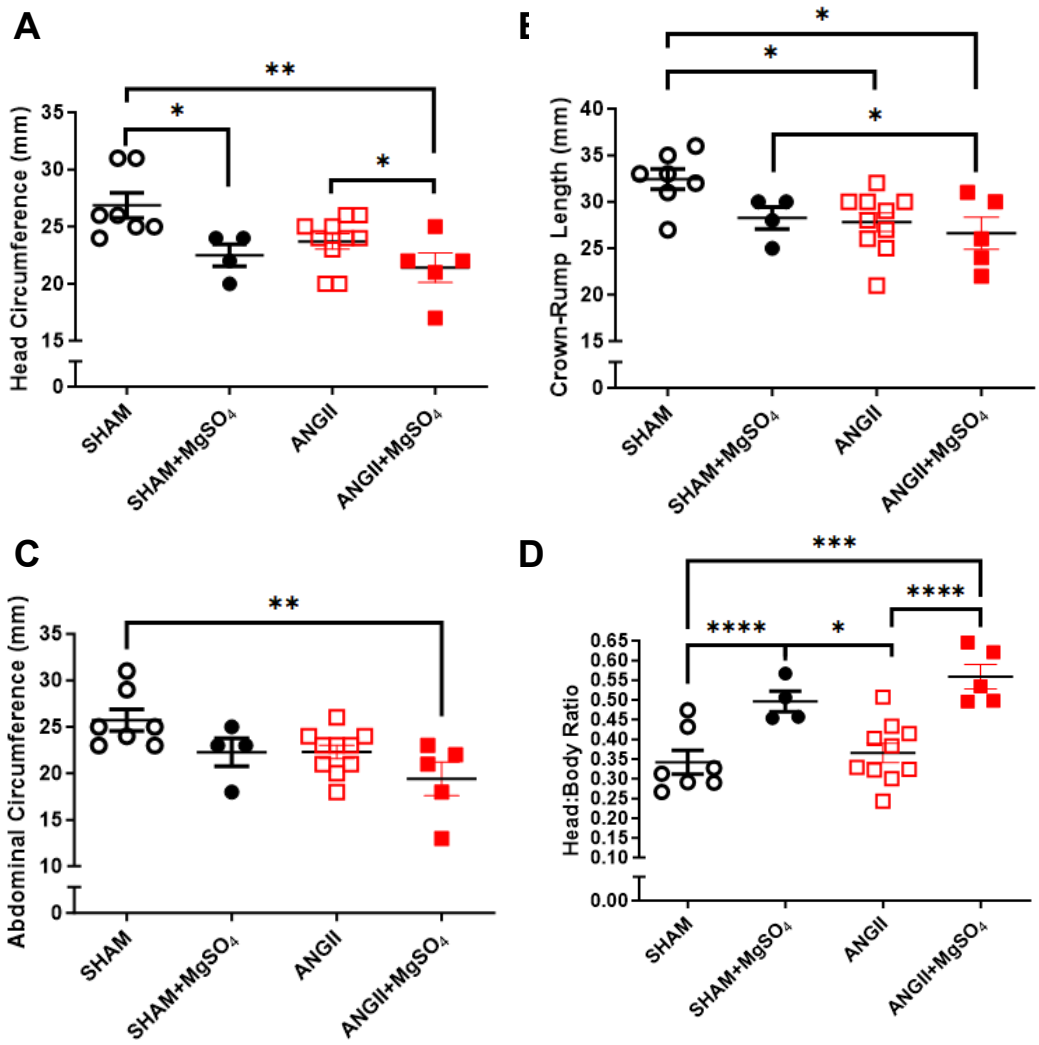

Figure 4.8: Anthropometric Measurements of Fetal Growth

At GD18.5, fetuses were removed from the uterine horn and all amniotic fluid, placental tissue and associated membranes were removed. (A) A significant main effect was detected for ANGII (p=0.0219) and MgSO4 (p=0.0051) in head circumference; SHAM+$MgSO_4$ (*N*=4), ANGII (*N*=10) and ANGII+$MgSO_4$ (*N*=5) groups relative to SHAM (*N*=7) controls. $MgSO_4$ alone or in combination with ANGII resulted in a significant decrease in head circumference relative to SHAM (**p*<0.05) or ANGII alone (**p*<0.05). There was a main effect of ANGII (*p*=0.0092) but not $MgSO_4$ in crown-rump length (B). ANGII resulted in a significant decrease in crown-rump length compared to SHAM (**p*<0.05) that was not reversed by $MgSO_4$ (**p*<0.05, **p*<0.05 vs. SHAM+$MgSO_4$). Abdominal circumference showed a significant main effect from both ANGII (*p*=0.0111) and $MgSO_4$ (*p*=0.0161, C). Abdominal circumference was significantly lower in ANGII+$MgSO_4$ offspring versus SHAM (***p*<0.01). There may also have been a decrease in SHAM+$MgSO_4$ relative to SHAM and ANGII relative to ANGII+$MgSO_4$. (D) Analysis by two-way ANOVA revealed a significant main effect in head:body ratio of $MgSO_4$ (*p*<0.0001) but not ANGII. Head:body ratio was calculated as an indicator of head-sparing fetal growth restriction and, following *post hoc* analysis, was found to be significantly increased for SHAM and ANGII in combination with $MgSO_4$ in comparison to SHAM or ANGII only (*****p*<0.0001 SHAM/ANGII vs SHAM+$MgSO_4$/ANGII+$MgSO_4$, ****p*<0.001 SHAM vs. ANGII+$MgSO_4$, **p*<0.05 SHAM +$MgSO_4$ vs. ANGII, respectively). Data analysed by two-way ANOVA with Tukey's *post hoc* testing, where appropriate.

4.4.2.2 Placental Characteristics

There was a significant main effect of both ANGII (p=0.0024) and $MgSO_4$ (p=0.0310) on placental weight. Placental weight was significantly reduced in those born to mothers infused with ANGII versus SHAM controls (0.225±0.01g vs. 0.288±0.02g, p<0.05, Fig. 4.9A). Offspring from ANGII+$MgSO_4$ dams (0.204±0.01g) also exhibited a significantly decreased placental weight relative to SHAM (p<0.01, p<0.05 vs 0.233±0.017; SHAM+$MgSO_4$ that was also lower than ANGII only (ns). Whilst not statistically significant, there appeared to be a nominal reduction in placental weight in SHAM+$MgSO_4$ offspring compared to SHAM (0.233±0.02g, ns.). The fetal:placental ratio did not differ significantly between groups, however, there was a pattern of a reduced ratio in both groups receiving ANGII that was more pronounced in offspring exposed to both ANGII and $MgSO_4$ *in utero* (4.43±0.32 ANGII, 3.96±0.49 ANGII+$MgSO_4$ vs. 4.93±0.23 SHAM, Fig. 4.9B, ns.). There did not seem to be an effect of $MgSO_4$ alone in SHAM animals (4.91±0.41 SHAM+$MgSO_4$, ns.).

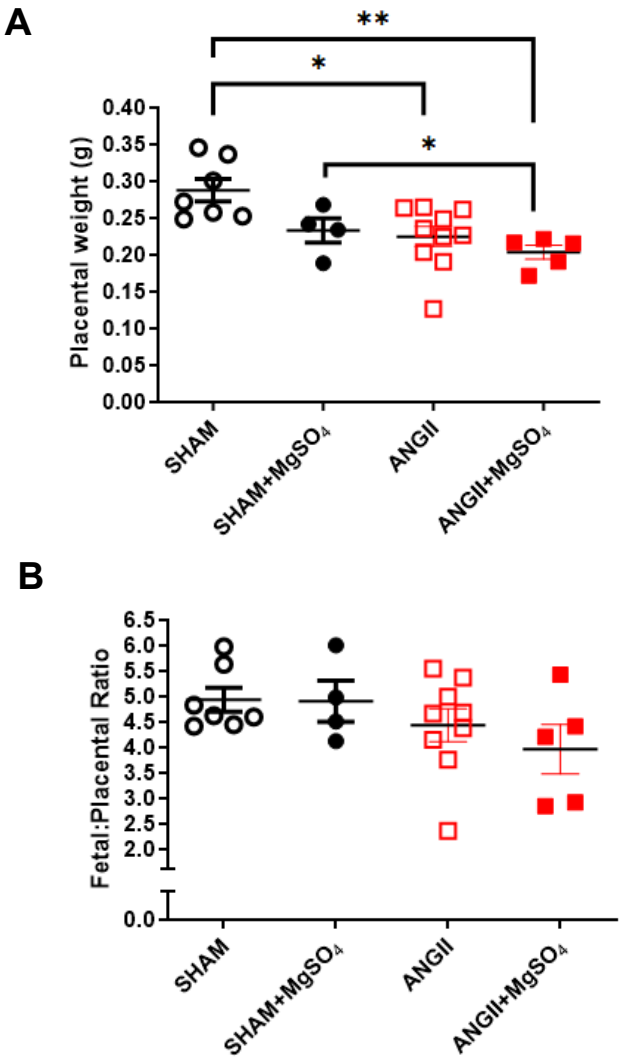

Figure 4.9: Placental Weight and the Fetal:Placental Ratio Following ANGII and $MgSO_4$

Once separated from the fetus, each placenta was gently blotted with absorbent paper to remove excess fluid. There was a significant main effect of both ANGII (p=0.0024) and $MgSO_4$ (p=0.0310) on placental weight. (A) Treatment with ANGII (N=10) resulted in a significant decrease in placental weight when compared to SHAM (N=7) placentae (*p<0.05). Placental weight was also significantly reduced in ANGII+$MgSO_4$ compared to SHAM+$MgSO_4$ (*p<0.05) and SHAM placentae (**p<0.01). (B) The fetal:placental ratio did not significantly differ between groups though there was a pattern of a decreased ratio in both ANGII and ANGII+$MgSO_4$ offspring when compared to both SHAM and SHAM+$MgsO_4$ offspring. Data analysed by two-way ANOVA with Tukey's *post hoc* testing, where appropriate.

4.5 Discussion

The work presented in this chapter has shown that administration of magnesium sulphate salt ($MgSO_4$) as a 1% w/v solution in place of normal drinking water as a preventative therapeutic during hypertensive pregnancy improves maternal weight gain, blood pressure and proteinuria. However, $MgSO_4$ treatment is detrimental to fetal growth and maternal cardiac function and did not improve indices of maternal uteroplacental blood flow. Further study and characterisation are required to understand the role of magnesium during hypertensive pregnancy and whether its use could open a new avenue of therapeutics, particularly in the case of super-imposed pre-eclampsia.

Reversible weight gain is an important indicator of a healthy pregnancy, with the fetus accounting for 28% of total gestational weight gain (Dalfra' *et al*, 2022). Other sources of maternal weight gain include amniotic fluid, uterine and breast tissue, fat stores and changes to blood and fluid volume (Thornburg *et* al, 2015; Dalfra' *et* al, 2022). Evidence in the literature shows that failure to gain an appropriate amount of gestational weight can result in adverse fetal and neonatal outcomes (Thornburg *et al*, 2015). In a meta-analysis of 196,670 participants examining weight gain across pregnancy, Voerman and colleagues (2019) showed that the risk of adverse outcomes was increased where gestational weight gain was either below or above the optimal range. All groups in this study demonstrated a consistent weight-gain throughout pregnancy. When non-gravid weight (total body weight minus the gravid uterus) was measured at GD18.5, it was found that ANGII-infusion at mid-gestation in the SHRSP may have resulted in a decrease in non-gravid weight relative to SHAM controls that was rescued by $MgSO_4$. Mg^{2+} is involved in protein synthesis, insulin metabolism and blood glucose control (Gröber *et al*, 2015). Subclinical hypomagnesemia is often associated with a loss of appetite and constipation (Gröber *et al*, 2015). Additionally, evidence suggests that a balanced magnesium status is an important factor in carbohydrate metabolism (Fiorentini *et al*, 2021). Thus, it appears that supplementation of SPE-like ANGII-infused dams with $MgSO_4$ may improve maternal weight gain via appetite control. Food intake was not measured in this study but could be investigated in the future using metabolic cages.

$MgSO_4$ resulted in a significant fall in systolic blood pressure, confirmed by tail-cuff plethysmography, in both ANGII-treated and SHAM mothers. Magnesium supplementation in those with hypertension as means to lower BP has yielded inconsistent results. Several studies have shown a significant reduction in BP alongside a significant increase in serum Mg^{2+} and urinary Mg^{2+} excretion when Mg^{2+} was used as an intervention in cases of mild to moderate hypertension (Kowano *et al*, 1998; Jee *et al*, 2002; Houston, 2011). Other studies have shown that there is no beneficial effect of Mg^{2+} supplementation in hypertension (Dickinson *et al*, 2006). With regards to pregnancy, serum Mg^{2+} has been shown to decline over the course of pregnancy and has been found to be significantly decreased in red blood cell membranes of individuals with pre-eclampsia versus normotensive pregnancies (Dalton *et al*, 2016; Nelander *et al*, 2017). Further, a deficiency of magnesium has been linked to the development of pre-eclampsia (Chiarello *et* al, 2018). Mg^{2+} is known to influence vascular tone via a number of mechanisms. Its action as a natural Ca^{2+} channel blocker results in the production of vasodilatory prostaglandins and competes for binding sites on vascular smooth muscle cells reducing intracellular calcium and sodium (Houston, 2011). Magnesium also increases the production of nitric oxide by endothelial cells, improving endothelial function and decreasing total peripheral resistance (Fiorentini *et al*, 2021; Schutten *et al*, 2018). It is unknown which of these actions may be responsible for the beneficial effect on maternal SBP in this study, or indeed if it is a combination of mechanisms.

In a normal pregnancy, changes to cardiac function are apparent as early as the first trimester, with rising cardiac output and stroke volume functioning to offset the decline in peripheral resistance and increase in left ventricular mass (Sanghavi and Rutherford, 2014; Soma-Pillay *et al*, 2016). This is not the case during hypertensive pregnancies, where volume-overload related stress results in diastolic dysfunction that is evidenced by increased left ventricular mass, vascular resistance and reduced SV and CO (Gyselaers and Thilaganathan, 2019; Castleman *et al*, 2016). In this study, ΔCO trended towards a reduction in the chronically hypertensive SHAM and SPE-like ANGII groups by GD12.5 (relative to PP values) before rising at GD18.5. SV tended to rise over the course of gestation in SHAM animals but tended towards an overall decrease across gestation in the ANGII group. $MgSO_4$ did not significantly improve either ΔCO or SV in ANGII-infused dams. Mg^{2+} is also known to influence myocardial metabolism and Ca^{2+}

homeostasis by preventing activation of L-type Ca^{2+} channels in the myocardium and modulation of intracellular ion concentrations by interactions with several transporters that regulate the cardiac action potential (Fiorentini *et al*, 2021). $MgSO_4$ has been shown to improve cardiac function in the L-NAME model of SPE (Coates *et al*, 2006). Further studies have shown that $MgSO_4$ increases CO and SV in both animal models and pre-eclamptic patients (James, 2010). There was no beneficial effect of $MgSO_4$ on ΔCO or SV in ANGII-infused SHRSP dams in this study. With regards to ΔCO, any potential beneficial effect of $MgSO_4$ may have been obscured by the batch variability introduced by the COVID-19 pandemic. To combat the small *n* numbers generated due to COVID-related restrictions, data points for the ANGII and SHAM groups from Chapter 3 were added to the results of Chapter 4. This non-contemporaneous study design introduced the batch variation observed in the raw heart rate and cardiac output data. Alternatively, this may be, in part, due to alterations in Mg^{2+} metabolism following ANGII. Both ANGII and aldosterone have been reported to alter intracellular concentrations of Mg^{2+} (Touyz *et al*, 2001). In human PE, it has been shown that though ANGII production is decreased there is an increased sensitivity to it as well as an accumulation of Mg^{2+} in the fetal circulation that may arise from altered Mg^{2+} metabolism (Verdonk *et al*, 2014; Chiarelllo *et al*, 2018). Therefore, it may be possible that infusion of ANGII resulted in a depletion of intracellular magnesium in maternal tissues and accumulation in fetal tissues. It should also be noted that due to the administration method of $MgSO_4$ in this study the exact dose delivered in drinking water cannot be accurately controlled and may have varied between individual animals which creates difficulties in ascertaining its beneficial effects. Measurement of the maternal magnesium status as well as that of the placenta and fetus would be of great interest in this model to understand how ANGII alters Mg^{2+} status and availability during hypertensive pregnancy.

Deficiencies in remodelling of the maternal uterine spiral arteries have long been associated with the development of hypertensive disorders of pregnancy and have been confirmed to occur in normal SHRSP pregnancies (Small *et al*, 2016a). There was no effect of either ANGII or $MgSO_4$ on indices of uteroplacental flow as measured by Doppler ultrasound in this study. This was unexpected, given the known actions of Mg^{2+} on the vasculature as discussed previously. However, the benefit of $MgSO_4$ on uteroplacental flow has been debated in the literature. Though Shcauf and colleagues (2009) showed an increase in blood volume in the

uterine arteries of pre-eclamptic patients, there was no statistical difference in resistance index 24 hours after intravenous $MgSO_4$. A similar finding was observed when $MgSO_4$ was given to a small cohort of individuals with pre-term labor, where RI did not change following a 6 hour infusion of $MgSO_4$ (Güden *et al*, 2016). Conversely, a study by Souza *et al*, (2010) found that both RI and S/D in the uterine artery decreased in severely pre-eclamptic individuals receiving an i.v. loading dose of $MgSO_4$ after 20 minutes. This was also seen by Maged and colleagues (2016) following a similar short-term protocol in a similar population. Much of the literature is comprised of small scale studies in local patient populations, thus larger-scale studies and further investigation of the effects of $MgSO_4$ during pregnancy are required to understand its actions on maternal and fetoplacental blood flow.

In agreement with results from Chapter 3, infusion of ANGII in pregnant SHRSP dams led to increased water intake and urine production alongside proteinuria at GD18.5 compared to SHAM. ANGII+$MgSO_4$ dams had significantly reduced intake, output and proteinuria at GD18.5 compared to ANGII alone, though none of these were similar to SHAM levels. Previous work in rodent models has shown a renoprotective effect of $MgSO_4$ in female diabetic rats, improving surgically induced renal ischemia/reperfusion injury (Akan *et al*, 2016). The kidneys play a major role in Mg^{2+} homeostasis, with the glomeruli filtering 70% of total serum Mg^{2+}, of which 96% is reabsorbed by the renal tubules (Blaine *et al*, 2015). Renal Mg^{2+} excretion is dependent on serum Mg^{2+}. However, due to the large stores of Mg^{2+} that exist within bone and soft tissue, it is possible for serum Mg^{2+} to present within the normal ranges, thereby maintaining renal excretion, even though intracellular stores may be depleted (Fiorentini *et al*, 2021). Indeed, this has been shown to occur in hypertensive humans and rats (Barbagallo *et al*, 2021). Therefore, $MgSO_4$ added to drinking water may have resulted in elevated intracellular renal Mg^{2+} prior to and following ANGII administration, preventing depletion due to worsening hypertension. In support of this, magnesium in drinking water generally has a higher bioavailability (Barbagallo *et al*, 2021). Additionally, Mg^{2+} is known to modulate the immune response and subclinical Mg^{2+} deficiency, as is observed in hypertensive pregnancies, creates a low-grade chronic state of inflammation which is theorised to underlie the proteinuria characteristic of pre-eclampsia (Maier *et al*, 2021; Karumanchi *et al*, 2005). Supplemental $MgSO_4$ may prevent this inflammation and resultant tissue damage, improving renal function

and decreasing proteinuria. Assessment of fibrosis and renal morphology, similar to the methods carried out in Chapter 3, would be of interest in this study.

Fetal growth restriction is known to occur in hypertensive disorders of pregnancy, including pre-eclampsia, and has been shown to occur in the pregnant SHRSP when infused with ANGII (Obata *et* al, 2020; Morgan *et al*, 2018). Magnesium has been linked to FGR whereby $MgSO_4$ treatment has been shown to reduce the risk of low birthweight, preterm birth and stillbirth (Fanni *et al*, 2021; Lassi *et al*, 2014). Similar findings have been seen in rodent models where $MgSO_4$ increased fetal and placental weights in a rat model of IUGR (Kazemi-Darabadi and Akbari, 2020). This was not the case in this study, where ANGII infusion combined with $MgSO_4$ drinking water resulted in a significant decrease in head circumference, fetal and placental weights and significantly increased head:body ratio relative to SHAM and ANGII alone. Some evidence exists that suggests antenatal $MgSO_4$ in pre-eclamptic women results in adverse neonatal outcomes due to fetal hypermagnesemia (Abbassi-Ghanavati *et al*, 2012; Elasy and Nafea, 2022; Mittendorf *et al*, 2002). Mg^{2+} has previously been shown to be actively transported against a maternal-fetal concentration gradient in the rat placenta (Greer, 1994). In humans, pre-eclamptic placentae have been found to exhibit a decreased clearance of $MgSO_4$ (Brookfield *et al*, 2016). It has been reported that fetuses exposed to prolonged administration of $MgSO_4$, as was the method of this study, experience a higher incidence of complications than those exposed for relatively short durations as is more common when used in clinical practice for the treatment of pre-eclampsia (Kamitomo *et al*, 2000; James, 2010; Narasimhulu *et al*, 2017). This may explain the effect of $MgSO_4$ on fetal and placental outcomes observed in this study. Further study on $MgSO_4$ and fetoplacental outcomes would be advantageous in understanding the detrimental impact of $MgSO_4$ in this model.

To conclude, pregnant SHRSP dams infused with ANGII experience the classical symptoms of super-imposed pre-eclampsia. Treatment of these dams with $MgSO_4$ improved maternal systolic blood pressure, weight gain and proteinuria but did not improve fetal and placental outcomes when compared to ANGII alone. Additionally, $MgSO_4$ in addition to ANGII administration showed a significantly worse outcome for multiple fetal and placental measures of *in utero* growth compared to ANGII alone and was ineffective in improving uteroplacental blood flow. The use of $MgSO_4$ in the treatment of pre-eclampsia and the benefit to

maternal and fetal outcomes is still widely debated. Many of the studies available on $MgSO_4$ use during hypertensive pregnancies are of low to moderate quality and large-scale meta-analyses fail to show a positive correlation. This study may be improved by monitoring the maternal, fetal and placental Mg^{2+} status as well as renal histopathology at time of sacrifice. It may also be of benefit to investigate alternative dosing routes and regimes in this model and comparing fetal outcomes to determine if prolonged exposure to $MgSO_4$ is the underlying cause of further FGR in this study.

Chapter 5: Distinct Uterine Artery Gene Expression Profiles During Early Gestation in the Stroke-Prone Spontaneously Hypertensive Rat

This work is published as an open-access article, cited as:

Scott, K.*, Morgan, H.L.*, Delles, C., Fisher, S., Graham, D. and McBride, M.W. (2021). Distinct uterine artery gene expression profiles during early gestation in the stroke-prone spontaneously hypertensive rat. *Physiological Genomics*. **53** (4), p.160-171.

Where * indicates an equal contribution.

Preface

The results contained in the following chapter were produced and analysed in collaboration with individuals at the University of Glasgow and Dr. Hannah L. Morgan. Contributions to the work of this chapter were as follows, in accordance with the CreDiT system:

Conceptualisation: Dr. Morgan, Dr. Graham and Dr. McBride.
Data Curation: Mx. K. Scott.
Formal Analysis: Mx. K. Scott and Dr. Morgan (IPA Analysis).
Investigation: Dr. Morgan (myography and RNA extractions) and Mx. K. Scott (IPA data generation).
Methodology: Dr. McBride, Dr, Graham, Dr. Morgan and Mx. K. Scott.
Project Administration: Dr. McBride, Dr. Graham and Dr. Delles.
Visualisation: Mx. K. Scott and Mr. S. Fisher.
Writing – Original Draft: Mx. K. Scott (results, discussion, conclusion) and Dr. Morgan (introduction, methods).
Writing – Review and Editing: Mx. K. Scott, Dr. Morgan, Dr. Graham, Dr. Delles and Dr. McBride.

Alterations to the original content of this article have been made in response to examiner comments for this thesis, thus the text and results presented in this chapter may differ in some places from the original published manuscript.

5.1 Introduction

Hypertensive complications during pregnancy are abundantly common worldwide and have been attributed as a leading cause of maternal mortality (Say *et al*, 2014). Hypertensive disorders of pregnancy (HDP) encompass both known hypertension before pregnancy and de novo hypertension; diagnosed on or after 20 wk gestation and includes gestational hypertension, preeclampsia, chronic hypertension, and superimposed preeclampsia (Brown *et al*, 2018b). The complicated multifactorial nature of these disorders means that there is large variability in clinical presentations and severity (Cunningham and LaMarca, 2018). Conditions such as preeclampsia are major contributors to poor fetal development, resulting in intrauterine growth restriction and premature birth (Stojanovska *et al*, 2016). Furthermore, these conditions can impact the health of both the mother and offspring in later life, with the increased risk of development of cardiovascular disease and type 2 diabetes (Barker and Osmond, 1986; Barker *et al*, 1989; Barker *et al*, 1993; Wilson *et al*, 2003; Sattar *et al*, 2003; Hubel *et al*, 2000).

Hypertensive pregnancies share similarities in the vascular dysfunction phenotypes observed in the placental bed and the phenotypes that underpin cardiovascular diseases (Sattar and Greer, 2002). During normal uncomplicated pregnancies, major uteroplacental vascular remodelling occurs transforming the uteroplacental vessels from narrow, muscular, and vasoactive arteries to more flaccid, open vessels that are less responsive to vasoconstrictive and dilatory agents (Pijenborg *et al*, 2006; Osol and Mandala, 2009). Maternal blood is then able to freely flow into the intervillous space, thus allowing adequate exchange of nutrients, gases, and waste products between mother and fetus, via the placenta. In HDP, the uteroplacental vasculature fails to remodel sufficiently, thus impairing uteroplacental blood flow. This has the potential to result in fetal growth restriction, placental ischemic-reperfusion damage, and increased antiangiogenic and proinflammatory factors, which are released into the circulation leading to systemic vascular dysfunction (Burton *et al*, 2009; Robertson *et al*, 1967). Spiral arteries from patients with preeclampsia have been found to have shallower remodelling, retain a contractile phenotype, and do not show a pregnancy-dependent increase in flow-mediated vasodilation (Lyall *et al*, 2013). Furthermore, there is evidence that this remodelling is initiated before the invasion of placental-derived trophoblast cells. A study by van der Heijden et al. (2005) in pseudopregnant mice

provides evidence that the initiation of uteroplacental vascular remodelling can occur in the absence of any conceptus material, suggesting that the uterine arteries can be “primed” by maternal factors to respond appropriately to more major placental-dependent remodelling events.

Examining the uteroplacental vascular gene expression in these early remodelling stages is a key for understanding the vascular responses to HDP. Studies have examined the differential gene expression over gestation in humans and rodents and found pregnancy-dependent changes in the expression of hormone receptors, calcium, and potassium channels and growth factors in the uterine artery (Osol and Mandala, 2009; Pastore *et al*, 2012; Mishira *et al*, 2018; Hu *et al*, 2019). However, studies examining the genetic profile of the uterine arteries response to pathophysiological pregnancy are lacking. The majority of studies investigating gene expression changes associated with abnormal vascular remodelling responses in HDP have focused on term placental or decidual gene expression (Lian *et al*, 2010; Herse *et al*, 2012; Wang *et al*, 2012). Thus, the mechanisms behind impaired early pregnancy-dependent remodelling are still elusive due to inaccessibility of uterine artery tissue and ethical issues with tissue from early-pregnancy timepoints. Animal models of HDP can be used to overcome this obstacle.

The stroke-prone spontaneously hypertensive rat (SHRSP) demonstrates an elevated blood pressure throughout gestation with evidence of reduced uteroplacental blood flow and fetal and placental abnormalities conjunctive with common hypertensive complications in human pregnancy (Small *et al*, 2016a). Furthermore, SHRSP demonstrates a failure to respond to the cardiovascular demands of pregnancy even in the absence of chronic hypertension. Nifedipine-treated SHRSP dams did not develop hypertension, yet still demonstrated a failure of uterine artery pregnancy-dependent remodelling and an impaired uteroplacental blood flow compared with the normotensive Wistar–Kyoto rat (WKY) (Small *et al*, 2016a), suggesting that the SHRSP-impaired remodelling is directed by maternal genetic differences and not pre-existing hypertension. This study aimed to determine the difference in gene expression response to early pregnancy between SHRSP and WKY, to identify differential gene expression patterns that may underlie adverse vascular remodelling response to pregnancy.

5.2 Hypothesis & Aims

It was hypothesised that uterine arteries harvested in early gestation from hypertensive SHRSP dams would show an altered gene expression profile relative to uterine arteries from normotensive WKY controls.

We aimed to investigate this by performing RNA sequencing and Ingenuity Pathway Analysis® of expression profiles for genes related to vascular function in RNA extracted from uterine arteries from non-pregnant and pregnant SHRSP and WKY animals on GD6.5.

5.3 Methods

5.3.1 Animals and Mating

All animal procedures were approved by the Home Office according to the Animals (Scientific Procedures) Act (1986) (Project License 60/9021) and followed ARRIVE guidelines. SHRSP and WKY rats (obtained via brother × sister mating in-house at the University of Glasgow) were housed in controlled 12-h light/dark conditions with a constant temperature (21 ± 3°C) with ad libitum access to water and standard diet (Rat and Mouse No.1 Maintenance Diet, Special Diet Services). Virgin females of each strain were time mated at 12 wk (±4 days) of age with stud males of the respective strain, with pregnancy (P) confirmed by the presence of copulation plug [gestational day (GD) 0.5]. On GD 6.5, dams were euthanized, and the uterine artery only was isolated and cleaned of connective tissue and adipose tissue for use in either myography experiments or snap-frozen for RNA extraction. Age-matched virgin SHRSP and WKY were used as nonpregnant (NP) controls.

5.3.2 Uterine Artery Myography

Uterine arteries were dissected and prepared for wire myography as previously described (Morgan *et al*, 2018). Main uterine artery segments only were used for all myography experiments and radial arteries along with any other vessels were dissected and discarded. Briefly, after mounting and normalization to 13.3 kPa, the contractile and relaxation responses of arteries were assessed using dose responses to noradrenaline (1×10^{-8} to 1×10^{-5} mol/L), carbachol, and sodium nitroprusside (both 1×10^{-9} to 2×10^{-5} mol/L). A pressure myograph system (Danish Myo Technology) was used to determine external and internal diameters over a range of physiological pressures (10–120 mmHg). These were then used to calculate the cross-sectional area (μm^2) = $4\pi \times (D_E^2 - D_I^2)$, where D_E = external diameter and D_I = internal diameter. Group sizes were between n = 5–11 animals.

5.3.3 RNA Sample Preparation and Sequencing

Uterine artery RNA was extracted using the miRNeasy Mini Kit (Qiagen) according to manufacturer's instructions after homogenization in Qiazol using a TissueLyserII. Total RNA quality was assessed using the Eukaryote Total RNA PicoChip on an Agilent Bioanalyzer 2100 (Agilent Technologies, UK). RNA quality

was accepted with an RNA Integrity Number (RIN) >7. RNA was extracted from *N* = 3 animals per group.

A minimum of 100 ng of total RNA was used for RNA-sequencing (RNA-Seq) library preparations. Total RNA libraries were prepared with ribosomal-depleted RNA using the Illumina TruSeq Stranded Total RNA with Ribo-Zero Gold Kit (Illumina), following manufacturer's instructions. Sequencing was performed on a NextSeq500 Illumina sequencing system, with paired-end sequencing at a depth of 50 million reads per sample. Adapter and quality trimming of the reads were performed using CutAdapt and Sickle software packages, with FastQC used to ensure suitable sequence quality throughout processing. Reads were aligned using TopHat and the gene annotation build used was the Ensembl Rnor_6 reference genome, version 81. Differential expression was assessed using DESeq2 software package (Bioconductor 3.6) across four comparisons: WKY NP vs. P, SHRSP NP vs. P, WKY NP vs. SHRSP NP, and WKY P vs. SHRSP P. Principal component analysis (PCA) was performed using Python with sklearn StandardScaler. Due to the design of this study, a gene's fold change was expressed relative to nonpregnant expression, thus a negative fold change implies a reduction in expression in the nonpregnant uterine artery compared with pregnant. RNA-Seq data were deposited to Annotare 2.0 (Accession No.:E-MTAB-10212).

5.3.4 Pathway Analysis

The differentially expressed protein coding transcripts were investigated using Ingenuity Pathway Analysis® (IPA®; Qiagen). This functionally correlated transcript expression profiles from each comparison group to gene expression and highlighted biologically relevant pathway changes. The differentially expressed transcripts were filtered with $p_{adj} < 0.05$, and to confirm quantifiable expression, the fragments per kilobase of transcript per million mapped reads (FPKM) criteria was >1.0. An expression analysis was conducted for each data set of differentially expressed genes (DEGs) specific to either WKY or SHRSP with common changes removed, to highlight key disease and functional pathway involvement. This was further investigated using a core comparison analysis of the strain-specific datasets to identify differences in canonical pathways and assign activation *z*-

scores for each comparison group. Comparisons were made between nonpregnant (NP) and GD 6.5 pregnant (P) for each strain.

5.3.5 Statistical Analysis

All data are presented as means ± SE, unless otherwise stated. No data points were excluded during analysis. Myography data were analysed using area under the curve compared using two-way ANOVA with Tukey *post hoc* test. Expression analyses within IPA® were conducted automatically, using the Fisher's exact test of significance ($P < 0.05$) to prevent over representation in relation to the knowledge database of IPA® which compares gene expression in the literature with the study set.

5.4 Results

5.4.1 Early Pregnancy Did Not Alter Uterine Artery Structure or Function

Significant main ANOVA effects were detected in active effective pressure (p=0.015), the relaxation response to sodium nitroprusside (p=0.05), external diameter (p=0.012) and internal diameter (p=0.0026) only. The contractile and relaxation responses of the uterine arteries to noradrenaline and carbachol were not significantly different between strains and pregnancy (Fig. 5.4A–B). The relaxation response to sodium nitroprusside was significantly reduced in SHRSP NP compared to WKY NP arteries (Fig. 5.4C, *P < 0.05). There were no significant uterine artery functional changes between NP and GD 6.5 in response to increasing luminal pressure (Fig. 5.4D–F). However, there was a strain-dependant response, whereby NP WKY uterine arteries demonstrated a significantly increased external and internal diameter compared with NP SHRSP arteries (*P < 0.05, **P < 0.01 NP WKY vs. NP SHRSP; Fig. 5.4D–E). There were no significant differences across pregnancy or strain in cross-sectional area (Fig. 5.4F).

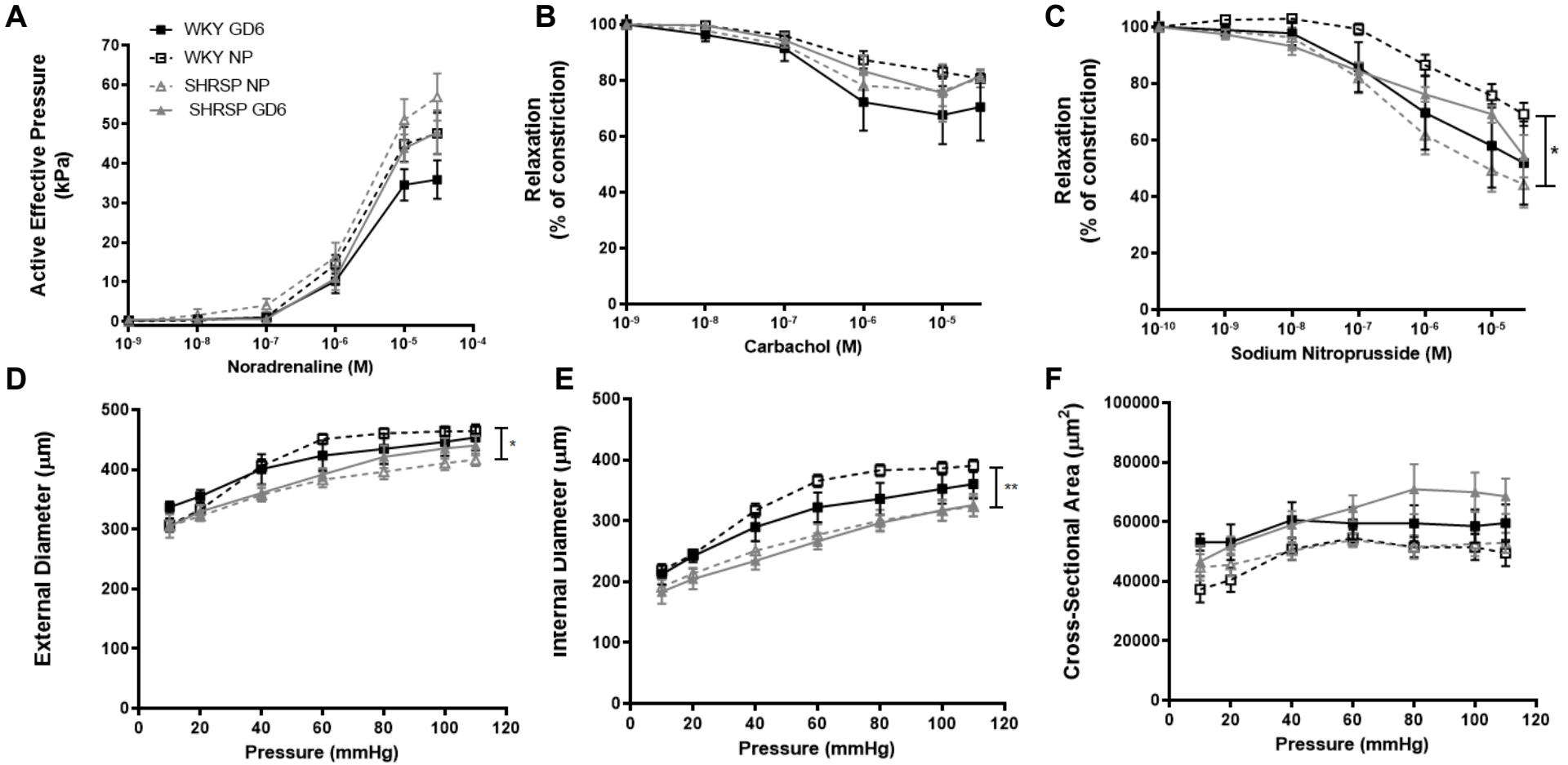

Figure 5.1: Isolated Uterine Artery Function & Structure

Isolated uterine artery function and structure was analysed *ex vivo* by wire and pressure myography in response to varying concentrations ($1x10^{-9}$ – $2x10^{-5}$M) of vasoactive stimuli and varying pressures along a gradient of 10-110mmHg. There was no significant difference in the area under the curve of the pregnancy-dependent responses to noradrenaline (A) or carbcachol (B). The area under the curve of the relaxation response to sodium nitroprusside was significantly reduced in SHRSP NP versus WKY NP arteries (*p<0.05, C). External (D) and internal (E) diameters were significantly increased in NP WKY uterine arteries compared to NP SHRSP arteries (*p<0.05, **p<0.01). There were no significant differences in uterine artery cross-sectional area (F). Data presented as mean ± SEM and analysed using two-way ANOVA with Tukey's post hoc test of the area under the curve; N=5-11. NP= non-pregnant.

5.4.2 Pregnancy Induces Strain-Specific Changes to Gene Expression as Early as GD6.5

The principal component analysis (PCA) plot (Fig. 5.2A) demonstrates a clear separation between both pregnancy state (PC1: 23.2% variance) and strain (PC2: 16.3% variance). The significant differentially expressed genes (DEGs) were separated by biotype [protein coding, long-noncoding intergenic RNA (lincRNA), microRNA (miRNA), small RNA, and pseudogenes] and the proportions represented were found to be similar in WKY and SHRSP across pregnancy (Fig. 5.2B). WKY uterine arteries were found to have 552 DEGs, with 173 DEGs upregulated and 379 DEGs downregulated in early pregnancy. SHRSP uterine arteries had 842 pregnancy-specific DEGs, with 180 DEGs upregulated and 662 DEGs downregulated (Table 5.1). The number of significant DEGs that were novel for each comparison group and those that were common between strains are shown in Fig. 5.2C. The biological relevance of these 188 common DEGs is outlined in Table 5.2, which details the 15 most significant biological functions predicted by IPA to be most likely influenced by pregnancy that are common to both strains achieved via pathway enrichment analysis based on gene expression profiles. All DEGs for both WKY and SHRSP that were altered by pregnancy were visualized by volcano plots, with the most significant genes [$-\log_{10}(P\text{-value}) \geq 10$] labelled by gene name (Fig. 5.2D).

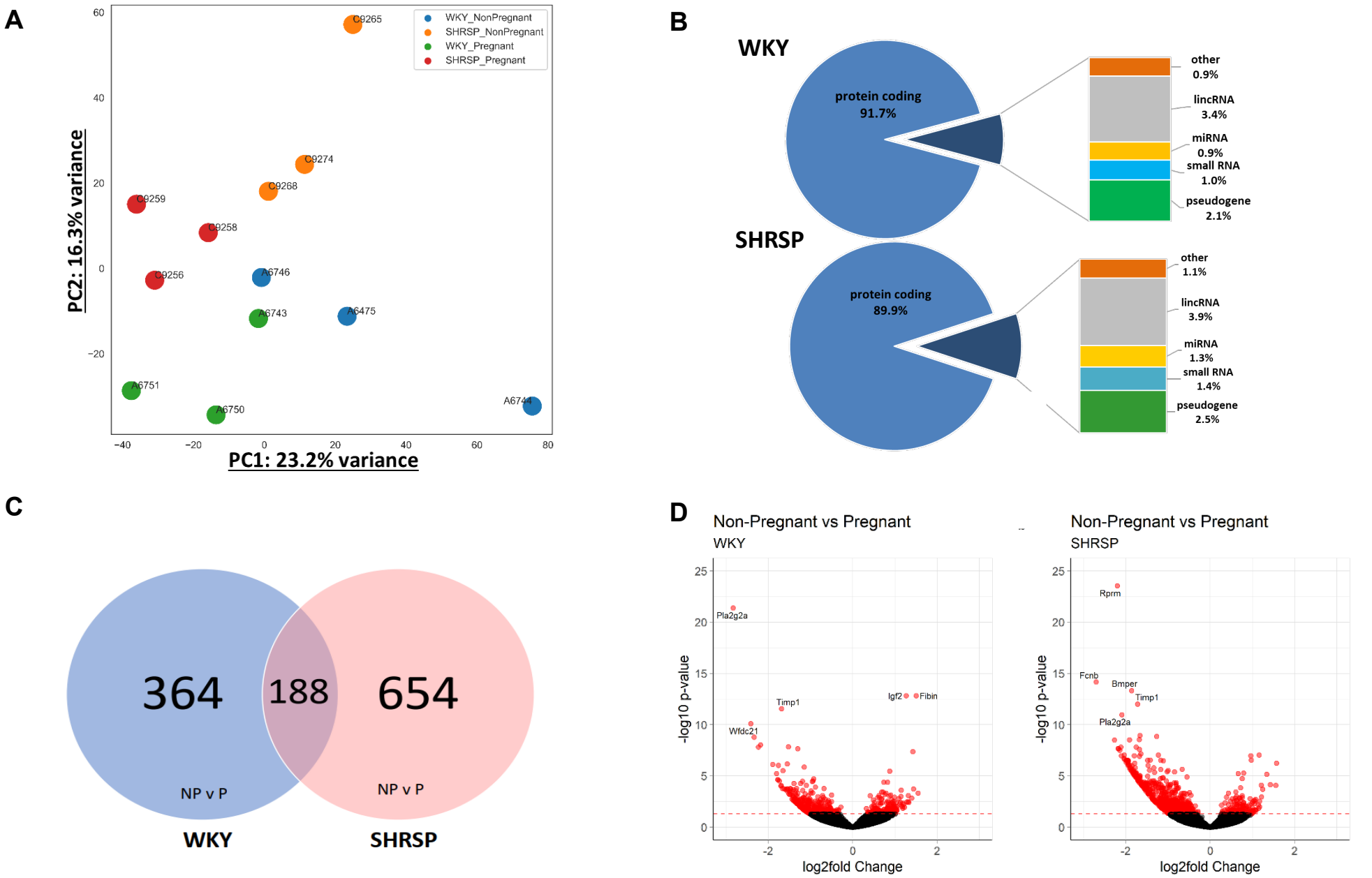
A
WKY_NonPregnant
SHRSP_NonPregnant
WKY_Pregnant
SHRSP_Pregnant
C9265
C9274
C9268
C9259
C9258
C9256
A6746
A6743
A6475
A6751
A6750
A6744
PC2: 16.3% variance
PC1: 23.2% variance
B
WKY
protein coding
91.7%
other
0.9%
lincRNA
3.4%
miRNA
0.9%
small RNA
1.0%
pseudogene
2.1%
SHRSP
protein coding
89.9%
other
1.1%
lincRNA
3.9%
miRNA
1.3%
small RNA
1.4%
pseudogene
2.5%
C
364
188
654
NP v P
NP v P
WKY
SHRSP
D
Non-Pregnant vs Pregnant
WKY
Pla2g2a
Timp1
Wfdc21
Igf2
Fibin
-log10 p-value
log2fold Change
Non-Pregnant vs Pregnant
SHRSP
Rprm
Fcnb
Bmper
Timp1
Pla2g2a
-log10 p-value
log2fold Change

Figure 5.2: Alterations in the Number of Differentially Expressed Genes and Composition of RNA Types in SHRSP and WKY

(A) The principal component analysis of non-pregnant (NP) and GD6.5 pregnant (P) uterine artery gene expression from WKY and SHRSP rats, showing the ordination of all samples and the top two principle components, PC1 (Pregnancy variance = 23.2%) and PC2 (Strain variance = 16.3%). (B) The biotype profiles demonstrate the proportions of the different biotypes represented by the significantly differentially expressed genes. lincRNA = long non-coding RNA, miRNA = microRNA. (C) Venn diagram showing the number of DEGs specific to SHRSP (654) or WKY (364), or in common between strains (188), across pregnancy determined by IPA®. (D) The DEGs altered by pregnancy in WKY and SHRSP represented by volcano plots. p-values were adjusted for multiple comparisons and transformed by $-\log_{10}$. DEGs with a $-\log_{10}(p\text{-value}) \geq 10$ are labelled by gene name.

Table 5.1 The number of up- and downregulated DEGs across pregnancy and strain, highlighting the number of DEGS in common or unique.

	Non-Pregnant vs Pregnant			**WKY vs SHRSP**		
	WKY	SHRSP	*Common*	Non-Pregnant	Pregnant	*Common*
Upregulated	173	180	*44*	214	131	*56*
Downregulated	379	662	*144*	179	75	*41*
Total	552	842	*188*	393	206	*97*

Table 5.2 The top 15 biological functions and diseases associated with the 188 DEGs associated with pregnancy in both SHRSP and WKY

Biological Diseases & Functions	-log(p-value)
Cell cycle	13.119
Cellular Assembly & Organisation	12.827
DNA Replication, Recombination & Repair	12.827
Cancer	11.570
Organismal Injury & Abnormalities	11.570
Reproductive System Disease	11.570
Cell Death & Survival	10.535
Protein Synthesis	8.391
Neurological Disease	8.156
Cellular Movement	8.099
Cardiovascular System Development & Function	7.533
Cellular Development	7.255
Cellular Growth & Proliferation	7.255
Gastrointestinal Disease	7.223
Hepatic System Disease	7.223

Biological diseases and functions were determined using ingenuity pathway analysis (IPA®) pathway enrichment analysis based on gene expression. The diseases and functions that the 188 in-common differentially expressed genes (DEGs) are most likely to influence are listed at the top, with a greater $-\log_{10}(P\text{-value})$ suggesting increased likelihood of involvement in the uterine arteries adaptation to pregnancy. SHRSP, spontaneously hypertensive stroke-prone rats; WKY, Wistar–Kyoto rats.

5.4.3 SHRSP and WKY Dams Show Distinct Differences in Pathway Activation During Early Pregnancy

Ingenuity pathway analysis® was used to correlate early pregnancy-dependent changes in gene expression to biologically relevant changes in canonical pathways. Core comparison analysis of pregnancy-dependant DEGs specific to either strain (WKY = 364, SHRSP = 654, Fig. 5.2C) revealed differences in activation z-score between several predicted canonical pathways and biological functions/diseases (Fig. 5.3). *Z*-scores, measures of predicted directional activity, were assigned by IPA® based on the pattern of gene expression changes across pregnancy and then ranked using hierarchical clustering. In our data set, an increased *z*-score implies an increased activation of that pathway in NP uterine arteries compared with GD 6.5, thus a pregnancy-associated reduction. WKY

dams demonstrated an increase in *z*-score, thus a reduced activity in pregnant uterine arteries, of several pathways involved in energy production and the renin-angiotensin-aldosterone system (RAAS) (Fig. 5.3A). In contrast, the SHRSP group demonstrated negative *z*-scores and pregnancy-associated activation of the aforementioned pathways alongside an increased activation of pathways related to the immune response and cell cycle control (Fig. 5.3A). While WKY and SHRSP shared similarities in activation predictions for apoptosis, morbidity/mortality and organismal death in disease and biological function pathways, although through different mechanisms, SHRSP-specific DEGs also influenced the response of several types of immune cells (Fig. 5.3B). Pathways with activation scores that were different between strains and/or known to affect vessel function were chosen for further analysis.

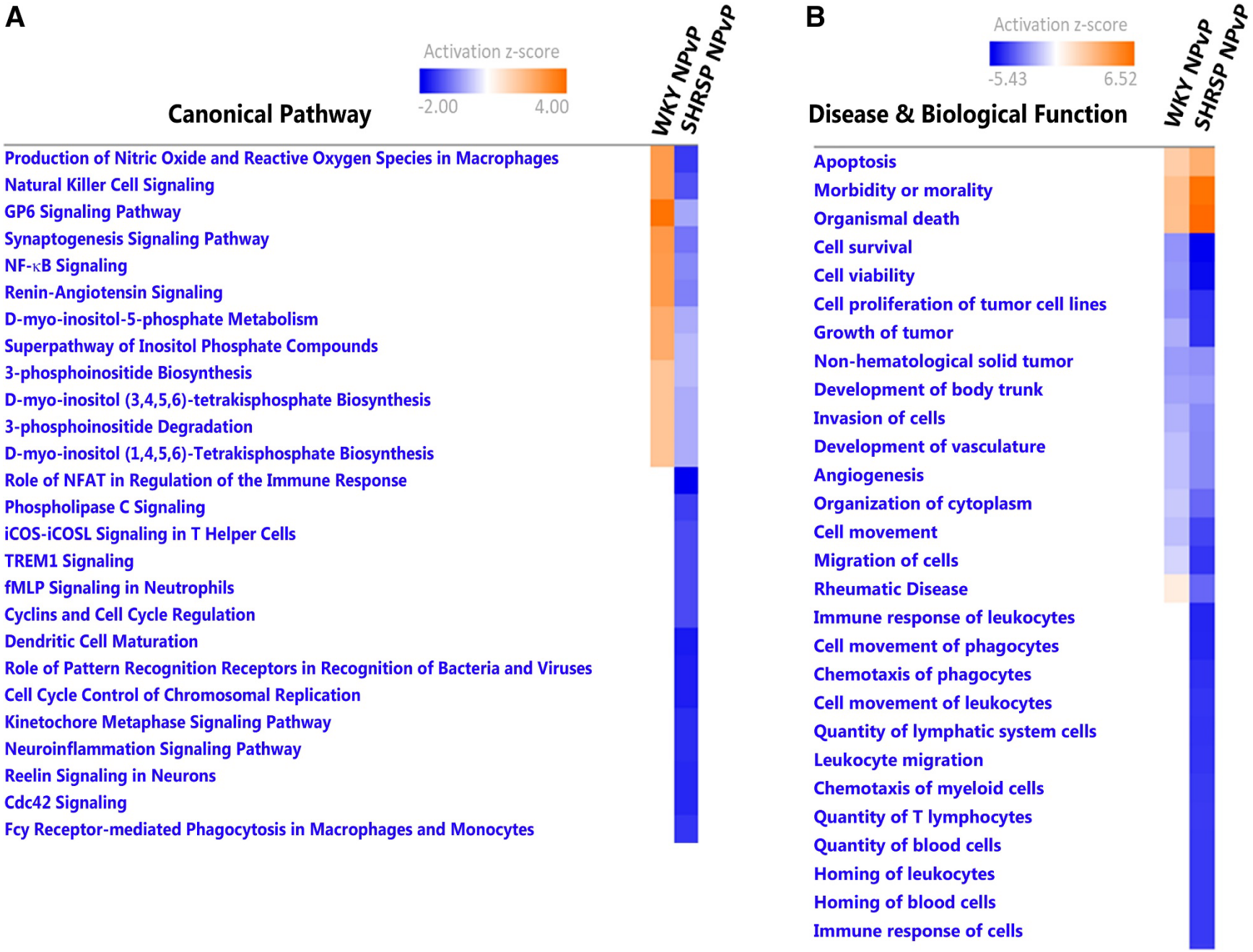
A
Activation z-score
-2.00
4.00
WKY NPvP
SHRSP NPvP
Canonical Pathway
Production of Nitric Oxide and Reactive Oxygen Species in Macrophages
Natural Killer Cell Signaling
GP6 Signaling Pathway
Synaptogenesis Signaling Pathway
NF-κB Signaling
Renin-Angiotensin Signaling
D-myo-inositol-5-phosphate Metabolism
Superpathway of Inositol Phosphate Compounds
3-phosphoinositide Biosynthesis
D-myo-inositol (3,4,5,6)-tetrakisphosphate Biosynthesis
3-phosphoinositide Degradation
D-myo-inositol (1,4,5,6)-Tetrakisphosphate Biosynthesis
Role of NFAT in Regulation of the Immune Response
Phospholipase C Signaling
iCOS-iCOSL Signaling in T Helper Cells
TREM1 Signaling
fMLP Signaling in Neutrophils
Cyclins and Cell Cycle Regulation
Dendritic Cell Maturation
Role of Pattern Recognition Receptors in Recognition of Bacteria and Viruses
Cell Cycle Control of Chromosomal Replication
Kinetochore Metaphase Signaling Pathway
Neuroinflammation Signaling Pathway
Reelin Signaling in Neurons
Cdc42 Signaling
Fcy Receptor-mediated Phagocytosis in Macrophages and Monocytes
B
Activation z-score
-5.43
6.52
WKY NPvP
SHRSP NPvP
Disease & Biological Function
Apoptosis
Morbidity or morality
Organismal death
Cell survival
Cell viability
Cell proliferation of tumor cell lines
Growth of tumor
Non-hematological solid tumor
Development of body trunk
Invasion of cells
Development of vasculature
Angiogenesis
Organization of cytoplasm
Cell movement
Migration of cells
Rheumatic Disease
Immune response of leukocytes
Cell movement of phagocytes
Chemotaxis of phagocytes
Cell movement of leukocytes
Quantity of lymphatic system cells
Leukocyte migration
Chemotaxis of myeloid cells
Quantity of T lymphocytes
Quantity of blood cells
Homing of leukocytes
Homing of blood cells
Immune response of cells

Figure 5.3: Pathway Activation Analysis in SHRSP and WKY Uterine Arteries

The core comparison pathway analysis of canonical pathways (A) and those related to biological functions/diseases (B) of non-pregnant (NP) and GD6.5 (P) uterine artery gene expression from WKY and SHRSP rats. Pathways were ranked by hierarchical clustering and assigned *z*-scores as area measures of the predicted direction of activity such that a positive score was associated with increased pathway activation in NP compared to GD6.5 uterine arteries, thus a pregnancy associated reduction.

5.4.4 Early Pregnancy Is Associated with Alterations in Inflammatory Response Genes

The increased activation of pathways related to the immune response in SHRSP uterine arteries directed the investigation into gene expression changes in inflammatory response. Both WKY and SHRSP arteries showed differential gene expression that suggests an increased local inflammatory response to pregnancy by GD 6.5 (Fig. 5.4). Nineteen DEGs were common to both strains (Fig. 5.4; Table 5.3); however, the number of genes influencing pregnancy-associated inflammatory response were greater in SHRSP uterine arteries than WKY (89 vs. 38, respectively) (Fig. 5.4; Tables 5.4 and 5.5). Taken together, these data suggest that hypertensive SHRSP dams experience an elevated immune response to pregnancy compared with WKY.

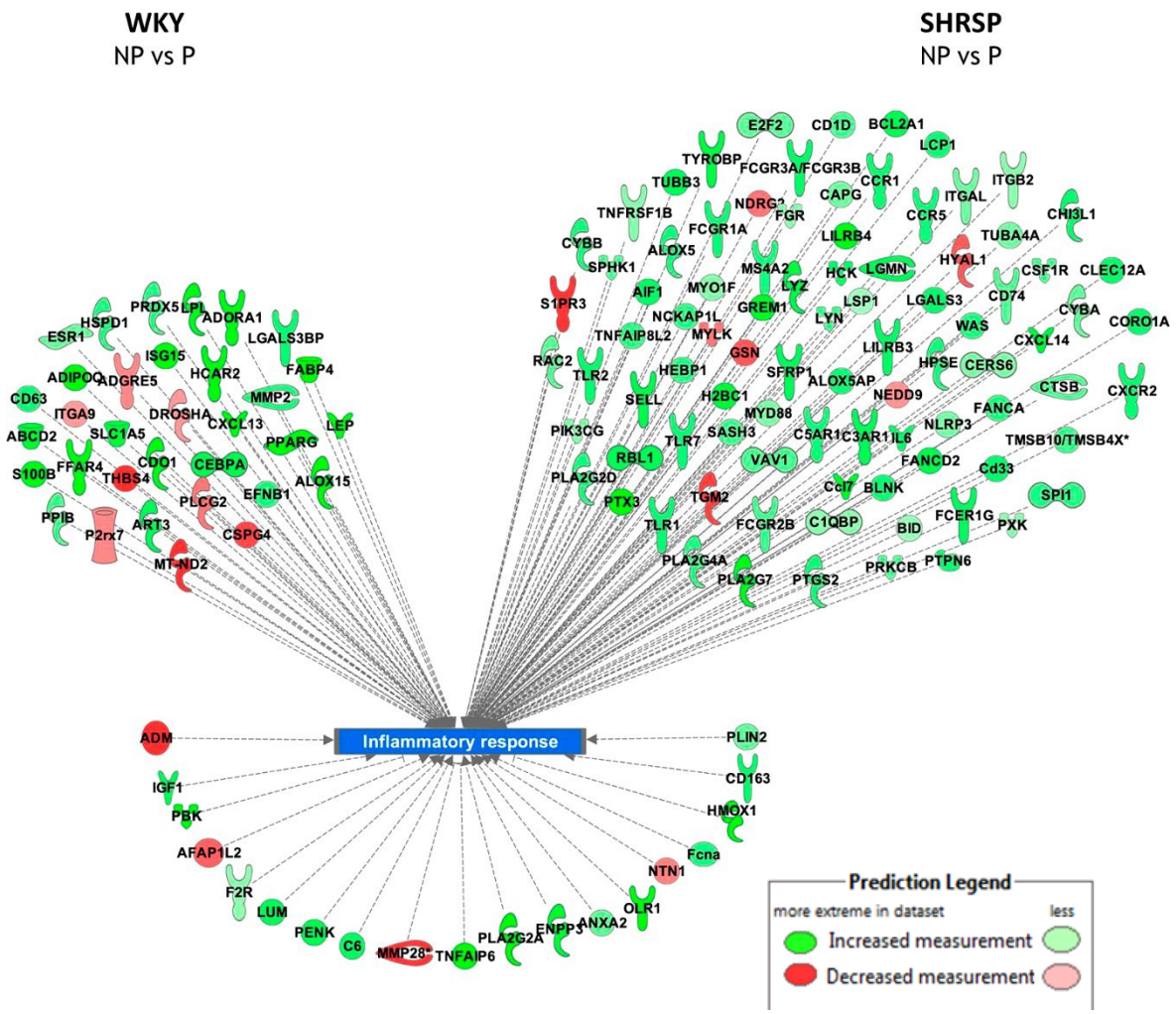

Figure 5.4: Predicted Interaction Network of Inflammatory Response Genes

Predicted interaction network of the inflammatory response in non-pregnant (NP) or GD6.5 (P) uterine arteries in SHRSP and WKY dams. The genes in common (same direction, similar fold-change) are shown in the lower semi-circle. There were more genes involved in this response in SHRSP uterine arteries than WKY. Here, **green** represents an increased expression and **red** a decreased expression in pregnant (GD6.5) vs non-pregnant uterine arteries.

Table 5.3 Common inflammatory genes that were differentially expressed in response to pregnancy.

Common Inflammatory genes	Gene Symbol	Ensembl Gene ID (ENSRNO)	WKY NP vs P		SHRSP NP vs P	
			padj	FC	padj	FC
Adrenomedullin	Adm	G00000027030	0.028520	1.76	$7.87x10^{-5}$	2.31
Phospholipase A2	Pla2g2a	G00000016945	$4.21x10^{-22}$	-7.11	$1.06x10^{-11}$	-4.27
Heme oxygenase 1	Hmox1	G00000014117	0.012645	-1.84	$2.84x10^{-9}$	-3.21
Actin Filament Associated Protein 1 Like 2	Afap1l2*	G00000017164	0.000383	1.60	0.001470	1.51
Insulin-like growth factor 1	Igf1*+	G00000004517	$1.36x10^{-6}$	-2.22	$2.97x10^{-7}$	-2.26
PDZ binding kinase	Pbk	G00000015308	0.016036	-2.27	$4.16x10^{-5}$	-3.21
TNF alpha induced protein 6	Tnfaip6	G00000050792	0.020741	-2.19	$5.37x10^{-5}$	-3.09
Oxidized low density lipoprotein (lectin-like) receptor 1	Olr1	G00000056219	0.002504	-2.60	0.000174	-2.89
Lumican	Lum	G00000004610	0.010963	-2.03	0.001921	-2.18
CD163 molecule	Cd163	G00000010253	0.006994	-1.76	0.000118	-2.01
Perilipin 2	Plin2	G00000007060	0.025994	-1.59	0.014596	-1.60
Proenkephalin	Penk*	G00000008943	0.007917	-2.13	0.001593	-2.24
Ficolin A	Fcna	G00000017063	0.013236	-1.87	0.014109	-1.80
Coagulation factor II (thrombin) receptor	F2r	G00000048043	0.005514	-1.59	0.024149	-1.46
Netrin 1	Ntn1	G00000003947	0.025481	1.41	0.025089	1.39
Complement C6	C6	G00000024115	0.000191	-2.91	0.014595	-2.10
Annexin A2	Anxa2	G00000010362	0.030614	-1.64	0.024361	-1.63
Matrix metalloproteinase-28	Mmp28	G00000061904	0.015311	1.78	0.022709	1.69
Ectonucleotide pyrophosphatase/phosphodiesterase 3	Enpp3	G00000013791	0.000830	-2.07	$1.60x10^{-6}$	-2.52

The fold change (FC) and false discovery rate (*padj*) of 20 significant (*padj* <0.05) DE genes that are common to both WKY and SHRSP uterine arteries during the first 6 days of pregnancy. *indicates 2 or more transcript variants for that gene.

Table 5.4 Differential gene expression of inflammatory genes specific to WKY pregnancy

WKY Specific Inflammatory	Gene Symbol	Ensembl Gene ID (ENSRNO)	WKY NP vs P	
			padj	FC
ATP binding cassette subfamily D, member 2	Abcd2	G00000173208	0.014944	-2.08
Adhesion G protein-coupled receptor E5	Adgre5	G00000123146	0.003724	1.43
Adenosine A1 receptor	Adora1	G00000163485	0.017430	-2.24
Peroxiredoxin 5	Prdx5	G00000126432	0.032492	-1.56
C-X-C motif chemokine ligand 13	Cxcl13	G00000156234	0.000031	-3.33
Solute carrier family 1 member 5	Slc1a5*	G00000105281	0.001642	-2.03
Peroxisome proliferator-activated receptor gamma	Pparg*	G00000132170	0.005440	-2.33
Heat shock protein family D member 1	Hspd1	G00000144381	0.028752	-1.57
Integrin subunit alpha 9	Itga9	G00000144668	0.032359	1.34
Cysteine dioxygenase type 1	Cdo1	G00000129596	0.001210	-2.24
Arachidonate 15-lipoxygenase	Alox15	G00000161905	0.003980	-2.41
Hydroxycarboxylic acid receptor 2	Hcar2	G00000182782	0.015378	-2.28
Galectin 3 binding protein	Lgals3bp	G00000108679	0.046384	-1.68
ISG15 ubiquitin-like modifier	Isg15	G00000021802	0.005119	-2.33
Fatty acid binding protein 4	Fabp4*	T00000014701	0.001000	-2.79
Adiponectin, C1Q and collagen domain containing	Adipoq*[a]	G00000181092	0.002005	-2.34
Free fatty acid receptor 4	Ffar4	G00000021763	0.016327	-2.27
Ephrin B1	Efnb1	G00000006877	0.037403	-1.60
ADP-ribosyltransferase 3	Art3*	G00000002256	0.022197	-1.85
Phospholipase C, gamma 2	Plcg2	G00000051986	0.001342	1.51
Drosha ribonuclease III	Drosha	G00000013451	0.035892	1.36
S100 calcium binding protein B	S100b	G00000001295	0.0021668	-2.27
Estrogen Receptor 1	Esr1	G00000019358	0.046925	-1.43
Matrix metallopeptidase 2	Mmp2	G00000016695	0.046187	-1.60
Leptin	Lep	G00000045797	0.007917	-2.34
Legumain	Lgmn	G00000007089	0.037070	-1.70
Lipoprotein lipase	Lpl	G00000012181	0.004264	-2.23
Mitochondrial NADH dehydrogenase II	Mt-nd2	G00000031033	0.045737	1.90
Purinergic receptor P2X 7	P2rx7	G00000001296	0.040142	1.43
Peptidylprolyl isomerase B	Ppib	G00000016781	0.047338	-1.52
Secreted fizzle related protein 1	Sfrp1	G00000017783	0.000471	-1.99
Thrombospondin 4	Thbs4	G00000012471	0.026375	1.91
CD63 molecule	Cd63	G00000007650	0.009079	-1.66
C-X-C motif chemokine ligand 14	Cxcl14	G00000011984	0.041624	-2.05
CCAAT enhancer binding protein alpha	Cebpa	G00000010918	0.046410	-1.92
Chondroitin sulfate proteoglycan 4	Cspg4	G00000017208	0.049504	1.73

The fold change (FC) and significance of this change (*padj*) of all 36 significant (*padj* <0.05) DE genes that are specific to WKY uterine arteries during the first 6 days of pregnancy. * indicates 2 or more transcript variants for that gene; [a]All transcripts of that gene were found to have a significantly altered expression.

Table 5.5 Differential expression of inflammatory response genes specific to SHRSP pregnancy

SHRSP Specific Inflammatory genes	**Gene Symbol**	**Ensembl Gene ID (ENSRNO)**	SHRSP NP vs P	
			padj	FC
Spi-1 proto-oncogene	Spi1	G00000012172	0.000059	-1.75
Pentraxin 3	Ptx3	G00000012280	0.000009	-3.19
Leukocyte immunoglobulin like receptor B4	Lilrb4*	G00000027811	0.000011	-3.02
Transglutaminase 2	Tgm2	G00000012956	0.000139	1.64
HCK proto-oncogene, Src family tyrosine kinase	Hck	G00000009331	0.000073	-2.01
Sphingosine-1-phosphate receptor 3	S1pr3*	G00000014524	0.000844	1.69
Lysozyme	Lyz	G00000005825	0.000138	-2.36
Phospholipase A2 group VII	Pla2g7	G00000025691	0.000093	-2.71
RB transcriptional corepressor like 1	Rbl1	G00000006921	0.000326	-2.20
Tyro protein tyrosine kinase binding protein	Tyrobp	G00000020845	0.000318	-2.35
Rac family small GTPase 2	Rac2	G00000007350	0.000893	-1.63
Leukocyte immunoglobulin like receptor B3	Lilrb3	G00000058422	0.000063	-2.08
Complement C3a receptor 1	C3ar1	G00000009211	0.000477	-2.21
Fc fragment of IgE receptor Ig	Fcer1g	G00000024159	0.000652	-2.12
Complement C5a receptor 1	C5ar1	G00000047800	0.002403	-1.84
BCL2-related protein A1	Bcl2a1	G00000047606	0.000652	-2.22
Coronin 1A	Coro1a	G00000019430	0.001174	-1.96
Myeloid differentiation primary response 88	Myd88	G00000013634	0.002852	-1.50
CD74 molecule	Cd74*	G00000018735	0.005292	-1.64
Arachidonate 5-lipoxygenase	Alox5*	G00000012972	0.000399	-1.86
Galectin 3	Lgals3*	G00000010645	0.002633	-1.95
Gremlin 1	Grem1	G00000026053	0.000604	-2.63
NCK associated protein 1 like	Nckap1l*	G00000036829	0.000171	-1.74
Phosphatidylinositol-4,5-bisphosphate 3-kinase γ	Pik3cg	G00000009385	0.004194	-1.51
Allograft inflammatory factor 1	Aif1*	G00000000853	0.008599	-2.07
Colony stimulating factor 1 receptor	Csf1r*+	G00000018414	0.014309	-1.68
LYN proto-oncogene, Src family tyrosine kinase	Lyn	G00000008180	0.004068	-1.70
Capping actin protein, gelsolin like	Capg	G00000013668	0.005868	-1.56
Lymphocyte cytosolic protein 1	Lcp1*	G00000010319	0.002581	-1.90
C-X-C motif chemokine ligand 14	Cxcl14	G00000011984	0.003266	-2.45
TNF alpha induced protein 8 like 2	Tnfaip8l2	G00000021100	0.006413	-1.76
Cytochrome b-245 alpha chain	Cyba	G00000013014	0.008045	-1.61
Complement C1q binding protein	C1qbp	G00000006949	0.001100	-1.46
Vav guanine nucleotide exchange factor 1	Vav1	G00000050430	0.008920	-1.67
phospholipase A2	Pla2g2d	G00000016826	0.008458	-1.82

SAM and SH3 domain containing 3	Sash3	G00000004409	0.008173	-1.69
Fc fragment of IgG receptor IIb	Fcgr2b*	G00000046452	0.013710	-1.67
Cytochrome b-245 beta chain	Cybb	G00000003622	0.010194	-1.84
CD33 molecule	Cd33	G00000037331	0.008200	-1.97
Cathepsin B	Ctsb	G00000010331	0.016124	-1.65
BH3 interacting domain death agonist	Bid	G00000012439	0.024038	-1.40
Integrin subunit beta 2	Itgb2	G00000001224	0.020822	-1.46
Chitinase 3 like 1	Chi3l1	G00000053272	0.012719	-1.97
Myosin IF	Myo1f	G00000008409	0.021748	-1.49
Fc fragment of IgG receptor Ia	Fcgr1a*	G00000021199	0.012514	-1.90
TNF receptor superfamily member 1B	Tnfrsf1b	G00000016575	0.023990	-1.48
B-cell linker	Blnk	G00000013967	0.014363	-1.89
Ceramide synthase 6	Cers6	G00000024595	0.025914	-1.51
NLR family, pyrin domain containing 3	Nlrp3*	G00000003170	0.044205	-1.52
Toll-like receptor 7	Tlr7	G00000004249	0.019507	-1.90
Protein tyrosine phosphatase, non-receptor type 6	Ptpn6*	G00000014294	0.000652	-1.94
Chemokine (C-C motif) receptor 5	Ccr5*	G00000049115	0.017069	-1.86
Lymphocyte-specific protein 1	Lsp1	G00000020300	0.046625	-1.36
Heparanase	Hpse	G00000002188	0.021449	-1.83
Toll-like receptor 2	Tlr2	G00000009822	0.022074	-1.98
Arachidonate 5-lipoxygenase activating protein	Alox5ap	G00000000907	0.022028	-1.91
Gelsolin	Gsn*	G00000018991	0.033501	1.55
Integrin subunit alpha L	Itgal	G00000017980	0.030319	-1.57
Myosin light chain kinase	Mylk*	G00000002215	0.046507	1.43
E2F transcription factor 2	E2f2	G00000047741	0.031763	-1.60
Hyaluronoglucosaminidase 1	Hyal1	G00000015858	0.033276	1.54
C-C motif chemokine receptor 1	Ccr1	G00000006715	0.026110	-1.93
Prostaglandin-endoperoxide synthase 2	Ptgs2	G00000002525	0.029288	-1.87
Chemokine (C-C motif) ligand 7	Ccl7	G00000000239	0.000907	-2.58
C-type lectin domain family 12 member A	Clec12a	G00000054860	0.008586	-1.95

FA complementation group A	Fanca	G00000016706	0.027502	-1.78
FA complementation group D2	Fancd2	G00000061085	0.003360	-2.25
Fc fragment of IgG receptor IIIa	Fcgr3a/Fcgr3b	G00000024382	0.006589	-2.02
PX domain containing serine/threonine kinase like	Pxk	G00000008024	0.000012	-1.47
Thymosin beta 4 X-linked	Tmsb10/Tmsb4x	G00000042499	0.003274	-1.71
Tubulin beta 3 class III	Tubb3	G00000017209	0.008508	-2.15
CD1d molecule	Cd1d	G00000016451	0.046340	-1.66
Fc fragment of IgG receptor Ig	Fcer1g	G00000024159	0.000652	-2.12
FGR proto-oncogene, Src family tyrosine kinase	Fgr	G00000009912	0.046468	-1.47
H2b clustered histone 1	H2bc1	G00000016865	0.002965	-2.46
Heme binding protein 1	Hebp1	G00000000024	0.043935	-1.74
Interleukin 6	Il6	G00000010278	0.037185	-2.03
Membrane spanning 4-domains A2	Ms4a2	G00000020993	0.035666	-1.81
NDRG family member 2	Ndgr2	G00000010389	0.001650	1.44
Neural precursor cell expressed, developmentally downregulated 9	Nedd9	G00000014548	0.036454	1.32
Phospholipase A2 group IVA	Pla2g4a	G00000002657	0.028490	-1.77
Protein kinase C beta	Prkcb	G00000012061	0.013710	-1.65
Selectin L	Sell	G00000002776	0.008520	-2.28
Sphingosine kinase 1	Sphk1	G00000010626	0.032870	-1.66
Toll-like receptor 1	Tlr1	G00000038722	0.029859	-1.94
Tubulin alpha 4a	Tuba4a	G00000003597	0.043889	-1.54
WASP actin nucleation promoting factor	Was	G00000031058	0.001202	-1.78

The fold change (FC) and false discovery rate (*padj*) of all 89 significant (*padj* <0.05) DE genes that are specific to SHRSP uterine arteries during the first 6 days of pregnancy. *indicates 2 or more transcript variants for that gene. $^{+}$ 2 or more transcripts of that gene were found to be significantly differentially expressed in one or both comparison group.

5.4.5 SHRSP Uterine Arteries Have a Pregnancy-Associated Increase in NOX2 Expression

Pathway analysis also revealed that SHRSP uterine arteries are associated with a prediction of increased production of reactive oxygen species (ROS) via NADPH oxidase in early pregnancy (*z*-score = 1.34 WKY vs. −3.05 SHRSP). The expression of key genes involved in the production of nitric oxide and reactive oxygen species in WKY uterine arteries did not change in response to pregnancy, whereas SHRSP arteries experience a pregnancy-associated increase in expression (Fig. 5.5, Table 5.5). SHRSP uterine arteries demonstrated an increased expression of two NADPH oxidase (NOX) subunits *p22-phox*, *p67-phox*, *gp91*, and *p40-phox* in the pregnant SHRSP compared with NP. This suggests an increase in NOX2 expression, and, therefore, ROS production in early pregnancy that does not occur in early WKY pregnancy.

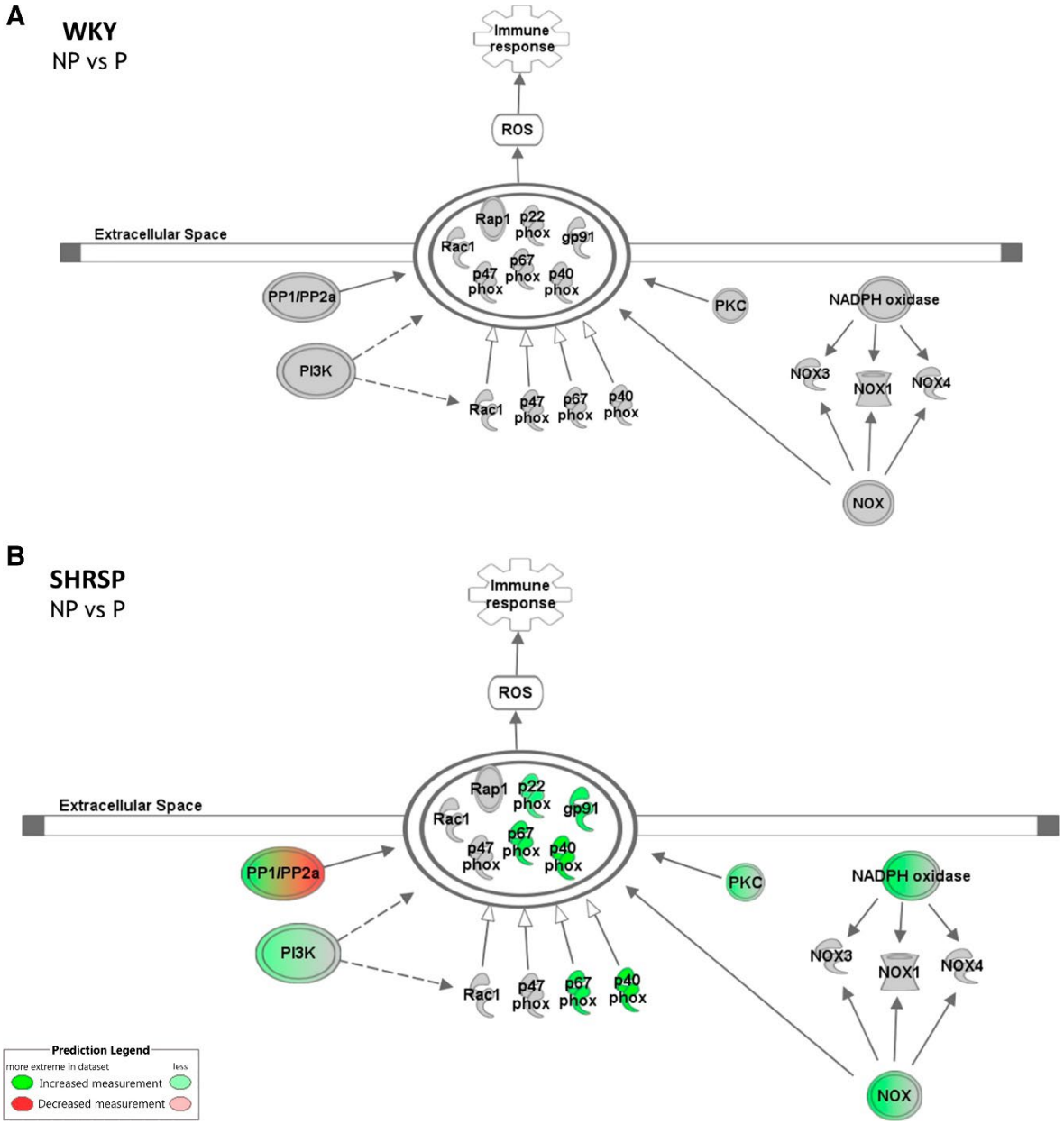

Figure 5.5: Predicted Interaction Network of NOX2 and ROS Production

Predicted expression network for the production of nitric oxide and reactive oxygen species (ROS) in non-pregnant (NP) or GD6.5 (P) uterine arteries in WKY (A) and SHRSP (B) dams. No changes were detected in WKY uterine arteries. SHRSP arteries showed an increased expression of four NOX2 subunits, PKC=protein kinase C, PP1/PP2a=protein phosphatase complex 1/2a and PI3K= phosphatidylinositol kinase complex 3. NOX2= NADPH oxidase 2. Here, **green** represents an increased expression, **red** a decreased expression, **grey** no change and a **green**/**red** representing conflicting expression in pregnant (GD6.5) vs non-pregnant uterine arteries.

Table 5.6 Genes involved in ROS production via NADPH Oxidase in the SHRSP pregnancy.

	Gene Symbol		SHRSP NP vs P	
Gene Name	Rat	Human	padj	FC
NADPH oxidase 2				
Cytochrome b-245 α chain	Cyba	p22-phox	***0.0080***	***-1.61***
Cytochrome b-245 ß chain	Cybb	Gp91	***0.0102***	***-1.84***
Neutrophil cytosolic factor 2	Ncf2*^{P}	p67-phox	***$5.75x10^{-5}$***	***-1.94***
Neutrophil cytosolic factor 4	Ncf4	p40-phox	***$9.59x10^{-5}$***	***-2.20***
Neutrophil cytosolic factor 1	Ncf1*	p47-phox	0.1881	-1.18
Phosphatidylinositol 3 kinase complex				
Fibroblast growth factor receptor 3	Fgfr3*	FGFR3	***0.0466***	***1.56***
Phosphatidylinositol-bisphosphate 3-kinase catalytic subunit γ	Pik3cg	PIK3CG	***0.0042***	***-1.51***
Protein phosphatase 1/2A complex				
Protein phosphatase, Mg^{2+}/Mn^{2+} dependent 1L	Ppm1l	PPM1L	***0.0431***	***1.37***
Protein phosphatase 1 regulatory inhibitor subunit 14B	Ppp1r14b	PPP1R14B	***$9.61x10^{-5}$***	***-1.74***
Protein phosphatase 1 regulatory subunit 3C	Ppp1r3c	PPP1R3C	***0.0141***	***1.74***

The NADPH oxidase subunit genes and the associated complexes had a significantly altered expression in SHRSP (*padj* <0.05; shown in bold). The same genes did not reach significance in WKY. * indicates 2 or more transcript variants for that gene. Ncf2^{P} is a non-coding processed transcript in rat.

5.4.6 Calcium Signalling Genes Were Differentially Altered in WKY and SHRSP Arteries in Response to Pregnancy

IPA® revealed gene expression patterns in WKY that suggested a reduction in Ca^{2+} signalling in GD 6.5 uterine arteries (Fig. 5.6). There was a significant decrease in expression of *Plcg2*, *Itpr2*, and *Myh6* and an increase in *Calm1* expression in pregnant WKY uterine arteries (Table 5.6). The same expression pattern was not observed in the DEGs from SHRSP arteries (Fig. 5.6B), where there was a decrease in expression of *Plcl1* and *Mylk* and an increase in *Prkcb* expression. This suggests a reduction in Ca^{2+} release and increased sequestering of Ca^{2+} in WKY pregnancy, whereas the DEGs in SHRSP uterine arteries suggest an activation of Ca^{2+} signal transduction in early pregnancy.

WKY vessels also demonstrated a pregnancy-dependant reduction in the expression of RAAS genes leading to a predicted decrease in Ca^{2+} release downstream of the angiotensin receptor type 1 (AT_1R) (Fig. 5.7A). In contrast, SHRSP pregnant vessels demonstrated an increase in expression of genes involved in RAAS signalling in the uterine artery (Fig. 5.7B), thus a predicted activation of pathways downstream of AT1R that results in the production of ROS and vasoconstriction (Table 5.7).

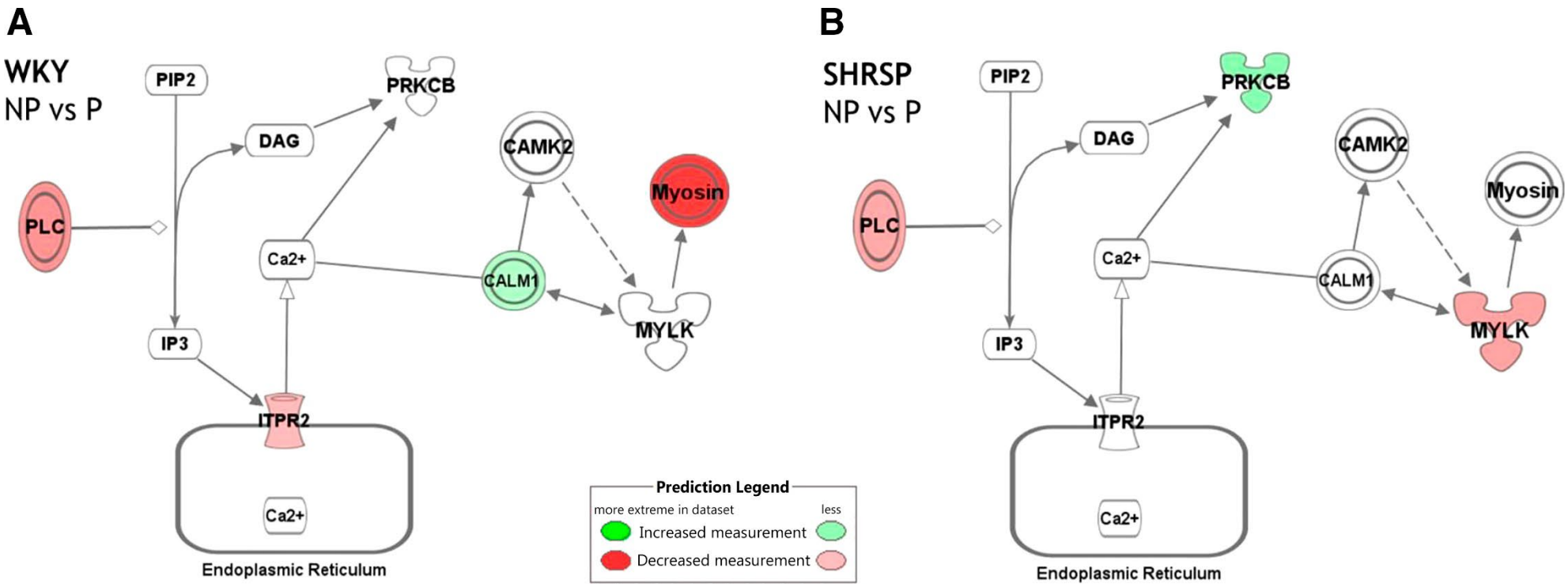

Figure 5.6: Predicted Interaction Network for Adrenergic Signalling

Predicted expression network for adrenergic calcium signalling in non-pregnant (NP) or GD6.5 (P) uterine arteries in WKY (A) and SHRSP (B) dams. WKY demonstrated a predicted pregnancy-dependant reduction in expression of PLC= phospholipase C, ITPR2= Inositol 1,4,5-triphosphate receptor type 2 and Myosin= Myosin heavy chain 6, alongside an increased expression of CALM1= calmodulin 1. SHRSP showed a pregnancy-dependant increase in the expression of PRKCB= protein kinase C beta and a reduced expression of MYLK= myosin light chain kinase and PLC= phospholipase C. Here, **green** represents an increased expression, **red** a decreased expression, **white** no change and a **green**/**red** representing conflicting expression in pregnant (GD6.5) vs non-pregnant uterine arteries.

Table 5.7 The significantly differentially expressed genes involved in calcium release and regulation.

Genes involved in Ca^{2+} release in **WKY**	Gene Symbol	Ensembl Gene ID	NP vs P	
			padj	FC
Calmodulin 1	Calm1	ENSG00000198668	0.013824	-1.45
Myosin heavy chain 6	Myh6	ENSG00000197616	0.029213	2.03
Inositol 1,4,5-trisphosphate receptor type 2	Itpr2	ENSG00000123104	0.037560	1.32
Phospholipase C gamma 2	Plcg2	ENSG00000197943	0.001342	1.51

Genes involved in Ca^{2+} release in **SHRSP**	Gene Symbol	Ensembl Gene ID	NP vs P	
			padj	FC
Protein kinase C beta	Prkcb	ENSG00000166501	0.013710	-1.65
Myosin light chain kinase	Mylk*	ENSG00000065534	0.046507	1.43
Phospholipase C like 1	Plcl1	ENSG00000115896	0.041570	1.40

The false discovery rate (*padj*) and fold change (FC) of significant (*padj* <0.05) DE gene transcripts in WKY and SHRSP intracellular calcium release. * indicates 2 or more transcript variants for that gene. $^{+}$ 2 or more transcripts of the gene were found to be significantly differentially expressed.

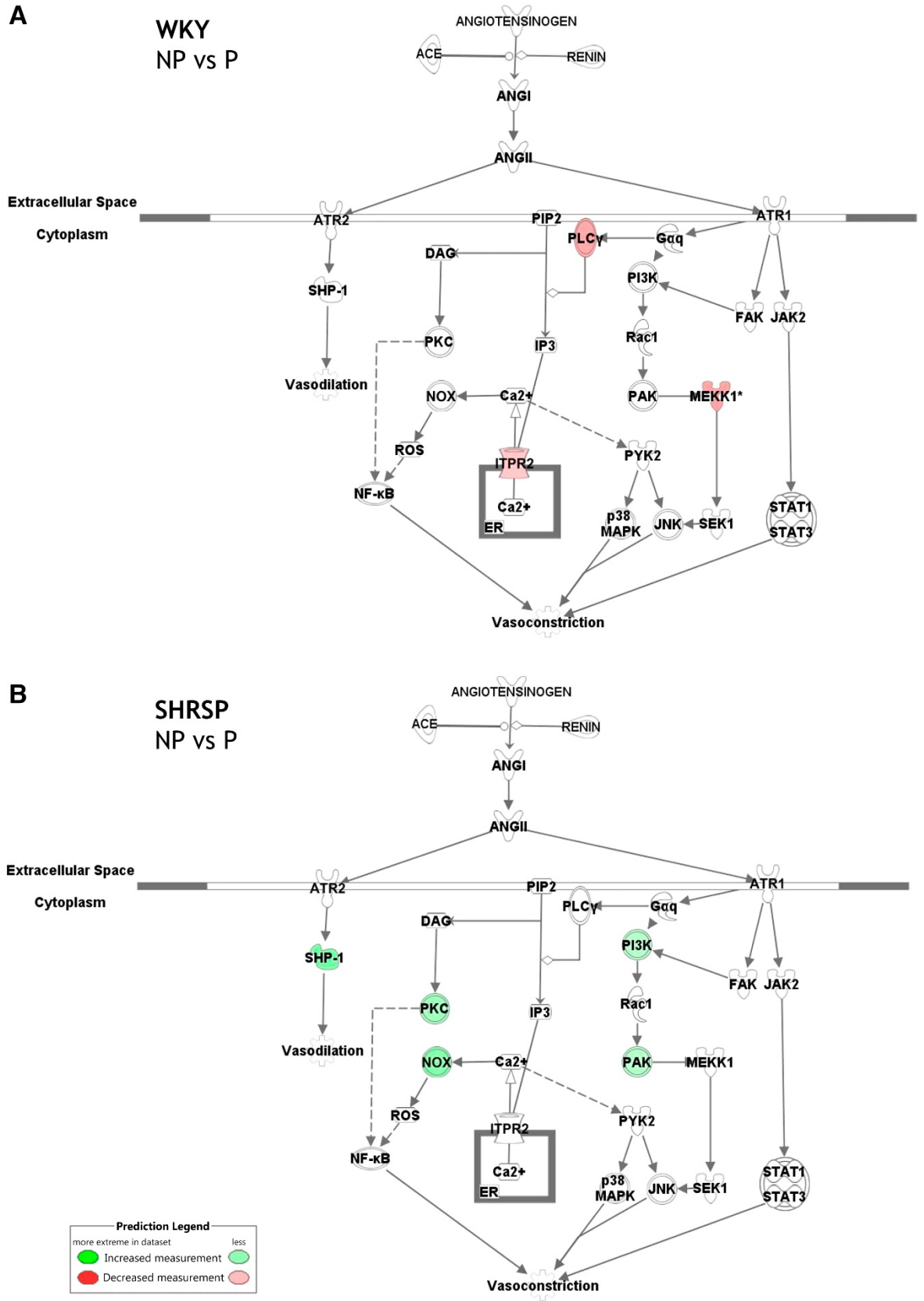
A
WKY
NP vs P
ANGIOTENSINOGEN
ACE
RENIN
ANGI
ANGII
Extracellular Space
Cytoplasm
ATR2
PIP2
ATR1
PLCγ
Gαq
DAG
PI3K
SHP-1
FAK
JAK2
Rac1
PKC
IP3
Vasodilation
NOX
Ca2+
PAK
MEKK1*
ROS
ITPR2
PYK2
NF-κB
Ca2+
ER
p38
MAPK
JNK
SEK1
STAT1
STAT3
Vasoconstriction
B
SHRSP
NP vs P
ANGIOTENSINOGEN
ACE
RENIN
ANGI
ANGII
Extracellular Space
Cytoplasm
ATR2
PIP2
ATR1
PLCγ
Gαq
DAG
SHP-1
PI3K
FAK
JAK2
Rac1
PKC
IP3
Vasodilation
NOX
Ca2+
PAK
MEKK1
ROS
ITPR2
PYK2
NF-κB
Ca2+
ER
p38
MAPK
JNK
SEK1
STAT1
STAT3
Vasoconstriction
Prediction Legend
more extreme in dataset
less
Increased measurement
Decreased measurement

Figure 5.7: Predicted Interaction Network for Renin-Angiotensin-Aldosterone System (RAAS) Signalling

Predicted expression network for renin-angiotensin-aldosterone system (RAAS) signalling in non-pregnant (NP) or GD6.5 (P) uterine arteries in WKY (A) and SHRSP (B) dams. WKY demonstrated a predicted pregnancy-dependant reduction in expression of PLCγ = phospholipase C gamma, ITPR2= Inositol 1,4,5-Trisphosphate receptor type 2, MEKK1= Mitogen-activated protein kinase kinase kinase 1. SHRSP showed a pregnancy-dependant increase in the expression of SHP-1= Protein tyrosine phosphatase non-receptor type 6, NOX = NADPH oxidase, PKC= protein kinase C, PAK= p-21 activated kinase 1, PI3K= Phosphatidylinositol-4,5-bisphosphate 3-kinase catalytic subunit gamma. Here, **green** represents an increased expression, **red** a decreased expression, white no change and a **green**/**red** representing conflicting expression in pregnant (GD6.5) vs non-pregnant uterine arteries.

Table 5.8 The significantly differentially expressed genes involved in the renin-angiotensin-aldosterone system.

Genes involved in RAAS in **WKY**	Gene Symbol	Ensembl Gene ID	NP vs P	
			padj	FC
Mitogen-activated protein kinase kinase kinase 12	Map3k12	ENSG00000139625	0.047338	1.30
Mitogen-activated protein kinase kinase kinase 1	Mekk1	ENSG00000095015	0.004423	1.54
Inositol 1,4,5-trisphosphate receptor type 2	Itpr2	ENSG00000123104	0.037560	1.32
Phospholipase C gamma 2	Plcg2	ENSG00000197943	0.001342	1.51

Genes involved in RAAS in **SHRSP**	Gene Symbol	Ensembl Gene ID	NP vs P	
			padj	FC
Protein kinase C beta	Prkcb	ENSG00000166501	0.013710	-1.65
Cytochrome B-245 β chain	Cybb	ENSG00000165168	0.010194	-1.84
p-21 activated kinase 1	Pak1	ENSG00000149269	0.024970	-1.52
Phosphatidylinositol-4,5-bisphosphate 3-kinase catalytic subunit γ	Pikc3g	ENSG00000105851	0.004194	-1.51
Protein tyrosine phosphatase non-receptor type 6	Shp-1	ENSG00000111679	0.000625	-1.94

The false discovery rate (*padj*) and fold change (FC) of significant (*padj* <0.05) DE gene transcripts in WKY and SHRSP RAAS signalling.

5.4.7 SHRSP and WKY Dams Show Distinct Differences in Genes Related to Energy Production During Early Pregnancy

WKY uterine arteries demonstrated an overall increase in the expression of genes related to oxidative phosphorylation in pregnant relative to nonpregnant arteries, with a *z*-score of −2.53. The *z*-score for SHRSP was 0, indicating that this pathway is not involved in the early adaptation to pregnancy in this strain. IPA® revealed the DEGs were related to increased expression of components of complexes I, III, IV, and V in WKY dams across the first 6 days of gestation (Table 5.9; Fig. 5.8A). This change in expression was not observed in SHRSP uterine arteries.

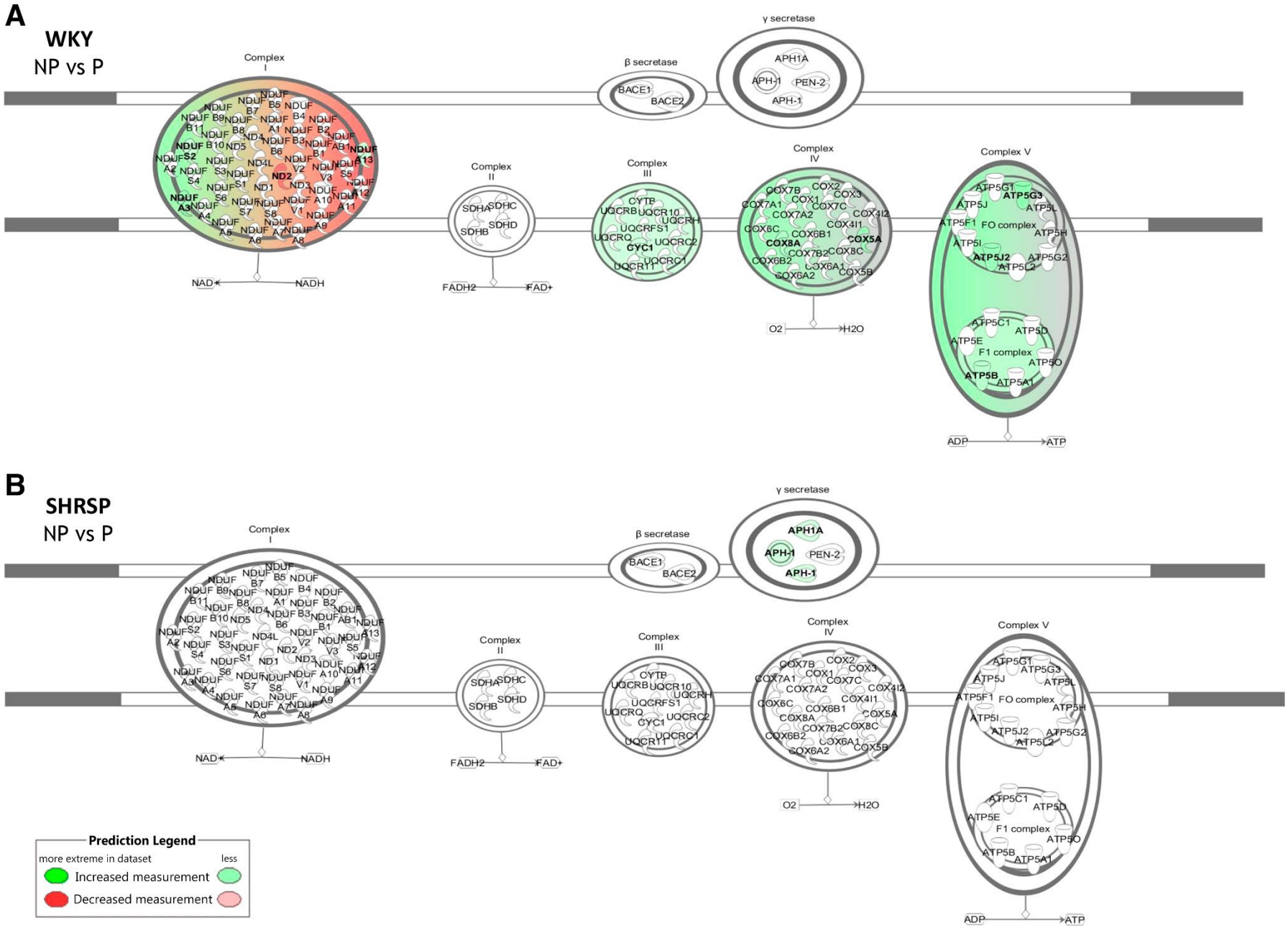
A
WKY
NP vs P
Complex I
β secretase
BACE1
BACE2
γ secretase
APH1A
APH-1
PEN-2
Complex II
SDHA
SDHB
SDHC
SDHD
Complex III
CYTB
UQCRB
UQCRC2
UQCRH
UQCRFS1
UQCRQ
CYC1
UQCRC1
UQCR11
Complex IV
COX7B
COX2
COX3
COX7A1
COX1
COX7C
COX7A2
COX4I2
COX6C
COX4I1
COX6B1
COX5A
COX8A
COX7B2
COX8C
COX6B2
COX6A1
COX5B
COX6A2
Complex V
ATP5G1
ATP5G3
ATP5J
ATP5L
ATP5F1
FO complex
ATP5H
ATP5I
ATP5J2
ATP5G2
ATP5L2
ATP5C1
ATP5D
ATP5E
F1 complex
ATP5O
ATP5B
ATP5A1
NAD
NADH
FADH2
FAD+
O2
H2O
ADP
ATP
B
SHRSP
NP vs P
Prediction Legend
more extreme in dataset
less
Increased measurement
Decreased measurement

Figure 5.8: Predicted Interaction Network for Oxidative Phosphorylation Signalling Complexes

Predicted expression network for oxidative phosphorylation signalling in non-pregnant (NP) or GD6.5 (P) uterine arteries in WKY (A) and SHRSP (B) dams. WKY demonstrated a predicted pregnancy-dependant increase in expression of components of complexes III, IV and V. WKY also demonstrated a conflicting expression in complex I. No changes were detected in SHRSP uterine arteries. Here, **green** represents an increased expression, **red** a decreased expression, white no change and a **green**/**red** representing conflicting expression in pregnant (GD6.5) vs non-pregnant uterine arteries.

Table 5.9 The differentially expressed genes involved in mitochondrial function changes due to pregnancy in WKY.

Gene name	Gene Symbol	Ensembl Gene ID	WKY NP vs P	
			padj	FC
Complex I				
Nadh:ubiquinone oxidoreductase subunit A3	Ndufa3	ENSG00000170906	***0.022197***	***-1.75***
Nadh:ubiquinone oxidoreductase subunit A13	Ndufa13	ENSG00000186010	***0.027977***	***-1.37***
Nadh:ubiquinone oxidoreductase core subunit S2	Ndufs2	ENSG00000158864	***0.047252***	***-1.41***
Mitochondrially encoded NADH:ubiquinone oxidoreductase core subunit 2	Nd2	ENSG00000198763	***0.045737***	***1.90***
Complex III				
Cytochrome I	Cyc1	ENSG00000179091	***0.038197***	***-1.35***
Complex IV				
Cytochrome c oxidase subunit 5A	Cox5a	ENSG00000178741	***0.021279***	***-1.73***
Cytochrome c oxidase subunit 8A	Cox8a	ENSG00000176340	***0.024036***	***-1.53***
Complex V				
F0 complex				
ATP synthase, H^+ transporting, mitochondrial f0 complex subunit C3 (subunit 9)	Atp5g3	ENSG00000249253	***0.015354***	***-1.79***
ATP synthase, H^+ transporting, mitochondrial f0 complex subunit F2	Atp5j2	ENSG00000254283	***0.004097***	***-1.69***
F1 complex				
ATP synthase, H^+ transporting, mitochondrial F1 complex, β polypeptide	Atp5b	ENSG00000110955	***0.011745***	***-1.49***

The fold change (FC) and false discovery rate (*padj*) of mitochondrial genes that were significantly differentially expressed in WKY non-pregnant (NP) vs pregnant (P) and the FC and *padj* of the same genes from SHRSP NP vs P. Significance is defined as *padj* <0.05. *genes which have multiple transcripts.

5.5 Discussion

This study focussed on specific changes in the gene expression profile of uterine arteries in WKY and SHRSP rats from nonpregnant to GD 6.5. It complements many other studies that have examined differential gene expression across pregnancy in both humans and rodents (Hubel *et al*, 2000; Lash *et al*, 2006; Lash *et al*, 2016; Robson *et al*, 2019). However, to our knowledge, it is the first to examine expression changes in early pregnancy, before functional and structural changes in the uterine arteries in a model of chronic hypertension. We identified differential expression of 364 pregnancy-specific genes in WKY and 654 in SHRSP. These specific DEGs in WKY were predicted to be involved in pathways related to increased energy production and reduced calcium signal transduction, whereas SHRSP-specific changes were predicted to influence the immune response and activate pathways leading to vasoconstriction. Despite similarities in pregnancy-associated gene expression in both strains, our data suggests that uterine arteries in SHRSP dams demonstrate an altered genetic response in early pregnancy that may lead to maladaptive changes and failed priming of the arteries and thus, deficient remodelling.

We have previously shown that the SHRSP exhibits deficient uterine artery remodelling, reflected by altered vascular structure and function and uteroplacental blood flow at GD 18.5 (Small *et al*, 2016a). This was not the case at the early pregnancy (GD 6.5) time point examined in the current study, with uterine arteries responding to vasoactive substances and having similar structure to WKY. From the prediction analysis performed using IPA®, we found that both SHRSP and WKY dams shared gene expression changes indicating that a necessary vascular response to pregnancy is conserved between strains. The biological functions associated with the 188 pregnancy-specific DEGs in common between WKY and SHRSP were associated with processes involved in vascular remodelling. However, out with this set of shared genes in common, the pregnancy-dependant specific gene expression changes were observed to differ greatly between WKY and SHRSP suggesting an additional stress response present in SHRSP only. This may be in part due to pre-existing hypertension in this strain. Blood pressure was not measured in this study, thus the assumption that the SHRSP dams included in this study were hypertensive relative to WKY controls was based on historical data from previous generations. Previously, in

chapter 3 of this thesis, results have shown no significant differences in blood pressure at pre-pregnancy between SHRSP and WKY dams, therefore this assumption may not be accurate. This may not be the case at GD6.5, where results in chapter 3 have shown a divergence in blood pressure between the two, though this was non-significant. However, it is worth noting that in previous studies amelioration of the SHRSP dam's pre-existing hypertension does not resolve their observed abnormal uterine artery remodelling at GD18.5. (Small *et al*, 2016a). We have previously shown that treatment with nifedipine before and throughout pregnancy in the SHRSP while controlling their blood pressure - and as a result limiting the known direct effects of hypertension on oxidative stress and inflammatory cell activation (Barakonyi *et al*, 2014; Yang *et al*, 2013; Paravicini and Touyz, 2008) - did not improve measures of uterine artery function including assessment via myography and Doppler ultrasound *in vivo* at GD 18.5 (Small *et al*, 2016a). We chose not to include a nifedipine-treated SHRSP control in this study based on these previous findings. It has been shown that nifedipine alters the expression of genes related to Ca^{2+}-signalling, inflammation and ROS production in the heart, brain and livers of SHR rats compared to non-treated SHR (Lee *et al*, 2012). It may be useful to investigate the gene expression of nifedipine-treated SHRSP uterine arteries in future work to understand how it exerts a beneficial effect on blood pressure without altering uterine artery function.

We chose to further investigate gene expression changes related to the inflammatory response pathway, given the known importance of uterine-specific natural killer (uNK) cells, decidual macrophages, and other maternal immune cells in coordinating appropriate trophoblast invasion into the spiral arteries (Mor *et al* 2011), and the association between an exaggerated inflammatory response in the placental bed of hypertensive pregnancies (Barakonyi *et al*, 2014). Although both strains demonstrated an increased local inflammatory response to pregnancy, this was much greater in the SHRSP suggesting that hypertensive SHRSP dams experience an abnormally elevated immune response in response to pregnancy, as early as GD 6.5. Indeed, an abnormal immune response has been implicated in early gestation as an initiating factor that may interfere with crucial interactions between uterine natural killer cells and trophoblasts, resulting in systemic inflammation, impaired placentation, and dysregulated vascular remodelling (Taylor and Sasser, 2017). An array of factors can contribute to impairment of the immune response, one of which is reactive oxygen species (ROS) produced by

NADPH oxidase (NOX). In macrophages, ROS released to the extracellular space by membrane-bound NOX in chronic inflammatory conditions has been shown to impair the function of T cells and NK cells (Yang *et al*, 2013). Oxidative stress, or ROS accumulation, produced by NOXs is also known to play a role in the development and maintenance of hypertension (Paravicini and Touyz, 2008). IPA predicted an increase in ROS production via increased expression of NOX2 in SHRSP but not WKY uterine arteries in early pregnancy. This suggests that hypertensive SHRSP dams experience an increase in ROS production in early pregnancy, which may contribute to the elevated immune response and abnormal uterine artery function observed in later pregnancy.

Mitochondrial function is crucial in early pregnancy, as in the first trimester there is a heavy reliance on glucose utilization for the increased production of ATP to meet the increased maternal and fetal energy requirements (Thornburg *et al*, 2000). Analysis of the proteome in placental tissue from normotensive and preeclamptic pregnancies demonstrates an association between preeclampsia, inflammation, and mitochondrial dysfunction (Xu *et al*, 2018). In our data, there was an overall increase in the expression of genes involved in oxidative phosphorylation in pregnant WKY uterine arteries. However, SHRSP uterine arteries did not demonstrate any gene expression changes in the pathway across pregnancy. This implies that in early hypertensive pregnancy either energy production is already at its peak preventing further increases or it is unable to respond to the demands of pregnancy. This inability to adapt to changing energy requirements may contribute to a dysregulated immune response, impaired later vascular remodelling, or predicted changes in calcium signalling and transduction.

Given the importance of Ca^{2+} signalling in a myriad of functions required to complete a healthy pregnancy, together with studies demonstrating a decrease in serum Ca^{2+} in hypertensive pregnancies (Adamova *et al*, 2009), we chose to investigate expression changes in the α-adrenergic signalling pathway in this study. The DEGs in WKY uterine arteries indicate a pregnancy-associated reduction in Ca^{2+} release and sequestering. This may contribute to the decrease in peripheral vascular resistance and blood pressure normally experienced during pregnancy. Gopalakrishnan *et al* (2020) highlighted that the typical transcriptome response to pregnancy, in the rat uterine artery, involves the downregulation of calcium signalling and vascular smooth muscle contraction pathways. In contrast,

SHRSP uterine arteries demonstrated an increased expression of *Prkcb*, a member of the protein kinase C (PKC) family, which is known to mediate vascular contraction independently of intracellular Ca^{2+} (Gutíerrez *et al*, 2019; Ringvold and Khalil, 2017), along with an expression pattern suggesting an increased overall activation of the Ca^{2+} signalling pathway. This suggests a potential mechanism for the increased contractile response observed in later gestation in SHRSP uterine arteries (Small *et al*, 2016a).

Normal pregnancy is associated with an upregulation of RAAS and concurrent increased resistance to angiotensin II (ANG II), whereas HDPs (particularly pre-eclampsia) are associated with an increased sensitivity to ANG II and suppression of the RAAS (Verdonk *et al*, 2014; Hussein and Lafayette, 2014). IPA analysis of the RAAS pathway revealed a pregnancy-dependant decrease in expression of RAAS genes in WKY uterine arteries and an increased expression of genes downstream of angiotensin receptor 1 (AT_1R) in SHRSP uterine arteries. These data suggest that although there is evidence of a decrease in Ca^{2+} release in WKY uterine arteries, in SHRSP arteries, the pathways downstream of AT_1R have an increased activation, leading to increased ROS production and vasoconstriction. However, animal models with excessive RAAS activation also result in preeclampsia like symptoms and there is evidence that demonstrates a role for autoantibody activation of AT_1R and its downstream effectors leading to vasoconstriction (Verdonk *et al*, 2014). Interestingly, these downstream effectors include NOX and other genes that were also implicated in the increased production of ROS and immune response demonstrated in SHRSP uterine arteries in early pregnancy.

This study sought to examine the specific differences in gene expression in response to early pregnancy in the normotensive WKY and hypertensive SHRSP uterine artery. Taken together, our data provides evidence that hypertension during pregnancy results in distinct gene expression changes in pathways influencing uterine artery vascular function that are not seen in normotensive pregnancy. These pathway changes may underlie or contribute to the adverse vascular remodelling and resultant placental ischemia and systemic vascular dysfunction in later stages of gestation seen in hypertensive disorders of pregnancy in rodents. In the absence of human uterine artery samples from an

early gestational time point, the results here may lend some insight into maladaptive responses in human hypertensive pregnancies.

Chapter 6: Genetic and Functional Validation of Early Pregnancy Expression Profiles in SHRSP and WKY Arteries

6.1 Introduction

During a normal pregnancy, calcium (Ca^{2+}) is important in the formation of the fetal skeleton. Indeed, studies have shown that maternal Ca^{2+} absorption significantly increases in the second and third trimesters and is directly correlated to maternal Ca^{2+} intake (Hacker et al, 2012). This is achieved by increased intestinal absorption, decreased renal excretion and increased bone resorption (Lafond and Simoneau, 2006). This increase in absorption is mediated by calcitrol in the absence of increases to parathyroid hormone serving to increase blood Ca^{2+} (Hacker et al, 2012; Lafond and Simoneau, 2006). The recommended Ca^{2+} intake per day for women 19-51 years old is 1000mg/day, with 78% of women over 20 years of age failing to meet this daily allowance (Adamova et al, 2009). In hypertensive pregnancies, serum concentrations of Ca^{2+} are reduced relative to a normal pregnancy (He et al, 2016).

Calcium signalling is exceptionally versatile, with elevated intracellular Ca^{2+} being responsible for the activation of many cellular processes including gene transcription, cell proliferation, differentiation, necrosis and apoptosis (Baczyk *et al*, 2011). Functioning of the cardiovascular system, in particular, is highly associated with changes in Ca^{2+}. Of note is the role of Ca^{2+} in the constriction of vascular smooth muscle cells (VSMCs) and vasodilation in endothelial cells (Adamova et al, 2009). A common feature of hypertensive disorders of pregnancy is endothelial dysfunction leading to an increase in vascular tone (Possomato-Vieira and Khalil, 2016). An inverse relationship between Ca^{2+} intake and symptoms of pre-eclampsia was first reported in 1980 (Belizán and Villar, 1980). Following several studies, it has now been shown that there is an association between serum hypocalcaemia and pre-eclampsia (Kumuru *et al*, 2003; Jain *et al*, 2009; Sukonpan and Phupong, 2004). Despite this, calcium supplementation in pre-eclampsia has produced mixed results. There are many studies in the literature that support the role for calcium supplementation to prevent pre-eclampsia occurrence in low Ca^{2+} intake, and thus increased PE risk, individuals (Patrelli *et al*, 2012; Hofmeyr *et al*, 2018). On the other hand, a World Health Organisation randomised controlled trial of 8,325 pregnant participants with low Ca^{2+} intake receiving supplementation showed that calcium supplementation did not prevent pre-eclampsia, though it did reduce its severity (Villar *et al*, 2006).

Due to the importance of Ca^{2+} in vascular function and its association with PE, studies utilising animal models have been conducted to assess how the expression of Ca^{2+} handling proteins may change in normotensive and hypertensive rodents in a pregnancy-dependant manner. Recent data generated from Ingenuity Pathway Analysis (Chapter 5) shows that in normotensive uterine arteries, pregnancy results in an increase in the expression of calmodulin-1 (CALM1; modulation of cardiac ion channel function, activation of contractile machinery), and a decreased expression of inositol-triphosphate receptor (ITPR2; release of Ca^{2+} from intracellular stores) and phospho-lipase C (PLC; generation of IP_3 and activation of IP_3R) (Scott *et al*, 2021). In contrast, hypertensive arteries show an increase in the expression of protein kinase C β (PRCKB; enhances Ca^{2+} currents) and a decrease in the expression of myosin-light chain kinase (MYLK; contractile machinery) and PLC (Scott *et al*, 2021). This indicates a differential response to Ca^{2+} between normal and hypertensive pregnancy, though the exact mechanisms that underlie this and their contribution to pathology are unclear.

Another important regulator of VSMC function are reactive oxygen species (ROS), (Bertero and Maack, 2018). ROS are widely recognised signalling molecules with functions across a broad range of cell types and are generated as by-products of mitochondrial activity or by enzymes out with the mitochondria such as NADPH oxidases (Görlach et al, 2015). ROS production is naturally balanced by endogenous antioxidant activity, with scavengers removing excess ROS to prevent oxidative stress (Zorov *et al*, 2014). Normal pregnancy is characterised by a pro-oxidant period where ROS production is heightened (Tenório *et al*, 2019). During hypertensive pregnancies, abnormal placentation leads to oxidative stress within the placenta that results from increased NADPH oxidase and mitochondrial activation, resulting in an increase in pro-inflammatory cytokines and endothelial dysfunction (Guerby *et al*, 2021; Phoswa and Haliq, 2021). Many studies have shown that pro-oxidant activity is exacerbated during hypertensive pregnancy (Rogers *et al*, 2006; Schoots *et al*, 2021). It has been documented that in hypertension, VSMC Ca^{2+} homeostasis is modulated by NAPDH oxidase activity and ROS production (Touyz *et al*, 2018). Previous work in Chapter 5 has shown that in uterine arteries from pregnant hypertensive rats, there is an increased expression of NADPH oxidase subunits that may result in an increase in ROS production, which may contribute to the vascular dysfunction and increased blood

pressure evident in late gestation in the SHRSP rat (Scott *et al*, 2021; Morgan *et al*, 2018).

Calcium and ROS go hand in hand in regulating vascular tone and VSMC function. A disruption in the production and maintence of either one has the potential to lead to pathological states. Though there is evidence in the literature to show a relationship between Ca^{2+}, ROS and VSMC function in hypertensive pregnancy the mechanisms that underlie any potential pathology are unclear. In this study, we sought to validate the gene expression patterns observed in Chapter 5 in pregnant and non-pregnant WKY and SHRSP uterine arteries to further investigate the influence of these on uterine artery function in early pregnancy.

6.2 Hypothesis & Aims

Based on evidence generated in Chapter 5, we hypothesised that there would be a functional difference in Ca^{2+} handling, ROS generation and NOX subunit expression between WKY and SHRSP uterine arteries on gestational day 6.5 relative to non-pregnant controls.

We aimed to investigate this by performing live cell fluorescent Ca^{2+} imaging in uterine artery vascular smooth muscle cells (UAVSMCs) to assess intracellular Ca^{2+} release. We also performed electron paramagnetic resonance (EPR) spectroscopy quantification of ROS production and Taqman® gene expression assays for NOX2 subunits *p22-phox* and g*p91*.

6.3 Materials and Methods

Animals were housed and mated as outlined in section 2.3.1. Animals were randomly allocated to one of four groups: WKY non-pregnant (NP), WKY pregnant (P; gestational day 6.5), SHRSP NP or SHRSP P. Uterine or mesenteric arteries from pregnant WKY or SHRSP rats or virgin, age-matched controls were dissected as in the general materials and methods (2.4.3). These arteries were either stored at -80°C until use in either EPR or Taqman®, or immediately used to isolated uterine artery vascular smooth muscle cells for live-cell fluorescent Ca^{2+} imaging.

6.3.1 Validation of NOX2 Subunit Gene Expression via Taqman® Gene Expression Assay

RNA was extracted from whole, frozen uterine or mesenteric arteries harvested at time of sacrifice (section 2.2.1). Following quality control, cDNA was generated from these RNA samples via RT-PCR (2.2.2). This was then utilised in a qPCR Taqman® gene expression assay to determine the relative expression of NOX2 subunits *p22-phox* (Human: *Cyba*) and *gp91* (Human: *Cybb*). Details of the Taqman® assay and the specific probes used can be found in section 2.2.3.1.

6.3.2 Measurement of ROS Production via Superoxide anion ($O_2^{\bullet-}$) Quantification by Electron Paramagnetic Resonance (EPR) Spectroscopy

The cell-permeable spin-trapping probe CMH (1-hydroxy-3-methoxycarbonyl-2,2,5,5-tetramehtylpyrrolidine; Enzo Life Sciences, Exeter, UK) was used to detect intracellular superoxide anion concentration. Frozen uterine or mesenteric arteries were homogenised by addition of 100µL of lysis buffer (Tissue Protein Extraction Reagent, ThermoFisherScientific, Paisley, UK) and disruption using a TissueLyser II for 2 minutes at 25Hz (Qiagen, Manchester, UK).

Samples were then incubated for 30 minutes at 37°C following addition of 50µL of modified Krebs/HEPES buffer of pH 7.35 [99mM NaCl, 4.7mM KCl, 2.5mM $CaCl_2$, 2.5mM $MgSO_4$, 24.7mM NaH_2CO_3, 1.0mM $K(PH_2O_4)$, 11.1mM D-Glucose, 20mM HEPES-Na; additional 0.05mM CMH, 5µM DETC (diethyldithiocarbamate) and 25µM deferoxamine]. Following incubation, approximately 50µL of each sample was loaded into a capillary glass tube (Noxygen Science Transfer & Diagnostics, Elzach, Germany) and placed inside the e-scan spectrometer cavity for reading.

Samples were read using a benchtop Bruker e-scan EPR spectrometer (Blue Scientific, Cambridge, UK). The remaining 30µL of lysate was used to quantify total protein by the BCA method (Pierce™ BCA Protein Assay Kit, ThermoFisher Scientific, Paisley, UK).

Results are expressed as a percentage relative to WKY NP controls calculated from the spectrum amplitude value (arbitrary units) per µg of protein. Spectrometer acquisition parameters were microwave power 21.98mV; microwave frequency 9.463GHz; no. of scans 30; sweep width 50G; modulation amplitude 2G; conversion time 656ms; time constant 656ms; resolution 512 points and receiver gain $1x10^5$. Sample temperature was kept at 37°C by a NOX-E.4-TGC Temperature and Gas Controller unit (Noxygen Science Transfer & Diagnostics, Elzach, Germany) connected to the spectrometer. EPR spectra trace data was quantified using WinEPR software (Bruker, Coventry, UK).

6.3.3 Live-Cell Fluorescent Intracellular Calcium Imaging

Vascular smooth muscle cells from uterine arteries (UAVSMC) were isolated and cultured as outlined in general materials & methods section 2.5. Cells were used after reaching 80% confluency in a 12-well plate at p0. 72 hours prior to imaging, cells were starved using DMEM (-) L-glutamine starvation media [25mM D-glucose, 1mM sodium pyruvate, 44mM sodium bicarbonate] (Gibco™, ThermoFisher Scientific, Paisley, UK) and 100IU/mL penicillin, 100µg/mL streptomycin and 0.5% v/v fetal bovine serum (FBS). This ensured that all cells were at the same growth cycle stage and there was no FBS in the media during the experiment, as this can alter readings.

Intracellular calcium release was measured using the fluorescent calcium indicator Cal-520®AM (ab171868, Abcam, Cambridge, UK). This dye works by preloading the cells. Once inside the cell, lipophilic blocking groups are cleaved from the dye causing it to remain intracellularly. When calcium is released, the calcium-sensitive dye produces fluorescent signals that can be detected and quantified. Once cells had been starved for 72 hours, they were incubated with Cal-520®AM. Briefly, the starvation media was removed, and cells washed with sterile PBS. A working 5µM Cal-520®AM/DMEM-HEPES solution was created by addition of 2.5µL of 1mM Cal-520®AM stock to 1mL of DMEM-HEPES media [5.5mM D-Glucose, 25mM HEPES, 1mM sodium pyruvate] (Gibco™, ThermoFisher Scientific, Paisley, UK)

and 2mM L-glutamine, 100IU/mL penicillin, 100µg/mL streptomycin and 0.5% v/v FBS. 400µL of 5µM Cal-520®AM/DMEM-HEPES was added per well and the culture plate covered with tinfoil to protect the dye from light. The plate was then incubated at 37°C and 5% CO_2 in a Heracell™ 240i CO_2 incubator (FisherScientific, Loughborough, UK) for 75 minutes. After 75 minutes, the Cal-520®AM/DMEM-HEPES solution was removed and cells were washed once with 1mL of Ca^{2+}-free HEPES solution [20mM HEPES, 130mM NaCl, 5mM KCl, 1mM $MgCl_2$, 10mM D-glucose, 0.1mM EDTA; pH 7.4]. 800µL of Ca^{2+}-free HEPES solution was added to each well and cells were further incubated at room temperature for 30 minutes, protected from light.

Live-cell microscopy was used to visualise calcium release with a Zeiss Axio Observer Z1 microscope (Carl Zeiss Ltd, Cambridge, UK). Culture plates were placed on a heated mount set to 37°C and cells brought into focus with bright field microscopy settings at 10x magnification. Each well was recorded for 6 minutes in the dark. Once cells were located, the microscope was switched to fluorescence detection of wavelengths Ex/Em 460/525nm. Baseline fluorescence was recorded for 2 minutes. At 2 minutes, 100µL of 1mM ANGII (Abcam, Cambridge, UK) was added to the well and timed for 2 minutes. At 4 minutes, 100µL of 1mM ionomycin (ThermoFisher Scientific, Paisley, UK) was added and the well recorded for a further 2 minutes. This process was repeated for each well on each plate.

The mean fluorescence intensity in the field of vision was recorded every 1.2 seconds using ZEN Microscopy software (Carl Zeiss Ltd, Cambridge, UK). Average baseline values (0-2 minutes) were subtracted from all subsequent intensity measurements to construct a trace of intracellular Ca^{2+} release in response to ANGII and ionomycin. The difference in peak and baseline ANGII-stimulated or ionomycin-stimulated Ca^{2+} release was calculated.

6.4 Results

6.4.1 *Cyba* Expression in WKY and SHRSP Pregnant Uterine Arteries

The expressions of NOX2 subunits *Cyba (p22-phox)* and *Cybb (gp91*) in uterine and mesenteric arteries from NP and P WKY and SHRSP rats was validated by qRT-PCR. Alongside a possible increase in *Cyba* expression in WKY P vs NP uterine arteries, there appeared to be an increase in relative *Cyba* expression in pregnant WKY uterine arteries compared to SHRSP (Fig 6.1A). Pregnancy may have resulted in a decreased expression of *Cyba* in SHRSP uterine arteries, which appeared lower than WKY P uterine arteries (ns.). There were no apparent differences in relative *Cybb* expression between strains or as a result of pregnancy in uterine arteries (Fig. 6.1B).

Expression patterns of *Cybb* but not *Cyba* in response to pregnancy seemed to be similar between WKY and SHRSP mesenteric arteries. Whilst not statistically significant, there may have been an increase in the relative expression of *Cyba* in pregnant WKY mesenteric arteries. Pregnancy did not seem to elicit a change in expression in SHRSP mesenteric arteries (Fig. 6.1C). There appeared to be an overall increased relative expression of *Cybb* in WKY versus SHRSP mesenteric arteries (Fig. 6.1D; ns.). Both SHRSP and WKY mesenteric arteries seemed to exhibit a similar response to pregnancy, with decreased expression of *Cybb*.

It is not possible to draw firm conclusions from this data, as the operator variation that can be seen between samples creates a large degree of error, likely a result of pipetting error between replicates within each sample. Additionally, the high standard deviation value between technical replicates in the housekeeping gene *Gapdh* indicates that its expression is not stable (Table 6.1).

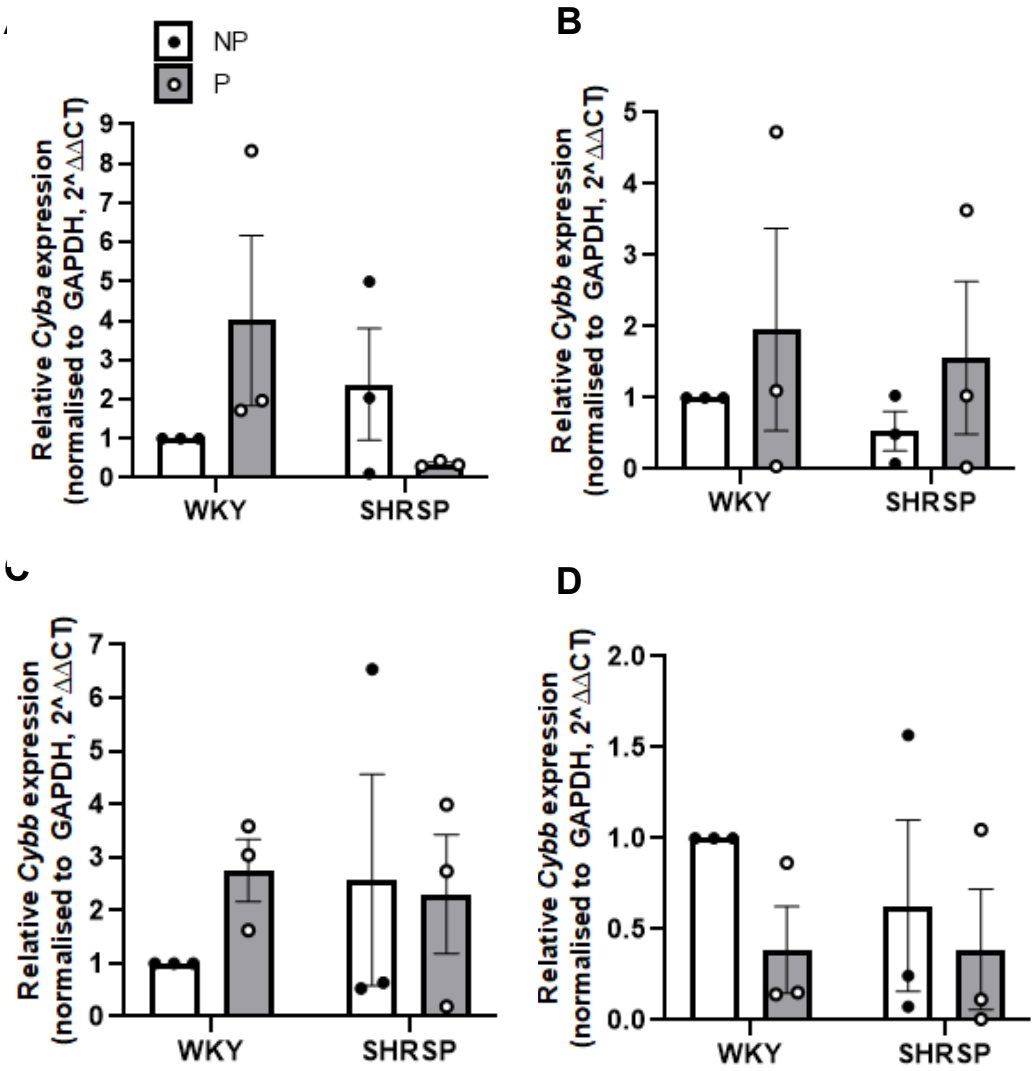

Figure 6.1: Validation of *Cyba* and *Cybb* Expression in Uterine & Mesenteric Arteries using Taqman® qRT-PCR

(A) *Cyba* expression appeared to be increased in pregnant WKY (*N*=3) uterine arteries relative to NP WKY (*N*=3) and pregnant SHRSP (*N*=3). Expression seemed to decrease in SHRSP pregnancy (*N*=3 NP). (B) There were no significant differences in *Cybb* expression across strain or pregnancy in uterine arteries. (C) No significant differences were detected in *Cyba* expression in WKY or SHRSP mesenteric arteries, though there appeared to be an increase in WKY pregnancy. (D) Whilst non-significant, there may have been a decrease in *Cybb* expression in response to pregnancy in WKY and SHRSP mesenteric arteries. Data analysed by two-way ANOVA with Tukey's *post hoc* testing. Values are expressed as the mean relative expression ± SEM normalised to the housekeeper gene *Gapdh* calculated from $2^{\Delta\Delta CT}$.

Table 6.1 Average Cycle Threshold Values and Standard Deviation for *Gapdh*, *Cyba* and *Cybb* in WKY and SHRSP arteries

GAPDH			CYBA			GAPH			CYBB		
Group	**Avg CT**	**Avg CT StDev**	**Group**	**Avg CT**	**Avg CT StDev**	**Group**	**Avg CT**	**Avg CT StDev**	**Group**	**Avg CT**	**Avg CT StDev**
WKY NP UA	31.342	3.26	***WKY NP UA***	30.462	0.93	***WKY NP UA***	31.460	2.50	***WKY NP UA***	31.019	0.59
WKY P UA	31.800	0.78	***WKY P UA***	29.315	0.37	***WKY P UA***	31.800	0.78	***WKY P UA***	29.135	0.24
SHRSP NP UA	31.466	1.96	***SHRSP NP UA***	30.555	0.56	***SHRSP NP UA***	31.466	1.96	***SHRSP NP UA***	29.630	0.17
SHRSP P UA	30.751	0.39	***SHRSP P UA***	31.383	0.24	***SHRSP P UA***	32.911	0.72	***SHRSP P UA***	30.557	0.28
WKY NP MA	30.580	2.60	***WKY NP MA***	33.638	0.34	***WKY NP MA***	35.195	4.19	***WKY NP MA***	34.838	0.12
WKY P MA	30.783	0.97	***WKY P MA***	31.949	0.58	***WKY P MA***	31.619	1.02	***WKY P MA***	33.173	0.48
SHRSP NP MA	29.321	0.25	***SHRSP NP MA***	31.491	0.07	***SHRSP NP MA***	31.022	0.99	***SHRSP NP MA***	32.371	0.34
SHRSP P MA	29.267	1.39	***SHRSP P MA***	31.465	0.42	***SHRSP P MA***	28.363	6.07	***SHRSP P MA***	31.363	0.38

The average cycle threshold (CT) values and standard deviation (StDev) of the cycle threshold value between technical replicates (measured in duplicate) for WKY and SHRSP pregnant (P) and non-pregnant (NP) uterine (UA) or mesenteric (MA) arteries. Values are given for the housekeeping gene *Gapdh* in relation to the target genes: either *Cyba* or *Cybb*. High standard deviation of CT values in the housekeeper indicated the assay was not of high quality.

6.4.2 ROS Production is Altered in Uterine and Mesenteric Arteries During Pregnancy in SHRSP and WKY

ROS production was measured in lysates generated from intact WKY and SHRSP NP and P uterine and mesenteric arteries by quantifying O^{-}_{2} via EPR. There were no significant differences in $O_2^{\bullet-}$ generation/µg of protein as a result of strain or pregnancy in uterine or mesenteric arteries (Fig. 6.2A, 6.2C). Superoxide anion generation was lower in SHRSP NP uterine arteries relative to WKY NP controls (12.7±1.7%, ns.) and appeared to increase in response to pregnancy (60.2±29.4% SHRSP P vs. WKY NP, ns., Fig. 6B). In mesenteric arteries, $O_2^{\bullet-}$ generation was reduced as a result of pregnancy in WKY rats (31.3±12.2% vs. WKY NP, p=0.09; Fig. 6D). There was significantly less ROS production in SHRSP NP compared to WKY NP mesenteric arteries (18.0±1.0%, p<0.05). Though there may have been an increase in ROS in SHRSP P mesenteric arteries compared to SHRSP NP, this was still lower than the WKY NP group (28.5±2.9%).

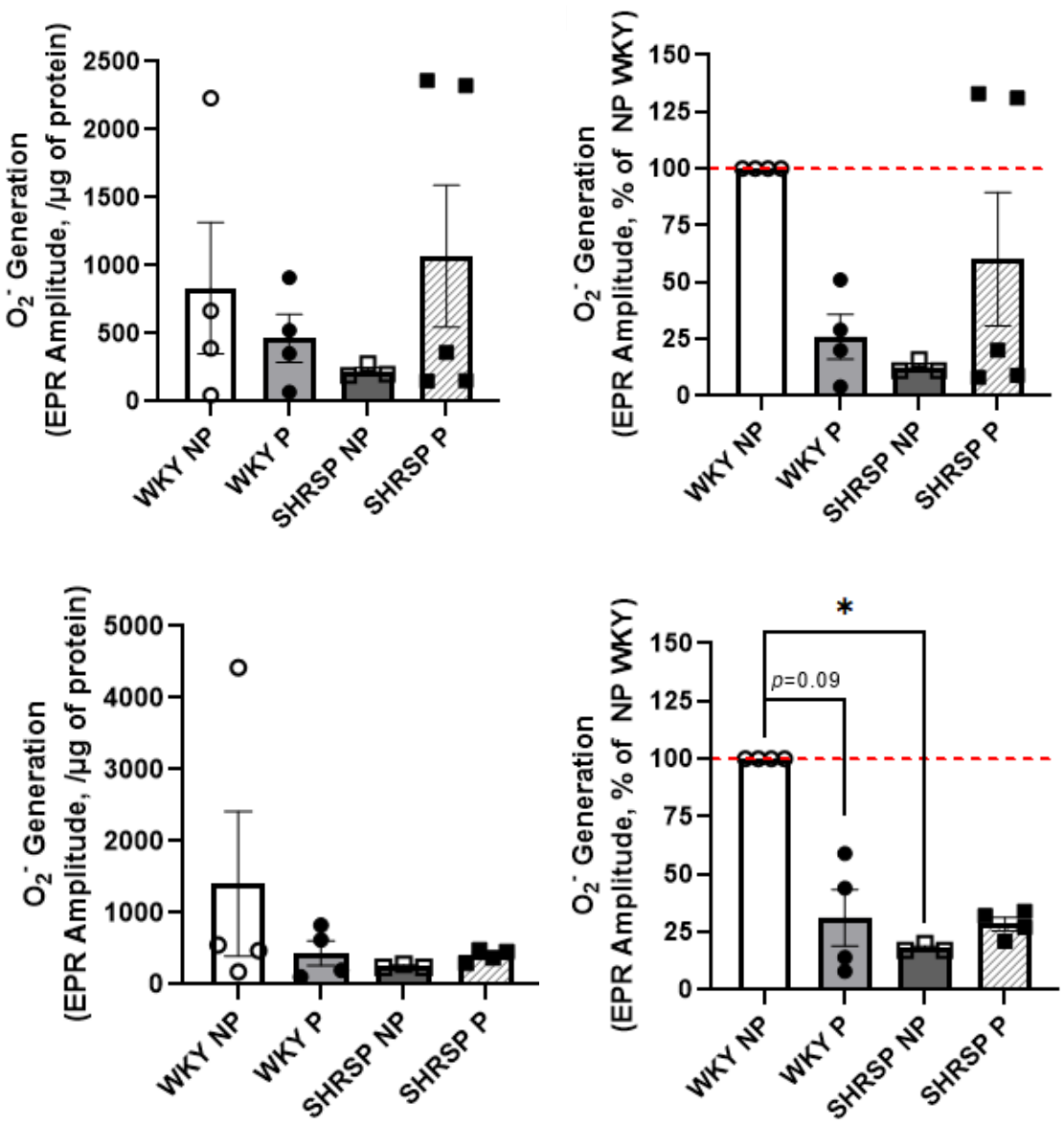

Figure 6.2: Superoxide Anion ($O_2^{\bullet-}$) Generation in Response to Pregnancy in WKY and SHRSP Arteries

(A, B) $O_2^{\bullet-}$ generation was not significantly different between groups in uterine arteries (WKY P (*N*=4); NP (*N*=4) arteries). There did appear to be an increased generation in SHRSP P (*N*=5) vs. NP (*N*=3) arteries. (C,D) There was a significant reduction in $O_2^{\bullet-}$ generation in SHRSP NP compared to WKY NP mesenteric arteries (*p<0.05). $O_2^{\bullet-}$ generation appeared to decrease in response to pregnancy in WKY (p=0.09). A similar pattern between WKY NP vs. P and SHRSP NP vs. P uterine artery ROS was observed in mesenteric arteries.. Raw EPR/µg values analysed by two-way ANOVA with Tukey's *post hoc* testing. Percentage values normalised to WKY NP as control analysed by Kruskal-Wallis test with Dunn's multiple comparisons *post hoc* testing.

6.4.3 Differences in Calcium Release in Uterine Arteries

Intracellular Ca^{2+} signalling was investigated using fluorescent Cal-520®AM. Figure 6.3A shows the trace of fluorescent intensity in UAVSMCs from non-pregnant and pregnant WKY and SHRSP rats in response to ANGII and ionomycin (Ca^{2+} ionophore). The first peak between 2-4 minutes represents ANGII-stimulated Ca^{2+} release. There was an accelerated response to ANGII in pregnant WKY UASMCs, peaking at approximately 2.7 minutes. The peak ANGII response in non-pregnant WKY UAVSMCs, on the other hand, did not occur until approximately 3.0 minutes. This was similar in SHRSP P cells. There was no difference in the area under the curve of ANGII-stimulated release between groups (Fig. 6.3B). This was not the case for ionomycin-stimulated release, represented by the second peak between 4-6 minutes. All groups reacted to ionomycin within a similar time. The peak response to ionomycin trended towards a reduction in pregnant SHRSP UAVSMCs compared to both WKY P and WKY NP cells (Fig. 6.3C, ns.). The area under the curve revealed a potential increase in ionomycin-stimulated Ca^{2+} release in pregnant WKY UAVSMCs compared to non-pregnant.

Due to technical issues with preparation of UAVSMCs and suspension of research activities due to COVID-19 disruptions (see Impact Statement) it was not possible to complete Ca^{2+} release experiments in non-pregnant SHRSP cells or to reach *n* numbers in all other groups that would have allowed for statistical testing

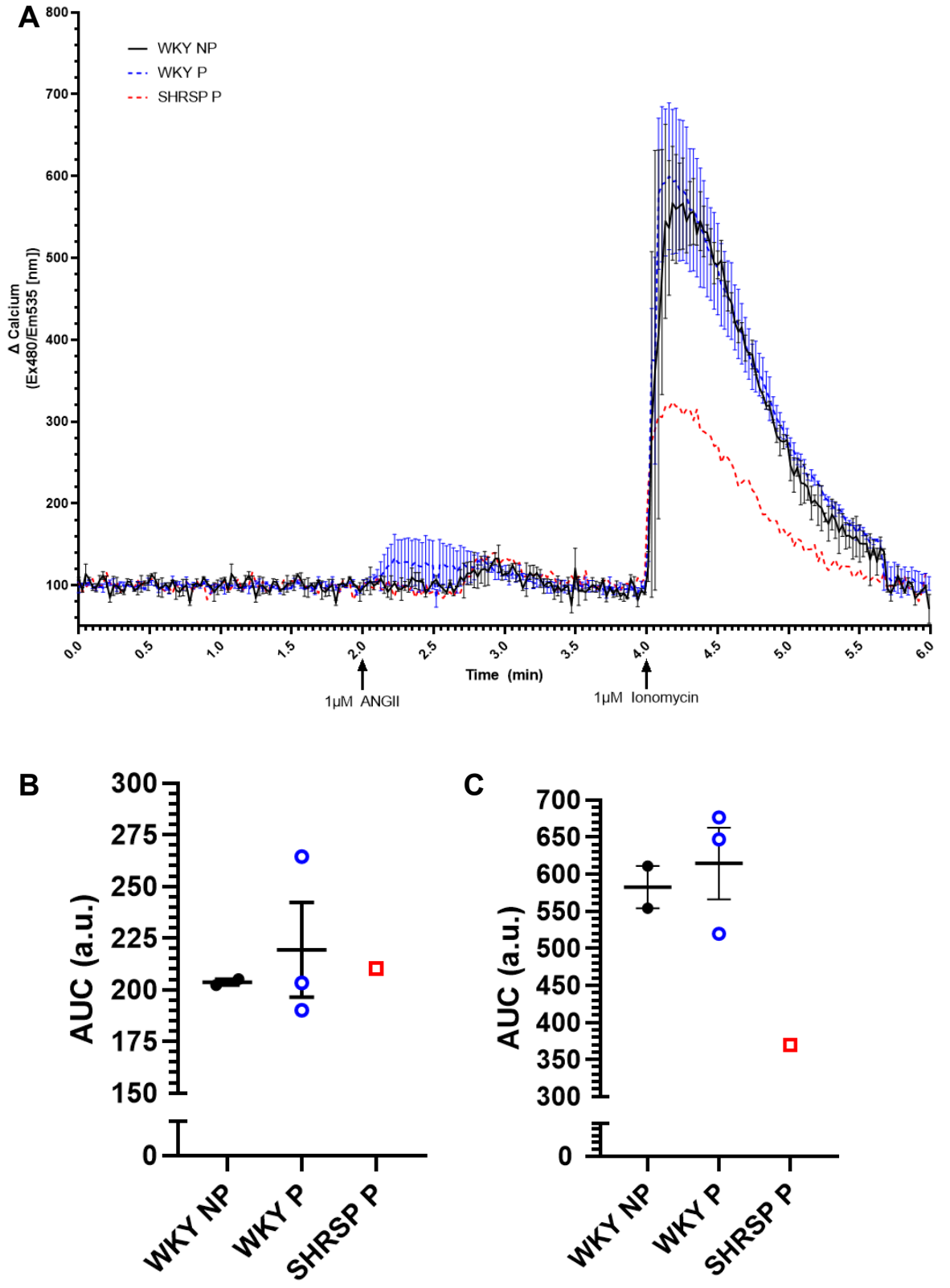
A
WKY NP
WKY P
SHRSP P
Δ Calcium
(Ex480/Em535 [nm])
800
700
600
500
400
300
200
100
0.0
0.5
1.0
1.5
2.0
2.5
3.0
3.5
4.0
4.5
5.0
5.5
6.0
Time (min)
1μM ANGII
1μM Ionomycin
B
AUC (a.u.)
300
275
250
225
200
175
150
0
WKY NP
WKY P
SHRSP P
C
AUC (a.u.)
700
650
600
550
500
450
400
350
300
0
WKY NP
WKY P
SHRSP P

Figure 6.3: Intracellular Calcium Release in WKY and SHRSP Uterine Artery Vascular Smooth Muscle Cells

(A) Intracellular Ca^{2+} release was measured over 6 minutes. Fluorescent baseline was established between 0-2 minutes and subtracted from the trace to calculate ∆Calcium. ANGII was added at 2 minutes and baseline re-established before addition of ionomycin at 4 minutes. The response to ANGII was delayed in WKY NP (*N*=2) and SHRSP P (*N*=1) UAVSMCs compared to WKY P (*N*=3). (B) The area under the curve for peak ANGII-stimulated Ca^{2+} release. No differences were observed between groups. (C) The area under the curve for peak ionomycin-stimulated Ca^{2+} release. There was an increase in WKY P vs. WKY NP cells. AUC seemed to decrease in cells from pregnant SHRSP uterine arteries versus WKY NP and WKY P. No statistical testing.

6.5 Discussion

This chapter focused on validating the gene expression profiles of age-matched, non-pregnant and gestational day 6.5 WKY and SHRSP uterine arteries. Few studies have investigated gene expression during early pregnancy, and far fewer have focused specifically on changes in the maternal vasculature despite its central involvement in the development of hypertensive disorders of pregnancy. Combined with the findings of Chapter 5, these results provide some insight into the strain-dependant differences between WKY and SHRSP in early pregnancy. These changes in gene expression and vascular function may contribute to defective maternal vascular remodelling normally observed in the SHRSP as a model of chronic hypertension during pregnancy.

We have previously reported that in early pregnancy, SHRSP but not WKY uterine arteries have an increased expression of NADPH oxidase 2 (nicotinamide adenine dinucleotide phosphate oxidase 2; NOX2) subunits *p22-phox (Cyba)* and *gp91 (Cybb)* that were predicted to increase ROS production (Scott *et al*, 2021). The family of NOX enzymes is unique in that their sole function is to generate ROS in the form of either superoxide anion ($O_2^{\bullet-}$) or hydrogen peroxide (Görlach *et al*, 2015). Hyperactivation of NOX leads to an accumulation of $O_2^{\bullet-}$ and subsequently reduces NO bioavailability and uncouples eNOS (Guerby *et al*, 2021). This can lead to endothelial dysfunction. The results of this study confirm that there is a strain-dependent response to pregnancy between WKY and SHRSP. However, there is disagreement between qRT-PCR results and those generated in Chapter 5. Here, we observed a non-significant increase in *p22-phox* expression in pregnant WKY that was not indicated by previous results. This does, however, agree with the literature that normal pregnancies are characterised by an initial pro-oxidant period (Tenório *et al*, 2019). This pro-oxidant period is a result of vascular plug formation in the maternal spiral arteries that functions to promote trophoblast invasion, vascular remodelling, early placental development and protection of the fetus against oxidative stress (Pijenborg *et al*, 2006). The results of this study indicate that despite an increase in *p22phox* expression, there appears to be a reduced generation of $O_2^{\bullet-}$ in response to pregnancy in WKY. As it is a regulatory subunit, *p22phox* does not only form NOX2 but rather is able to form heterodimers that create any one of the NOX isoforms as well as bind to the other regulatory subunits (Bedard and Krause, 2007). One such isoform is NOX4,

which in contrast to the other NOX isoforms has been shown to have a protective role in the vasculature (Vermot *et al*, 2021). NOX4 produces hydrogen peroxide which stimulates vasodilation during hypertensive or inflammatory stress (Schröder *et al*, 2012). NOX4 is unique in that it does not require the other cytosolic subunits to activate and appears to be constitutively active (Bedard and Krause, 2007). Thus, the increase in *p22phox* expression but resultant decrease in $O_2^{\bullet-}$ generation in pregnant WKY arteries may be due to activation of NOX4, which would agree with the protective pro-oxidant activity described in literature, rather than NOX2. This may also explain why this was not detected in the results of Chapter 5, where IPA specifically focused on the NOX2 pathway of ROS generation. It is important to note that standard curves were not performed for qPCR reactions, thus the efficiency for the target and control genes (i.e., double the cDNA exhibits the expected cycle threshold value) was not validated, thus the data cannot be accurately quantified.

Previous work suggested that there would be an increased expression of both NOX2 subunits in pregnant SHRSP uterine arteries (Scott *et al*, 2021). There appeared to be an increase in *gp91* but not *p22-phox* expression in pregnant SHRSP. *Gp91* is a catalytic subunit that forms the membrane-bound core of active NOX2 (Bedard and Krause, 2007; Vermot *et al*, 2021). NOX2 is expressed in a variety of cell types including endothelial cells, vascular smooth muscle cells, cardiomyocytes, fibroblasts and inflammatory cells (Bedard and Krause, 2007). As these experiments utilised intact arteries, it is unclear which cell type is responsible for the increased *gp91* expression. *P22-phox* normally associates with *gp91* to provide stability and it was believed that both subunits were required to produce an active enzyme (Vermot *et al*, 2021). *Gp91* was shown by Görlach and colleagues (2000) to contribute to endothelial dysfunction and impaired vascular relaxation in mouse aortae via endothelial specific $O_2^{\bullet-}$ production. Further research has shown that even when *p22phox* expression is low or absent, *gp91* is still able to oxidise NADPH and thus produce superoxide (Ezzine *et al*, 2014). Additionally, sera from pre-eclamptic patients have been shown to induce the expression of *gp91* but not *p22phox* in human umbilical vein endothelial cells (Matsubara *et al*, 2010). The hypothesis that *gp91* may produce $O_2^{\bullet-}$ independently of *p22phox* expression in SHRSP pregnancy may be supported by EPR results. Whilst non-significant, there seemed to be an increase in $O_2^{\bullet-}$ generation in pregnant SHRSP uterine arteries. Previous studies have shown that in aortic

VSMCs and ring preparations, $O_2^{\bullet-}$ generation is generally increased in untreated SHRSP rats compared to WKY, as measured both by chemiluminescence and EPR (Lappas *et al*, 2005; Kerr *et al*, 1999; Wu *et al*, 2001). This was not the case in our study where superoxide generation was lower in SHRSP NP versus WKY NP uterine arteries. ROS are relatively short-lived and can be altered by the process of homogenisation as disruption of cellular membranes can alter substrate concentrations (Murphy *et al*, 2022). This may explain the variability present in the WKY NP control and the differences in $O_2^{\bullet-}$ production compared to literature, as results of previous studies were performed in intact tissue or cultured cells as opposed to homogenates as in this study. These differences may also be explained by the differences in vascular beds studied. Further study of the specific types of ROS generated in WKY and SHRSP uterine arteries would be advantageous in understanding the role of ROS in the maternal uterine vasculature during normotensive and hypertensive pregnancy.

The interactions that occur between ROS and Ca^{2+} can be considered bi-directional, whereby changes in the signalling of one can alter the other and are highly cell-type specific (Görlach *et al*, 2015). In addition to the predicted changes in ROS production identified in Chapter 5, results also predicted a strain-dependent response in Ca^{2+} signalling between WKY and SHRSP pregnancies. To investigate this, functional Ca^{2+} signalling in UAVSMCs was performed. There was no difference in the ANGII response, however, there may have been an increase in ionomycin-induced intracellular Ca^{2+} release in pregnant WKY UAVSMCs versus non-pregnant. Though the expression patterns generated previously may suggest reduced Ca^{2+} release, they also suggest this may be due to accumulation of Ca^{2+} intracellularly. Ionomycin is a narrow-spectrum ionophore with a strong attraction to divalent cations such as Ca^{2+}, and even low concentrations can cause the sarcoplasmic reticulum to empty as much as 70% into the extracellular space (Smith *et al*, 1989). Thus, the absence of effect by ANGII on intracellular release coupled with the concurrent increased release by ionomycin in pregnant WKY UAVSMCs may provide evidence that though intracellular Ca^{2+} is not reduced, it is sequestered in the sarcoplasmic reticulum, which agrees with the expression patterns observed previously (Scott *et al*, 2021). Ionomycin-induced calcium release was reduced in UAVSMCs from pregnant SHRSP, however as this was a preliminary study (due to COVID-19 related disruptions) the sample size of this group was N=1 so it is unclear whether this

result is representative or anomalous. Conducting further experiments with greater numbers as well as performing qRT-PCR experiments for the specific genes related to Ca^{2+} signalling identified by IPA would be of great interest in validating and understanding the functional implications of hypertension on Ca^{2+} signalling in early pregnancy.

In summary, this study provides further evidence that there is a strain-dependent response to pregnancy between normotensive WKY uterine arteries and hypertensive SHRSP. Though this study was unable to fully validate the previously reported gene expression patterns of Chapter 5, we have shown that NOX subunit expression and ROS production are significantly altered between WKY and SHRSP early pregnancies, prior to any structural remodelling. To support this, we observed differences in ROS generation between the two in local uterine and systemic mesenteric arteries. We have also provided preliminary functional evidence that there may be alterations to Ca^{2+} handling in response to pregnancy in the WKY, however further study and inclusion of SHRSP cells would be advantageous in understanding the consequences of pregnancy on uterine artery Ca^{2+} handling in normotensive and hypertensive circumstances.

Chapter 7: General Discussion

Pregnancy may be considered one of the most physiologically stressful tests of an individual's life. Adapting to pregnancy challenges almost all of the major maternal systems and derangement of any one of these processes can result in pathological states (Wenger, 2014). Hypertension is increasing in prevalence rapidly in modern society, with an estimated one third of the adult population worldwide affected (Singh *et al*, 2016). This, in turn, has resulted in an increased incidence of hypertensive disorders of pregnancy (Agrawal and Wenger, 2020). The impact of this has been significant, with a long-term increase in the risk for adverse cardiovascular health in both mothers and offspring becoming apparent (de Martelly *et al*, 2021; Tooher *et al*, 2017; Cirillo and Cohn, 2015; Stojanovska *et al*, 2016; Bokslag *et al*, 2016). Further, the influence of the maternal cardiovascular, renal and immune systems have now been identified as key components in the development of hypertensive disorders of pregnancy (Gyselaers and Thilaganathan, 2019). Though our understanding of the underlying pathology of these disorders has improved, there is still much to learn. Combined with the ethical and legal limitations within pregnancy research, now more than ever there is a prominent need for the development of animal models that can recapitulate these disorders and inform future research directions.

The stroke-prone spontaneously hypertensive (SHRSP) rat is a known model of chronic hypertension that persists throughout pregnancy and has been well characterised over the years (Yamada *et al*, 1981; Fuchi *et al*, 1995a; Small *et al*, 2016a). Recently, the SHRSP has been utilised to produce a model of super-imposed pre-eclampsia. This stems from evidence in the literature that shows the noticeable involvement of the RAAS in pre-eclampsia development, specifically that of ANGII. Research has shown that in patients with PE, there is an increased sensitivity to circulating ANGII that impacts vascular function and placental development (Hussein and Lafayette, 2014; Chaiworapongsa *et al*, 2014). This is in conjunction with an increase in AT_1 receptor autoantibodies, which stimulate ROS production via NOX (Chen *et al*, 2014). Furthermore, ANGII is routinely used in non-pregnant normotensive animals to induce hypertension (Nishiyama *et al*, 2001; Lauresen *et al*, 1997) and has been noted to produce a PE-like phenotype when administered during normotensive rodent pregnancy (Xue *et al*, 2017; Shirasuna *et al*, 2015). Initially developed by the Graham group, the SHRSP model of SPE is achieved by infusion of ANGII from mid-gestation, specifically at the point of placental development (Morgan *et al*, 2018). Prior to the work of this

thesis, this model had been tested at two doses of ANGII: a 'low' dose of 500ng/kg/min and a 'high' dose of 1000ng/kg/min. This was novel as it showed an adaptability of the model to study variations in severity, a known characteristic of PE and SPE (Anthony *et al*, 2016). However, the 'low' dose did not fully recapitulate all indicators of SPE, whilst animals receiving the 'high' dose had a reduced survival rate, reduction in maternal body weight, deterioration of general animal health and total pregnancy loss giving rise to welfare concerns. The work of this thesis sought to optimise this model at a mid-dose of 750ng/kg/min in hopes that animals would exhibit the signs and symptoms of SPE whilst protecting their overall welfare and improving survival. As detailed in Chapter 3, this study found that pregnant SHRSP rats infused with 750ng/kg/min of ANGII developed a disease phenotype that was highly similar to human patients with SPE. ANGII infusion resulted in a significant, detrimental impact to maternal cardiovascular and renal function; altered placental development and potentially restricted fetal growth. This provides evidence that this optimised dose creates a replicable SPE phenotype that shows high similarity to the human condition whilst protecting animal welfare and could prove to be a useful tool in PE research.

The patterns suggestive of fetal growth restriction following ANGII in the pregnant SHRSP in this thesis are somewhat in contrast with results reported in the literature. Some studies conclude that the SHRSP does not experience FGR by GD18.5 in comparison to normotensive pregnancy, even though there is evidence of abnormal uterine artery remodelling and reduced uteroplacental flow (Small *et al*, 2016a; Small *et al*, 2016b; Morgan *et al*, 2018). Indeed, this agreed with our observations of untreated SHRSP. Conversely, other studies have shown evidence that SHRSP offspring do experience FGR (Barrientos *et al*, 2017). Reduced uteroplacental perfusion associated with maternal vascular disease is considered responsible for a majority of FGR cases, particularly concerning hypertensive disorders of pregnancy (Nardozza *et al*, 2017; Tannetta and Sargent, 2013; Fisher, 2016). The increase in circulating ANGII in this study resulted in an increase in the percentage of offspring considered growth restricted, in agreement with results generated at the previous 'high' dose of ANGII (Morgan *et al*, 2018), alongside significant reductions in fetal weight and crown-rump length. However, this was in the absence of any additive effect of ANGII on uteroplacental perfusion. Interrupted uteroplacental blood flow has long been considered as one of the main pathological factors that give rise to the abnormal placentation associated with PE.

Even so, not all individuals with PE experience altered placentation and FGR. Research now suggests that FGR is associated with early-onset PE as opposed to late-onset PE, where there is an absence of abnormal uterine artery Doppler leading to the suggestion this PE sub-type is driven by maternal and not placental factors (Gatford *et al*, 2020; Madazli *et al*, 2014). Similar findings in cases of SPE have also been reported, with a decreased frequency of abnormal uterine artery Doppler and FGR despite having lower placental weights at term (Stanek, 2017). Indeed, there appears to be a dose-response relationship between uteroplacental ischaemia and PE onset (Ismail, 2018). Given that the pregnant SHRSP already experiences impaired uteroplacental flow, the addition of systemic ANGII may have significantly stressed maternal systems towards a PE phenotype but may have been unable to cross this potential ischaemia threshold to affect uteroplacental flow. The study results made clear the effect of ANGII on the placenta itself, evidenced by reduced placental weight and histological abnormalities relative to SHAM and WKY, similar to human SPE. A possible suggestion is that the pre-existing hypertension in the SHRSP confers some sort of protective effect within the uteroplacental circulation against the additional hypertensive stress of ANGII infusion. There is certainly room for further characterisation in this model to identify the underlying mechanisms that may explain the disconnect between uteroplacental flow, FGR and placental outcomes and how this may potentially translate to similar findings in SPE patients.

Though the exact cause of the adverse *in utero* environment in this model is not clear, what is apparent are the potential long-term effects of such an environment to offspring. Literature has documented the increased cardiovascular risk in offspring born from hypertensive pregnancies, however, few studies have sought to investigate the mechanisms by which this occurs. Thus, this thesis aimed to provide insight into these mechanisms by assessing neonatal outcomes. The observed tendency for FGR in ANGII fetuses was preserved and more prominent in ANGII neonates, suggesting these offspring acquired a developmental handicap as a result of ANGII. To explore this further, qRT-PCR was performed for genes known to relate to vascular function and cardiovascular disease in SHAM and ANGII neonates. The small sample size did not allow for firm conclusions,. Although no significant results were generated, this work offers potential insight into the pathways that may be involved in the increased risk for adverse cardiovascular health in hypertensive pregnancy offspring. Further investigation to

validate this finding has already begun, with a follow-up study of these offspring into adulthood underway by another member of the Graham lab. These findings will be advantageous in understanding the underlying pathology of increased cardiovascular risk in offspring born to hypertensive pregnancies. It would also be beneficial to further investigate the placentae of affected dams in this model to gain insight as to how ANGII infusion creates an adverse *in utero* environment.

Treatment options for hypertensive disorders of pregnancy are severely lacking, with currently available options aimed at either controlling maternal blood pressure or preventing progression to a more severe form of disease. Though several agents do exist that lower maternal blood pressure (Lassi *et al*, 2014; Moussa *et al*, 2014), this alone does not resolve any of the underlying pathology. Magnesium sulphate is a commonly used agent in SPE patients to prevent seizures and the progression to HELLP syndrome (Moussa *et al*, 2014). Despite the widespread clinical use of $MgSO_4$ in these patients, relatively little is understood of its mechanism of action. Some studies have investigated the effect of antenatal $MgSO_4$ on rodent maternal outcomes and have observed improvements to blood pressure, cardiac function, proteinuria and decreased production of PE biomarkers (Coates *et al*, 2016; Korish, 2012). However, these studies were conducted in normotensive Sprague-Dawley or Wistar rats with artificially-induced hypertension, thus they do not accurately depict SPE. To our knowledge, there are no studies examining maternal, fetal and placental outcomes in response to $MgSO_4$ treatment in the pregnant SHRSP. Therefore, the work presented in Chapter 4 of this thesis sought to investigate these outcomes in both the untreated and ANGII-infused pregnant SHRSP.

A key distinction between this study and those previously published on $MgSO_4$ therapy in human PE is that normally, $MgSO_4$ is given as an initial large intravenous loading dose (4-6g) followed by a twenty-four-hour infusion at a smaller maintenance dose (1-2g/h) (Moussa *et al*, 2014). Once patients are stabilised they undergo delivery. In contrast, we used $MgSO_4$ in our rodent model as a preventative measure against SPE itself, rather than to prevent its progression to eclampsia, by administering $MgSO_4$ continuously from conception to delivery. We observed significant improvements to maternal weight, systolic blood pressure and proteinuria. However, $MgSO_4$ also reduced maternal cardiac function and inhibited fetal growth further than ANGII alone. The kidneys play a

key role in the regulation of Mg^{2+} homeostasis, primarily through re-absorption in the thick ascending limb of the loop of Henle and distal convoluted tubule (Fanni *et al*, 2021). SPE is associated with glomerular lesions and loss of size and charge selectivity of the glomerular barrier alongside a reduction of 30-50% in glomerular filtration rate (Karumanchi *et al*, 2005). Magnesium deficiency, though not shown to be a direct cause of PE, is considered a predisposing factor in its generation with PE patients presenting with decreased serum Mg^{2+} due to accumulation in the fetal circulation (Chiarello *et al*, 2018). Together, this suggests that in this rodent model of SPE, ANGII-infusion may lead to renal intracellular Mg^{2+} deficiency that is prevented by daily $MgSO_4$ administration, thereby preventing damage to the glomeruli and thus proteinuria. These protective effects to kidney function may also underlie the improvements in blood pressure noted in this model, though this is unconfirmed. Previous studies have shown evidence of a renoprotective effect of $MgSO_4$, reversing histopathological changes to the glomerular capillaries and Bowman's capsule as well as improving maternal blood pressure in an L-NAME model of PE (Korish, 2012). Whilst this work did not investigate any specific mechanisms, it did generate evidence that was suggestive of an improvement in kidney function following $MgSO_4$ that agrees with evidence in the literature. Further characterisation of the use of $MgSO_4$ in this model has the potential to lend further insight into its mechanism of action in maternal systems.

An unexpected outcome of this study was that $MgSO_4$ therapy resulted in worsening fetal growth restriction and did not improve indices of uteroplacental flow. In both humans and rodents, $MgSO_4$ has been shown to reduce the incidence of FGR and increase both fetal and placental weights in hypertensive pregnancy (Fanni *et al*, 2021; Kazemi-Darabadi and Akbari, 2020). This may be explained by the method of $MgSO_4$ administration in this study. Though $MgSO_4$ is often used in clinical practice, it is less often given in a preventative context but rather in circumstances where the patient is already eclamptic to prevent seizure reoccurrence, therefore the length of treatment is reduced in comparison to our study (Gordon *et al*, 2014). Further, $MgSO_4$ therapy in rodent models is usually initiated in mid-gestation, rather than at time of conception. Antenatal $MgSO_4$ use has been suggested by many studies to result in fetal hypermagnesemia and adverse neonatal outcomes, particularly where administration is prolonged (Karimoto *et al*, 2000; James, 2010; Narasimulu *et al*, 2017). We have previously hypothesised that infusion of pregnant SHRSP rats with ANGII results in an

accumulation of Mg^{2+} in the fetal circulation, as is observed in human PE (Chiarello *et al*, 2018). Therefore, the added Mg^{2+} provided by long-term $MgSO_4$ drinking water (which has a higher bioavailability (Barbagallo *et al*, 2021)) may have resulted in fetal hypermagnesemia in ANGII-infused dams, leading to significantly reduced fetal and placental growth. Though the work presented in Chapter 4 supports a harmful rather than a beneficial role of $MgSO_4$ in fetal outcomes, it highlights the dangers of antenatal $MgSO_4$ use and reinforces the need for a structured and optimised dosing regimen when used in pregnancy, particularly in cases of PE and eclampsia where fetal toxicity is more likely (Brookfield *et al*, 2016). Assessing outcomes in response to varied dosing regimens and/or routes of $MgSO_4$ as well as assessment of the maternal and fetoplacental Mg^{2+} status in this model in future work would be beneficial.

Given that neither ANGII-infusion nor $MgSO_4$ therapy altered uteroplacental flow, we hypothesised that the pregnant SHRSP may already have a predisposition to dysfunctional vascular remodelling of the uterine arteries. Therefore, one of the main aims of this thesis was to investigate the underlying mechanisms that may be responsible at an early gestational time-point, prior to any functional or structural changes to the uterine artery. In the rodent pregnancy by GD6.5 implantation is complete, but the placenta has not developed, thus only maternal effectors are responsible for any potential differences observed (Soares *et al*, 2012). It was confirmed via myography that at GD6.5 there were no significant differences in vessel properties between NP and GD6.5 arteries for both strains. This suggested that the impairments observed in late gestation were not due to maternal hypertension alone but may have a genetic component, supported by evidence in the literature of abnormal remodelling in SHRSP dams where their hypertension was ameliorated by nifedipine (Small *et al*, 2016a). Few studies have investigated gene expression changes in the uterine arteries in the context of hypertensive pregnancy and even fewer at an early gestational time point. To our knowledge, this is the first to study gene expression patterns at an early gestational time point in a rodent model of chronic hypertension during pregnancy. Ingenuity Pathway Analysis® revealed a vast number of pregnancy-dependant expression changes in both WKY and SHRSP, however only a small portion of these were investigated further in subsequent analysis. Whilst there were distinct differences in expression patterns between GD6.5 WKY and SHRSP arteries, there were also a number of changes in common between the two strains. This provides evidence that there

are essential, conserved pregnancy adaptations that occur in both strains regardless of hypertensive status.

In the context of the WKY, IPA® identified an expression profile with overarching themes of increased energy production and reduced Ca^{2+} signalling whilst the SHRSP profile presented a pattern of expression suggestive of exacerbated immune involvement, increased oxidative stress and vasoconstriction. SHRSP uterine arteries were shown to have an increased gene expression of NOX2 subunits *gp91* and *p22-phox* that was linked to increased ROS production. NOX2 is widely distributed in the vasculature and has been shown to contribute to ROS-induced vascular damage when overactivated, as in hypertension (Forte *et al*, 2016). Indeed, inhibition or depletion of NOX2 in animal models has been shown to be protective against ANGII-induced oxidative stress and hypertension (Fan *et al*, 2022; Chan and Baumbach, 2013). In Chapter 6 we aimed to confirm these findings by qRT-PCR of NOX2 subunits and quantification of superoxide production, as superoxide is the main ROS species produced by NOX2 (Görlach *et al*, 2015). In agreement with IPA® data, there appeared to be an increased expression of *gp91* but did not observe an increase in *p22-phox* expression in GD6.5 SHRSP uterine arteries. Though this disagrees with the predictions of IPA® somewhat, it does agree with the finding that *gp91* but not *p22-phox* expression is increased in the sera of PE patients (Matsubara *et al*, 2010). We also observed what appeared to be an increase in $O_2^{\bullet-}$ production in response to pregnancy at a local and systemic level in arteries from GD6.5 SHRSP dams. This led to the hypothesis that *gp91*, the catalytic subunit that forms the core of active NOX2, is able to generate ROS independently of *p22-phox*, which is normally required for stability (Bedard and Krause, 2007; Vermot *et al*, 2021). This is supported by evidence in the literature that shows ROS production via activation of *gp91* in the absence of *p22-phox* (Ezzine *et al*, 2014). Results of this study were suggestive of a decrease in $O_2^{\bullet-}$ generation in GD6.5 WKY uterine arteries as hypothesised, however this was in the presence of an increase in *p22-phox* expression that was not highlighted by IPA® analysis. This may be explained by the fact that *p22-phox* is a regulatory subunit that forms a part of any one of the NOX isoforms, including the constituently active NOX4 which produces hydrogen peroxide (Vermot *et al*, 2021; Bedard and Krause, 2007). Hydrogen peroxide is known to be protective in the vasculature by promoting vasodilation (Schröder *et al*, 2012). This may explain the decrease in $O_2^{\bullet-}$ generation despite an increase in *p22-phox* expression in

WKY uterine arteries in response to pregnancy and provides evidence of a protective pro-oxidant period in early rodent pregnancy that mirrors that seen in healthy human pregnancy (Tenório *et al*, 2019). The contrast between the WKY and SHRSP early response to pregnancy provides new insights on the impact of chronic maternal hypertension on oxidative stress and may, in part, explain the observed vascular dysfunction of these arteries in late gestation, similar to that observed in humans.

The expression patterns produced by IPA® also highlighted the involvement of vascular smooth muscle cell Ca^{2+} signalling, whereby normotensive pregnancy was characterised by a decrease in Ca^{2+} signalling and possible retention of Ca^{2+} in the sarcoplasmic reticulum whilst hypertensive pregnancy showed an increased expression of *Prkcb*, which is known to induce vascular contraction independently of Ca^{2+} (Gutíerrez *et al*, 2019; Ringvold and Khalil, 2017). Functional Ca^{2+} signalling in uterine artery vascular smooth muscle cells from GD6.5 WKY and SHRSP uterine arteries was performed to validate these expression patterns. Due to research limitations out-with our control, the data could not be analysed statistically and only a small number of samples were used. Despite this, there appeared to be an increase in ionomycin-induced but not ANGII-induced Ca^{2+} release in pregnant WKY UAVSMCs. This appears to contrast with earlier predictions of reduced Ca^{2+} in WKY pregnancy. Ionomycin was used in these experiments as its strong attraction to divalent cations promotes sarcoplasmic emptying of Ca^{2+}, even at relatively low concentrations (Smith *et al*, 1989). Taking this into consideration, this work suggests that rather than a reduction in intracellular Ca^{2+}, WKY pregnancy results in sequestering of Ca^{2+} and reduced release of Ca^{2+} from the sarcoplasmic reticulum. This also explains the reduced expression of *Itpr2* identified by IPA®. The lack of SHRSP cells did not allow for any investigation of the effect of hypertension on intracellular Ca^{2+} in early pregnancy. It would be beneficial to extend this work in the future to include more *n* numbers to fully validate these findings at the functional and genetic level as well as investigate other important pathways identified in previous analysis. The work presented in this thesis has highlighted the involvement of both ROS and Ca^{2+} in the uterine artery response to early hypertensive pregnancy and has identified further pathways and molecules of interest. Though it must be acknowledged that blood pressure was not measured in the animals used for IPA® analysis and results in chapter 3 showed no difference in blood pressure at pre-pregnancy

between WKY and control SHRSP dams. Therefore, the assumption that the SHRSP animals included in this study were hypertensive may not be accurate. Future studies of this nature should include systolic blood pressure measurement in dams prior to uterine artery harvest. These novel insights will undoubtedly prove useful in understanding how chronic maternal hypertension can alter the genetic priming of the uterine arteries during pregnancy and could have the potential to deepen our understanding of the same early pregnancy processes in human hypertensive pregnancy. This may have the potential to improve future prediction and prevention efforts.

It is important to note that for all studies, calculations of power and sample size were not performed in advance. Therefore, it is possible that the work presented in this thesis may not be sufficiently powered to prevent against type I or type II error, particularly where samples sizes are small. Prospective power calculations are used to estimate the probability of rejecting the null hypothesis in a larger population by observing the effects in a sample of said population. Though it is possible to calculate study power retrospectively based on the chosen level of significance, sample effect size and sample size, these results are not informative. By assuming that the sample effect size is equivalent to the population effect size, one assumes that the study sample is not biased and represents a random set of observations. However, this random component disappears once data from the study sample is collected. In other words, these 'random' observations become fixed constants (Dziak *et al*, 2018). Additionally, *post hoc* power is intrinsically linked to the chosen *p*-value, such that low values (high significance) will always have high power and high values (low significance) will always have low power (Hoenig and Heisey, 2001). Therefore, retrospective calculations of power are conceptually flawed and as such were not performed in this thesis. Given the analysis issues relating to small sample sizes throughout this thesis, it is imperative that future work includes power and sample size calculations prior to data collection to ensure a robust study design.

The work of this thesis has provided information on an optimised, novel rodent model of super-imposed pre-eclampsia that may be used as a potential tool in investigating the pathophysiology of the condition or in assessing the long-term consequences of an adverse *in utero* environment. This tool was utilised to explore whether a routinely used seizure prophylaxis in severe pre-eclamptic

patients could be used as a preventative therapeutic in SPE. This study has furthered our understanding of the effects of $MgSO_4$ in the context of hypertensive pregnancy for both maternal and fetal outcomes and highlighted the unmet need for research on standardised dosing regimens to prevent negative impacts to fetal health. Finally, this thesis has provided novel insights into the genetic factors that may influence uterine artery remodelling in early hypertensive pregnancy and has generated preliminary evidence of direct functional consequences of these genetic alterations that has the potential to inform future research directions in humans.

Chapter 8: Appendix

8.1 Sacrifice Sheet

8.1.1 GD18.5 Maternal Data

Date	GD
Strain	
ID	
Maternal Weight	
Tibia	

Heart	Whole- LV- EDTA ☐ Heparin ☐ Fix ☐ Freeze ☐
Lungs	Whole- Fix ☐ Freeze ☐
Liver	Whole- Fix ☐ Freeze ☐
Spleen	Whole- Fix ☐ Freeze ☐
Kidneys	R- L- Fix ☐ Freeze ☐
Brain	Whole- Fix ☐ Freeze ☐
Adrenals	Fix ☐ Freeze ☐
Uterus	Whole- ARTERY Fix ☐ Freeze ☐
Placentas	Formalin ☐ JB ☐ Freeze: Dec ☐ Lab ☐ Jx ☐ Chorionic

8.1.2 Fetal and Placental Data

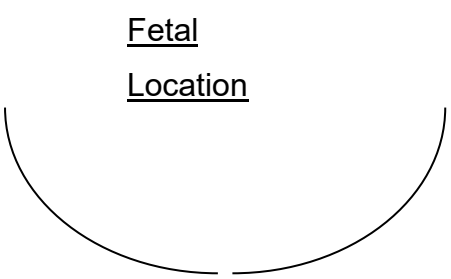

Date:

Strain:

Maternal ID:

Maternal weight:
GD .....

Fetal ID	Fetal whole weight	Placental weight	Fetal weights					Notes
			Head	Body	C:R	HC	AC	

8.2 Echocardiographic Calculations

Stroke volume (ml) = EDV/ESV

Cardiac output (ml/min) = $SV \times HR$

Ejection Fraction (%) = $(SV/EDVol) \times 100$

Fractional shortening (%) = $(EDD-ESD/EDD) \times 100$

Left ventricular mass (g) = $(0.8 \times ASEcube) + 0.6/1000$

Where ASEcube = $1.04 \times (IVSTd + LVIDd + PWTd)3 - LVIDd3$

LVIDd = average EDD x 10

IVSTd = average AWTd x 10

APWTd = average PWTd x 10

EDVol = $1.047 \times LVIDd3$

ESV = $1.047 \times (Average\ EDDs)3$

HR = Determined by counting the number of peaks observed in 1000msec during M-mode imaging

List of References

Abbas, A.E., Lester, S.J. and Connolly. H. (2005). Pregnancy and the cardiovascular system. *International Journal of Cardiology*. **98** (22), p.179-189.

Abbassi-Ghanavanti, M., Alexander, J.M., McIntire, D.D., Savani, R.C. and Lenovo, K.J. (2012). Neonatal Effects of Magnesium Sulfate Given to the Mother. *American Journal of Perinatology*. **29** (10), p.795-800.

Adam, K. (2017). Pregnancy in Women with Cardiovascular Disease. *Methodist DeBakey Cardiovascular Journal*. **13** (4), p.209-215.

Adamova, Z., Ozkan, S. and Khalil, R.A. (2009). Vascular and Cellular Calcium in Normal and Hypertensive Pregnancy. *Current Clinical Pharmacology*. **4** (3), p.172-190.

Agrawal, A. and Wenger, N.K. (2020). Hypertension During Pregnancy. *Current Hypertension Reports*. **22** (Article ID 64), p.1-9.

Ahmad, A. and Ahmed, A. (2004). Elevated placental soluble vascular endothelial growth factor receptor-1 inhibits angiogenesis in preeclampsia. *Circulation Research*. **95** (9), p.884-891.

Ahmed, A., Rezai, H., and Broadway-Stringer, S. (2016). Evidence-Based Review of the Pathophysiology of Preeclampsia. In: Islam, S *Hypertension: from basic research to clinical practice volume 2, Advances in Experimental Medicine and Biology*. Switzerland: Springer International Publishing AG. pp.355-374.

Akan, M., Ozbilgin, S., Boztas, N., Celik, A., Ozkardesler, S., Ergur, B.U., Guneli, E., Sisman, A.R., Akokay, P. and Meseri, R. (2016). Effect of magnesium sulfate on renal ischemia-reperfusion injury in streptozotocin-induced diabetic rats. *European Review for Medical and Pharmacological Sciences*. **20** (8), p.1642-1655.

Alexander, B.T., Kassab, S.E., Miller, M.T., Abram, S.R., Reckelhoff, J.F., Bennett, W.A. and Granger, J.P. (2001). Reduced Uterine Perfusion Pressure During Pregnancy in the Rat Is Associated With Increases in Arterial Pressure and Changes in Renal Nitric Oxide. *Hypertension*. **37** (4), p.1191-1195.

Ali, A.M.J. and Khalil, R.A. (2015). Genetic, Immune and Vasoactive Factors in the Vascular Dysfunction Associated with Hypertension in Pregnancy. *Expert Opinion on Therapeutic Targets*. **19** (11), p.1495-1515.

Alpoim, P.N., Godoi, L.C., Freitas, L.G., Gomes, K.B. and Drusse, L.M. (2013). Assessment of L-arginine asymmetric 1 dimethyl (ADMA) in early-onset and late-onset (severe) preeclampsia. *Nitric Oxide*. **33**, p.81-82.

Alpoim, P.N., Gomes, K.B., Pinheiro, M. de B., Godoi, L.C., Jardim, L.L., Muniz, L.G., Sandrim, V.C., Fernandes, A.P. and Dusse, L.M.S. (2014). Polymorphisms in endothelial nitric oxide synthase gene in early and late severe preeclampsia. *Nitric Oxide*. **42**, p.19-23.

Anthony, J., Damasceno, A. and Ojjii, D. (2016). Hypertensive disorders of pregnancy: what the physician needs to know. *Cardiovascular Journal of Africa*. **27** (2), p.104-110.

Ardense, L.B., Danser, A.H.J., Poglitsch, M., Touyz, R.M., Burnett, J.C., Llorens-Cortes, C., Ehlers, M.R. and Sturrock, E.D. (2019). Novel Therapeutic Approaches Targeting the Renin-Angiotensin System and Associated Peptides in Hypertension and Heart Failure. *Pharmacological Reviews*. **71** (4), p.539-570.

Baczyk, D., Kingdom, J.C.P. and Uhlén, P. (2011). Calcium signalling in the placenta. *Cell Calcium*. **49** (5), p.350-356.

Barakonyi, A., Miko, E., Szereday, L., Polgar, P.D., Nemeth, T.N., Szekeres-Bartho, J. and Engels, G.L. (2014). Cell Death Mechanisms and Potentially Cytotoxic Natural Immune Cells in Human Pregnancies Complicated by Preeclampsia. *Reproductive Sciences*. **21**, p.155-166.

Bakrania, A., George, E.M. and Granger, J.P. (2022). Animal models of preeclampsia: investigating pathophysiology and therapeutic targets. *American Journal of Obstetrics and Gynecology*. **226** (Supplement), p.S973-S987.

Barker, D.J., Gluckman, P.D., Godfrey, K.M., Harding, J.E., Owens, J.A. and Robinson, J.S. (1993). Fetal nutrition and cardiovascular disease in adult life. *The Lancet*. **341** (8850), p.938-941.

Barker, D.J. and Osmond, C. (1986). Infant mortality, childhood nutrition, and ischaemic heart disease in England and Wales. *The Lancet*. **327** (8489), p.1077-1081.

Barker, D.J., Winter, P.D., Osmond, C., Margetts, B. and Simmonds, S.J., (1989). Weight in infancy death and death from ischaemic heart disease. *The Lancet*. **334** (8663), p.577-580.

Barrientos, G., Pusssetto, M, Rose, M., Staff, A.C., Blois, S.M. and Toblli, J.E. (2017). Defective trophoblast invasion underlies fetal growth restriction and preeclampsia-like symptoms in the stroke-prone spontaneously hypertensive rat. *Molecular Human Reproduction*. **23** (7), p.509-519.

Bedard, K. and Krause, K-H. (2007). The NOX Family of ROS-Generating NADPH Oxidases: Physiology and Pathophysiology. *Physiological Reviews*. **87** (1), p.245-313.

Belizán, J.M. and Villar, J. (1980). The relationship between calcium intake and edema-, proteinuria-, and hypertension-gestosis: an hypothesis. *The American Journal of Clinical Nutrition*. **33** (10), p.2202-2210.

Benny, P.A., Al-Akwaa, F.M., Schlueter, R.J., Lassiter, C.B. and Garmire, L.X. (2020). A Review of Meta-analysis of Omics Approach to Study Preeclampsia. *Placenta*. **92**, p.17-27.

Bertero, E. and Maack, C. (2018). Calcium Signaling and Reactive Oxygen Species in Mitochondria. *Circulation Research*. **122** (10), p.1460-1478.

Bhat, R.A. and Kushtagi, P. (2006). A re-look at the duration of human pregnancy. *Singapore Medical Journal*. **47** (12), p.1044-1048.

Blaine, J., Choncol, M. and Levi, M. (2015). Renal Control of Calcium, Phosphate, and Magnesium Homeostasis. *Clinical Journal of the American Society of Nephrology*. **10** (7), p.1257-1272.

Blanc, J., Lacolley, P., Laurent, S. and Elghozi, J-L. (2004). Comparison of Angiotensin II‐Induced Blood Pressure and Structural Changes in Fischer 344 and Wistar Kyoto Rats. *Clinical and Experimental Pharmacology and Physiology*. **31** (7), p.466-473.

Bohlender, J., Ganten, D. and Luft, F.C. (2000). Rats Transgenic for Human Renin and Human Angiotensinogen as a Model for Gestational Hypertension. *Journal of the American Society of Nephrology*. **11** (11), p.2056-2061.

Bokslag, A., Teunissen, P.W., Franssen, C., Kesteren, van F., Kamp, O., Ganzevoort, W., Paulus, W.J. and de Groot, C.J.M. (2017). Effect of early-onset preeclampsia on cardiovascular risk in the fifth decade of life. *American Journal of Obstetrics and Gynecology*. **216** (5), p.523.E1-523.E7.

Bokslag, A., Weissenbruch, van M., Mol, B.W. and de Groot, C.J.M. (2016). Preeclampsia: short and long-term consequences for mother and neonate. *Early Human Development*. **102**, p.47-50.

Borekci, B., Gulaboglu, M. and Gul, M. (2009). Iodine and Magnesium Levels in Maternal and Umbilical Cord Blood of Preeclamptic and Normal Pregnant Women. *Biological Trace Element Research*. **129** (1), p.1-8.

Boutet, M., Roland, L., Thomas, N. and Bilodeau, J-F. (2009). Specific systemic antioxidant response to preeclampsia in late pregnancy: the study of intracellular glutathione peroxidases in maternal and fetal blood. *American Journal of Obstetrics and Gynecology*. **200** (2), p.530.e1-530.e7.

Bouvier-Colle, M-H., Mohangoo, A.D., Gissler, M., Novak-Antolic, Z., Vutuc, C., Szamotulska, K. and Zeitlin, J. for The Euro-Peristat Scientific Committee. (2012). What about the mothers? An analysis of maternal mortality and morbidity in perinatal health surveillance systems in Europe. *British Journal of Obstetrics and Gynaecology*. **119** (7), p.880-890.

Brookfield, K., Su, F., Elkomy, M.H., Drover, D.R., Lyell, D.J. and Carvalho, B. (2016). Pharmacokinetics and placental transfer of magnesium sulfate in pregnant women. *American Journal of Obstetrics & Gynecology*. **214** (6), p.737.e1-737.e9.

Brown, M.A., Magee, L.A., Kenny, L.C., Karumanchi, S.A., MCCarthy, F.P., Saito, S., Hall, D.R., Warren, C.E., Adoyi, G., Ishaku, S., International Society for the Study of Hypertension in Pregnancy. (2018a). Hypertensive Disorders of Pregnancy. *Hypertension*. **72** (1), p.24-43.

Brown, M.A., Magee, L.A., Kenny, L.C., Karumanchi, S.A., McCarthy, F.P., Saito, S., Hall, D.R., Warren, C.R., Adoyi, G., Ishaku, S., International Society for the Study of Hypertension in Pregnancy. (2018b). The hypertensive disorders of pregnancy: ISSHP classification, diagnosis & management recommendations for international practice. *Pregnancy Hypertension*. **13**, p.291-310.

Buddeberg, B.S., Sharma, R., O'Driscoll, J.M., Agten, A.K., Khalil, A. and Thilaganathan, B. (2018). Cardiac maladaptation in term pregnancies with preeclampsia. *Pregnancy Hypertension*. **13**, p.198-203.

Burke, S.D., Barrette, V.F., Bianco, J., Thorne, J.G., Yamada, A.T., Pang, S.C., Adams, M.A. and Croy, B.A. (2010). Spiral arterial remodelling is not essential for normal blood pressure regulation in mice. *Hypertension*. **55** (3), p.729-737.

Burton, G.J. and Fowden, A.L. (2012). Review: The placenta and developmental programming: Balancing fetal nutrient demands with maternal resource allocation. *Placenta*. **33** (Supplement), p.S23-S27.

Burton, G.J., Redman, C.W., Roberts, J.M. and Moffett, A. (2019). Pre-eclampsia: pathophysiology and clinical implications. *BMJ*. **366**, l2381.

Burton, G.J., Woods, A.W., Jauniaux, E. and Kingdom, J.C. (2009). Rhelogical and physiological consequences of conversion of the maternal spiral arteries for uteroplacental blood flow during human pregnancy. *Placenta*. **30** (6), p.473-482.

Bytautiene, E., Lu, F., Tamayo, E.H., Hankins, G.D.V., Longo, M., Kublickiene, K. and Saade, G.R. (2010). Long-term maternal cardiovascular function in a mouse model of sFlt-1-induced preeclampsia. *American Journal of Physiology, Heart and Circulatory Physiology*. **298** (1), p.H189-H193.

Campbell, N., LaMarca, B. and Cunningham, M.W. (2018). The role of Agonistic Autoantibodies to the Angiotensin II Type 1 Receptor (AT1-AA) in Pathophysiology of Preeclampsia. *Current Pharmaceutical Biotechnology*. **19** (10), p.781-785.

Carlin, A. and Alfirevic, Z. (2008). Physiological changes of pregnancy and monitoring. *Best Practice & Research Clincal Obstetrics & Gynaecology*. **22** (5), p.801-823.

Carswell, H.V.O., McBride, M.W., Graham, D., Dominiczak, A.F. and Macrae, I.M. (2005). Mutant Animal Models of Stroke and Gene Expression. In: Read, S.J. and Virley, D. *Stroke Genomics. Methods in Molecular Medicine*. Totowa, New Jersey: Humana Press. pp.49-74.

Casamassimi, A., Federico, A., Rienzo, M., Esposito, S. and Ciccodicola, A. (2017). Transcriptome Profiling in Human Diseases: New Advances and Perspectives. *International Journal of Molecular Sciences*. **18** (8; 1652), p.1-15.

Casper, F. and Seufert, R. (1995). Atrial natriuretic peptide (ANP) in preeclampsia-like syndrome in a rat model. *Experimental and Clinical Endocrinology & Diabetes*. **103** (3), p.292-296.

Castleman, J.S., Ganapathy, R., Taki, F., Lip, G.Y.H., Steeds, R.P. and Kotecha, D. (2016). Echocardiographic Structure and Function in Hypertensive Disorders of Pregnancy: A Systematic Review. *Circulation: Cardiovascular Imaging*. **9** (9), e004888.

Cavanagh, D., Rao, P.S., Tsai, C.C. and O'Connor, T.C. (1977). Experimental toxemia in the pregnant primate. *American Journal of Obstetrics and Gynecology*. **128** (1), p.75-85.

Chaiworapongsa, T., Chaemsaithong, P., Yeo, L. and Romero, R. (2014). Pre-eclampsia part 1: current understanding of its pathophysiology. *Nature Reviews Nephrology*. **10** (8), p.466-480.

Chan, S-L. and Baumbach, G.L. (2013). Nox2 Deficiency Prevents Hypertension-Induced Vascular Dysfunction and Hypertrophy in Cerebral Arterioles. *International Journal of Hypertension*. **2013** (Article ID 793630), p.1-9.

Chapman, A.B., Abraham, W.T., Zamudio, S., Coffin, C., Merouani, A., Young, D., Johnson, A., Osorio, F., Goldberg, C., Moore, L.G., Dahms, T. and Schrier, R.W. (1998). Temporal relationships between hormonal and hemodynamic changes in early human pregnancy. *Kidney International*. **54** (6), p.2056-2063.

Chen, C.W., Jaffe, I.Z. and Karumanchi, S.A. (2014). Pre-eclampsia and cardiovascular disease. *Cardiovascular Research*. **101** (4), p.579-586.

Chen, J. Z-J., Sheehan, P.M., Brennecke, S.P. and Keogh, R.J. (2012). Vessel remodelling, pregnancy hormones and extravillous trophoblast function. *Molecular and Cellular Endocrinology*. **349** (2), p.138-144.

Cheung, K.L. and Lafayette, R.A. (2013). Renal Physiology of Pregnancy. *Advances in Chronic Kidney Disease*. **20** (3), p.209-214.

Chiarello, D., Marín, R., Proverbio, F., Coronado, P., Toledo, F., Salsoso, R.,Gutiérrez, J. and Sobrevia, L. (2018). Mechanisms of the effect of magnesium salts in preeclampsia. *Placenta*. **69**, p.134-139.

Chrysant, S.G. and Chrystant G.S. (2019). Association of hypomagnesemia with cardiovascular diseases and hypertension. *International Journal of Cardiology and Hypertension*. **1**, 100005.

Cicinelli, E., Einer-Jensen, N., Galatnino, P., Alfonso, R. and Nicoletti, R. (2006). The Vascular Cast of the Human Uterus: From Anatomy to Physiology. *Annals of the New York Academy of Sciences*. **1034** (1), p.19-26.

Cirillo, P.M. and Cohn, B.A. (2015). Pregnancy Complications and Cardiovascular Disease Death 50-Year Follow-Up of the Child Health and Development Studies P. *Circulation*. **132** (13), p.1234-1242.

Clapp, J.F. and Capeless, E. (1997). Cardiovascular function before, during, and after the first and subsequent pregnancies. *American Journal of Cardiology*. **80** (11), p.1469-1470.

Clift, D. and Schuh, M. (2013). Re-starting life: Fertilization and the transition from meiosis to mitosis. *Nature Reviews Molecular Cell Biology*. **14** (9), p.549-562.

Coan, P.M., Conroy, N., Burton, G.J. and Freguson-Smith, A.C. (2006). Origin and characteristics of glycogen cells in the developing murine placenta. *Developmental Dynamics*. **235** (12), p.3280-3294.

Coates B.J., Broderick, T.L., Batia, L.M. and Standley, C.A. (2006). MgSO4 prevents left ventricular dysfunction in an animal model of preeclampsia. *American Journal of Obstetrics and Gynecology*. **195** (5), p.1398-1403.

Cohen, J.B., Hanff, T.C., Bress, A.P. and South, A.M. (2020). Relationship Between ACE2 and Other Components of the Renin-Angiotensin System. *Current Hypertension Reports*. **22** (7), p.44-49.

Coorens, T.H.H., Oliver, T.R.W., Sanghvi, R., Sovio, U., Cook, E., Vento-Tormo, R., Haniffa, M., Young, M.D., Rahbari, R., Sebire, N., Campbell, P.J., Charnock-Jones, D.S., Smith, G.C.S. and Behjati, S. (2021). Inherent mosaicism and extensive mutation of human placentas. *Nature*. **592** (7852), p.80-85.

Cornelius, D.C., Cottrell, J., Amaral, L.M. and LaMarca, B. (2019). Inflammatory mediators: a causal link to hypertension during preeclampsia. *British Journal of Pharmacology*. **176** (12), p.1914-1921.

Cox, B., Leavey, K., Nosi, U., Wong, F. and Kingdom, J. (2015). Placental transcriptome in development and pathology: expression, function, and methods of analysis. *American Journal of Obstetrics and Gynecology*. **213** (4), p.S138-S151.

Cunningham, M.W. and LaMarca, B. (2018). Risk of cardiovascular end-stage renal disease, and stroke in postpartum women and their fetuses after a hypertensive pregnancy. *American Journal of Physiology Regulatory, Integrative and Comparative Physiology*. **315** (3), p.R521-R528.

Cunningham, M.W., Vaka, V.R., McMaster,, K., Ibrahim, T, Cornelius, D.C., Amaral, L., Campbell, N., Wallukat, G., McDuffy, S., Usry, N., Dechend, R. and LaMarca, B. (2019). Renal natural killer cell activation and mitochondrial oxidative stress; new mechanisms in AT1-AA mediated hypertensive pregnancy. *Pregnancy Hypertension*. **15**, p.72-77.

Cushen, S.C. and Goulopoulou, S. (2017). New Models of Pregnancy-Associated Hypertension. *American Journal of Hypertension*. **30** (11), p.1053-1062.

Dadelszen, P. von and Magee, L.A. (2016). Preventing deaths due to the hypertensive disorders of pregnancy. *Best Practice & Research Clincal Obstetrics & Gynaecology*. **36**, p.83-102.

Dalfra', M.G., Burlina, S. and Lapolla, A. (2022). Weight gain during pregnancy: A narrative review on the recent evidences. *Diabetes Research and Clinical Practice*. **188** (109913), p.1-8.

Dalton, L.M., Ní Fhloinn, D.M., Gaydadzhieva, G.T., Mazurkiewicz, O.M., Leeson,. (2016). Magnesium in pregnancy. *Nutrition Reviews*. **74** (9), p.549-557.

Davidson, A.O., Schork, N., Jaques, B.C., Kelman, A.W., Sutcliffe, R.G., Reid, J.L. and Dominiczak, A.F. (1995). Blood Pressure in Genetically Hypertensive Rats. *Hypertension*. **26** (3), p.452-459.

Davis, E.F., Newton, L., Lewandowski, A.J., Lazdam, M., Kelly, B.A., Kyriakou, T. and Leeson, P. (2012). Pre-eclampsia and offspring cardiovascular health: mechanistic insights from experimental studies. *Clinical Science (London)*. **123** (2), p.53-72.

Davison, J.M. and Dunlop, W. (1980). Renal hemodynamics and tubular function in normal human pregnancy. *Kidney International*. **18** (2), p.152-161.

Davisson, R.L., Hoffmann, D.S., Butz, G.M., Aldape, G., Schlager, G., Merrill, D.C., Sethi, S., Weiss, R.M. and Bates, J.N. (2002). Discovery of a Spontaneous Genetic Mouse Model of Preeclampsia. *Hypertension*. **39** (2), p.337-342.

de Araújo, C.A.L., Oliveira, L. de S., de Gusmão I.M.B., Guimarães, A., Ribeiro, M. and Alves, J.G.B. (2020). Magnesium supplementation and preeclampsia in low-income pregnant women – a randomized double-blind clinical trial. *BMC Pregnancy and Childbirth*. **20** (208), p.1-6.

De Rijk, E.P.C.T., van Esch, E. and Flik, G. (2002). Pregnancy Dating in the Rat: Placental Morphology & Maternal Blood Parameters. *Toxicologic Pathology*. **30** (2), p.271-282.

Deak, T.M. and Moskovitz, J.B. (2012). Hypertension and Pregnancy. *Emergency Medicine Clinics of North America*. **30** (4), p.903-917.

deMartelly, V.A., Dreixler, J., Tung, A., Mueller, A., Heimberger, S., Fazal, A.A., Naseem, H., Lang, R., Kruse, E., Yamat, M., Granger, J.P., Bakrania, B.A., Rodriguez-Kovacs, J., Rana, S. and Shahul, S. (2021). Long-Term Postpartum Cardiac Function and Its Association With Preeclampsia. *Journal of the American Heart Association*. **10** (5), e018526.

Dickinson, H.O., Nicolson, D.J., Campbell, F., Cook, J.V., Beyer, F.R., Ford, G.A. and Mason, J. (2006). Magnesium supplementation for the management of essential hypertension in adults. *Cochrane Database of Systematic Reviews*. **19** (3), CD004640.

Doridot, L., Passet, B., Méhats, C., Rigourd, V., Barbaux, S., Ducat, A., Mondon, F., Vilotte, M., Castille, J., Breuiller-Fouché, M., Daniel, N., le Provost, F., Bauchet, A-L., Baudrie, V., Hertig A., Buffat, C., Simeoni, U., Germain, G., Vilotte, J-L., and Vaiman, D. (2013). Preeclampsia-Like Symptoms Induced in Mice by Fetoplacental Expression of STOX1 Are Reversed by Aspirin Treatment. *Hypertension*. **61** (3), p.662-668.

Dziak, J.J., Dierker, L.C. and Abar, B. (2018). The interpretation of statistical power after the data have been gathered. *Current Psychology*. **39**, p.870-877.

Ebbing, C., Rasmussen, S., Skjærven, R. and Irgens, L.M. (2017). Risk factors for recurrence of hypertensive disorders of pregnancy, a population-based cohort study. *Acta Obstetricia et Gynecologica Scandinavica*. **96** (2), p.243-250.

Eggenhuizen, G.M., Go, A., Koster, M.P.H., Baart, E.B. and Galjaard, R.J. (2021). Confined placental mosaicism and the association with pregnancy outcome and fetal growth: a review of the literature. *Human Reproduction Update*. **27** (5), p.885-903.

Elasy, A.N. and Nafea, O.E. (2022). Critical Hypermagnesemia in Preeclamptic Women Under a Magnesium Sulfate Regimen: Incidence and Associated Risk Factors. *Biological Trace Element Research*. [Online]. Available at: https://doi.org/10.1007/s12011-022-03479-x [Accessed 6 February 2023].

Erfanian, S., Yazdanpour, L., Javeshghani, D., and Roustazadeh, A. (2019). Association of arginine vasopressin (AVP) promoter polymorphisms with preeclampsia. *Pregnancy Hypertension*. **18**, p.122-125.

Ezzine, A., Souabni, H., Bizouarn, T. and Baciou, L. (2014). Recombinant form of mammalian gp91^{phox} is active in the absence of p22^{phox}. *Biochemical Journal*. **462** (2), p.337-345.

Fanni, D., Gerosa, C., Nurchi, V.M., Manchia, M., Saba, L., Coghe, F., Crisponi, G., Gibo, Y., Eyken, P.V., Fanos, V. and Faa, G. (2021). The Role of Magnesium in Pregnancy and in Fetal Programming of Adult Diseases. *Biological Trace Element Research*. **199** (10), p.3647-3657.

Fiorentini, D., Cappadone, C., Farruggia, G. and Prata, C. (2021). Magnesium: Biochemistry, Nutrition, Detection, and Social Impact of Diseases Linked to Its Deficiency. *Nutrients*. **13** (4), p.1136-1180.

Fisher, S.J. (2016). Why is placentation abnormal in preeclampsia?. *American Journal of Obstetrics & Gynecology*. **213** (4), p.S115-S122.

Folk, D.M. (2018). Hypertensive Disorders of Pregnancy: Overview and Current Recommendations. *Journal of Midwifery & Women's Health*. **63** (3), p.289-300.

Fonseca, B.M., Correia-da-Silva, G. and Teixeira, N.A. (2012). The rat as an animal model for the fetoplacental development: a reappraisal of the post-implantation period. *Reproductive Biology*. **12** (2), p.97-118.

Forrester, S.J., Booz, G.W., Sigmund, C.D., Coffman, T.M., Kawai, T., Rizzo, V.,. (2018). Angiotensin II Signal Transduction: An Update on Mechanisms of Physiology and Pathophysiology. *Physiological Reviews*. **98** (3), p.1627-1738.

Forte, M., Nocella, C., de Falco, E., Palmerio, S., Schirone, L., Valenti, V., Frati, G., Carnevale, R. and Sciarretta, S. (2016). The Pathophysiological Role of NOX2 in Hypertension and Organ Damage. *High Blood Pressure & Cardiovascular Prevention*. **23**, p.355-364.

Founds, S.A., Conley, Y.P., Lyons-Weiler, J.F., Jeyabalan, A., Hogge, W.A. and Conrad, K.P. (2009). Altered Global Gene Expression Changes in First Trimester Placentas of Women Destined to Develop Preeclampsia. *Placenta*. **30** (1), p.15-24.

Fowden, A.L. and Moore, T. (2012). Maternal-fetal resource allocation: Co-operation and conflict. *Placenta*. **33** (Supplement 2), p.e11-e15.

Frank, H.G. (2017). Placental Development. In: Polin, R.A., Abman, S.H., Rowitch, D.H., Benitz, W.E. and Fox, W.W. *Fetal and Neonatal Physiology*. 5th ed. Philadelphia: Elsevier. pp.101-113.

Fu, Z., Hu, J., Zhou, L., Chen, Y., Deng, M., Liu, X., Su, J., Lu, A., Fu., X. and Yang, T. (2019). (Pro)renin receptor contributes to pregnancy-induced sodium-water retention in rats via activation of intrarenal RAAS and α-ENaC. *American Journal of Renal Physiology*. **316** (3), p.F530-F538.

Fuchi, I., Noda, K., and Matsubara, Y. (1995a). Studies on Pregnancy Hypertension and IUGR-SFD: Effects of Drugs on the Blood Vessels in the Placenta of Pregnant SHRSP. *Clinical and Experimental Pharmacology and Physiology*. **22** (Suppl 1), p.S286-S287.

Fuchi, I., Higashino, H., Noda, K., and Suzuki, A. (1995b). Placental Na^+, K^+ Activated ATP-ase Activity in SHRSP in Connection with Pregnancy Induced Hypertension and Intra-Uterine Growth Retardation. *Clinical and Experimental Pharmacology and Physiology*. **22** (Suppl 1), p.S283-S285.

Furukawa, S., Kuroda, Y. and Sugiyama, A. (2014). A Comparison of the Histological Structure of the Placenta in Experimental Animals. *Journal of Toxicologic Pathology*. **27** (1), p.11-18.

Furukawa, S., Tsuji, N and Sugiyama, A. (2019). Morphology and physiology of rat placenta for toxicological evaluation. *Journal of Toxicologic Pathology*. **32**, p.1-17.

Fushima, T., Sekimoto, A., Minato, T., Ito, T., Oe, Y., Kisu, K., Sato, E., Funamoto, K., Hayase, T., Kimura, Y., Ito, S., Sato, H. and Takahashi, N. (2016). Reduced Uterine Perfusion Pressure (RUPP) Model of Preeclampsia in Mice. *PLoS One*. **11** (5), e0155426.

Gaffey, M.F., Das, J.K. and Bhutta, Z.A. (2015). Millennium Development Goals 4 and 5: Past and future progress. *Seminars in Fetal and Neonatal Medicine*. **20** (5), p.285-292.

Gatford, K.L., Andraweera, P.H., Roberts, C.T. and Care, A.S. (2020). Animal Models of Preeclampsia. *Hypertension*. **75** (6), p.1363-1381.

Gerbaud, P. and Pidoux, G. (2015). Review: An overview of molecular events occurring in human trophoblast fusion. *Placenta*. **36** (S1), p.S35-S42.

Gobbo, G.D.E., Konwar, C. and Robinson, W.P. (2020). The significance of the placental genome and methylome in fetal and maternal health. *Human Genetics*. **139** (9), p.1183-1196.

Gong, S., Gaccioli, F., Dopierala, J., Sovio, U., Cook, E., Volders, P-J., Martens, L., Kirk, P.D.W., Richardson, S., Smith, G.C.S. and Charnock-Jones, D.S. (2021). The RNA landscape of the human placenta in health and disease. *Nature Communications*. **12** (2639), p.1-17.

Gopalakrishnan, K., and Kumar, S. (2020). Whole-Genome Uterine Artery Transcriptome Profiling and Alternative Splicing in Rat Pregnancy. *Internal Journal of Molecular Science*. **21** (6), p.1-18.

Gordon, R., Magee, L.A., Payne, B., Firoz, T., Sawchuck, D., Tu, D., Vidler, M., de Silva, D., von Dadelszen, P. and the Community Level Interventions for Pre-eclampsia (CLIP) Working Group. (2014). Magnesium Sulphate for the Management of Preeclampsia and Eclampsia in Low and Middle Income Countries: A Systematic Review of Tested Dosing Regimens. *Journal of Obstetrics and Gynaecology Canada*. **36** (2), p.154-163.

Görlach, A., Bertram, K., Hudecova, S. and Krizanova, O. (2015). Calcium and ROS: A mutual interplay. *Redox Biology*. **6**, p.260-271.

Görlach, A., Brandes, R.P., Nguyen, K., Amidi, M., Dehghani, F. and Busse, R. (2000). A gp91phox Containing NADPH Oxidase Selectively Expressed in Endothelial Cells Is a Major Source of Oxygen Radical Generation in the Arterial Wall. *Circulation Research*. **87** (1), p.26-32.

Graham, D., McBride, M.W., Brain, N.J.R. and Dominiczak, A.F. (2005). Congenic/Cosmic Models of Hypertension. In: Fennell, J.P. and Baker, A.H. *Hypertension. Methods in Molecular Medicine*. Totowa, New Jersey: H. pp.3-15.

Grigsby, P.L. (2016). Animal Models to Study Placental Development and Function Throughout Normal and Dysfunctional Human Pregnancy. *Seminars in Reproductive Medicine*. **34** (1), p.11-16.

Greer, F.R. (1994). Calcium, phosphorus, magnseium and the placenta. *Acta Paediatrica*. **83** (S405), p.20-24.

Gröber, U., Schmidt, J. and Kisters, K. (2015). Magnesium in Prevention and Therapy. *Nutrients*. **7** (9), p.8199-8226.

Gude, N.M., Roberts, C.T., Kalionis, B. and King, R.G. (2004). Growth and function of the normal human placenta. *Thrombosis Research*. **114** (5-6), p.397-407.

Güden, M., Akkurt, M.Ö., Yalçin, S.E., Coşkun, B., Akkurt, I., Yavuz, A., Yirci, B. and Kandemir, N.Ö. (2016). A comparison of the effects of the most commonly used tocolytic agents on maternal and fetal blood flow. *Turkish Journal of Obstetrics and Gynecology*. **13** (2), p.85-89.

Guedes-Martins, L. (2016). Superimposed Preeclampsia. In: Islam, S. *Hypertension: from basic research to clinical practice volume 2, Advances in Experimental Medicine and Biology*. Switzerland: Springer International Publishing AG. pp.409-417.

Guerby, P., Tasta, O., Swiader, A., Pont, F., Byjold, E., Parant, O., Vayssiere C., Salvayre, R., and Negre-Salvayre, A. (2021). Role of oxidative stress in the dysfunction of the placental endothelial nitric oxide synthase in preeclampsia. *Redox Biology*. **40**, ID 101861.

Guerrera, M.P., Volpe, S.L. and James, J. (2009). Therapeutic Uses of Magnesium. *American Family Physician*. **80** (2), p.157-162.

Gutíerrez, A., Contreras, C., Sánchez, A. and Prieto, D. (2019). Role of Phosphatidylinositol 3-Kinase (PI3K), Mitogen-Activated Protein Kinase (MAPK), and Protein Kinase C (PKC) in Calcium Signaling Pathways Linked to the α1-Adrenoceptor in Resistance Arteries. *Frontiers in Physiology*. **10** (55), p. 1-14.

Guttmacher, A.E., Maddox, Y.T. and Spong, C.Y. (2014). The Human Placenta Project: Placental Structure, Development, and Function in Real Time. *Placenta*. **35** (5), p.303-304.

Gyselaers, W. and Thilaganathan, B. (2019). Preeclampsia: a gestational cardiorenal syndrome. *The Journal of Physiology*. **597** (18), p.4695-4714.

Hacker, A.N., Fung, E.B. and King, J.C. (2012). Role of calcium during pregnancy: maternal and fetal needs. *Nutrition Reviews*. **70** (7), p.397-409.

Harvey, A.P., Montezano, A.C., Hood, K.Y., Lopes, R.A., Rios, F., Ceravolo, G., Graham, D. and Touyz, R.M. (2017). Vascular dysfunction and fibrosis in stroke-prone spontaneously hypertensive rats: The aldosterone-mineralocorticoid receptor-Nox1 axis. *Life Sciences*. **179**, p.110-119.

Hasanein, P., Parviz, M., Keshavarz, M., Javanmardi, K., Mansoori, M. and Soltan, N. (2006). Oral magnesium administration prevents thermal hyperalgesia induced by diabetes in rats. *Diabetes Research and Clinical Practice*. **73** (1), p.17-22.

He, L., Lang, L., Li, Y., Liu, Q. and Yao, Y. (2016). Comparison of serum zinc, calcium, and magnesium concentrations in women with pregnancy-induced hypertension and healthy pregnant women: A meta-analysis. *Hypertension in Pregnancy*. **35** (2), p.202-209.

He, D-H., Zhang, L-M., Lin, L-M., Ning, R-B., Wang, H-J., Xu, C-S. and Lin, J-X. (2014). Effects of Losartan and Amlodipine on Left Ventricular Remodeling and Function in Young Stroke-Prone Spontaneously Hypertensive Rats. *Acta Cardiologica Sinica*. **30** (4), p.316-324.

Hering, L., Herse, F., Geusens, N., Verlohren, S., Wenzel, K., Staff, A.C., Brosnihan, K.B., Huppertz, B., Luft, F.C., Müller, D.N., Pijnenborg, R., Cartwright, J.E. and Dechend, R. (2010). Effects of Circulating and Local Angiotensin II in Rat Pregnancy. *Hypertension*. **56** (2), p.311-318.

Herrera-Garcia, G. and Contag, S. (2014). Maternal Preeclampsia and Risk for Cardiovascular Disease in Offspring. *Current Hypertension Reports*. **16** (475), p.1-10.

Herse, F., LaMarca, B., Hubel, C.A., Kaartokallio, T., Lokki, A.I., Ekholm, E., Laivuori, H., Gauster, M., Huppertz, B., Sugulle, M., Ryan, J.M., Novotny, S., Brewer, J., Park, J-K., Kacik, M., Hoyer, J., Verlohen, S., Wallukat, G., Rother, M., Luft, F.C., Muller, D.N., Schunck, W-H., Staff, A.C. and Dechend, R. (2012). Cytochrome P450 Subfamily 2J Polypeptide 2 Expression and Circulating Epoxyeicosatrienoic Metabolites in Preeclampsia. *Circulation*. **126** (25), p.2990-2999.

Herse, F., Staff, A.C., Hering, L., Muller, D.N., Luft, F.C. and Dechend, R. (2008). AT_1-receptor autoantibodies and uteroplacental RAS in pregnancy and pre-eclampsia. *Journal of Molecular Medicine*. **86**, p.697-703.

Hoenig, J.M. and Heisey, D.M. (2001). The Abuse of Power The Pervasive Fallacy of Power Calculations for Data Analysis. *The American Statistician*. **55** (1), p.19-24.

Hofmeyr, G.J., Lawrie, T.A., Atallah, Á.N., Torloni, M.R. and Cochrane Pregnancy and Childbirth Group. (2018). Calcium supplementation during pregnancy for preventing hypertensive disorders and related problems. *Cochrane Database of Systematic Reviews*. **2018** (10), CD001059.

Houston, M. (2011). The Role of Magnesium in Hypertension and Cardiovascular Disease. *Journal of Clinical Hypertension (Greenwich)*. **13** (11), p.843-847.

Hu, C., Wu, Z., Huang, Z., Hao, X., Wang, S., Deng, J., Yin, Y. and Tan, C. (2021). Nox2 impairs VEGF-A-induced angiogenesis in placenta via mitochondrial ROS-STAT3 pathway. *Redox Biology*. **45**, ID 102051.

Hu, X-Q., Song, R., Romero, M., Dasgupta, C., Huang, X., Holguin, M.A., Williams, V., Xiao, D., Wilson, S.M. and Zhang, L. (2019). Pregnancy Increases Ca^{2+} Sparks/Spontaneous Transient Outward Currents and Reduces Uterine Arterial Myogenic Tone. *Hypertension*. **73** (3), p.691-702.

Huang, P.L., Huang, Z., Mashimo, H., Bloch, K.D., Moskowitz., M.A., Bevan, J.A. and Fishman, M.C. (1995). Hypertension in mice lacking the gene for endothelial nitric oxide synthase. *Nature*. **377** (6546), p.239-242.

Hubel, C.A., Snaedal, S., Ness, R.B., Wiessfeld, L.A., Giersson, R.T., Roberts, J.M. and Arngrimsson, R. (2000). Dyslipoproteinaemia in postmeno-pausal women with a history of eclampsia. *BJOG: An International Journal of Obstetrics & Gynecology*. **107** (6), p.776-784.

Hussein, W. and Lafayette, R.A. (2014). Renal function in normal and disordered pregnancy. *Current Opinion in Nephrology and Hypertension*. **23** (1), p.46-53.

Hutcheon, J.A., Lisonkova, S., Joseph, K.S. (2011). Epidemiology of pre-eclampsia and the other hypertensive disorders of pregnancy. *Best Practice & Research Clinical Obstetrics & Gynaecology*. **25** (4), p.391-403.

Ismail, B. (2018). Pre-eclampsia and the foetus: a cardiovascular perspective. *Cardiovascular Journal of Africa*. **29** (6), p.387-393.

Jabrane-Ferrat, N. and Siewiera, J. (2014). The upside of decidual natural killer cells: new developments in the immunology of pregnancy. *Immunology*. **141** (4), p.490-497.

Jain, S., Sharma, P., Kulshreshtha, S., Mohan, G. and Singh, S. (2009). The Role of Calcium, Magnesium, and Zinc in Pre-Eclampsia. *Biological Trace Elements*. **133**, p.162-170.

James, J.L., Chamley, L.W. and Clark, A.R. (2017). Feeding Your Baby In Utero: How the Uteroplacental Circulation Impacts Pregnancy. *Physiology*. **32** (3), p.234-245.

James, M.F.M. (2010). Magnesium in obstetrics. *Best Practice & Research in Clinical Obstetrics and Gynaecology*. **24** (3), p.327-337.

Jee, S.H., Miller, E.R., Guallar, E., Singh, V.K., Appel, L.J. and Klag, M.J. (2002). The effect of magnesium supplementation on blood pressure: a meta-analysis of randomized clinical trials. *American Journal of Hypertension*. **15** (8), p.691-696.

Ji, L., Brkić, J., Liu, M., Fu, G., Peng, C. and Wang, Y-L. (2013). Placental trophoblast cell differentiation: Physiological regulation and pathological relevance to preeclampsia. *Molecular Aspects of Medicine*. **34** (5), p.981-1023.

Kaleta, B. (2019). The role of osteopontin in kidney diseases. *Inflammation Research*. **68** (2), p.93-102

Karumanchi, S.A., Maynard, S.E., Stillman, I, E., Epstein, F.H. and Sukhatme, V.P. (2005). Preeclamspia: A renal perspective*. Kidney International*. **67** (6), p.2101-2113.

Kassebaum, N.J. *et al* (2014). Global, regional, and national levels and causes of maternal mortality during 1990–2013: a systematic analysis for the Global Burden of Disease Study 2013. *The Lancet*. **384** (9947), p.980-1004.

Kato, T., Mizuguchi, N. and Ito, A. (2015). Blood pressure, renal biochemical parameters and histopathology in an original rat model of essential hypertension (SHRSP/Kpo strain). *Biomedical Research (Tokyo)*. **36** (3), p.169-177.

Kawano, Y., Matsuoka, H., Takishita, S. and Omae, T. (1998). Effects of magnesium supplementation in hypertensive patients: assessment by office, home, and ambulatory blood pressure. *Hypertension*. **32** (2), p.260-265.

Kazemi-Darabadi, S. and Akbari, G. (2020). Evaluation of magnesium sulfate effects on fetus development in experimentally induced surgical fetal growth restriction. *The Journal of Maternal-Fetal & Neonatal Medicine*. **33** (14), p.2459-2465.

Kedia, K., Smith, S.F., Wright, A.H., Barnes, J.M., Tolley, H.D., Esplin, M.S.E. and Graves, S.W. (2016). Global "omics" evaluation of human placental response to preeclamptic conditions. *American Journal of Obstetrics and Gynecology*. **215** (2), p.238.e1-238.e20.

Kerr, S., Brosnan, M.J., McIntyre, M., Reid, J.L., Dominiczak, A.F. and Hamilton, C.A. (1999). Superoxide Anion Production Is Increase in a Model of Genetic Hypertension. *Hypertension*. **33** (6), p.1353-1358.

Khedagi, A.M. and Bello, N.A. (2021). Hypertensive Disorders of Pregnancy. *Cardiology Clinics*. **39** (1), p.77-90.

Khedun, S.M., Ngotho, D., Moodley, J. and Naicker, T. (1998). Plasma and Red Cell Magnesium Levels in Black African Women with Hypertensive Disorders of Pregnancy. *Hypertension in Pregnancy*. **17** (2), p.125-134.

Kobayashi, H. (2015). The Impact of Maternal-Fetal Genetic Conflict Situation on the Pathogenesis of Preeclampsia. *Biochemical Genetics*. **53**, p.223-234.

Korish, A. (2012). Magnesium sulfate therapy of preeclampsia: an old tool with new mechanism of action and prospect in management and prophylaxis. *Hypertension Research*. **35**, p.1005-1011.

Kumuru, S., Aydin, S., Simsek, M., Sahin , K., Yaman, M., and Ay, G. (2003). Comparison of serum copper, zinc, calcium, and magnesium levels in preeclamptic and healthy pregnant women. *Biological Trace Elements Research*. **94** (2), p.105-112.

Kuriakose, J., Montezano, A.C. and Touyz, R.M. (2021). ACE2/Ang-(1-7)/Mas1 axis and the vascular system: vasoprotection to COVID-19-associated vascular disease. *Clinical Science (London)*. **135** (2), p.387-407.

Kusinski, L.C., Stanley, J.L., Dilworth, M.R., Hirt, C.J., Andersson, I.J., Renshall, L.J., Baker, B., Baker, P.N., Sibley, C.P., Wareing, M. and Glazier, J.D. (2012). eNOS knockout mouse as a model of fetal growth restriction with an impaired uterine artery function and placental transport phenotype. *American Journal of Physiology Regulatory, Integrative and Comparative Physiology*. **303** (1), p.R86-R93.

Lafond, J. and Simoneau, L. (2006). Calcium Homeostasis in Human Placenta: Role of Calcium-Handling Proteins. *International Review of Cytology*. **250**, p.109-174.

Lai, C., Coulter, S.A. and Woodruff, A. (2017). Hypertension and Pregnancy. *Texas Heart Institute Journal.* **44** (5), p.350-351.

LaMarca, B., Parrish, M., Ray, L.F., Murphy. S.R., Roberts, L., Glover, P., Wallukat, G., Wenzel, K., Cockrell, K., Martin, J.N., Ryan, M.J. and Dechend, R. (2009). Hypertension in response to autoantibodies to the angiotensin II type I receptor (AT1-AA) in pregnant rats: role of endothelin-1. *Hypertension*. **54** (4), p.905-909.

LaMarca, B., Parrish, M.R. and Wallace, K. (2012). Agonistic Autoantibodies to the Angiotensin II Type I Receptor Cause Pathophysiologic Characteristics of Preeclampsia. *Gender Medicine*. **9** (3), p.139-146.

Lappas, G., Daou, G.B. and Anand-Srivastava, M.B. (2005). Oxidative stress contributes to the enhanced expression of Giα proteins and adenylyl cyclase signalling in vascular smooth muscle cells from spontaneously hypertensive rats. *Hypertension*. **23** (12), p.2251-2261.

La Rovere, M.T., Pinna, G.D. and Raczak, G. (2008). Baroreflex Sensitivity: Measurement and Clinical Implications. *Annals of Noninvasive Electrocardiology*. **13** (2), p.191-207.

Lassi, Z.S., Mansoor, T., Salam, R.A., Das, J.K. and Bhutta, Z.A. (2014). Essential pre-pregnancy and pregnancy interventions for improved maternal, newborn and child health. *Reproductive Health*. **11** (Suppl 1), S2.

Lash, G.E., Pitman, H., Morgan, H.L., Innes, B.A., Agwu, C.N. and Bulmer, J.N. (2013). Decidual macrophages: key regulators of vascular remodelling in human pregnancy. *Journal of Leukocyte Biology*. **100** (2), p.315-325.

Lash, G.E., Schiessl, B., Kirkley, M., Innes, B.A., Cooper, A., Searle, R.F., Robson, S.C. and Bulmer, J.N. (2006). Expression of angiogenic growth factors by uterine natural killer cells during early pregnancy. *Journal of Leukocyte Biology*. **80** (3), p.572-580.

Lassi, Z.S., Mansoor, T., Salam, R.A., Das, J.K. and Bhutta, Z.A. (2014). Essential pre-pregnancy and pregnancy interventions for improved maternal, newborn and child health. *Reproductive Health*. **11** (S1), p.S2-S21.

Laursen, J.B., Rajaopalan, S., Galis, Z., Tarpey, M., Freeman, B.A. and Harrison, D.G. (1997). Role of Superoxide in Angiotensin II–Induced but Not Catecholamine-Induced Hypertension. *Circulation*. **95** (3), p.588-593.

Lee, K-M., Kang, H-A., Ko, C-B., Park, M., Lee, H-Y., Choi, H-R., Yun, C-H., Jung, W-W., Oh, J-W. and Kang, H-S. (2012). Differential gene expression profiles in spontaneously hypertensive rats induced by administration of enalapril and nifedipine. *International Journal of Molecular Medicine.* **31** (1), p.179-187.

Leeman, L., Dresang, L.T. and Fontaine, P. (2016). Hypertensive Disorders of Pregnancy. *American Family Physician*. **93** (2), p.121-127.

Leno-Durán, E., Hatta, K., Bianco, J., Yamada, A.T., Ruiz-Ruiz, C., Olivares, E.G. and Croy, B.A. (2010). Fetal-placental hypoxia does not result from failure of spiral arterial modification in mice. *Placenta*. **31** (8), p.731-737.

Li, F., Fushima, T., Oyanagi, G., Townley-Tilson, H.W.D., Sato, E., Nakada, H., Oe, Y., Hagaman, J.R., Wilder, J., Li, M., Sekimoto, A., Saigusa, D., Sato, H., Ito, S., Jennette, J.C., Maeda, N., Karumanchi, S.A., Smithies, O., and Takahashi, N. (2016). Nicotinamide benefits both mothers and pups in two contrasting mouse models of preeclampsia. *Proceedings of the National Academy of Sciences of the United States of America*. **113** (47), p.13450-13455.

Li, J., LaMarca, B. and Reckelhoff, J.F. (2012). A model of preeclampsia in rats: the reduced uterine perfusion pressure (RUPP) model. *American Journal of Physiology, Heart and Circulatory Physiology*. **303** (1), p.H1-H8.

Li, J., Wang, L., Ding, J., Cheng, Y., Diao, L., Li, L., Zhang, Y. and Yin, T. (2022). Multiomics Studies Investigating Recurrent Pregnancy Loss: An Effective Tool for Mechanism Exploration. *Frontiers in Immunology*. **13** (826198), p.1-12.

Lian, I.A., Toft, J.H., Olsen, G.D., Langaas, M., Bjørge, L., Eide, I.P., Børdahl, P.E. and Austgulen, R. (2010). Matrix Metalloproteinase 1 in Pre-eclampsia and Fetal Growth

Restriction: Reduced Gene Expression in Decidual Tissue and Protein Expression in Extravillous Trophoblasts. *Placenta*. **31** (7), p.615-620.

Lisonkova, S. and Joseph, K.S. (2013). Incidence of preeclampsia: risk factors and outcomes associated with early- versus late-onset disease. *American Journal of Obstetrics and Gynecology*. **209** (6), p.544.e1-544.e12.

Liu, L.X. and Arany, Z. (2014). Maternal cardiac metabolism in pregnancy. *Cardiovascular Research*. **101** (4), p.545-553.

Liu, M. and Dudley Jr., S.C. (2020). Magnesium, Oxidative Stress, Inflammation, and Cardiovascular Disease. *Antioxidants*. **9** (10), p.907-938.

Liu, X. and Pan, Z. (2022). Store-Operated Calcium Entry in the Cardiovascular System. In: Crusio, W.E., Dong, H., Radeke, H.H., Rezaei, N., Steinlein, O. and Xiao, J. *Advances in Experimental Medicine and Biology*. Singapore: Springer Nature. pp.303-333.

Liu, S., Xie, X., Lei, H., Zou, B. and Xie, L. (2019). Identification of Key circRNAs/lncRNAs/miRNAs/mRNAs and Pathways in Preeclampsia Using Bioinformatics Analysis. *Medical Science Monitor*. **25**, p.1679-1693.

Livak, K.J. and Schmittgen, T.D. (2001). Analysis of Relative Gene Expression Data Using Real-Time Quantitative PCR and the 2−ΔΔCT Method. *Methods*. **25** (4), p.402-408.

Louwen, F., Muschol-Steinmetz, C., Reinhard, J., Reitter, A. and Yuan, J. (2012). A lesson for cancer research: placental microarray gene analysis in preeclampsia. *Oncotarget*. **3** (8), p.759-773

Lumbers, E.R., Delforce, S.J., Arthurs, A.L. and Pringle K.G. (2019). Causes and Consequences of the Dysregulated Maternal Renin-Angiotensin System in Preeclampsia. *Frontiers in Endocrinology*. **10**, p.1-13.

Lumbers, E.R. and Pringle, K.G. (2014). Roles of the circulating renin-angiotensin-aldosterone system in human pregnancy. *Regulatory, Integrative and Comparative Physiology*. **306** (2), p.R91-R101.

Lyall, F., Bulmer, J.N., Duffie, E., Cousin, F., Theriault, A. and Robson, S.C. (2001). Human Trophoblast Invasion and Spiral Artery Transformation: The Role of PECAM-1 in Normal Pregnancy, Preeclampsia and Fetal Growth Restriction. *The American Journal of Pathology*. **158** (5), p.1713-1721.

Lyall, F., Robson, S.C. and Bulmer, J.N. (2013). Spiral Artery Remodelling and Trophoblast Invasion in Preeclampsia and Fetal Growth Restriction: Relationship to Clinical Outcome. *Hypertension*. **62** (6), p.1046-1054.

Ma'ayeh, M., Rood, K.M., Kniss, D. and Costantine, M.M. (2020). Novel Interventions for the Prevention of Preeclampsia. *Current Hypertension Reports*. **22** (17), p.1-8.

Madazli, R., Yuksel, M.A., Imamoglu, M., Tuten, A., Oncul, M., Aydin, B. and Dem. (2014). Comparison of clinical and perinatal outcomes in early- and late-onset preeclampsia. *Maternal-Fetal Medicine*. **290**, p.53-57.

Magee, L.A., Pels, A., Helewa, M., Rey, E. and von Dadelszen, P. (2015). The hypertensive disorders of pregnancy. *Best Practice & Research Clinical Obstetrics & Gynaecology*. **29** (5), p.643-657.

Maier, J.A., Castiglioni, S., Locatelli, L, Zocchi, M. and Mazur, A. (2021). Magnesium and inflammation: Advances and perspectives. *Seminars in Cell & Developmental Biology*. **115**, p.37-44.

Makrides, M., Crosby, D.D., Shepherd, E. and Crowther, C.A. (2014). Magnesium supplementation in pregnancy. *Cochrane Database of Systematic Reviews*. **4**, p.1-54.

Maltepe, E. and Fisher, S.J. (2015). Placenta: The Forgotten Organ. *Annual Review of Cell and Developmental Biology*. **31** (1), p.523-552.

Mandala, M. and Osol, G. (2011). Physiological Remodelling of the Maternal Uterine Circulation During Pregnancy. *Basic & Clinical Pharmacology & Toxicology*. **110** (1), p.12-18.

Maric-Bilkan, C., Gilbert, E.L. and Ryan, M.J. (2014). Impact of ovarian function on cardiovascular health in women: focus on hypertension. *International Journal of Womens Health*. **6**, p.131-139.

Mary, S., Small, H., Herse, F., Carrick, E., Flynn, A., Mullen, W., Dechend, R. and Delles, C. (2021). Preexisting hypertension and pregnancy-induced hypertension reveal molecular differences in placental proteome in rodents. *Physiological Genomics*. **53** (6), p.259-268.

Masineni, S., Chaner, P.N., Singh, G.D., Powers, A. and Stier, C.T. (2005). Male Gender and Not the Severity of Hypertension Is Associated With End-Organ Damage in Aged Stroke-Prone Spontaneously Hypertensive Rats. *American Journal of Hypertension*. **18** (6), p.878-884.

Matsubara, K., Matsubara, Y., Hyodo, S., Katayama, T. and Ito, M. (2010). Role of nitric oxide and reactive oxygen species in the pathogenesis of preeclampsia. *Journal of Obstetrics and Gynaecology*. **36** (2), p.239-247.

Maynard, S.E., Min, J-Y., Merchan, J., Lim, K-H., Li, J., Mondal, S., Libermann, T.A., Morgan, J.P., Sellke, F.W., Stillman, I.E., Epstein, F.H., Sukhatme, V.P. and Karumanchi, S.A. (2003). Excess placental soluble fms-like tyrosine kinase 1 (sFlt1) may contribute to endothelial dysfunction, hypertension, and proteinuria in preeclampsia. *Journal of Clinical Investigation*. **111** (5), p.649-658.

McCarthy, R. and Kopin, I.J. (1978). Pregnancy: Its Effects on Blood Pressure, Heart Rate and Sympatho-Adrenal Activity in Spontaneously Hypertensive Rats. *Experimental Biology and Medicine*. **158** (2), p.242-244.

Melchiorre, K., Rajan, S. and Thilaganathan, B. (2012). Cardiac structure and function in normal pregnancy. *Current Opinion in Obstetrics and Gynaecology*. **24** (6), p.413-421.

Mirabito Colafella, K.M., Boveé, D.M. and Danser, A.H.J. (2019). The renin-angiotensin-aldosterone system and its therapeutic targets. *Experimental Eye Research*. **186** (107680), p.1-7.

Miralles, F., Collinot, H., Boumerdassi, Y., Ducat, A., Duché, A., Renault, G., Marchiol, C., Lagoutte, I., Bertholle, C., Andrieu, M., Jacques, S., Méhats, C. and Vaiman, D. (2019). Long-term cardiovascular disorders in the STOX1 mouse model of preeclampsia. *Scientific Reports*. **9** (11918), p.1-13.

Mishra, J.S., Gopalakrishnan, K. and Kumar, S. (2018). Pregnancy upregulates angiotensin type 2 receptor expression and increases blood flow in uterine arteries of rats. *Biology of Reproduction*. **99** (5), p.1091-1099.

Mittendorf, R., Dambrosia, J., Pryde, P.G., Lee, K-S., Gianopoulos, J.G., Besing. (2002). Association between the use of antenatal magnesium sulfate in preterm labor and adverse health outcomes in infants. *American Journal of Obstetrics & Gynecology*. **186** (6), p.1111-1118.

Mizuno, Y., Sotomaru, Y., Katsuzawa, Y., Kono, T., Meguro, M., Oshimura, M., Kawai, J., Tomaru, Y., Kiyosawa, H., Nikaido, I., Amanuma, H., Hayashizake, Y. and Okazaki, Y. (2002). Asb4, Ata3, and Dcn are novel imprinted genes identified by high-throughput screening using RIKEN cDNA microarray. *Biochemical and Biophysical Research Communications*. **290** (5), p.1499-1505.

Mohamed, M.A., Manzor, N.F.M., Zulkifli, N.F., Zainal, N., Hayati, A.R. and Asnawi, A.W.A. (2020). A Review of Candidate Genes and Pathways in Preeclampsia- An Integrated Bioinformatical Analysis. *Biology*. **9** (4), p.62-81.

Mor, G., Cardenas, I., Abrahams, V. and Guller, S. (2011). Inflammation and pregnancy: the role of the immune system at the implantation site. *Annals of the New York Academy of Sciences*. **1221** (1), p.80-87.

Morgan, H.L., Butler, E., Ritchie, S., Herse, F., Dechend, R., Beattie, E., McBride, M.W. and Graham, D. (2018). Modelling Superimposed Preeclampsia Using Ang II (Angiotensin II) Infusion in Pregnant Stroke-Prone Spontaneously Hypertensive Rats. *Hypertension*. **72** (1), p.208-218.

Morton, J.S., Levasseur, J., Ganguly, E., Quon, A., Kirschenman, R., Dyck, J.R.B., Fraser, G.M. and Davidge, S.T. (2019). Characterisation of the Selective Reduced Uteroplacental Perfusion (sRUPP) Model of Preeclampsia. *Scientific Reports*. **9** (9565), p.1-13.

Moussa, H.N., Arian, S.E. and Sibai, B.M. (2014). Management of Hypertensive Disorders in Pregnancy. *Women's Health*. **10** (4), p.385-404.

Murphy, M.P., Bayir, H., Belousov, V., Chang, C.J., Davies, K.J.A., Davies, M.J. (2022). Guidelines for measuring reactive oxygen species and oxidative damage in cells and in vivo. *Nature Metabolism*. **4** (6), p.651-662.

Nabika, T., Ohara, H., Kato, N. and Isomura, M. (2012). The stroke-prone spontaneously hypertensive rat: still a useful model for post-GWAS genetic studies?. *Hypertension Research*. **35** (5), p.477-484.

Naderi, S., Tsai, S.A. and Khandelwal, A. (2017). Hypertensive Disorders of Pregnancy. *Current Atherosclerosis Reports*. **19** (3), p.15-21.

Narasimhulu, D., Brown, A., Egbert, N.M., Haberman, S., Bhutada, A., Minkoff, H. and Rastogi, S. (2017). Maternal magnesium therapy, neonatal serum magnesium concentration and immediate neonatal outcomes. *Journal of Perinatology*. **37**, p.1297-1303.

Nardozza, L.M.M., Caetano, A.C.R., Zamarian, A.C.P., Mazzola, J.B., Silva, C.P., Marçal, V.M.G., Lobo, T.F., Peixoto, A.B. and Júnior, E.A. (2017). Fetal growth restriction: current knowledge. *American Journal of Obstetrics and Gynecology*. **295** (5), p.1061-1077.

National Institute for Health and Care Excellence. (2019). *Reducing the risk of hypertensive disorders in pregnancy.* Available: https://www.nice.org.uk/guidance/ng133/chapter/Recommendations#management-of-chronic-hypertension-in-pregnancy. Last accessed 08 April 2022.

Nelander, M, Weis, J., Bergman, L., Larsson, A., Wikström, A-K. and Wikström, J. (2017). Cerebral Magnesium Levels in Preeclampsia; A Phosphorus Magnetic Resonance Spectroscopy Study. *American Journal of Hypertension*. **30** (7), p.667-672.

Nelson, A.C., Mould, A.W., Bikoff, E.K. and Robertson, E.J. (2016). Single-cell RNA-seq reveals cell type-specific transcriptional signatures at the maternal-foetal interface during pregnancy. *Nature Communications*. **7** (11414), p.1-13.

Nguyen, M.T.X., Han, J., Ralph, D.L., Veiras, L.C. and McDonough, A.A. (2015). Short-term nonpressor angiotensin II infusion stimulates sodium transporters in proximal tubule and distal nephron. *Physiological Reports*. **3** (9), p. e12496.

Nishiyama, A., Fukui, T., Fujisawa, Y., Rahman, M., Tian, R-X., Kimura, S. and Abe, Y. (2001). Systemic and Regional Hemodynamic Responses to Tempol in Angiotensin II–Infused Hypertensive Rats. *Hypertension*. **37** (1), p.77-83.

Novakovic, B., Yuen, R.K., Gordon, L., Penaherrera, M.S., Sharkey, A., Moffett, A., Craig, J.M., Robinson, W.P. and Saffery, R. (2011). Evidence for widespread changes in promoter methylation profile in human placenta in response to increasing gestational age and environmental/stochastic factors. *BMC Genomics*. **12** (529), p.1-14.

Obata, S., Toda, M., Tochio, A., Hoshino, A., Miyagi, E. and Aoki, S. (2020). Fetal growth restriction as a diagnostic criterion for preeclampsia. *Pregnancy Hypertension*. **21**, p.58-62.

Ocaranza, M.P., Riquelme, J.A., García, L., Jalil, J.E., Chiong, M., Santos, R.A.S. and Lavandero, S. (2020). Counter-regulatory renin-angiotensin system cardiovascular disease. *Nature Reviews Cardiology*. **17** (2), p.116-129.

O'Day, M.P. (1997). Cardio-respiratory physiological adaptation of pregnancy. *Seminars in Perinatology*. **21** (4), p.268-275.

Odenkirk, M.T., Stratton, K.G., Gritsenko, M.A., Bramer, L.M., Webb-Robertson, B-J.M., Bloodsworth, K.J., Weitz, K.K., Lipton, A.K., Monroe, M.E., Ash, J.R., Fourches, D., Taylor, B.D., Burnum-Johnson, K.E. and Baker, E.S. (2020). Unveiling Molecular Signatures of Preeclampsia and Gestational Diabetes Mellitus with Multi-Omics and Innovative Cheminformatics Visualization Tools. *Molecular Omics*. **16** (6), p.521-532.

Odutayo, A. and Hladunewich, M. (2012). Obstetric Nephrology: Renal Hemodynamic and Metabolic Physiology in Normal Pregnancy. *Clinical Journal of American Society of Nephrology*. **7** (12), p.2073-2080.

Okamoto, K., Yamori, T. and Nagaoka, A. (1974). Establishment of the SHRSPs (SHR). *Circulation Research*. **34** (Suppl 1), p.I143-I153.

Oparil, S. and Schmieder, R.E. (2013). New Approaches in the Treatment of Hypertension. *Circulation Research.* **116** (6), p.1074-1095.

Osol, G. and Mandala, M. (2009). Maternal Uterine Vascular Remodelling During Pregnancy. *Physiology (Bethesda)*. **24**, p.58-71.

Osol, G. and Moore, L.G. (2013). Maternal Uterine Vascular Remodelling During Pregnancy. *Microcirculation*. **21** (1), p.38-47.

Paravicini, T.M. and Touyz, R.M. (2008). NADPH Oxidases, Reactive Oxygen Species, and Hypertension: Clinical implications and therapeutic possibilities. *Diabetes Care*. **31** (Supplement 2), p.S170-S180.

Parham, P. (2004). NK Cells and Trophoblasts. *Journal or Experimental Medicine*. **200** (8), p.951-955.

Pastore, M.B., Jobe, S.O., Ramadoss, J. and Magness, R.R. (2012). Estrogen Receptor-α and Estrogen Receptor-β in the Uterine Vascular Endothelium during Pregnancy: Functional Implications for Regulating Uterine Blood Flow. *Seminars in Reproductive Medicine*. **30** (1), p.46-61.

Patel, S., Rauf, A., Khan, H. and Abu-Izneid, T. (2017). Renin-angiotensin-aldosterone (RAAS): The ubiquitous system for homeostasis and pathologies. *Biomedicine & Pharmacotherapy*. **94**, p.317-325.

Patel, V.B., Zhong, J-C., Grant, M.B. and Oudit, G.Y. (2016). Role of the ACE2/Angiotensin 1-7 axis of the Renin-Angiotensin System in Heart Failure. *Circulation Research*. **118** (8), p.1313-1326.

Patrelli, T.S., Dall'Asta, A., Gizzo, S., Pedrazzi, G., Piantelli, G., Jasonni,V.M. and Modena, A.B. (2012). Calcium supplementation and prevention of preeclampsia: a meta-analysis. *The Journal of Maternal-Fetal and Neonatal Medicine*. **25** (12), p.2570-2574.

Paull, J.R.A, Bunting, M.W. and Widdop, R.E. (1997). Role of the Brain Renin-Angiotensin System in the Maintenance of Blood Pressure in Conscious Spontaneously Hypertensive and Sinoarortic Baroreceptor Reflex-Denervated Rats. *Clinical and Experimental Pharmacology and Physiology*. **24** (9-10), p.667-672.

Paul, M., Mehr, A.P. and Kreutz, R. (2006). Physiology of Local Renin-Angiotensin Systems. *Physiological Reviews*. **86** (3), p.747-803.

Phoswa, W.N. and Khaliq, O.P. (2021). The Role of Oxidative Stress in Hypertensive Disorders of Pregnancy (Preeclampsia, Gestational Hypertension) and Metabolic Disorder of Pregnancy (Gestational Diabetes Mellitus). *Oxidative Medicine and Cellular Longevity*. **2021**, ID 5581570.

Pijenborg, E., Vercruysse, L. and Hanssens, M. (2006). The Uterine Spiral Arteries In Human Pregnancy: Facts and Controversies. *Placenta*. **27** (9-10), p.939-958.

Plevkova, J., Brozmanova, M., Harsanyiova, J., Sterusky, M., Honetschlager, J. and Buday, T. (2020). Various Aspects of Sex and Gender Bias in Biomedical Research. *Physiological Research*. **69** (Suppl 3), p.S367-S378.

Poon, L.C.Y., Kametas, N.A., Maiz, N., Akolekar, R. and Nicolaides, K.H. (2009). First-trimester prediction of hypertensive disorders of pregnancy. *Hypertension*. **53** (3), p.812-818.

Possomato-Vieira, J. and Khalil, R.A. (2013). Mechanisms of Endothelial Dysfunction in Hypertensive Pregnancy and Preeclampsia. *Advances in Pharmacology*. **77**, p.361-431.

Pruthi, D., Khankin, E.V., Blanton, R.M., Aronovitz, M., Burke, S.D., McCurley, A., Karumanchi, S.A. and Jaffe, I.Z. (2003). Exposure to Experimental Preeclampsia in Mice Enhances the Vascular Response to Future Injury. *Hypertension*. **65** (4), p.863-870.

Raffaelli, R., Prioli, M.A., Parissone, F., Prati, D., Carli, M., Bergamini, C., Cacici, G., Balestreri, D., Vassanelli, C. and Franchi, M. (2014). Pre-eclampsia: evidence of altered ventricular repolarisation by standard ECG paramters and QT dispersion. *Hypertension Research*. **37** (11), p.984-988.

Ramesar, S.V., Mackraj, I., Gathiram, P. and Moodley, J. (2011). Sildenafil citrate decreases sFlt-1 and sEng in pregnant l-NAME treated Sprague–Dawley rats. *European Journal of Obstetrics & Gynecology and Reproductive Biology*. **157** (2), p.136-140.

Rieber-Mohn, A.B., Sugulle, M., Wallukat, G., Alnæs-Katjavivi, P., Størvold, G.L., Bolstad, N., Redman, C.W.G., Dechend, R. and Staff, A.C. (2018). Auto-antibodies against the angiotensin II type I receptor in women with uteroplacental acute atherosis and preeclampsia at delivery and several years postpartum. *Journal of Reproductive Immunology*. **128**, p.23-29.

Ringvold, H.C. and Khalil, R.A. (2017). Chapter Six - Protein Kinase C as Regulator of Vascular Smooth Muscle Function a. In: Khalil, R.A. *Vascular Pharmacology Smooth Muscle*. London: Academic Press. pp.203-301.

Reinke, E., Supriyatiningsih and Haier, J. (2017). Maternal mortality as a Millennium Development Goal of the United Nations: a systematic assessment and analysis of available data in threshold countries using Indonesia as example. *Journal of Global Health*. **7** (1) [Online]. Available at: https://www.ncbi.nlm.nih.gov/pmc/articles/PMC5370209/ [Accessed 01 April 2022].

Robertson, W.B., Brosens, I. and Dixon, H.G. (1967). The pathological response of the vessels of the placental bed to hypertensive pregnancy. *Journal of Pathology and Bacteriology*. **93** (2), p.581-592.

Robson, A., Harris, L.K., Innes, B.A., Lash, G.E., Aljunaidy, M.M., Aplin, J.D., Baker, P.N., Robson, S.C. and Bulmer, J.N. (2012). Uterine natural killer cells initiate spiral artery remodelling in human pregnancy. *The FASEB Journal*. **26** (12), p.4876-4885.

Robson, A., Lash, G.E., Innes, B.A., Zhang, J.Y., Robson, S.C., and Bulmer, J.N. (2019). Uterine spiral artery muscle dedifferentiation. *Human Reproduction*. **34** (8), p.1428-1238.

Rogers, M.S., Wang, C.C.R., Tam, W.H., Li, C.Y., Chu, K.O. and Chu, C.Y. (2006). Oxidative stress in midpregnancy as a predictor of gestational hypertension and pre-eclampsia. *BJOG: An International Journal of Obstetrics & Gynecology*. **113** (9), p.1053-1059.

Ruddy, J.M., Akerman, A.W., Kimbrough, D., Nadeau, E.K., Stroud, R.E., Mukherjee, R., Ikonomidis, J.S. and Jones, J.A. (2017). Differential hypertensive protease expression in the thoracic versus abdominal aorta. *Journal of Vascular Surgery*. **66** (5), p.1543-1552.

Rylander, R. (2015). Pre-eclampsia during pregnancy and cardiovascular disease later in life: the case for a risk group. *Archives of Gynaecology and Obstetrics*. **292**, p.519-521.

Saavedra, J.M. (2009). Opportunities and limitations of genetic analysis of hypertensive rat strains. *Journal of Hypertension*. **27** (6), p.1129-1133.

Sanghavi, M. and Rutherford, J.D. (2014). Cardiovascular Physiology of Pregnancy. *Circulation*. **130** (12), p.1003-1008.

Santillan, M.K., Santillan, D.A., Scroggins, S.M., Min, J.Y., Sandgren, J.A., Pearson, N.A., Leslie, K.K., Hunter, S.K., Zamba, G.K.D., Gibson-Corley, K.N. and Grobe, J.L. (2014). Vasopressin in preeclampsia: a novel very early human pregnancy biomarker and clinically relevant mouse model. *Hypertension*. **64** (4), p.852-859.

Sattar, N. and Greer, I.A. (2002). Pregnancy complications and maternal cardiovascular risk: opportunities for intervention and screening? *BMJ*. **325**, p.157-160.

Sattar, N., Ramsay, J., Crawford, L., Cheyne, H., Greer, I.A. (2003). Classic and novel risk factor parameters in women with a history of preeclampsia. *Hypertension*. **42** (1), p. 39-42.

Say, L., Chou, D., Gemmill, A., Tunçalp, Ö., Moller, A-B., Daniels, J., Gülmezoglu, A.M., Temmerman, M. and Alkema, L. (2014). Global causes of maternal death: a WHO systematic analysis. *The Lancet Global Health*. **2** (6), p.E323-E333.

Schiffrin, E.L. (2001). Role of endothelin-1 in hypertension and vascular disease. *American Journal of Hypertension*. **14** (S3), p.83S-89S.

Schlegel, R.N., Spiers, J.G., Moritz, K.M., Cullen, C.L., Björkman, S.T. and Paravicini, T.M. (2017). Maternal hypomagnesemia alters hippocampal NMDAR subunit expression and programs anxiety-like behaviour in adult offspri. *Behavioural Brain Research*. **328**, p.39-47.

Schoots, M.H., Bourgonje, M.F., Bourgonje, A.R., Prins, J.R., van Hoorn, E.G.M., Abdulle, A.E., Kobold, A.C.M., van der Heide, M., Hillebrands, J-L., van Goor, H. And Gorijn, S.J. (2021). Oxidative stress biomarkers in fetal growth restriction with and without preeclampsia. Placenta. **115**, pp.87-96.

Schutten, J.C., Joosten, M.M., de Borst, M.H. and Bakker, S.J.L. (2018). Magnesium and Blood Pressure: A Physiology-Based Approach. *Advances in Kidney Disease and Health*. **25** (3), p.244-250.

Scott, K., Morgan, H.L., Delles, C., Fisher, S., Graham, D. and McBride, M.W. (2021). Distinct uterine artery gene expression profiles during early gestation in the stroke-prone spontaneously hypertensive rat. *Physiological Genomics*. **53** (4), p.160-171.

Scott, P-A., Provencher, M., Guérin, P and St-Louis, J. (2009). Gestation-Induced Vascular Remodelling. In: Vaillancourt, C. and Lafond, J. *Human Embryogenesis Methods and Protocols*. New York: Humana Press. pp.103-102.

Severino, P., Netti, L., Mariani, M.V., Maraone, A., D'Amato, A., Scarpati, R. (2019). Prevention of Cardiovascular Disease: Screening for Magnesium Deficiency. *Cardiology Research and Practice*. **2019**, ID 4874921.

Shankar, K., Zhong, Y., Kang, P., Blackburn, M.L., Soares, M.J., Badger, T.M. and Gomez-Acevedo, H. (2012). RNA-Seq Analysis of the Functional Compartments within the Rat Placentation Site. *Endocrinology*. **153** (4), p.1999-2011.

Sharma, S., Godbole, G. and Modi, D. (2016). Decidual Control of Trophoblast Invasion. *American Journal of Reproductive Immunology*. **75** (3), p.341-350.

Shesely, E.G., Gilbert, C., Granderson, G., Carretero, C.D., Carretero, O.A. and Beierwaltes, W.H. (2001). Nitric oxide synthase gene knockout mice do not become hypertensive during pregnancy. *American Journal of Obstetrics and Gynecology*. **185** (5), p.1198-1203.

Shirasuna, K., Karasawa, T., Usui, F., Kobayashi, M., Komada, T., Kimura, H., Kawashima, A., Ohkuchi, A., Taniguchi, S., and Takahashi, M. (2015). NLRP3 Deficiency Improves Angiotensin II-Induced Hypertension But Not Fetal Growth Restriction During Pregnancy. *Endocrinology*. **156** (11), p.4281-4292.

Sholook, M.M., Gilbert, J.S., Sedeek, M.H., Huang, M., Hester, R.L. and Granger, J.P. (2007). Systemic hemodynamic and regional blood flow changes in response to chronic reductions in uterine perfusion pressure in pregnant rats. *American Journal of Physiology, Heart and Circulatory Physiology*. **293** (4), p.H2080-H2084.

Si, W., Xie, W., Deng, W., Xiao, Y., Karnik, S.S., Xu, C., Chen, Q. and Wang, Q.K. (2018). Angiotensin II increases angiogenesis by NF-κB-mediated transcriptional activation of angiogenic factor AGGF1. *The FASEB Journal*. **32** (9), p.5051-5062.

Singh, A., Singh, A.K., Pandey, P., Chandra, S., Singh, K.A. and Gambhir, I.S. (2016). Molecular genetics of essential hypertension. *Clinical and Experimental Hypertension*. **38** (3), p.268-277.

Small, H.Y., Morgan, H., Beattie, E., Griffin, S., Indahl, M., Delles, C. and Graham, D. (2016a). Abnormal uterine artery remodelling in the stroke prone spontaneously hypertensive rat. *Placenta*. **37**, p.34-44.

Small, H.Y., Nosalski, R., Morgan, H., Beattie, E., Guzik, T.J., Graham, D. and Delles, C. (2016b). Role of Tumor Necrosis Factor-α and Natural Killer Cells in Uterine Artery Function and Pregnancy Outcome in the Stroke-Prone Spontaneously Hypertensive Rat. *Hypertension*. **68** (5), p.1298-1307.

Smith, S.D., Dunk, C.E., Aplin, J.D., Harris, L.K. and Jones, R.L. (2009). Evidence for Immune Cell Involvement in Decidual Spiral Arteriole Remodeling in Early Human Pregnancy. *The American Journal of Pathology*. **174** (5), p.1959-1971.

Smith, J.B., Zheng, T. and Lyu, R-M. (1989). Ionomycin releases calcium from the sarcoplasmic reticulum and activates $Na^{+}Ca^{2+}$ exchange in vascular smooth muscle cells. *Cell Calcium*. **10** (3), p.125-134.

Soares, M.J., Chakraborty, D., Rumi, M.A.K., Konno, T. and Renaud, S.J. (2012). Rat Placentation: An Experimental Model For Investigating the Hemochorial Maternal-Fetal Interface. *Placenta*. **33** (4), p.233-243.

Soltani, N., Keshavarz, M., Sohanaki, H., Dehpour, A.R. and Asl, S.Z. (2005). Oral magnesium administration prevents vascular complications in STZ-diabetic rats. *Life Sciences*. **76** (13), p.1455-1464.

Soma-Pillay, P., Catherine, N-P., Tolppanen, H., and Mebazaa, A. (2016). Physiological changes in pregnancy. *Cardiovascular Journal of Africa*. **27** (2), p.89-94.

Souza, A.S.R., Amorim, M.M.R., Coutinho, I.C.A.N.C., Lima, M.M. de S., Neto, C.N. and Figueroa, I.N. (2010). Effect of the Loading Dose of Magnesium Sulfate (MgSO4) on the Parameters of Doppler Flow Velocity in the Uterine, Umbilical and Middle Cerebral Arteries in Severe Preeclampsia. *Hypertension in Pregnancy*. **29** (2), p.123-134.

Sparks, M.A., Crowley, S.D., Gurley, S.B., Mirotsou, M. and Coffman, T.M. (2014). Classical Renin-Angiotensin System in Kidney Physiology. *Comprehensive Physiology*. **4** (2), p.1201-1228.

Stojanovska, V., Scherjon, S.A. and Plösch, T. (2016). Preeclampsia As Modulator of Offspring Health. *Biology of Reproduction*. **94** (3), p.1-10

Stott, D., Nzelu, O., Nicolaides, K.H. and Kametas, N.A. (2018). Maternal hemodynamics in normal pregnancy and in pregnancy affected by pre-eclampsia. *Ultrasound in Obstetrics and Gynaecology*. **52** (3), p.359-364.

Sukonpan, K. and Phupong, V. (2005). Serum calcium and serum magnesium in normal and preeclamptic pregnancy. *Archives of Gynecology & Obstetrics*. **273**, p.12-06.

Sunderland, N., Hennessy, A. and Makris, A. (2010). Animal Models of Pre-eclampsia. *American Journal of Reproductive Immunology*. **65** (6), p.533-541.

Takimoto, E., Ishida, J., Sugiyama, F., Horiguchi, H., Murakami, K. and Fukamizo, A. (1996). Hypertension Induced in Pregnant Mice by Placental Renin and Maternal Angiotensinogen. *Science*. **274** (5289), p.995-998.

Tan, E.K. and Tan, E.L. (2013). Alterations in physiology and anatomy during pregnancy. *Best Practice & Research Clinical Obstetrics & Gynaecology*. **27** (6), p.791-802.

Tannetta, D. and Sargent, I. (2013). Placental Disease and the Maternal Syndrome of Preeclampsia: Missing Links?. *Current Hypertension Reports*. **15**, p.590-599.

Taylor, E.B. and Sasser, J.M. (2017). Natural killer cells and T lymphocytes in pregnancy and pre-eclampsia. *Clinical Science (London)*. **131** (24), p.291-2917.

Tenório, M.B., Ferreira, R.C., Moura, F.A., Bueno, N.B., de Oliveira, A.C.M. and Goulart, M.O.F. (2019). Cross-Talk Between Oxidative Stress and Inflammation in Preeclampsia. *Oxidative Medicine and Cellular Longevity*. **2019**, ID 8238727.

Thompson, L.P., Pence, L., Pinkas, G., Song, H. and Telugu, B.P. (2016). Placental Hypoxia During Early Pregnancy Causes Maternal Hypertension and Placental Insufficiency in the Hypoxic Guinea Pig Model. *Biology of Reproduction*. **95** (6), p.128-138.

Thornburg, K.L., Bagby, S.P. and Giraud, G.D. (2015). Chapter 43 - Maternal Adaptations to Pregnancy. In: Plant, T.M., Zeleznik, A.J., Albertini, D.F., Goodman, R.L., Hereison, A.E., McCarthy, M.M., Muglia, L.J. and Richards, J.S. *Knobil and Neill's Physiology of Reproduction*. 4th ed. London: Academic Press. pp.1927-1957.

Thornburg, K.L., Jacobson, S-L., Giraud, G.D. and Morton, M.J. (2000). Hemodynamic Changes in Pregnancy. *Seminars in Perinatology*. **24** (1), p.11-14.

Tooher, J., Thornton, C., Makris, A., Ogle, R., Korda, A. and Hennessy, A. (2017). All Hypertensive Disorders of Pregnancy Increase the Risk of Future Cardiovascular Disease. *Hypertension*. **70** (4), p.798-803.

Touyz, R.M., Alves-Lopes, R., Rios, F.J., Camargo, L.L., Anagnostopoulou, A., Arner, A. and Montezano, A.C. (2018). Vascular smooth muscle cell contraction in hypertension. *Cardiovascular Research*. **114** (4), p.529-539.

Touyz, R.M., Chantal, M. and Reudelhuber, T.L. (2001). Angiotensin II Type I Receptor Modulates Intracellular Free Mg^{2+} in Renally Derived Cells via Na^{+}-dependent Ca^{2+}-independent Mechanisms. *Journal of Biological Chemistry.* **276** (17), p.13657-13663.

Townley-Tilson, W.H.D., Wu, Y., Ferguson, J.E. and Patterson, C. (2014). The Ubiquitin Ligase ASB4 Promotes Trophoblast Differentiation through the Degradation of ID2. *PLoS One*. **9** (2), e89451.

Turanov, A.A., Lo, A., Hassler, R.M., Makris, A., Ashar-Patel, A., Alterman, J.F., Coles, A.H., Haraszti, R.A., Roux., L., Godinho, B.M.D.C., Echeverria, D., Pears, S., Iliopoulos, J., Shanmugalingam, R., Ogle, R., Zsengeller, Z.K., Hennessy, A., Karumanchi, S.A., Moore, M.J. and Khorova, A. (2018). RNAi modulation of placental sFLT1 for the treatment of preeclampsia. *Nature Biotechnology*. **36**, p.1164-1173.

Umesawa, M. and Kobashi, G. (2017). Epidemiology of hypertensive disorders in pregnancy: prevalence, risk factors, predictors and prognosis. *Hypertension Research*. **40**, p.213-220.

United Nations. (2015). *The Millennium Development Goals Report 2015*. [Online]. Available: http://www.un.org/millenniumgoals/2015_MDG_Report/pdf/MDG%202015%20rev%20(July%201).pdf [Accessed 01 April 2022].

Vagena, E., Crneta, J., Engström, P., He, L., Yulyaingsih, E., Korpel, N.L., Cheang, R.T., Bachor, T.P., Huang, A., Michel, G., Attal, K., Berrios, D.I., Valdearcros, M., Koliwad, S.K., Olson, D.P., Yi, C-X. and Xu, A.W. (2022). ASB4 modulates central melanocortinergic neurons and calcitonin signaling to control satiety and glucose homeostasis. *Science Signalling*. **15** (733), eabj8204.

Valensise, H., Vasapollo, B., Gagliardi, G. and Novelli, G.P. (2008). Early and late preeclampsia: two different maternal hemodynamic states in the latent phase of the disease. *Hypertension*. **52** (5), p.873-880.

van der Heijden, O.W.H., Essers, Y.P.G., Spaanderman, M.E.A., de Mey, J.G.R., van Eys, J.J.M. and Peeters, L.L.H. (2005). Uterine Artery Remodelling in Psuedopregnancy Is Comparable to That in Early Pregnancy. *Biology of Reproduction*. **73** (6), p.1289-1293.

Venkatesha, S., Toporsian, M., Lam, C., Hanai, J., Mammoto, T., Kim, Y., Bdolah, Y., Lim, K-H., Yuan, H-T., Libermann, T.A., Stillman, I.E., Roberts, D., D'Amore, P.A., Epstein, F.H., Sellke, F.W., Romero, R., Sukhatme, V.P., Letarte, M. and Karumanchi, S. (2006). Soluble endoglin contributes to the pathogenesis of preeclampsia. *Nature Medicine*. **12** (6), p.642-649.

Verdonk, K., Visser, W., Meiracker, A.H.V.D. and Danser, A.H. (2014). The renin–angiotensin–aldosterone system in pre-eclampsia: the delicate balance between good and bad. *Clinical Science (London)*. **126** (8), p.537-544.

Vermot, A., Petit-Härtlein, I., Smith, S.M.E. and Fieschi, F. (2021). NADPH Oxidases (NOX): An Overview from Discovery, Molecular Mechanisms to Physiology and Pathology. *Antioxidants*. **10** (6), p.890-945.

Vest, A.R. and Cho, L.S. (2014). Hypertension in Pregnancy. *Current Atherosclerosis Reports*. **16** (3), p.1-11.

Villar, J., Abdel-Aleem, H., Merialdi, M., Mathai, M., Ali, M.M., Zavaleta, N., Purwar, M., Hofmeyr, J., Nguyen, T.N.N., Campódonico, L., Landoulsí, S., Carroli, G., Lindheimer, M. and World Health Organisation Calcium Supplementation for the Prevention of Preeclampsia Trial Group. (2006). World Health Organization randomized trial of calcium supplementation among low calcium intake pregnant women. *American Journal of Obstetrics & Gynecology*. **194** (3), p.639-649.

Voerman, E., Santos, S., Inskip, D., Amiano, P., Barros, H., Charles, M-A., Chatzi, L., Chrousos, G.P., Corpeleijn, E., Crozier, S., Doyon, M., Eggesbø, M., Fantini, M.P., Farchi, S., Forastiere, F., Georgiu, V., Gori, D., Hanke, W., Hertz-Picciotto, I., Heude, B., Hivert, M-F., Hryhorczuk, D., Iñiguez, C., Karvonen, A.M., Küpers, L.K., Lagström, H., Lawlor, D.A., Lehmann, I., Magnus, P., Majewska, R., Mäkelä, J., Manios, Y., Mommers, M., Morgen, C.S., Moschonis, G., Nohr, E.A., Andersen, A-M. N., Oken, E., Pac, A., Papadopoulou, E., Pekkanen, J., Pizzi, C., Polanska, K., Porta, D., Richiardi, L., Rifas-Shiman, S.L., Roeleveld, N., Ronfani, L, Santos, A.C., Standl, M., Stigum, H., Stoltenberg, C., Thiering, E., Thijs, C., Torrent, M., Trnovec, T., van Gelder, M.M.H.J., van Rossem, L., von Berg, A., Vrijheid, M., Wijga, A., Zvinchuck, O., Sørensen, T.I.A., Godfrey, K., Jaddoe, V.W.V. and Gaillard, R. (2019). Association of Gestational Weight Gain With Adverse Maternal and Infant Outcomes. *Journal of the American Medical Association*. **321** (17), p.1702-1715.

Wallace, J.M., Bhattacharya, S. and Horgan, G.W. (2017). Weight change across the start of three consecutive pregnancies and the risk of maternal morbidity and SGA birth at the second and third pregnancy. *PLoS One*. **12** (6), p. e0179589.

Wallace, A.E., Fraser, R. and Cartwright, J.E. (2012). Extravillous trophoblast and decidual natural killer cells: a remodelling partnership. *Human Reproduction Update*. **18** (4), p.458-471.

Walshe, T.E., Dole, V.S., Maharaj, A.S.R., Patten, I.S., Wagner, D.D. and D'Amore, P.A. (2009). Inhibition of VEGF or TGF-β signaling activates endothelium and increases leukocyte rolling. *Arterioscleorisis, Thrombosis, and Vascular Biology*. **29** (8), p.1185-1192.

Wang, H.D., Xu, S., Johns, D.G., Du, Y., Quinn, M.T., Cayatte, A.J. and Cohen, R. A. (2001). Role of NADPH Oxidase in the Vascular Hypertrophic and Oxidative Stress Response to Angiotensin II in Mice. *Circulation Research*. **88** (9), p.947-953.

Wang, Y., Fan, H., Zhao, G., Liu, D., Du, L., Wang, Z., Hu, Y. and Hou, Y. (2012). miR-16 inhibits the proliferation and angiogenesis-regulating potential of mesenchymal stem cells in severe pre-eclampsia. *The FEBS Journal*. **279** (24), p.4510-4524.

Wenger, N.K. (2014). Recognizing Pregnancy-Associated Cardiovascular Risk Factors. *The American Journal of Cardiology*. **113** (2), p.406-409.

Wilson, B.J., Watson, M.S., Prescott, G.J., Sunderland, S., Campbell, D.M., Hannaford, P. and Smith, W.C.S. (2003). Hypertensive diseases of pregnancy and risk of hypertension and stroke in later life: results from cohort study. *BMJ*. **326**, p.845-892.

World Health Organisation. (2019). *Maternal mortality.* Available: https://www.who.int/en/news-room/fact-sheets/detail/maternal-mortality. Last accessed 01 April 2022.

Wu, R., Milette, E., Wu, L. and de Champlain, J. (2001). Enhanced superoxide anion formation in vascular tissues from spontaneously hypertensive and deoxycorticosterone acetate-salt hypertensive rats. *Journal of Hypertension*. **19** (4), p.741-748.

Xu, Z., Jin, X., Cai, W., Zhou, M., Shao, P., Yang, Z., Fu, R., Cao, J., Liu, Y., Yu, F., Fan, R., Zhang, Y., Zou, S., Zhou, X., Yang, N., Chen, X. and Li, Y. (2018). Proteomics Analysis Reveals Abnormal Electron Transport and Excessive Oxidative Stress Cause Mitochondrial Dysfunction in Placental Tissues of Early-Onset Preeclampsia. *Proteomics Clinical Applications*. **12** (5), e1700165.

Xue, B., Yin, H., Guo, F., Beltz, T.G., Thunhorst, R.L. and Johnson, A.K. (2017). Maternal Gestational Hypertension-Induced Sensitization of Angiotensin II Hypertension Is Reversed by Renal Denervation or Angiotensin-Converting Enzyme Inhibition in Rat Offspring. *Hypertension*. **69** (4), p.669-677.

Yallampali, C. and Garfield, R. (1993). Inhibition of nitric oxide synthesis in rats during pregnancy produces signs similar to those of preeclampsia. *American Journal of Obstetrics and Gynecology*. **169** (5), p.1316-1320.

Yamada, N., Kido, K., Tamai, T., Mukai, M. and Hayashi, S. (1981). Hypertensive effects on pregnancy in spontaneously hypertensive rats (SHR) and stroke-prone SHR (SHRSP). *International Journal of Biological Research in Pregnancy*. **2** (2), p.80-84.

Yang, Y., Bazhin, A.V., Werner, J. and Karakhanova, S. (2012). Reactive Oxygen Species in the Immune System. *International Reviews of Immunology*. **32** (3), p.249-270.

Yang, H., Kim, T-H., Lee, G-S., Hong, E-J. and Jeung, E-B. (2014). Comparing the expression patterns of placental magnesium/phosphorus-transporting channels between healthy and preeclamptic pregnancies. *Molecular Reproduction and Development*. **81** (9), p.851-860.

Yeh, H-L., Kuo, L-T., Sung, F-C. and Yeh, C-C. (2018). Association between Polymorphisms of Antioxidant Gene (MnSOD, CAT, and GPx1) and Risk of Coronary Artery Disease. *Biomed Research International*. **2018** (Article ID 5086869), p.1-8.

Yin, F.C., Spurgeon, H.A., Rakusan, K., Weisfeldt, M.L. and Lakatta, E. G. (1982). Use of tibial length to quantify cardiac hypertrophy: application in the aging rat. *American Journal of Physiology Heart and Circulatory Physiology*. **243** (6), p.H941-H947.

Yong, H.E.J. and Chan, S-Y. (2020). Current approaches and developments in transcript profiling of the human placenta. *Human Reproduction Update*. **26** (6), p.799-840.

Yong, H.E.J., Murthi, P., Brennecke, S.P. and Moses, E.K. (2018). Genetic Approaches in Preeclampsia. In: Murthi, P. and Vaillancourt, C *Preeclampsia. Methods in Molecular Biology, vol 1710*. New York: Humana Press. pp.53-72.

Zorov, D.B., Juhaszova, M. and Sollott, S.J. (2014). Mitochondrial Reactive Oxygen Species (ROS) and ROS-Induced ROS Release. *Physiological Reviews*. **94** (3), p.909-950.